An Investigation of Copper(I) Active Metal Template Synthesis of Interlocked Structures for Anion Binding

Sam Sutton

Wolfson College, University of Oxford



A thesis submitted for the degree of Doctor of Philosophy

Inorganic Chemistry Laboratory

University of Oxford

Trinity Term 2019

An Investigation of Copper(I) Active Metal Template Synthesis of Interlocked Structures for Anion Binding

Sam Sutton, Wolfson College, University of Oxford

Abstract of thesis submitted for the degree of D. Phil., Trinity Term 2019

This thesis describes the synthesis and study of a series of novel macrocycles containing propyl-, 1,2-hydroxymethyl benzene-, and 1,3-benzene-linked bis(iodo)triazole motifs, as well as computational investigation of these and further bis(iodo)triazole marcrocycles

Chapter One introduces the field of supramolecular chemistry, highlighting areas of particular relevance to this thesis *viz* halogen bonding, anion coordination, recognition, and templation routes to the synthesis of interlocked structural frameworks.

Chapter Two describes the synthesis of a series of macrocycles, containing propyl- and 1,2-hydroxymethyl benzene-linked bis(iodo)triazole motifs. Attempts to include them into [2]rotaxanes, pursuing understanding of how macrocycle flexibility impacts active metal templation outcomes are reported.

Chapter Three details computational methods used to determine if a simplified computational model has potential as a predictor for macrocycle viability in an active metal template reaction. Minimal conformations of known and novel macrocycles are generated complexed with Cu^{I} cations and the results presented for comparison with experimental outcomes.

Chapter Four focuses on the study of how macrocycle size variation impacts active metal template yield. A series of novel macrocycles containing the 1,3-bis(iodo)triazole benzene motif were prepared, then used in active metal template reactions to generate novel [2]rotaxanes for yield comparison.

Chapter Five provides a summary of the major conclusions of this thesis.

Chapter Six contains procedures pertaining to chemicals, instrumentation, data handling and analytical protocols, as well as detailing synthetic methods and characterisation of novel compounds.

Chapter Seven provides the references cited within Chapters One to Six.

Acknowledgements

As with many endeavours of such scope, this thesis could not have been completed without the support of others: Prof. Paul D. Beer, who gave me the opportunity to undertake a DPhil within his group, consistently shaping and guiding my research goals and experiences, while supporting my forays from synthetic into computational chemistry. This support included his petitioning on my behalf for the help of Prof. John McGrady, whose guidance and gentle criticism enabled me to realise my ideas, developing them into a proof of concept computational study, and hopefully opening up future avenues of investigation and collaboration.

Recognition for assistance in chemical matters goes to: Dr Sean Robinson, for patient, and particular, guidance in my first year on iodotriazole synthesis; Dr Asha Brown, a font of synthetic tips, tricks, and quiet reassurance; Dr Jason Lim, for fielding endless questions and discussion of many ideas, helping me direct my focus. Dr Tim Barendt, Dr Valentine Bunchuay and Andrew Docker all helped me on many occasions, whether brainstorming reactions gone awry, or reordering a synthetic route. Dr Bob Edkins brought me up to speed in the dark arts of Gaussian input files and wrangling the computational cluster. I am grateful to Dr Jess Pancholi, Valentine, Phil Marks, Jason and Andrew for taking the trouble to proof-read my thesis: all errors of course remain my own.

As the 'louder' of the two Beer group labs, S8 was a vibrant and musically eclectic environment. Nowhere else have I listened to pop-rock, choral, metal, orchestral and electronic music, and sung along to Disney... in the same working day! The diverse and stimulating experience S8, and its sister lab S7, offered me was a direct consequence of the people in the Beer group over that time: Lydia Gilday, Tom Mole, Dan Lucy, Will Arter, Stuart Cornes, Alex Hess, Hena Bagha, Anna Spearing-Ewyn, Grace Turner, Harry Klein, George Li, Arseni Borissov, Luiza Bondila, Robert Hein, Jane Liew, Richard Tse, Edward Mitchell, Tanya Rogova, Michael Ahrens, Niles Beadman and Jonny Moloney. They all have my gratitude for their engaging company and diverse discourse.

While it is impossible to list everyone else who has enriched my time in Oxford outside the Beer group individually, I should however especially like to thank my friends at Wolfson and in the Oxford University Rifle Club for making me feel welcome and valued. I apologise for the odd rant when synthesis was not going according to plan! Finally, I would like to thank my parents for all their support during this undertaking, without which it would not have been possible.

Abbreviations

$\Delta\delta$	change in chemical shift relative to free host
μ	micro
Å	Angstrom
A	hydrogen or halogen bond acceptor
aq.	aqueous
Bn	benzyl
br.	broad
calc.	calculated
°C	degrees Celsius
conc.	concentrated
COSY	homonuclear correlation spectroscopy
CuAAC	copper(I)-catalysed azide alkyne cycloaddition
d	doublet
dd	doublet of doublets
D	hydrogen bond donor
DCM	dichloromethane
DIPEA	*N,N'*-diisopropylethylamine
DMF	*N,N'*-dimethylformamide
DMSO	dimethylsulfoxide
DNA	deoxyribonucleic acid
e.g.	*exempli gratia*
EI	electron ionisation
equiv.	equivalent
ESI	electrospray ionisation
Et	ethyl
g	gram
HRESI-MS	high resolution electrospray ionisation mass spectrometry
Hz	Hertz
i.e.	*id est*
IPA	isopropyl alcohol
IUPAC	International Union of Pure and Applied Chemistry
J	joule
J	coupling constant
K	Kelvin
K_a	association constant
L	litre
LRESI-MS	low resolution electrospray ionisation mass spectrometry
m	*meta*

m	metre, milli, multiplet
M	moles per litre
MD	molecular dynamics
Me	methyl
MIM	mechanically interlocked molecule
MM	molecular mechanics
mol	mole
n	nano
neg.	negative
NMR	nuclear magnetic resonance
p	*para*
Ph	phenyl
pH	-$\log_{10}[H^+]$
pK_a	-$\log_{10}K_a$
pos.	positive
Pr	propyl
q	quartet
QM	quantum mechanics
quart.	quartet
quint.	quintet
R	chemical substituent
ROESY	rotating-frame nuclear Overhauser effect correlation spectroscopy
s	singlet
S	entropy
syn	synperiplanar
t	triplet
TBA	tetrabutylammonium cation
TBTA	tris[1-benzyl-1,2,3-triazol-4-yl)methyl]amine
^{t}Bu	*tert*-butyl
THF	tetrahydrofuran
TLC	thin layer chromatography
tosyl	4-toluenesulfonyl
Ts	4-toluenesulfonyl
TTF	tetrathiafulvalene
UV	ultraviolet

Contents

1 Introduction **1**

1.1 Supramolecular Chemistry . . . 2

1.1.1 Traditional Non-covalent Interactions . . . 3

1.1.2 σ-Hole Interactions . . . 6

1.2 Host-Guest Chemistry . . . 9

1.2.1 Importance of Anions . . . 10

1.2.2 Challenges in Anion Recognition . . . 11

1.2.3 Anion Receptors in Nature . . . 13

1.3 Synthetic Receptors for Anion Recognition and Sensing . . . 15

1.3.1 Hydrogen Bonding Receptors . . . 15

1.3.2 Halogen Bonding Receptors . . . 22

1.3.3 Anion Sensing . . . 26

1.3.4 Applications of Anion Recognition . . . 28

1.4 Mechanically Interlocked Molecules . . . 32

1.5 The Mechanical Bond . . . 33

1.6 Synthesis of Mechanically Interlocked Molecules . . . 34

1.6.1 Cation Template Synthesis . . . 35

1.6.2 Neutral Template Synthesis . . . 39

1.6.3 Anion Template Synthesis . . . 40

1.7 Applications of Mechanically Interlocked Molecules . . . 42

1.7.1 Receptors and Sensors . . . 42

1.7.2 Switches and Machines . . . 44

1.7.3 Catalytic Applications . . . 45

1.8 Project Aims . . . 47

2 Novel motifs for active metal template rotaxanation **48**

2.1 Introduction . . . 49

2.1.1 AT-CuAAC Synthesis of Interlocked Structures . . . 49

2.2 Chapter Aims . . . 52

2.3 Propyl Bis-iodotriazole Macrocycle . . . 53
2.3.1 Design and Synthesis of Hydrogen and Halogen Bonding Macrocycles . 53
2.4 1,2-Hydroxymethyl Benzene Bis-iodotriazole Macrocycle . . . 55
2.4.1 Design and Rationale . . . 55
2.4.2 Synthesis of Hydrogen and Halogen Bonding Macrocycles . . . 55
2.4.3 Attempted AT-CuAAC Rotaxane Formation with Propyl Spaced Bis-iodotriazole Macrocycle . . . 59
2.4.4 Qualitative Cu^{I}-binding . . . 60
2.4.5 Attempted AT-CuAAC Rotaxane Formation with 1,2-hydroxymethyl Benzene Spaced Bis-iodotriazole Macrocycle . . . 61
2.4.6 Synthesis of Smaller Ring-size 1,2-hydroxymethyl Benzene Bis-iodotriazole Containing Macrocycles . . . 65
2.4.7 Small Macrocycle AT-CuAAC Rotaxane Formation Investigation . . . 69
2.5 Conclusions . . . 73
2.6 Future Work . . . 73

3 Computational study of copper(I) binding conformation 74
3.1 Introduction . . . 75
3.1.1 Density Functional Theory in Brief . . . 75
3.1.2 Hartree-Fock Theory . . . 76
3.1.3 Kohn-Sham Density Functional Theory . . . 78
3.1.4 Functionals . . . 79
3.1.5 Basis Sets . . . 80
3.1.6 Chapter Aims . . . 81
3.2 Methodology . . . 82
3.2.1 Functionals . . . 83
3.2.2 Basis Sets . . . 84
3.2.3 Conformational Sampling . . . 85
3.2.4 Limitations of Approach . . . 87
3.2.5 Predictive Capacity . . . 88
3.3 Results . . . 88
3.3.1 Macrocycles with Known AT-CuAAC Performance . . . 89

3.3.2 Comparison of Minimal Conformations and AT-CuAAC Yield 99
3.3.3 Prospective Macrocycles 101
3.3.4 Comparison of Novel Macrocycle Conformations 115
3.4 Conclusions 119
3.5 Further Work 120

4 Effect of bis-triazole macrocycle size on AT-CuAAC yield 122
4.1 Introduction 123
4.2 Chapter Aims 126
4.3 Synthesis of Smaller Ring-size 1,3-bis(iodo)triazole Benzene Containing Macrocycles 127
4.3.1 Design and Rationale 127
4.3.2 Synthesis 128
4.4 AT-CuAAC [2]rotaxane Formation Investigation 133
4.4.1 Synthesis 133
4.5 Conclusions 139
4.6 Future Work 139

5 Conclusions 141

6 Experimental 144
6.1 General Considerations 145
6.1.1 Chemicals and Solvents 145
6.1.2 Instrumentation 145
6.1.3 Titration Protocols 146
6.1.4 Computational Methods 146
6.2 Synthesis 147
6.2.1 General Synthetic Methods 147
6.2.2 Compounds from Chapter 2 148
6.2.3 Compounds from Chapter 4 170

7 References 176

Chapter 1

Introduction

1.1 Supramolecular Chemistry

Supramolecular chemistry, a term coined by Lehn,[1] concerns the study of non-covalent intermolecular interactions toward the design and assembly of complex multi-component molecular architectures. The field was born out of the work of Pedersen,[2] Lehn[1,3] and Cram,[4] studying alkali metal binding using crown ethers, cryptands and spherands respectively (Figure 1.1), resulting in their being awarded the 1987 Nobel Prize in Chemistry *"for their development and use of molecules with structure-specific interactions of high selectivity."* From these beginnings great advances have been made, especially in the application of this relatively new, and undeniably powerful field, in areas such as biomaterials,[5] chemical analytics,[6,7] medicine[8,9] and resource reclamation[10] among many others. Now, through rational design, the construction of supramolecules from appropriately functionalised molecular components is being developed through a shift away from thermodynamically driven assemblies, to harness the possibilities afforded by non-equilibrium systems.[11] The importance of this new direction was highlighted[12] by the award of the 2016 Nobel Prize in Chemistry to Jean-Pierre Sauvage, Fraser Stoddart and Ben Feringa for *"the design and synthesis of molecular machines"*.

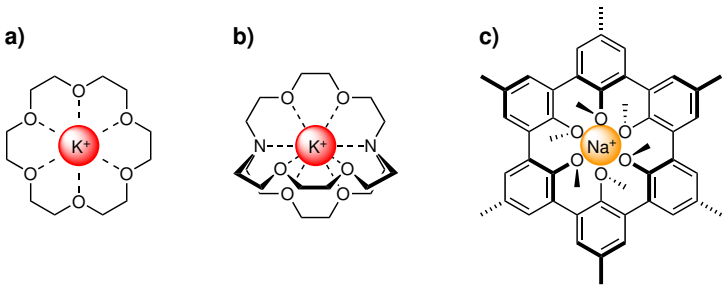

Figure 1.1: Early examples of cation binding: (a) Pedersen's crown ether,[2] (b) Lehn's Cryptand[1] and (c) Cram's Spherand[4]

The field of supramolecular chemistry has two main aspects: self-assembly, *i.e.* the spontaneous association of small molecules into larger and more complicated assemblies, and host-guest chemistry, *i.e.* the recognition and binding of a chemical entity, such as an anion or cation, by another. The subject of this thesis is the exploration of a novel method for template-directed construction of a host for recognizing anion guest species.

This introductory chapter will first address the interactions that drive supramolecular self-assembly, focusing on halogen bonding. From this basis, host-guest chemistry and the design of receptors for anion binding will be considered. This leads on to a discussion of the mechanical bond, and the application of host-guest chemistry to the assembly of mechanically

interlocked molecules (MIMs), with particular attention given to active metal template synthesis, which is the main focus of the work reported within this thesis.

1.1.1 Traditional Non-covalent Interactions

Supramolecular chemistry concerns intermolecular interactions, particularly as they can be used to affect or understand self assembly and host-guest association. These interactions are non-covalent, largely reversible, and operate under thermodynamic control. Aside from electrostatic attractions, the strength of these interactions typically falls short of covalent single bonds, with a typical single supramolecular bond enthalpy being < 200 kJ mol^{-1} compared to 300-500 kJ mol^{-1} for a C – C single bond.[13] This deficit in strength is more than made up for by the use of supramolecular interactions in a concerted fashion, yielding highly stable assemblies. The most studied interactions are discussed below, before moving on to cover the more recently harnessed σ-hole interactions.

Coulombic Interactions

Electrostatic interactions, divided between *ion–ion*, *ion–dipole* and *dipole–dipole* (Figure 1.2) occur as a result of Coulombic attraction or repulsion between charged species, and can be comparable in strength to covalent bonds. *Ion–ion* interactions, governed by Coulomb's law, are solely dependent on separation and charge density, lacking the directional component needed to enhance binding selectivity.[14] By contrast, *ion–dipole* interactions, which include hydrogen bonding and σ-hole interactions, though considerably weaker and effective only at shorter distances (again E $\propto$ r^{-2}), have greater potency in guest discrimination due to their much greater directionality;[15] the strength of interaction is dependent on the vector between the ion and dipole moment. For this reason, these interactions are heavily exploited in molecular recognition.

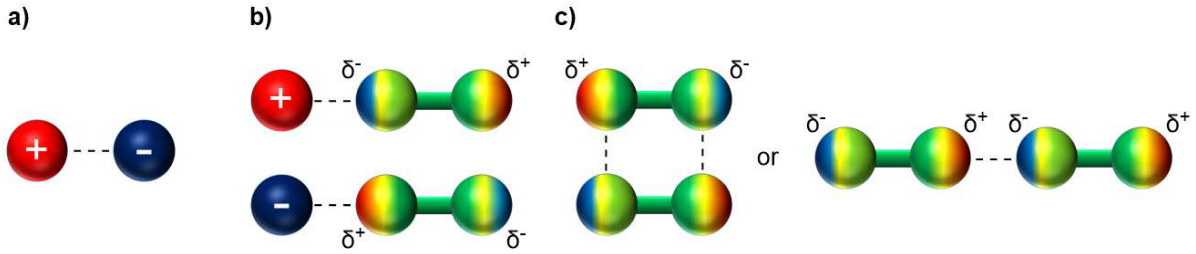

Figure 1.2: The three classes of Coulombic forces: (a) ion–ion, (b) ion–dipole and (c) dipole–dipole interactions.

Hydrogen Bonding

Hydrogen bonds are abundant throughout nature, being responsible for DNA base-pair recognition (Figure 1.3), as well as the primary means by which secondary and tertiary protein and enzyme structures are stabilized. Predominantly electrostatic in nature,[16] the hydrogen bond is defined by IUPAC as *an attractive interaction between a hydrogen atom from a molecule or fragment* $X{-}H$ *wherein* X *is more electronegative than* H*, and a group of atoms in the same, or another molecule*.[17] An electron donor interacts with the permanent dipole formed as electron density is drawn away from the hydrogen atom by its more electronegative neighbour. As a class of *ion–dipole* interaction, the interaction strength is at its greatest for linear geometries, ranging from 1-162 kJ mol^{-1} with non-linear arrangements occurring at the cost of bond enthalpy[18].

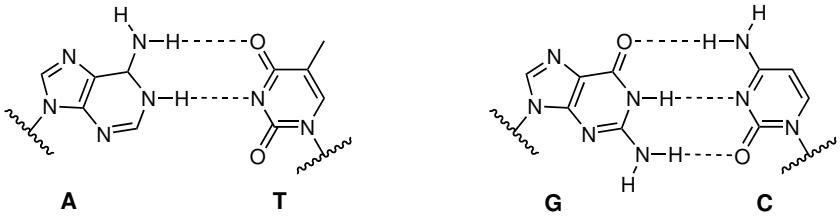

Figure 1.3: Hydrogen bonding between complementary DNA base pairs.

Cation- and Anion-π Interactions

Cation-π interactions are well studied. They are driven by electrostatic attraction between a cationic species and the electron-rich, partially negative quadrupole of an aromatic π-system[19,20] (Figure 1.4a), displaying interaction energies of 1-50 kJ mol^{-1}.[21] Anion-π interactions occur when an electron deficient aromatic system interacts with an anion (Figure 1.4b). They are infrequent in nature due to mutual electrostatic repulsion between anions and electron-rich amino acid side chains.[22] The interaction arises largely from electrostatic and anion-induced polarization effects,[23,24] which are strongest in non-polar aprotic solvents with small charge-dense anions, both conditions facilitating close approach of the charged species to the aromatic ring system. Multiple hapticities have been discerned by X-ray crystallographic studies, demonstrating little variation in interaction energies between them (1-25 kJ mol^{-1}), only significantly varying as distance from the ring changes.[25,26]

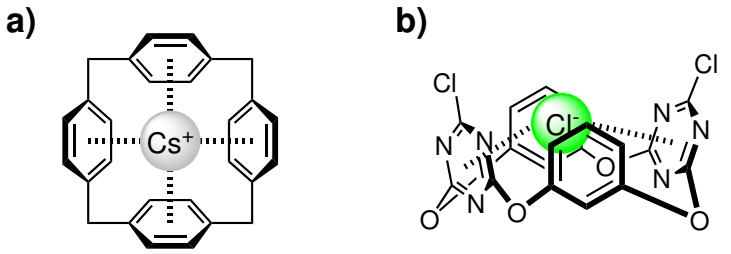

Figure 1.4: Examples of ion–π interactions: (a) cation–π interaction[27], (b) anion–π interaction.[28]

$\pi - \pi$, Donor-Acceptor Interactions

Spontaneous alignment of aromatic rings in an offset parallel *face-to-face* manner commonly termed $\pi - \pi$ stacking has been noted for a while,[29,30] with directly stacked and *face-to-edge* geometries also observed (Figure 1.5). $\pi - \pi$ stacking arises from a combination of electrostatics, dispersion forces and solvation effects,[31,32] and despite relatively weak enthalpies, these donor-acceptor interactions between aromatic rings are commonly used in supramolecular chemistry. Arising from a favourable association between an electron-rich and electron-poor ring system, and enhanced by the incorporation of electrostatic charge in one or both rings, alignment of the contact between rings can be highly susceptible to electronic effects resulting from their substituents,[33] with interaction energies reaching 75 kJ mol^{-1} in extended aromatic systems.[34]

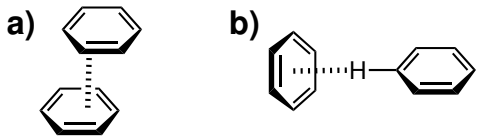

Figure 1.5: Aromatic π–π donor–acceptor interactions: (a) face-to-face, (b) face-to-edge.

Solvophobic Interactions

In polar solvents like water or acetonitrile, non-polar molecules interact weakly with the solvent, favouring aggregation with each other to minimize system energy. Termed the *Hydrophobic Effect* in water, this poorly understood phenomenon is now recognized to play an important role in biomolecular interactions,[35] as well as host-guest recognition in water.[36] The classical hydrophobic effect is predominantly driven by favourable entropic contributions from the release of water molecules in the hydration shells of molecular species during association.[37] The non-classical hydrophobic effect is dominated by an enthalpic contribution arising from the hydrogen bonding networks formed by the liberated water molecules with the bulk.[38,39] Exact energetic

contributions of solvophobic effects prove difficult to obtain, but studies with simple molecules have shown contributions up to approximately 10 kJ mol^{-1} in water.[40]

Coordinate Bonding

Lewis acid–base coordination, including metal–ligand coordination arises from the ability of a chemical species (Lewis acid) to accept a pair of electrons into a suitable, empty orbital, from a species (Lewis base) capable of donating such a pair of electrons, *e.g.* an anion. Despite being classified as molecular, rather than supramolecular, Lewis acid-base interactions possess many of the same qualities as supramolecular interactions, especially lability and reversibility of coordinate bonds and possession of specific geometric requirements.[41] Thus they have been relied on for the formation of strong host–guest complexes and higher order supramolecular polymetallic cage-like systems (Figure 1.6), as well as being harnessed for anion recognition through use of Lewis acidic components such as transition metals,[42] tin and three-coordinate boron species.[43]

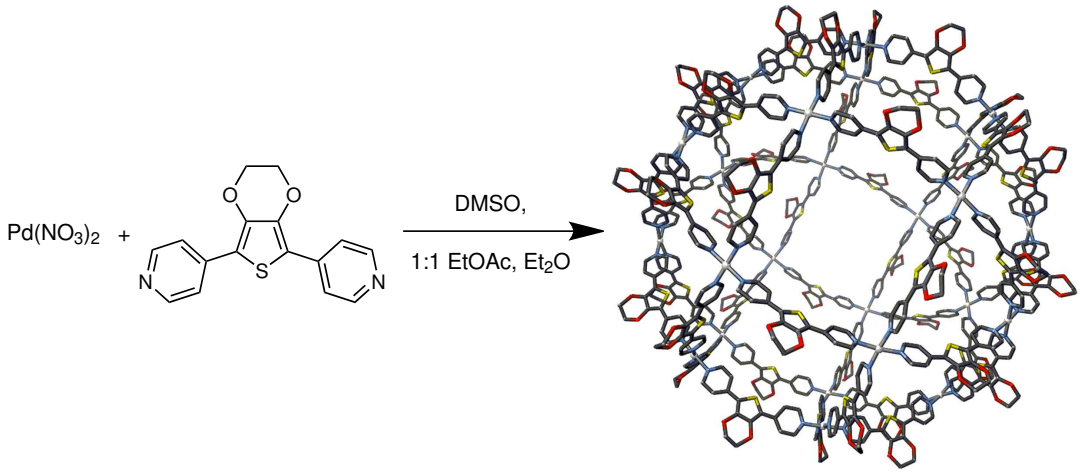

Figure 1.6: Example of a supramolecular $M_{24}L_{48}$ cage structure assembled *via* metal–ligand coordinate bonds between simple starting components.[44]

1.1.2 σ-Hole Interactions

Isolated atoms have spherically symmetric, positive electrostatic potential, as nuclear charge dominates the dispersed electrons. When a main group atom (D) is covalently bonded to a more electronegative functionality (R), its electron density is drawn toward the bond, resulting in an equatorial belt of partial negative charge, and a polar region of partial positive charge forming colinear to the R–D bond, termed a σ-hole. The magnitude of this σ-hole is dependent on the

polarizability of the atom D and the electron-withdrawing strength of the covalently attached group R.

The σ-hole is known to form non-covalent interactions with electron-rich Lewis bases (neutral and anionic). These interactions combine orbital contributions, as the σ-hole corresponds to the location of the σ^*-antibonding orbital of the R–D bond, with electrostatic,[45,46] charge transfer[47,48] and dispersion contributions,[49] though the relative magnitudes of these will be dependent on the particular donor and acceptor atoms.[50] These non-covalent interactions have been observed empirically and computationally for atoms in groups 14 (tetrel), 15 (pnictogen), 16 (chalcogen), 17 (halogen) and 18 (aerogen).[51,52] The computed molecular electrostatic potential (MEP) surfaces are shown below (Figure 1.7). As a result σ-hole interactions are increasingly employed in anion coordination. It is perhaps interesting to note that hydrogen bonding could be considered a special class of σ-hole interaction, meeting as it does many of the definition criteria.[53,54]

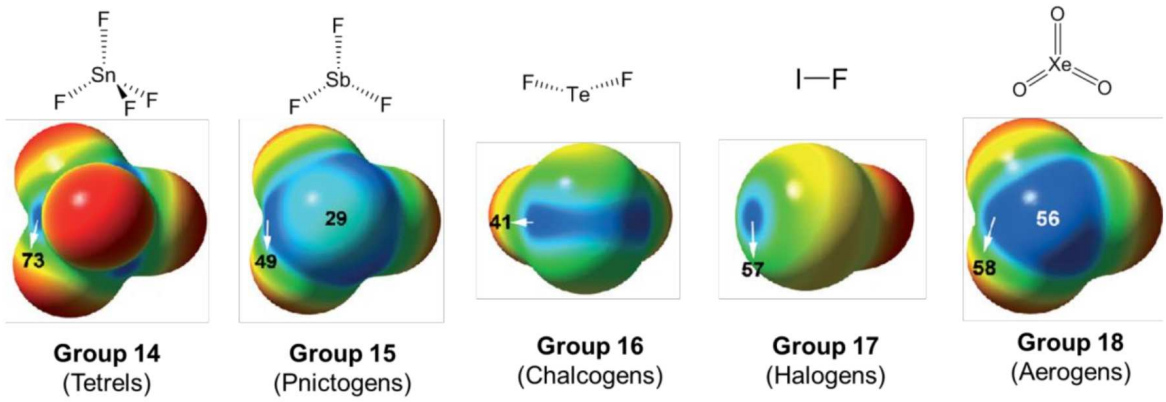

Figure 1.7: Computed MEP surfaces (MP2/aug-cc-pVTZ level) showing location of σ-holes (in blue). MEP values of σ-holes are indicated in kJmol^{-1}. Figure reproduced from reference.[55]

Halogen Bonding

The most studied of the σ-hole interactions, halogen bonding (XB) is similar to hydrogen bonding (HB), also being a special class of dipole–dipole or ion–dipole interactions. Defined by IUPAC[56] to occur where *'There is evidence of a net attractive interaction between an electrophilic region associated with a halogen atom in a molecular entity, and a nucleophilic region in another, or the same, molecular entity'*, it was first observed in the 19th century[57,58], but only identified in the 1950s by Mulliken and Hassel.[59–61] Subsequent calculations by Politzer and co-workers in the 1990s revealed the physical properties and potential utility in solution-phase supramolecular chemistry.[62–64] Their calculations suggested that when a R–X bond was

formed by a halogen atom X of valence electronic configuration $\ldots(n)s^2(n)p_x^2p_y^2p_z^1$, the electron in the p_z orbital (defined as pointing in the R–X bond direction) localizes in the σ bonding orbital. The equatorial belt of partial negative charge consists of the filled, non-bonding p_x and p_y orbitals, and the σ-hole is a consequence of the σ^* antibonding orbital, which dictates the highly directional nature of the halogen bond, with angles of interaction constrained to near 180° (Figure 1.8). This combination of negative belt and positive pole confers amphoteric behavior to the halogen, as electrophiles approaching orthogonally to the R–X bond can interact with the partial negative charge of the equatorial belt. It is important to note that although there is a significant covalent contribution, comparable to metal–ligand bonds of transition metal complexes,[65] it is generally understood that halogen bonding is primarily an electrostatic interaction, with further contributions from charge-transfer and dispersion forces. For σ-hole forming elements, heavier, more polarizable donors form stronger bonds, (F $<<$ Cl $<$ Br $<$ I) particularly when attached to strongly electron-withdrawing moieties, and typical interaction energies span the range of 10-200 kJ mol^{-1}.[50] This exceeds the strength of hydrogen bonding, in part due to greater tolerance of solvent polarity.[66]

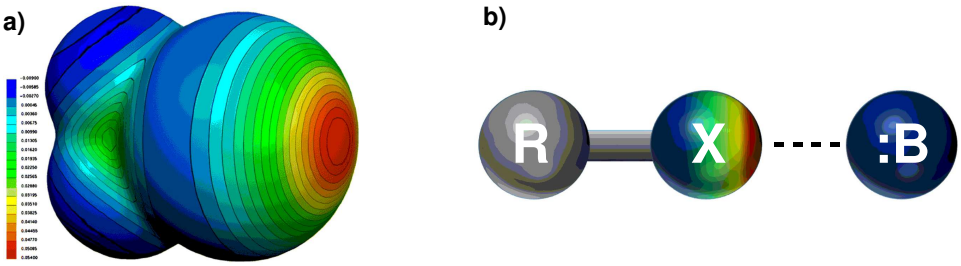

Figure 1.8: Halogen bonding: (a) electrostatic potential diagram of CF_3I showing the σ-hole as the region of positive potential (red) in Hartrees, at the 0.001 electrons Bohr^{-3} iso-density surface,[67] and (b) cartoon representation of a halogen bond with a Lewis base (R = halogen, aryl, alkyl, etc.; X = Cl, Br, I; B = N, O, S, Se, Cl, Br, I, F$^-$, Cl$^-$, Br$^-$, I$^-$, etc.)

Chalcogen, Pnictogen and Tetrel Bonding

Chalcogen bonding (ChB)[68] was defined in 2009[69] as operating *via* an analogous mechanism to halogen bonding, involving the formation of σ-holes on a chalcogen atom (number dependent on sp hybridisation of the center, *i.e.* sp^2 or sp^3). Theoretical studies have determined an expected interaction energy range of 3.5-46 kJ mol^{-1} for ChB complexes.[69] While still far less studied than XB, ChB interactions have been identified as contributing to the biological activity of organo-sulfur and organo-selenium compounds involved in protein structure stabilization and enzymatic regulation.[70,71] A key limiting factor impeding their broad utility is the air and

moisture sensitivity of the more potent ChB donors,[72] arising from weak $C–D$ bonds (C – Te bond strength is around 200 kJ mol^{-1}),[73] which has restricted their study to simple acyclic molecules. The search for more stable ChB donor motifs is ongoing.

Pnictogen (PnB) and Tetrel (TrB) bonding are largely unexplored, and very little is known about them beyond that they function in a similar manner to other σ-hole donors. Examples of supramolecular systems are rare, with most studies being computational or in the solid state.[74–76] They are difficult to study empirically as the increasing steric bulk of substituents around three-coordinate (pnictogen) or four-coordinate (tetrel) atoms likely blocks the electropositive σ-holes, preventing significant interaction with Lewis Bases. Further, the heavier members of the pnictogen (Sb, Bi) and tetrel (Sn, Pb) families, expected to have the strongest σ-hole interactions, have significant metallic character, participating more in traditional metallic coordination chemistry.[77,78]

1.2 Host-Guest Chemistry

The field of host-guest chemistry takes its inspiration from nature, specifically the many molecular recognition events that occur as a matter of course in biochemical processes, such as host binding of a substrate in a protein or enzyme. Introduced by Fischer at the end of the 19th century, the 'lock and key' model[79] describes the specific binding of a substrate 'key' to an enzyme active site 'lock'. This concept was expanded to include the idea of 'induced fit' *i.e.* the ability of a substrate molecule to induce a conformational change in the host, with an observable enhancement to recognition as a result (Figure 1.9).[80,81] Both of these ideas are encompassed by the principle of complementarity, formalised by Cram: *'to complex, hosts must have binding sites which can simultaneously contact and attract the binding sites of guests, without generating internal strains or strong non-bonded repulsions.'*[82]

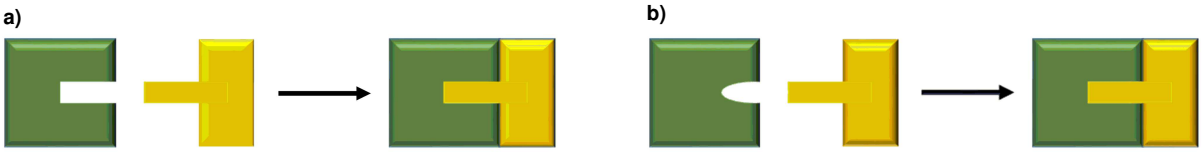

Figure 1.9: Models of host–guest binding: (a) Fischer's 'lock and key,'[79] and (b) Koshland's 'induced fit.'[80,81]

A second key concept, more easily observed in relatively crude synthetic receptors than their biological analogues, is that of preorganisation. First introduced in the 1980s by Cram

and co-workers,[83] it was later codified as *'the more highly hosts and guests are organised for binding and low solvation prior to their complexation, the more stable will be their complexes.'*[4] A particular manifestation of this is termed the *macrocyclic effect*, whereby hosts possessing enclosed structural frameworks often bind guests more strongly than their acyclic analogues.[84] This is due to several factors: greater rigidity and lower initial solvation result in fewer degrees of freedom lost on complexation, which is entropically favorable, as well as diminished enthalpic penalty from desolvation prior to guest binding. A well-defined and rigid structure also offers more ready access to shape and size complementarity, affording more favorable binding enthalpies.[85] Substrates within the scope of these concepts range from simple metal cations such as potassium, through simple anions such as chloride, small organic species (neutral and charged) all the way through to large biomolecules like proteins or enzymes.

The importance of the host-guest chemistry of anions is explored in the following section, addressing challenges faced in realizing it effectively, and touching upon examples of how nature achieves the specificity it does. This is followed by a review of the major types of artificial receptor design, detailing some of the history, and current state of the art of anion host-guest supramolecular chemistry.

1.2.1 Importance of Anions

Anions serve many vital physiological roles, with approximately seventy percent of enzymatic reactions being catalysed by anionic species.[86] The most abundant extracellular anion in the human body, chloride, acts to maintain cellular osmotic balance and regulates the electrical neutrality of extracellular fluid.[87] More complex organic anions such as glutamate[88] and aspartate[89] function as neurotransmitters, lactate[90] and pyruvate[91] serve as metabolic intermediates, while adenosine triphosphate (ATP), the energy currency of the cell, and deoxyribonucleic acid (DNA), are larger biological polyanions still. Anions even have physiological function in areas such as immune response, and biological mis-regulation can result in conditions such as cystic fibrosis.[92]

This is not to say that anion importance is limited to physiology. They can have profound and far-reaching impact on the wider environment: anthropogenic overabundance of anions such as nitrate and phosphate in the water system resulting from the overuse of fertilizers in arable farming causes eutrophication, leading to oxygen depletion and ecosystem damage or destruction.[93] Other less immediately obvious industrial activities cause influx and accumula-

tion of toxic cyanide, perchlorate and transition metal based oxoanions.[94] Of particular harm are the radioactive pertechnetate ($^{99}TcO_4^-$),[95] a byproduct of nuclear fuel reprocessing, and chromate (CrO_4^-).[96] Selective detection and sequestration of these pollutants, as well as more nuanced physiological interactions are current research targets.

1.2.2 Challenges in Anion Recognition

Anions present a double-edged sword as targets for recognition: the very properties that make high specificity possible also cause greater difficulties in the design of synthetic receptors. This in part explains why the supramolecular chemistry of anions has been historically less mature than that of cations, despite their clear importance.

Firstly, anions are larger in radius than comparable cations (1.81 Å for Cl^- versus 1.37 Å for K^+)[97] due to a lower effective nuclear charge. This results in lower charge densities, and consequently weaker electrostatic and ion–dipole interactions with receptors, in turn requiring supplementary interactions for effective recognition. That said, the greater polarizability compared to their isoelectronic cations affords a larger contribution from dispersive interactions in stabilizing anion–receptor complexes.

Secondly, anions exhibit a wide variety of geometries (Figure 1.10) which, while affording potential advantages in selectivity through more defined host–guest complementarity, renders design and synthesis of such well matched hosts a more elaborate and hence synthetically challenging affair.

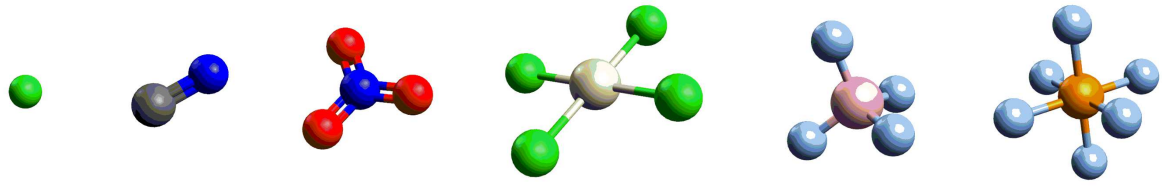

Figure 1.10: Examples of different anion geometries.

Anions can be pH-sensitive, potentially possessing multiple protonation equilibria, and may lose their negative charge entirely at low pH, which can nullify the use of electrostatic interactions for anion binding. Important examples of anions subject to this phenomenon include oxoanions such as phosphate, and biological derivatives such as ATP. Highly basic anions such as fluoride or carboxylates can even abstract acidic protons from receptor molecules.[98] Anion

pH-dependence can also limit the usable recognition groups, or viable pH windows, of receptors containing groups such as ammonium, which only function in low pH environments where they remain protonated.[99]

Lastly, when compared to their isolectronic cations, anions possess greater free energies of solvation, with greater dependence on both the nature of the anion and solvent. This energetic penalty must be overcome for host–guest complexation to occur. Solvation of both host and guest dictates the enthalpic and entropic contributions to the binding event: Considering the process in two stages, desolvation of host and guest incurs an enthalpic penalty, but ejection of solvent molecules from the host cavity is entropically favorable. Subsequent re-solvation of the host–guest complex is enthalpically favorable but entropically disfavored. Overall the binding event may be driven enthalpically and/or entropically, and this is highly system dependent. In polar protic solvents such as water, this hydration enthalpy must be taken into consideration during design, as the host molecule must effectively compete with, and displace, the hydration shell for binding to occur. In aprotic organic solvents with low dielectric constants, such as dichloromethane or chloroform, the more important association to overcome is that of ion pairing between the anion and its counter-cation,[100] but typically weak solvation results in lower energy barriers, allowing neutral receptors more viability.

The Hofmeister series (Figure 1.11) provides an approximation of the hydrophobicity, and hence hydration energy of anions, based upon their impact on the aqueous solubility of a protein.[101] Hydrophobic anions, typically larger and less charge dense, are preferentially bound by hydrophobic binding sites in aqueous solvent media due to their poorer solvation. Commensurately, hydrophilic anions with higher hydration energies are more challenging targets for anion recognition in equivalent aqueous conditions, due to the higher energy barrier that must be overcome.[102]

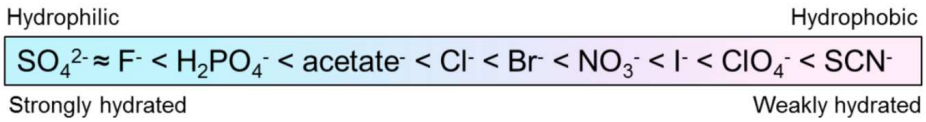

Figure 1.11: The Hofmeister series.

The impact of the hydrophobic effect on anion binding in water has not yet been well-explored, but several notable recent successes have been attributed to it. These hosts rely on deep hydrophobic cavities which shield the bound anions from bulk water, having higher affinities for larger, more charge diffuse and more poorly hydrated anions, such as I^- and

ClO_4^-. Examples include the bambusuril macrocycle (Figure 1.12a) reported by Sindelar and co-workers in 2015[103] capable of binding these anions with affinities in excess of 10^7 M^{-1} in aqueous phosphate buffer at pH 7.1, and the octa-acid cavitand (Figure 1.12b) reported by Gibb and coworkers in 2016[104] which binds the PF_6^- anion with K_a = 790 M^{-1}, again in phosphate buffer, but at pH 11.3. These systems are particularly notable for their anion affinity, as they are themselves polyanions. Gains in enthalpy and losses in entropy observed on binding in both cases suggest the non-classical hydrophobic effect is the driving factor.

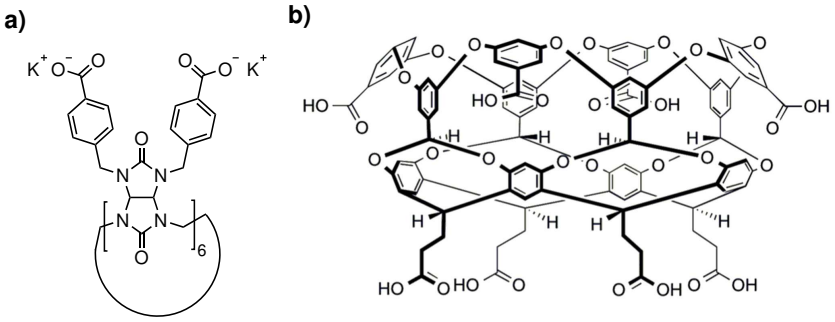

Figure 1.12: (a) A bambusuril macrocycle from the Sindelar group,[103] and (b) an octa-acid cavitand from the Gibb group.[104]

1.2.3 Anion Receptors in Nature

As effective anion binding presents more challenges than cation binding, it is useful to illustrate how nature has evolved to overcome these difficulties, and how this has inspired and informed synthetic anion receptor design. Natural anion binding cavities have been determined to be composed of a surprisingly small series of different binding motifs, recently considered to be modular in their construction. Two of the most important bases of which, the 'nest'[105] and C$^\alpha$NN,[106] are illustrated below (Figure 1.13).

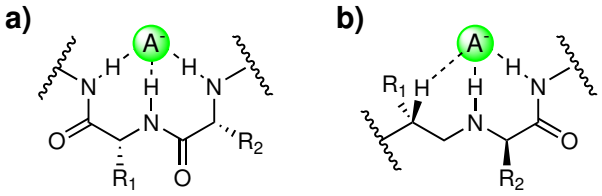

Figure 1.13: (a) The nest, and (b) C$^\alpha$NN motifs.

The nest is the result of a pair of neighbouring amino acid residues having dihedral angles of $\pm 70°$, $\pm 40°$, forming a depression from the main-chain NH groups of these and a third following residue. This depression is capable of accommodating an atom with a whole or partial negative charge. Examples of suitable guests include carbonyl oxygen, as in the oxoanion hole

of serine proteases, or a phosphate group, such as in the P-loop superfamily that binds ATP and GDP. The P-loop superfamily is further seen to exhibit compound nests of five successive NH groups.[107] The C$^{\alpha}$NN motif, usually found in protein loop regions preceding a helix, is structurally similar, again being comprised of a pair of neighboring NH donor residues, but an adjacent α-carbon replaces the third NH donor residue. This motif is found in sulfate and phosphate recognition sites.[108]

Often, the nature of the binding site complements the desired guest's hydrophobicity. Strongly hydrated anions are often bound in sites containing metal cations[102] or many convergent hydrogen bonding interactions.[109] Poorly hydrated anions such as halides tend to be bound by similarly hydrophobic residues, such as lysine, proline or leucine.[87] The impact of the relative affinity of the host and guest for water can significantly influence the favorability of the binding process, as has been recently shown by Whitesides *et al.*[110] The selectivity of natural binding sites is perhaps best illustrated by phosphate binding proteins, which are able to discriminate hydrogen phosphate from hydrogen arsenate even up to 4500-fold excess in water (Figure 1.14). This is particularly impressive given the identical charges and near identical pK_a values and hydration enthalpies of the oxoanions, and has been attributed to a loss of low energy barrier hydrogen bonding as a result of the 4% size difference.[111]

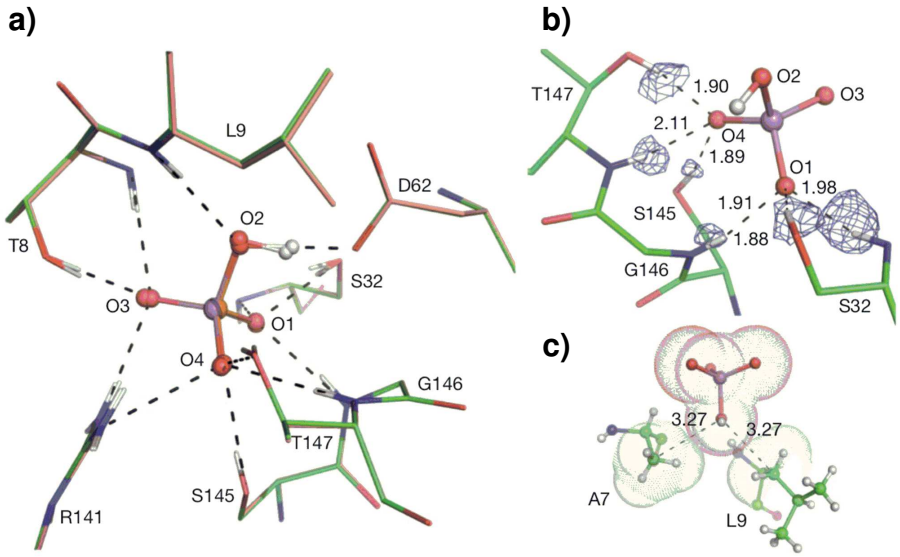

Figure 1.14: (a) A superposition of the $HAsO_4^{2-}$ and HPO_4^{2-} anions within the GFAJ-1 phosphate binding protein, (b) key ion-dipole interactions in the $HAsO_4^{2-}$ structure, and (c) steric clash between the bound $HAsO_4^{2-}$ and the protein. Figure reproduced from reference.[111]

1.3 Synthetic Receptors for Anion Recognition and Sensing

Guided by an ever-increasing understanding of how nature achieves specificity and strength in anion binding, a broad range of neutral and charged synthetic anion receptors have been reported, incorporating many chemical functionalities, and ranging from simple acyclic receptors to complex polydentate interlocked systems. Neutral receptor systems have most frequently been employed in largely apolar, aprotic solvents, while the high dielectric constants and free energies of anion solvation in protic solvents such as water usually necessitates positively charged receptors, using Coulombic attraction to outcompete the solvent and complex the anion. This increase in affinity comes at the cost of selectivity, due to the lack of directionality inherent to electrostatic interactions. Thus the ideal cationic binding motif is capable of strong, directional, charge-assisted ion–dipole interactions with anions, affording receptors with high affinity and selectivity. Hydrogen bonding is the most common ion–dipole interaction to be harnessed, with exploitation of the uniquely directional halogen bonding being a more recent, and burgeoning, undertaking. Various receptor examples incorporating these key non-covalent interactions are discussed below, as well as applications of these receptors.

1.3.1 Hydrogen Bonding Receptors

Hydrogen bonding (HB) donor motifs incorporated into synthetic anion hosts principally consist of neutral or cationic N–H and C–H donors. The origin of anion supramolecular chemistry is considered by many to be the observation of halide ion binding by a lipophilic macrobicyclic cage reported in 1968 by Park and Simmons.[112] Evidence of an encapsulated halide complex driven by electrostatics and hydrogen bonding, was observed by ^{1}H NMR after addition of chloride to an acidic aqueous solution of the protonated bis-amine. Little further progress was reported until 1976, when Graf *et al* published polyammonium cryptand-like hosts capable of binding chloride and bromide in aqueous media, employing hydrogen bonding and Coulombic attraction (Figure 1.15a).[113] This was followed in 1981 by Schmidtchen, who reported pH-independent quaternary ammonium cages which combined geometry and electrostatics to bind halide guests (Figure 1.15b).[114] These works have proven seminal, the design principles demonstrated providing the basis for much subsequent work.

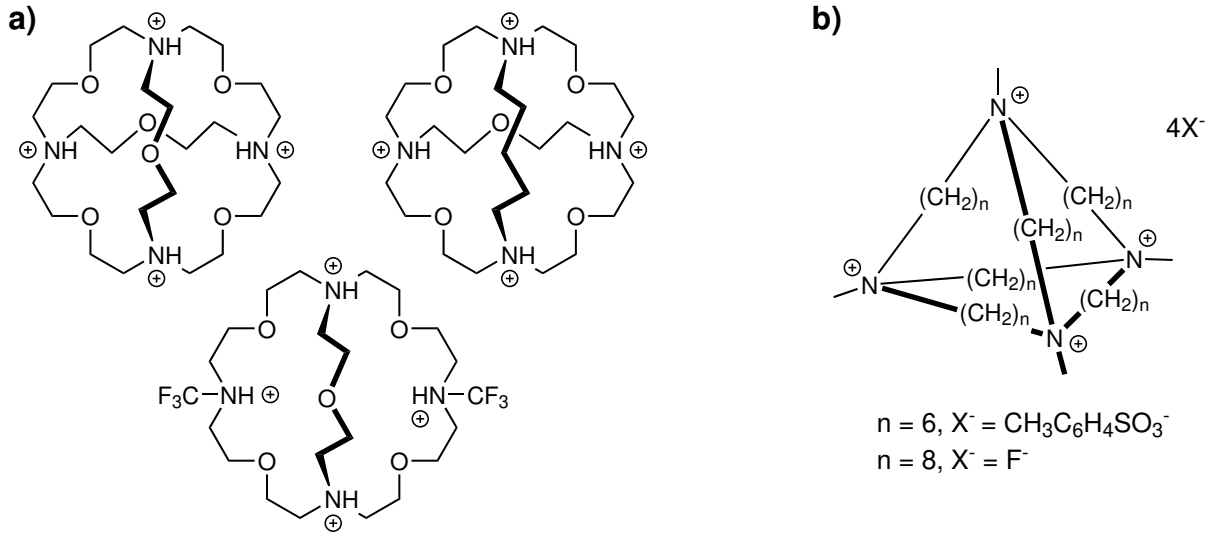

Figure 1.15: (a) Lehn's polyammonium cryptates,[113] (b) Schmidtchen's quarternary ammonium cages.[114]

The first example of a neutral receptor, operating solely *via* hydrogen bond donors was published in 1986 by Pascal *et al*, wherein they reported evidence for fluoride binding in DMSO-d_6 by a tris-amide cyclophane (Figure 1.16a).[115] Since these early systems, hydrogen bonding has continued to be harnessed in a variety of synthetic anion receptors. Neutral hydrogen bonding systems see most common demonstration in aprotic solvents, with amides proving popular choices for HB donor groups due to their ubiquity in nature and ready synthetic accessibility. An important isophthalamide-based acyclic structure capable of binding halides was reported in 1997 by Crabtree and co-workers (Figure 1.16b),[116] which drove incorporation of this style of motif into a range of anion hosts.[117] Adopting a thermodynamically favorable *syn-anti* conformation in the absence of an anion, it adopts a *syn-syn* conformation in the presence of halides, binding them in 1:1 stoichiometry in DCM *via* two convergent amide hydrogen bonds. Peptides, particularly cyclopeptides, offer another accessible route to multiple amide HB donors, a recent example being the cyclo-peptide 'molecular oyster' receptor reported by Kubik and co-workers (Figure 1.16c),[118] which is impressively capable of strongly binding I^- and $SO_4{}^{2-}$ anions in a competitive aqueous solvent medium of 95% water 5% MeOH by sandwiching anions between both rings *via* a combination of convergent ammonium HB interactions and the hydrophobic effect.

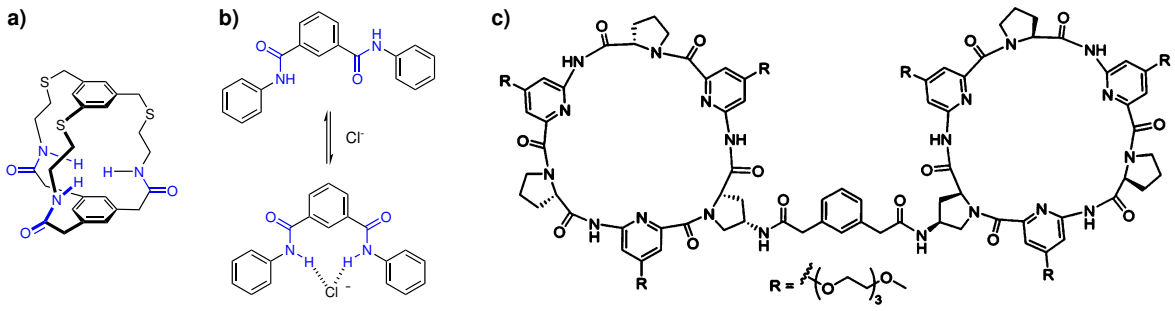

Figure 1.16: Neutral hydrogen bonding receptors: (a) A tris-amide cyclophane[115] (b) an isophthalamide-based acyclic,[116] and (c) a cyclopeptide-based 'molecular oyster.'[118]

First exploited in anion receptor design by Bowman-James and co-workers in 2003,[119] thioamide motifs are less well studied. Thioamides are stronger HB donors than amides, a result of the increased polarizability of sulfur decreasing N–H bond energies by $\sim$10kJ mol^{-1}, so they are more susceptible to deprotonation. In this work, a series of macrocyclic (Figure 1.17) and macrobicyclic hosts were shown to possess increased affinity for a range of anionic guests including $H_2PO_4^-$, HSO_4^- and the halides over their amide analogues, a finding mirrored by the work of Jurczak and co-workers,[120] who found a two-fold increase in affinity for chloride and benzoate compared to the amide analogue in a series of acyclic receptors, both sets of studies conducted in DMSO-d_6.

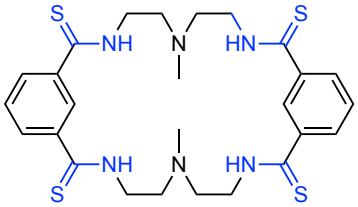

Figure 1.17: An example of a tetra-thioamide macrocycle.[119]

An obvious extension to the use of amides and thioamides, ureas and thioureas have also been exploited as potent HB donors.[121,122] Again, substitution of the amide oxygen for a sulfur increases acidity and thus HB donor strength, at the cost of increased ease of deprotonation. The two parallel N–H HB donors prove optimally spaced for interaction with Y-shaped anions such as carboxylates, nitrates and phosphates.[123] First reported in 1992 by Wilcox and co-workers (Figure 1.18a),[124] ureas and their thiourea analogues have since been incorporated into a variety of host molecules. Enhanced anion binding, as a direct result of two adjacent N–H donors from a single urea group compared to two separate amide groups, was reported by Jia *et al.*[125] A tris-thiourea tripodal receptor (Figure 1.18b) reported by Gale and

co-workers[126] demonstrates high binding affinity for SO_4^{2-} in 0.5% water in DMSO, while a C_3-symmetric metacyclophane-based receptor (Figure 1.18c) reported by Hong and coworkers[127] binds AcO^- and $H_2PO_4^-$ preferentially over Cl^- and N_3^- in pure DMSO.

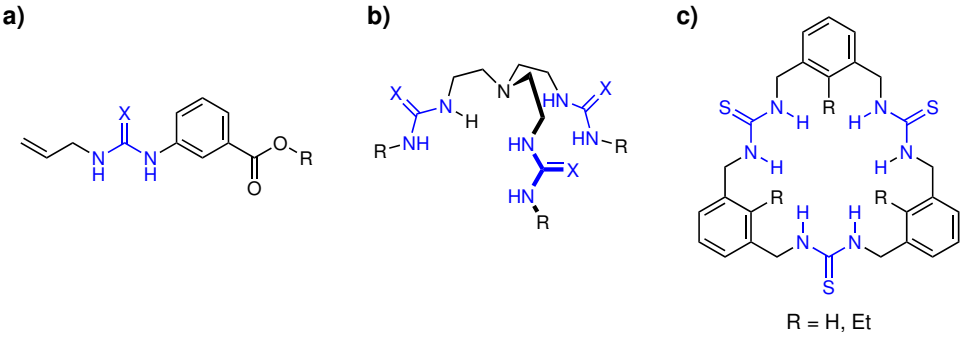

Figure 1.18: Neutral urea- and thiourea-based receptors, X = O, S.

Squaramides and thiosquaramides, derivatives of 3,4-diaminocyclobutane-1,2-dione, are a more recently utilized class of neutral N–H HB donor. First reported as an anion binding motif in 1998 by Ballester and co-workers after preceding theoretical calculations.[128,129] Many subsequent examples of receptors harnessing squaramides have been reported, with comparison between squaramide-based receptors and their urea-based analogues published in 2011 by Fabbrizzi and co-workers demonstrating the superior anion binding strength of squaramides.[130] The authors reported that this enhanced binding is due to a thermodynamic contribution resulting from the increased aromatic character of the four-membered ring on anion complexation. Thiosquaramides were first demonstrated as pH-dependent anion transporters in 2014 by Gale and co-workers (Figure 1.19a).[131] Thiosquaramides were predicted computationally to exhibit higher anion affinities than squaramide analogues,[132] however for the thiosquaramide receptors tested, similar or considerably lower binding affinities for Cl^- in DMSO-d_6 were observed. This was attributed to the higher conformational freedom of thiosquaramides resulting in a greater entropic penalty paid on anion binding. Recently a squaramide macrocycle was reported by Joliffe and co-workers that binds SO_4^{2-} selectively in 2:1 DMSO:water (Figure 1.19b).[133]

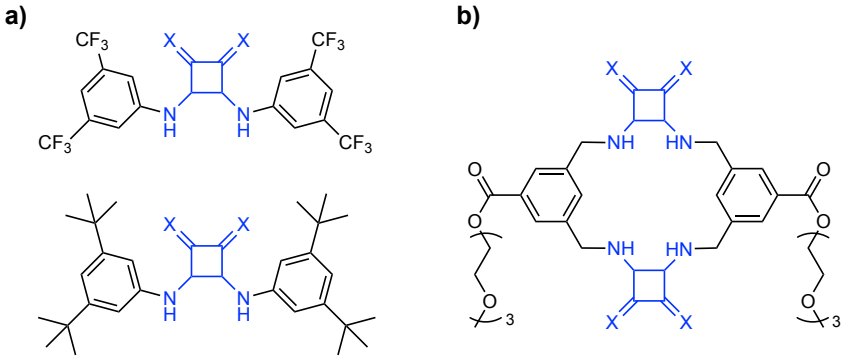

Figure 1.19: Neutral squaramide-based receptors. X = O, S.

Pyrrole offers a strong HB donor for anion recognition, with the further advantage that it lacks a HB accepting moiety, preventing competitive intra- or intermolecular host–host association. As a result, it has been incorporated into various anion hosts, most notably the calix[4]pyrroles. Pioneered by Sessler and co-workers in 1996,[134] calix[4]pyrroles are macrocycles containing four pyrrole units arranged with N-H HB donor groups pointing towards the central cavity. They adopt a cone formation on addition of an anion, with all four pyrrole units forming linear hydrogen bonds, preferentially binding F^- and Cl^- in a range of polar organic solvents. Additional functional groups can be used in combination to alter or improve anion affinities, demonstrated in a later dicationic pyridinium-functionalized calix[4]pyrrole derivative (Figure 1.20a) which strongly binds pyrophosphate ($HP_2O_7^{3-}$) in acetonitrile.[135] Higher order calix[n]pyrroles have also been reported to preferentially bind larger anions.[136] Pyrroles can also be used as part of extended aromatic systems such as indolocarbazoles or expanded porphyrins,[137] where the additional rigidity enhances preorganisation, and the HB donor ability is improved through increased acidity, with indolocarbazole-based foldamer examples binding Cl^- in pure water (Figure 1.20b).[138]

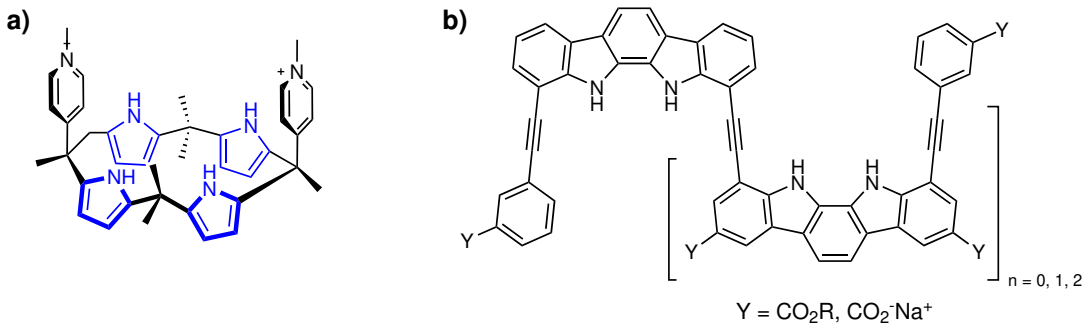

Figure 1.20: Pyrrole-based receptors.

Hydrogen bonding C–H donors were initially considered only capable of augmenting other stronger HB interactions, but are now established as anion binding motifs in their own right. One of the first anion binding systems with solely C–H donors, a fluorinated macrocyclic ether (Figure 1.21a), was reported in 1990 by Kaftory and co-workers.[139] It was determined to associate with F^- *via* four polarized CH_2 groups in solution and the solid state. C–H donors are also found in resorcinarene and bambus[6]uril derivatives, which bind anions in the central cavity. An example of a water soluble bambus[6]uril derivative was published in 2015 by Sindelar and co-workers (shown previously in Figure 1.12a), which is capable of strong anion binding in pure water, proving selective for more hydrophobic anions such as $ClO_4{}^-$ and I^-.[103]

Highly polarized C–H donors of the 1,2,3-triazole functional group have been exploited as an anion binding motif, in spite of being weaker than more acidic N–H donors, due to the electron-withdrawing sp^2-hybridized carbon and three heterocyclic nitrogen atoms. Pioneered by a seminal report by Flood and co-workers in 2008,[85] who described a neutral preorganized triazolophane macrocycle (Figure 1.21b), which was found to bind Cl^- strongly and selectively in CH_2Cl_2 with K_a = 1.3 x 10^5 M^{-1}. The subsequent popularity of the triazole motif has been driven by its ease of accessibility *via* the Huisgen copper(I)-catalyzed azide-alkyne cycloaddition (CuAAC) reaction, which has proved tolerant to a wide range of conditions and functional groups.[?] The same group recently reported the 'cyanostar', a novel macrocycle, possessing an electropositive cavity comprised of repeating cyanostilbene monomers, and shown to bind large anions such as PF_6 and $ClO_4{}^-$ in mixtures of methanol and DCM (Figure 1.21c).[140]

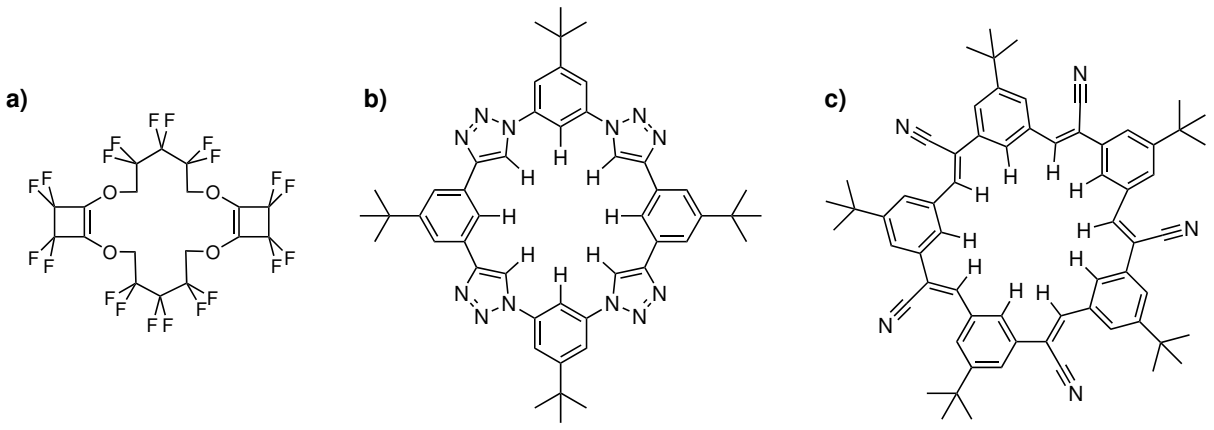

Figure 1.21: Neutral C–H donor-based receptors.

Electrostatic *ion–ion* interactions are the strongest of the non-covalent interactions, resulting in strong anion binding, but the purely radial dependence of electrostatic interaction strength results in a loss of selectivity. A combination of electrostatic charge and other non-covalent interactions, particularly directionally dependent ones like HB, allows this limitation to be overcome, yielding a strong and selective receptor even in competitive polar, protic solvent mixtures including pure water. Successfully harnessed motifs include pyridinium, guanidinium, imidazolium and triazolium. Guanidinium is a naturally occurring anion binding motif, found in arginine residues within proteins and enzymes such as carboxypeptidase-A, where its basic nature ($pK_a \sim 13.5$) allows it to function over a broad pH range.[141] Early receptors incorporating these motifs are simple in nature, such as the series of bis-pyridinium receptors reported in 1997 by Jeong *et al*, an example of which is shown below (Figure 1.22a), which proved capable of carboxylate binding $>10^3$ M^{-1} in 9:1 DMSO:water,[142] or the bis-guanidinium motifs investigated in 2001 by Hamilton and co-workers, capable of binding dicarboxylates in 3:1 water:methanol (Figure 1.22b).[143]

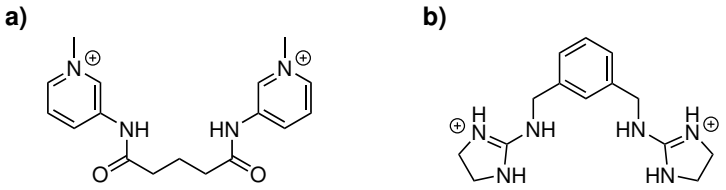

Figure 1.22: Early examples of charged hydrogen bonding receptors.

Soon these dual-interaction motifs were incorporated into more elaborate receptors. Examples include the tripodal tris-pyridinium benzene host (Figure 1.23a) reported by Steed and co-workers in 2003, capable of binding Br^- in CH_3CN,[144] and the tetracationic macrocycle reported by Sessler and co-workers in 2010, containing two pyridine bis-imidazolium motifs (Figure 1.23b), which binds mono- and di-terephthalate anions in DMSO with K_a = 2.1 x 10^3 M^{-1} and 3.3 x 10^3 M^{-1} respectively.[145]

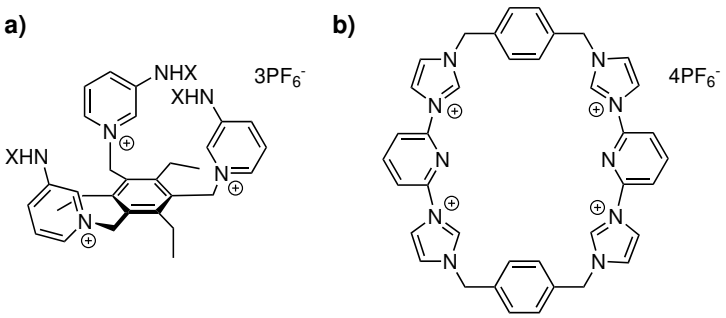

Figure 1.23: Charged HB receptor examples.

The triazolium cation has proved to be a strong and versatile anion binding motif, easily incorporated through N-methylation of a triazole. Triazolium groups have been leveraged heavily by many groups after first being reported in 2008 by Kumar *et al*, whose steroid-based bis-triazolium receptor bound $H_2PO_4^-$ (K_a = 1920 M^{-1}) selectively over halides ($K_a \sim$ 300 M^{-1}) and acetate (K_a = 30 M^{-1}) in chloroform.[146] Interestingly, the macrocyclic analogue exhibited lower affinity for this anion (K_a = 1100 M^{-1}) than the acyclic receptor, which was thought to be due to a loss of flexibility, which prevented a suitably complementary geometry. Subsequent examples were reported by the groups of Schubert and Beer, the former a bis-triazolium acyclic (Figure 1.24a) binding sulfate in a 2:1 host–guest complex, the latter a tetra-triazolium macrocycle (Figure 1.24b) capable of strong anion binding in 1:1 DMSO:H_2O, highlighting the power of the motif.[147,148]

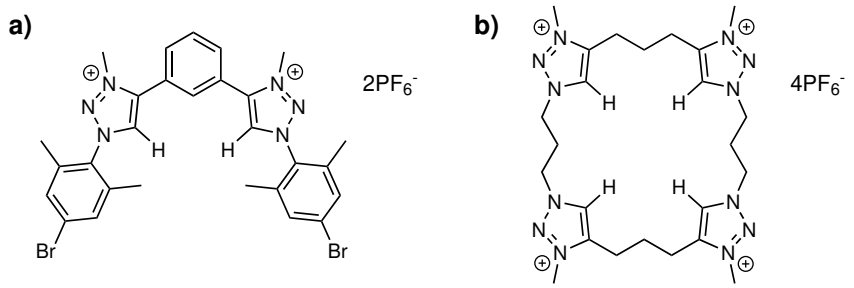

Figure 1.24: Example triazolium-based HB receptors.

1.3.2 Halogen Bonding Receptors

While still less common than their HB counterparts, XB donor anion hosts are a burgeoning means of achieving high anion affinity and selectivity. Iodine is the predominant halogen used in XB hosts, due to its high polarisability allowing it to form highly electrophilic σ-holes, which engender strong XB interactions, though bromine is also used.[149] As with HB receptors, neutral and cationic motifs are known, with cationic motifs seeing wider use due to the stronger charge-assisted XB that results. A key advantage of XB-anion interactions is the high linearity: revealed by crystal structures, this is a natural consequence of the polar position of the electropositive σ-hole of the halogen donor atom. Predominantly explored for solid-state chemistry and materials design, and studied extensively crystallographically, the potential of XB for solution-phase supramolecular chemistry has only truly started to be explored in the last decade. The known motifs can be grouped into three classes: haloperfluoroarene, halotriazole, haloimidazolium, and halotriazolium (Figure 1.25).



Figure 1.25: Common neutral and cationic XB-donor motifs for anion recognition, X = Br, I.

The first example of solution-phase XB anion recognition was a tripodal haloperfluoroaryl heteroditopic receptor (Figure 1.26a) reported in 2005 by Resnati and co-workers, which was shown to bind a separated sodium iodide ion pair in chloroform strongly (K_a = 2.6 x 10^5 M^{-1}).[150] Comparison of the perfluoro- and perfluoroiodo-analogues showed the potency of the XB-iodide interaction, with the perfluoro-analogue having significantly diminished binding strength (K_a = 1.3 x 10^3 M^{-1}) under the same conditions. Haloperfluoroarenes can be functionalized with the donor halogen at any position on the ring, so have an advantage over the other XB motifs in that their geometry can be tuned to match the requirements of the receptor design. This property is seen in the first example of anion recognition achieved by halogen bonding alone. Reported by Taylor and co-workers in 2010, it uses *ortho*-substituted iodines, allowing anionic guests to be coordinated in a tridentate XB manner within the receptor cavity (Figure 1.26b).[151] In acetone, this tripodal receptor bound halides $Cl^- > Br^- > I^-$ selectively over oxoanions TsO^-, $HSO_4{}^-$ and $NO_3{}^-$, suggesting an intrinsic preference of XB for soft-soft interactions with the halides rather than hard-soft interactions with the oxoanions. Later work from the Taylor group combined two perfluoroaryl groups with a urea motif (Figure 1.26c) in a neutral acyclic receptor capable of strongly binding benzoate anions in acetonitrile.[152]

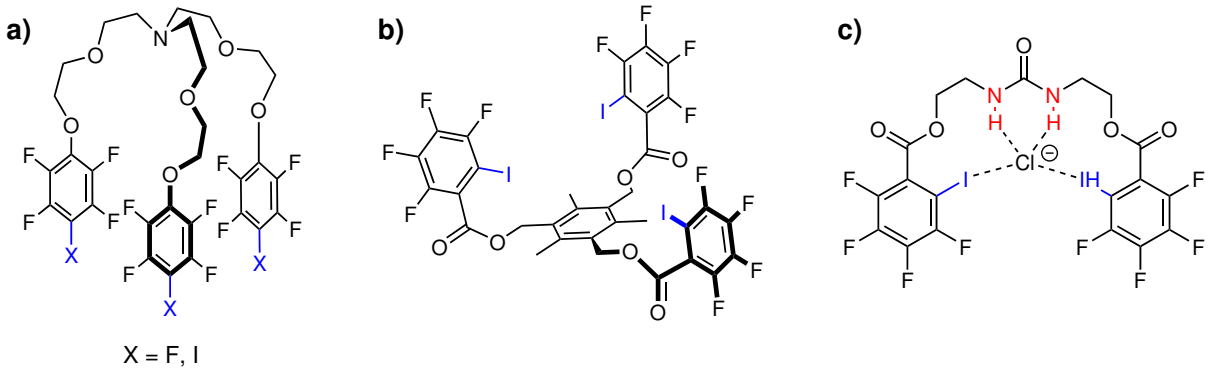

Figure 1.26: Early XB receptors.

The 5-iodo-1,2,3-triazole heterocycle was first shown to be a potent anion binding motif by Beer and coworkers in 2013 (Figure 1.27a),[153] shortly after it was shown to be readily accessible through one- or two-pot synthetic routes.[154,155] This tetrakis-zinc[4]metalloporphyrin-based iodotriazole receptor was found to bind halides in chloroform with approximately twice the strength of its prototriazole analogue while possessing the same selectivity trend. Subsequently, Schubert and co-workers reported the preparation of a series of anion receptors with bidentate halotriazole groups, to study the effect of different bite angles and differing degrees of polarization of the C–X bond.[156] The example shown below harnesses cooperative HB interactions to support the halogen bonding interaction through additional polarization of the triazoles (Figure 1.27b). From their studies they conclude that iodine was the best XB donor atom, and that due to the strict linearity of the halogen bond angle, there is a strong preference for monodentate XB if the spacer unit does not allow the ideal linear C – X···A geometry to be realized.

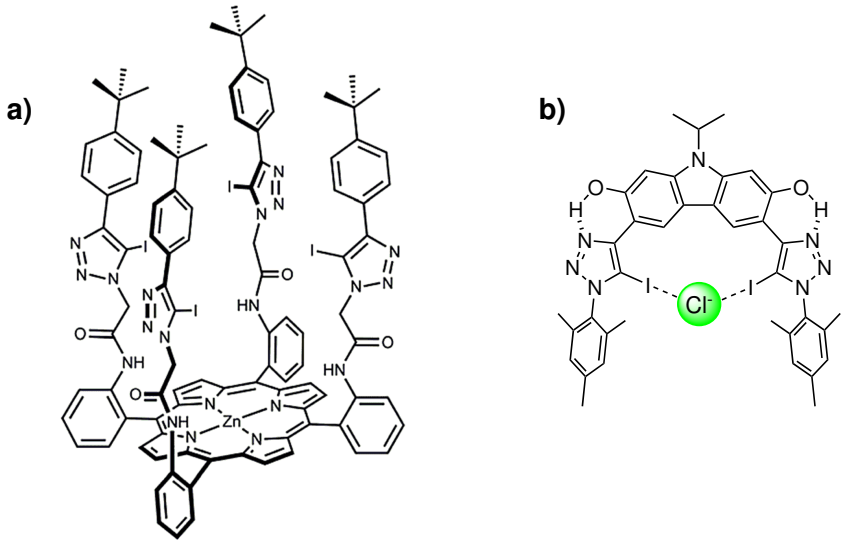

Figure 1.27: Early halotriazole receptors.

The magnitude of the σ-hole of an iodotriazole conjugated to a species such as pyridine can be increased by up to a factor of two *via* N-methylation to the corresponding cationic pyridinium. This was used to great effect by Beer and co-workers, yielding association constants an order of magnitude greater than the HB analogue (Figure 1.28).[65]

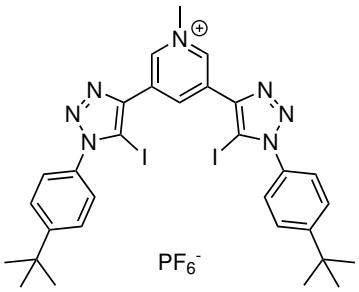

Figure 1.28: A charge-assisted iodotriazole pyridinium receptor.

Observed as early as 1993 in the solid state,[157] the solution state anion binding properties of haloimidazolium XB donors were not investigated until 2010,[158] precipitating the publishing of a series of papers by a number of groups. A bis-iodoimidazolium acyclic receptor (Figure 1.29a) reported by Huber and co-workers in 2011 was demonstrated to bind halides strongly in acetonitrile ($>10^5$ M^{-1}), compared to $<$100 M^{-1} for the prototriazolium analogue.[159,160] Resnati and co-workers described a simple mono-functionalized iodoimidazolium receptor in 2012, which was selective for $H_2PO_4^-$ (K_a = 1100 M^{-1}) over the halides (K_a $<$200 M^{-1}) in DMSO (Figure 1.29b).[161] These motifs have proven capable of strong binding even in highly competitive aqueous solvent mixtures, with haloimidazoliophane macrocycles reported by Beer and co-workers binding bromide and iodide selectively in 9:1 methanol:water, a competitive aqueous mixture, with K_a $>10^5$ M^{-1} (Figure 1.29c).[162]

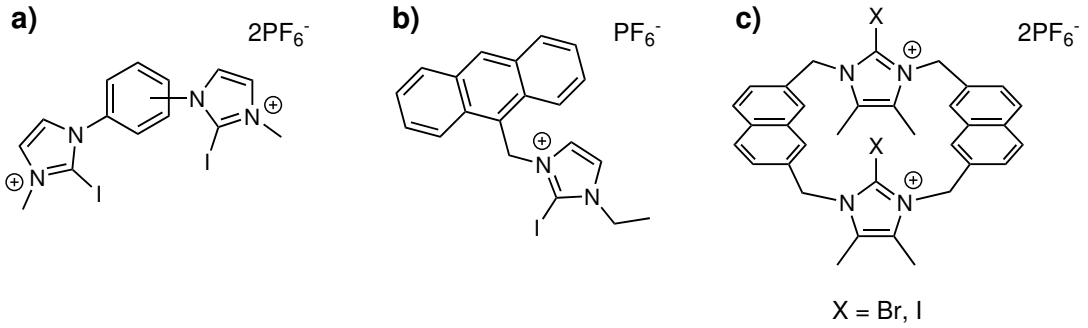

Figure 1.29: Examples of haloimidazolium receptors.

One of the limiting factors behind haloimidazolium incorporation and utilization in anion hosts is the intolerance of the motif to subsequent synthetic processes, resulting in decomposition and loss of anion binding capacity. The more stable, and even more highly polarized, iodotriazolium species can be efficiently accessed through direct halotriazole N-methylation, using methylating agents such as trimethyloxonium tetrafluoroborate[147] and methyl triflate.[163] Many groups have made use of this charge-assisted σ-hole, with a tendency towards strong

oxoanion binding evident in examples such as the series of bromo- and iodotriazolium receptors reported by Schubert and co-workers (Figure 1.30a),[164] and the 1,1'-bi-2-napthol (BINOL) bis-iodotriazolium receptors reported by Molina and co-workers (Figure 1.30b).[165]

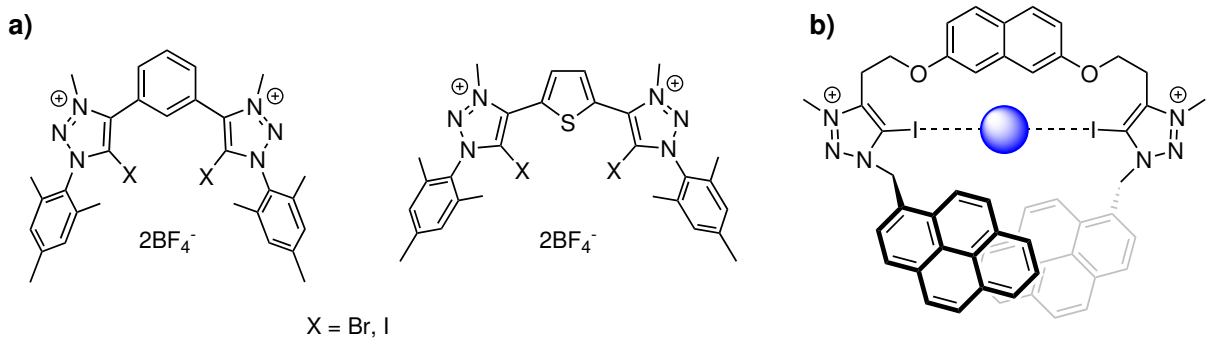

Figure 1.30: (a) Bidentate bromo- and iodotriazolium anion receptors,[164] (b) BINOL-based dicationic hosts for oxoanions.[165]

1.3.3 Anion Sensing

Anion sensor design typically entails the incorporation of signalling or reporter groups into the host structure in close proximity to, or as part of the binding site, such that the presence of a bound anion induces a measurable change in a macroscopic property of the host molecule. This may be electrochemical, *i.e.* a change in redox potential, conductivity, impedance, or optical, *i.e.* a change in colour or fluorescent/luminescent intensity.

Electrochemical anion sensing was first demonstrated by ferrocene- and cobaltocenium-containing host systems, where a cathodic shift of the respective redox couple resulting from anion binding stabilising the ferrocenium or cobaltocenium oxidised state.[166] An early cobaltocenium macrocycle (Figure 1.31a) reported in 1995 by Beer *et al*[167] was shown electrochemically to be selective for chloride in acetonitrile (ΔE = 35 mV), while a later ferrocenyl urea-based acyclic receptor reported by Tucker and co-workers in 2008[168] acts as an enantioselective voltammetric anion sensor for chiral carboxylate anions, demonstrating almost a two-fold preference for the (S)-enantiomer of N-benzenesulphonyl proline. The organic redox-active motif tetrathiafulvalene (TTF) has also been used as an electrochemical reporting group. It was incorporated into a receptor based on a calix[4]pyrrole by Nielsen *et al* in 2003 which proved F^--selective,[169] and more recently into a dual-signaling optically and electrochemically active receptor by Bejger *et al* in 2010, which displayed $H_2PO_4^-$ selectivity (Figure 1.31b).[170]

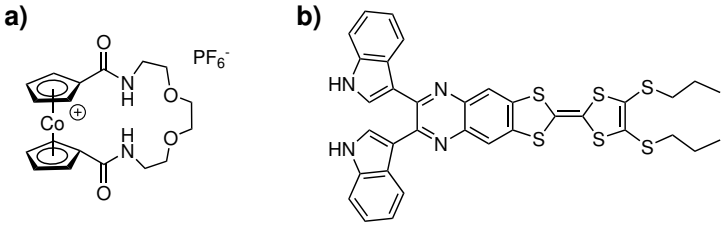

Figure 1.31: Electrochemical anion sensor examples: (a) a cobaltocenium macrocycle,[167] (b) a bis-indole-tetrathiofulvalene receptor.[170]

Redox anion sensing on surfaces, achieved by adsorption of appropriate anion receptors as ordered self-assembled monolayers (SAMs) on surfaces such as silicon, gold or metal oxide, offers the advantages of reuse, solvent-indifference and greater anion sensitivity. The first use of a ferrocene surface-confined anion sensor was reported in 1999 by Alonso *et al* and proved selective for $H_2PO_4^-$ in CH_2Cl_2 (Figure 1.32).[171] A later ferrocene urea disulfide acyclic example, reported by Beer and co-workers in 2010, displayed enhanced affinities for all anions tested compared to solution state when attached to gold electrodes.[172] Recent developments include electrochemical impedance spectroscopy sensing, where accumulation of anions on a suitably functionalised surface repels charged redox probes, leading to altered resistance to charge-transfer of the monolayer. This method has particular power in that it does not require redox-active groups to be incorporated into the receptor comprising the SAM, allowing the possibility of any existing receptor to be surface mounted for sensing in this manner.[173] A recent example by Minami *et al* was shown to be sensitive to biologically relevant basic anions such as F^-, AcO^- and $H_2PO_4^-$.[174]

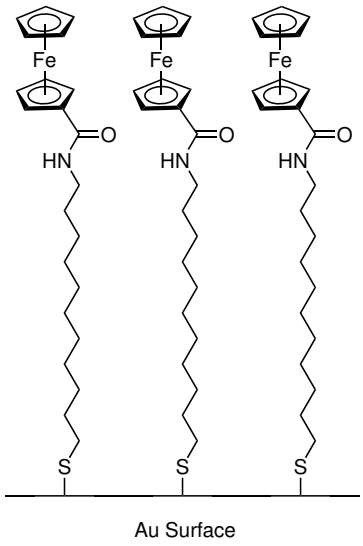

Figure 1.32: An early example of electrochemical sensing on surfaces using a simple ferrocene-based acyclic receptor.[171]

Optical anion sensors are usually fluorescent or colorimetric, and can also roughly be split between metal-based and organic-based sensing groups. Colorimetric sensing has obvious appeal in that it can present a response discernible by the naked eye. Sessler and co-workers reported anthraquinone-appended calix[4]pyrroles in 2000, which give anion-specific colour changes in DCM, with F^- inducing red to blue, Cl^- red to purple, and $H_2PO_4^-$ red to dark purple (Figure 1.33a).[175] Organic fluorophores can also be incorporated as part of the core scaffold of the sensor: a macrocycle reported by Kim and co-workers in 2011, comprised of two anthracene units linked at each end by imidazolium (Figure 1.33b), exhibits selective fluorescence quenching in the presence of $H_2PO_4^-$, K_a = 1.5 x 10^5 M^{-1} in 10:1 CH_3CN:DMSO.[176] Aldridge and co-workers reported a ferrocene-indenyl receptor in 2015[177] which underwent a color change from green to pink in the presence of F^- in THF, while a bis Eu^{III} sensor reported by Plush *et al* in 2007[178] only exhibited luminescent enhancement in the presence of malonate in water. A more recent lanthanide-based sensing system published by Smith *et al* in 2012 relied on a mixture of Eu^{III} and Tb^{III} complexes of the receptor to permit ratiometric quantification of bicarbonate levels in mitochondria (Figure 1.33c).[179]

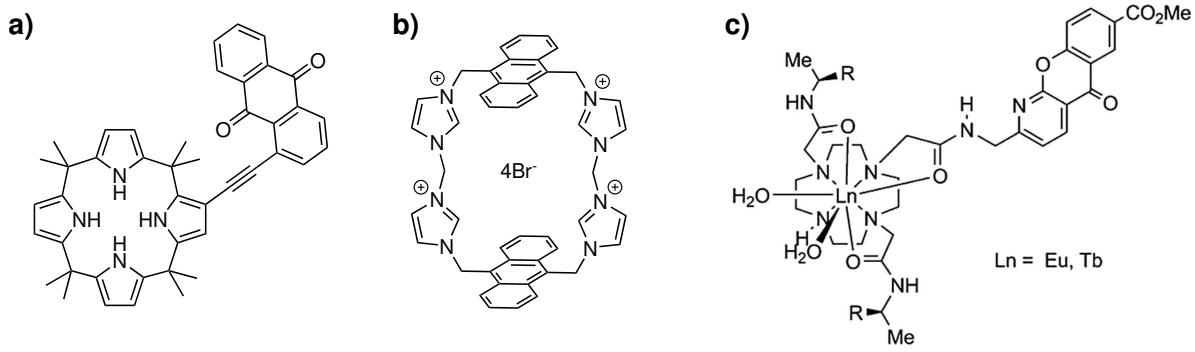

Figure 1.33: (a) an anthraquinone-appended calix[4]pyrrole,[175] (b) an anthracene-imidazolium based macrocycle,[176] and (c) a ratiometric sensor based on lanthanide binding sites.[179]

1.3.4 Applications of Anion Recognition

In addition to anion sensing applications, anion recognition has been exploited in abiotic systems for purposes as diverse as extraction, chiral recognition, organocatalysis (with asymmetric catalysis being a particular focus) and responsive materials such as gels and liquid crystals.

Extraction

Extraction research has mainly focused on two areas: removal of environmental contaminants such as fertilizer run-off anions nitrate or phosphate, and radioactive nuclear waste byproduct pertechnetate, as well as the reclamation of precious metals, generally via halo-metallates such as $[PtCl_6]^{2-}$ or $[AuBr_4]^-$. Examples include a tren-thiourea receptor reported by Warr *et al* as capable of almost quantitative extraction of $[PtCl_6]^{2-}$ from an aqueous 0.6M HCl solution into chloroform,[180] and a similar tren-urea receptor by Rajbanshi *et al* in 2011 capable of selective crystallization with sulfate in the presence of competing anions and highly basic conditions (Figure 1.34b).[181]

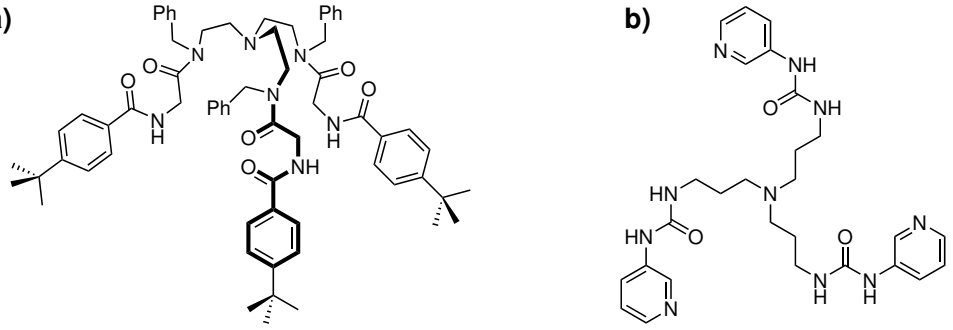

Figure 1.34: (a) a tripodal receptor capable of near quantitative platinum extraction,[180] (b) a sulfate extractant.[181]

Chiral Recognition

Chiral recognition and asymmetric catalysis both depend on the ability of the receptor to bind one enantiomer of a guest over another. The former is particularly crucial for biological processes, where different enantiomers can produce contrasting biochemical responses, with research driven by biological anions such as lactate (metabolism) and glutamate (signal transduction)[182] as well as medicinal compounds such as ibuprofen which are chiral anions at physiological pH. Amino acids and sugars form an important pool of chirality, core to many abiotic chiral anion receptors, but axially chiral motifs such as BINOL are also readily employed.[183–185] These chiral anion receptors can also be functionalized with redox-active or photo-active reporter groups, as in Willener's ferrocenyl urea-based acyclic mentioned previously.[168] The need for more architectural complexity in order to facilitate chiral discrimination was highlighted by work reported by Ulatowski *et al*, who only achieved a selectivity of 1.2 ± 0.1 for (R)-mandelate on screening a library of acyclic chiral receptors.[186]

Catalysis

As anions feature heavily among the ranks of reagents, intermediates or counterions, judicious application of anion binding affords the opportunity to control reaction outcomes and alter rates. The former is demonstrated by chiral 1,2,3-triazoliums reported by Ohmatsu *et al* in 2011, which confer up to 97% e/e in the asymmetric alkylation of oxindoles (Figure 1.35a).[187] A later bis-2-iodobenzimidazolium-based molecule reported by Huber and co-workers in 2017 yielded a 50-fold acceleration in the reaction of 1-chloroisochroman with a silyl enol ether (Figure 1.35b).[188] The authors suggest that the strong chloride binding of this molecule K_a = 3.5 x 10^6 M^{-1} assists in halide abstraction.

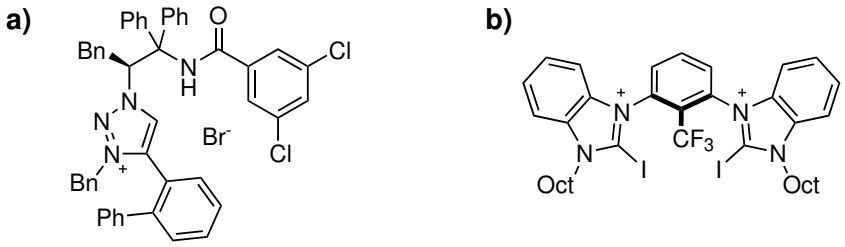

Figure 1.35: Anion receptor organocatalyst examples.[187,188]

Gels

Gels are a colloidal state of matter, comprising a multicomponent fibrous solid-like phase, about 1% by weight, which immobilizes a much larger solvent volume. Anion responsive supramolecular gels enable the detection of the presence or absence of an anion through bulk viscosity changes, running the gamut between a self-supporting structure and a solution of the gelator with the viscosity of its solvent. An important example of a gel that is broken down by the presence of anion was reported by Steed and co-workers in 2010, wherein a bisurea gelator used as a scaffold for pharmaceutical crystal growth was broken down by the addition of acetate (Figure 1.36a). This enabled crystal collection, facilitating macromolecular crystallography.[189] A more recent supramolecular gelator, reported by Lin *et al* in 2016, possesses competing binding interactions that yield an array of different fluorescent responses allowing identification of a range of anionic and cationic guests in water.[190] While anion-mediated XB gelators are rare, Liu *et al* reported a dendritic organogelator (Figure 1.36b) in 2016 that forms a gel *via* aromatic stacking of iodoperfluoroaryl groups, which is disrupted on the addition of chloride, resulting in a gel–sol transition.[191]

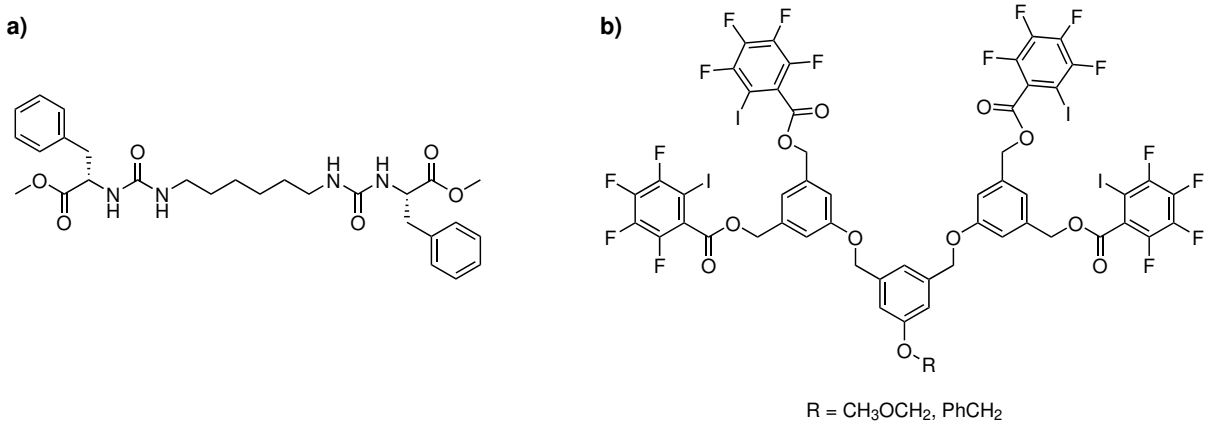

Figure 1.36: (a) a bisurea gelator that breaks down in the presence of acetate,[189] (b) a chloride-disrupted iodoperfluoroaryl gelator.[191]

Active Transport

With the ultimate objective of combating diseases resulting from anion misregulation, such as cystic fibrosis, relatively simple lipophilic anion receptors have been designed to alter anion transport across cellular membranes.[192] Artificial transport can occur across bilayer membranes *via* discrete molecules (anionophores) which bind to and convey the anion across the membrane, or by means of membrane spanning anion channels which result in a continuous path for anion movement. A tripodal fluorinated thiourea host (Figure 1.37a) reported by Gale and co-workers in 2011 provides a relatively early example of the first mechanism, and has shown promising anticancer activity, inducing apoptosis in lung, colon and tongue cancer cells by lowering cell pH through transport of HCl across cell membranes.[126] A triazole-based anionophore reported by Shang *et al* in 2014 uses intramolecular hydrogen bonding of amide groups to aid preorganization and resultant chloride transport,[193] while an even more recent system reported by Hernando *et al* in 2018 approaches the transport efficiency of cystic fibrosis transmembrane regulator (CFTR) protein (Figure 1.37b).[194] Reported examples of synthetic anion channels have harnessed self-assembly of macrocycles into porous channels as well as covalently-linked oligomeric assemblies of repeated anion binding motifs. A recent example of the former was published by Wei *et al* in 2016, forming a transmembrane pore *via* stacking of approx. 10 oligoamide macrocycles to yield a nanotube $\sim$34 Å long (Figure 1.37c).[195] They showed that the chloride transport activity of this pore could be tuned by altering the internal functionality of the macrocycles. A transmembrane halogen bonding cascade was reported by Matile and co-workers in 2013, wherein an octameric rail comprised of repeating iodoperfluoroaryl monomers transports chloride by a hopping mechanism (Figure 1.37d).[196]

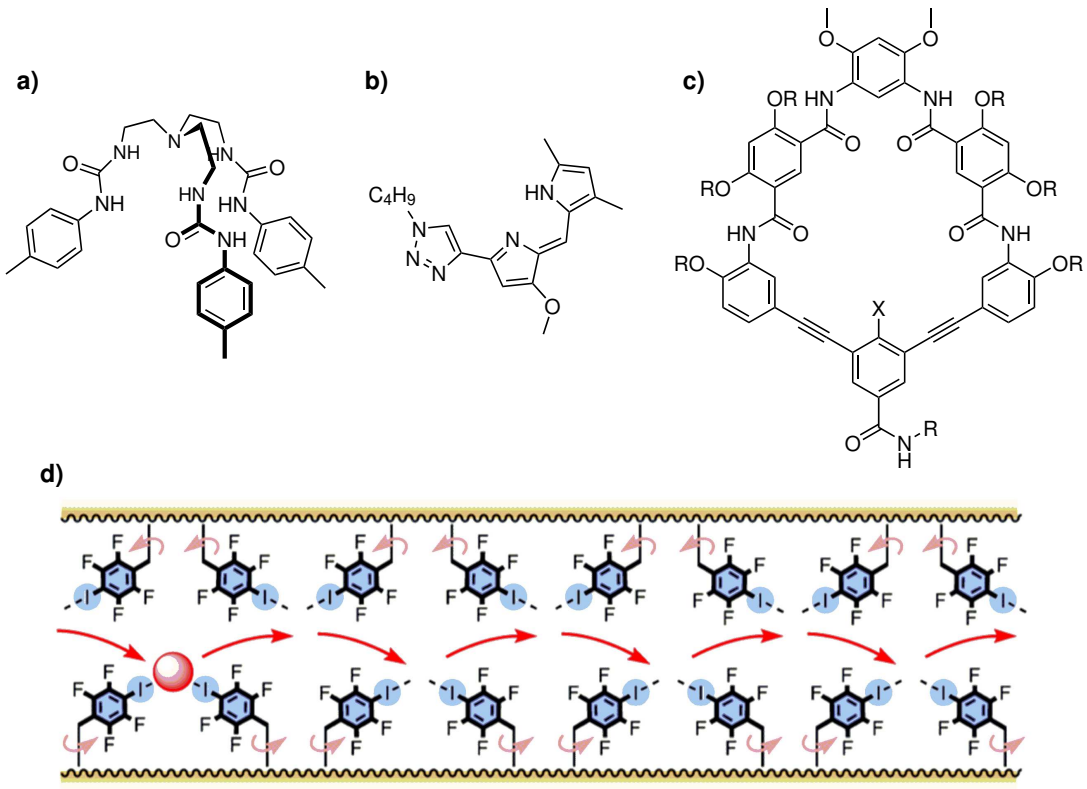

Figure 1.37: (a) a tripodal thiourea chloride host,[126] (b) a triazole-based chloride host,[194] (c) a macrocyclic unit from a chloride channel-forming nanotube,[195] and (d) an oligomeric anion cascade, figure reproduced from reference.[196]

1.4 Mechanically Interlocked Molecules

A relatively recent class of molecules, attractive for their potential nanotechnological applications as molecular sensors, or machines such as switches and motors, mechanically interlocked molecules (MIMs) afford opportunities for the creation of highly tunable systems through a variety of principally well-understood synthetic steps. Understanding the factors affecting, and applicability of a recently demonstrated synthetic route to MIMs, for use as potential anion sensors, is the focus of this thesis. The unique topological nature of the three dimensional cavity of MIMs affords the dual benefits of solvent exclusion and increased number of supramolecular binding interactions. These two factors are a potent combination in driving the selectivity and strength of binding interactions, illustrated in nature by biological anion receptors (Figure 1.14). Mechanical bonds are potent beyond altering binding affinity however, being able to convey kinetic stability, and alter reactivity of functionalities, through the shielding afforded by the more encapsulating nature of the scaffold.[197] These properties are exploited in drug delivery,[198] and are being investigated for catalytic applications.[199] Consequently, chemists have sought

more, higher yielding synthetic routes to these topologically elaborate interlocked motifs. The following section will discuss strategies used to access MIMs, focusing on template directed synthesis, in particular the relatively recent field of active metal template synthesis.

1.5 The Mechanical Bond

The term 'mechanical bond' was coined by Frisch in 1953,[200] existing where two or more molecular components are interlocked, such that their separation requires cleavage of a covalent bond. The diminished degrees of freedom afforded by the mechanical bond serve to enhance non-covalent interactions.[201] Termed the *catenand effect*, it is observed in metal complexes, which show enhanced stability when ligated by MIMs.[202] The first example of a MIM was reported by Wasserman in 1960, a [2]catenane, being comprised of two interlocked rings (Figure 1.38a),[203] with a yield too low to isolate, followed by the first [2]rotaxane synthesis by Harrison in 1967 with 6% isolated yield, comprising a macrocycle and a threaded chain with stoppers to prevent separation (Figure 1.38b).[204] While other more complex topologies such as Trefoil knots (Figure 1.38c) or higher order rotaxanes and catenanes exist, these first two represent the preponderance of interlocked molecules reported. Naturally observed examples of MIMs include enzymes such as DNA polymerase, which adopts a rotaxane structure,[205] and intermediates during DNA replication and recombination, which form catenanes.[206,207]

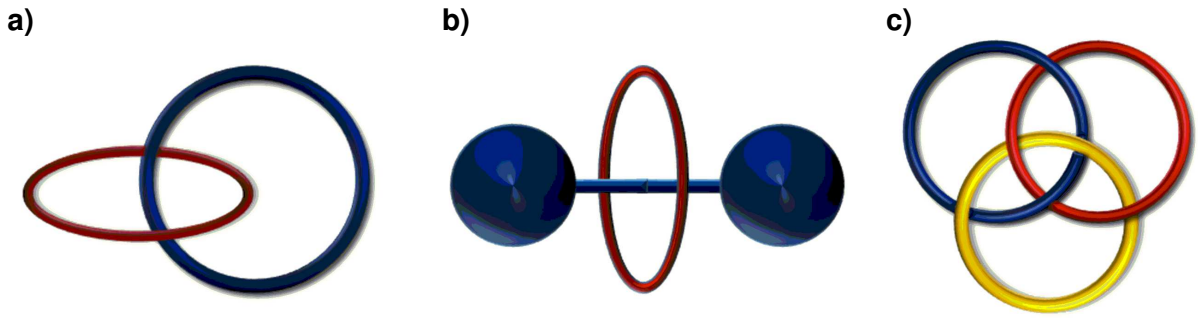

Figure 1.38: MIM archetype schematics: (a) Catenane, (b) Rotaxane, (c) Trefoil knot.

1.6 Synthesis of Mechanically Interlocked Molecules

Early examples of MIM synthesis depended on statistical outcomes to afford interlocked products, suffering low yields as a result ($<$10%).[203] Template-directed MIM synthesis has since become the norm. A chemical template *organizes an assembly of atoms, with respect to one or more geometric loci, in order to achieve a particular linking of atoms*.[208] This template can arise from mutual interactions from components in a system or be a separate chemical species, such as an additional guest.[209] Templation can operate under thermodynamic control, where an equilibrium between the components drives product formation, or kinetic control, where the desired transition state(s) are stabilized, facilitating irreversible product formation.[210]

There are many avenues by which templation can be exploited for the synthesis of MIMs, with more routes existing for rotaxane than catenane synthesis. Common methods for accessing rotaxanes include *stoppering*, the covalent addition of bulky stopper groups to a pseudorotaxane to prevent macrocycle dethreading,[211,212] *clipping*, where a macrocycle precursor undergoes a ring-closing reaction around a stoppered axle component,[213] and *snapping*, where two half-axle precursor components are joined through the macrocycle cavity.[214,215] More exotic, and significantly rarer, methods of rotaxane formation also exist, such as relying on elevated temperature to slide a macrocycle over a stopper group,[216] decreasing ring size[217] or increasing stopper size once a pseudorotaxane assembly has formed.[218,219] Catenanes have been accessed by two main routes, either a ring-closing *clipping* reaction of a macrocycle precursor passing through a preformed macrocycle,[220,221] or double cyclisations of orthogonal macrocycle precursors, being held together by a template, around each other.[222] An additional route to both rotaxanes and catenanes is the *magic rod* or *magic ring* ruthenium-catalyzed olefin metathesis.[223] These routes are shown schematically in Figure 1.39.

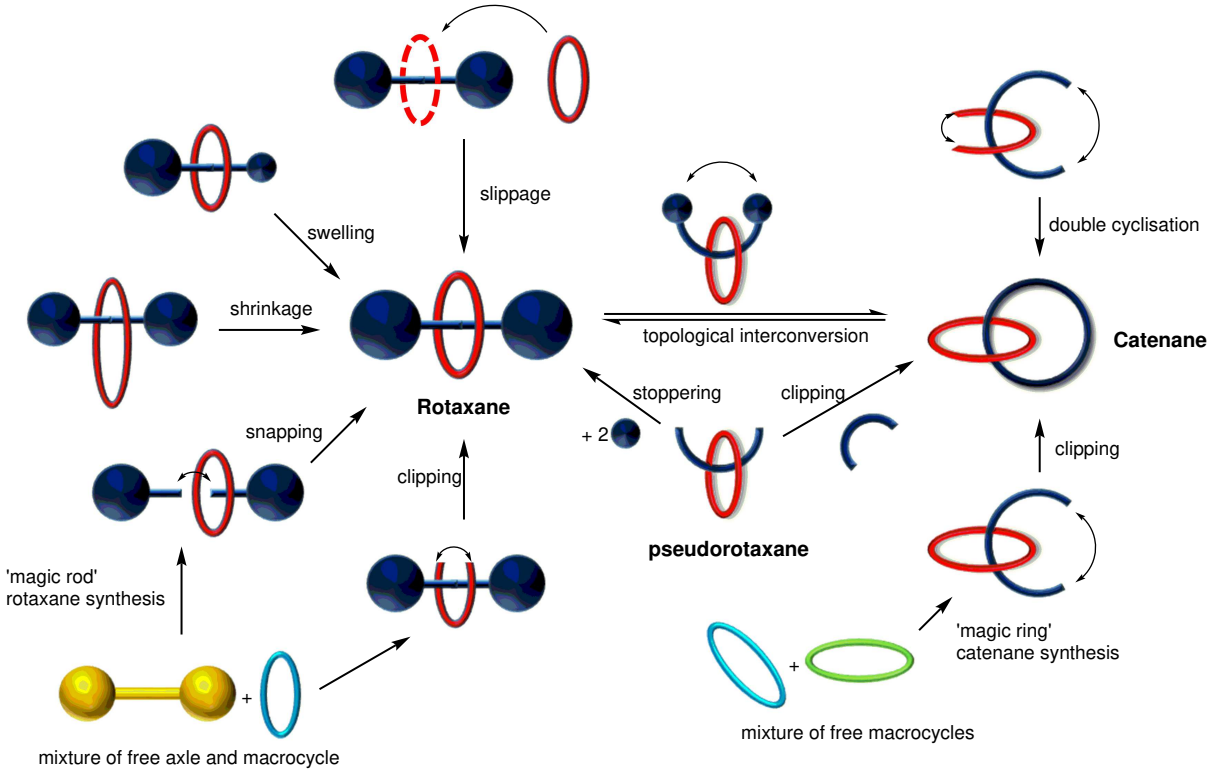

Figure 1.39: Schematic illustration of synthetic routes to rotaxanes and catenanes.

1.6.1 Cation Template Synthesis

Passive Metal Templation

The field of MIMs was revolutionized by the seminal report of a [2]catenane synthesized using a Cu^{I} template by Sauvage *et al* in 1983.[220] Exploiting the preferred tetrahedral coordination state of Cu^{I}, a phenanthroline ligand was threaded through a macrocycle incorporating the same motif, resulting in both ligands being coordinated to the copper orthogonally. A subsequent *clipping* reaction using the Williamson ether synthesis to close the ring, followed by decomplexation with KCN resulted in free catenane (Figure 1.40). This templation process is termed *passive metal templation*, as the metal cation is not a part of the MIM-forming reaction, only serving to organize the components.

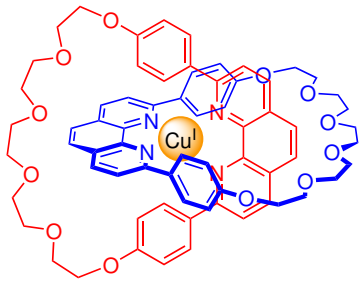

Figure 1.40: The first example of catenane formation through passive metal templation.[220]

Since this pioneering example, various metal cations of differing stereochemical and geometric preferences have been exploited for metal template synthesis, facilitating access to higher order structures. Geometries and metals successfully used include linear (Au^{I}),[224] square planar (Pd^{II}),[225] trigonal bipyramidal (Cu^{II}, Zn^{II})[226] and octahedral (Cd^{II}, Ru^{II}, Ni^{II}, Co^{II}, Fe^{II}).[227] Some structural examples of particular note are shown in Figure 1.41, including a Fe^{II} templated, triply interpenetrated 'Star of David' [2]catenane reported by Leigh *et al* in 2014,[228] a trefoil knot formed *via* the self-assembly of a heteroleptic triangular framework reported by Wood *et al* in 2015,[229] and a daisy chain polyrotaxane family reported by Chang *et al* in 2017, the formation of which is Zn^{II} directed.[230]

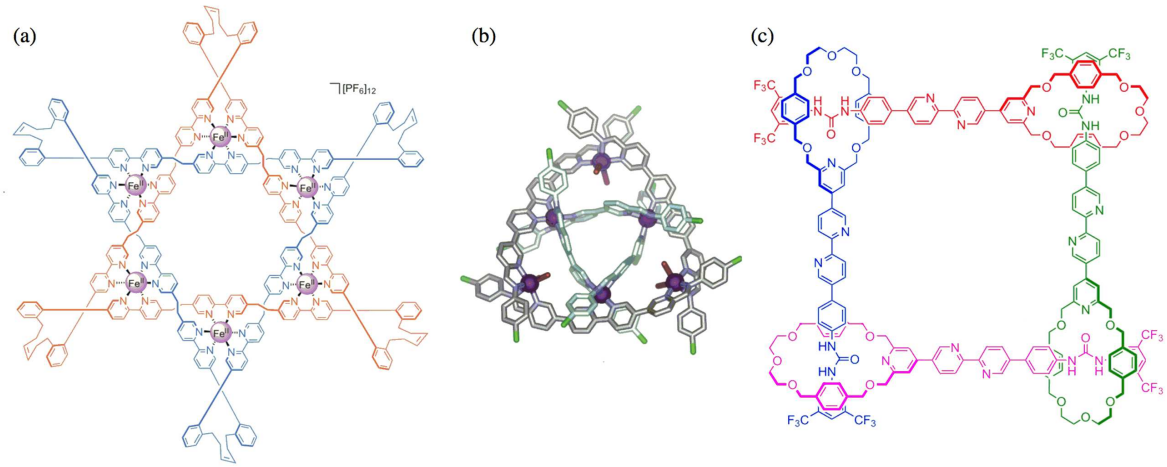

Figure 1.41: Example architectures achieved through passive metal templation: (a) a Star of David [2]catenane,[228] (b) a trefoil knot,[229] and (c) a cyclically penetrated oligorotaxane (4-mer shown).[230] Figures reproduced from references.

Further examples of the potency of passive metal template synthesis in MIM construction may be found using alkali metals (Li^{+}, Na^{+}, K^{+})[231] alkali earth metals (Ca^{2+}, Ba^{2+})[232] and lanthanides.[233] These metals possess less well defined coordination geometries than the transition metals, and typically require the incorporation of motifs with which they can undergo

hard acid-hard base interactions, such as crown ethers, or the 2,6-diamidopyridyl motif used by Ayme *et al* in 2014 in the formation of an Eu^{II}-templated trefoil knot.[234]

Organic Cation Templation

Cationic organic molecules also provide an abundance of motifs suitable for MIM templation. Motifs exploited for this purpose are principally highly electron deficient polypyridinium motifs such as 4,4'-bipyridinium viologen, or secondary ammoniums. The former are used in conjunction with electron-rich motifs, associating strongly through aromatic donor-acceptor, $C-H\cdots\pi$ and HB interactions, while the latter are typically used in combination with crown ether macrocycles.[211,235] Viologen-containing axles have been used with macrocycles such as benzo-crown ethers,[236] calixarenes[237] and pillarenes[238] among others, while bis-viologen containing macrocycles have been exploited by the Stoddart group in catenane synthesis, including self-assembly of a [2]catenane in acidic aqueous media (Figure 1.42a).[239] Another polypyridinium example, reported by Li *et al* in 2015, was comprised of interlocked cages where the association is strengthened by the hydrophobic effect (Figure 1.42b).[240] Cationic organic motifs have also been used in the construction of even more elaborate MIM architectures such as suitanes, a term coined by Stoddart for a cage like structure consisting of a number of linked macrocycles through which an arm from a centrally linked core protrudes. The first example, an ammonium templated suit[2]ane, was reported in 2006 (Figure 1.42c).[241]

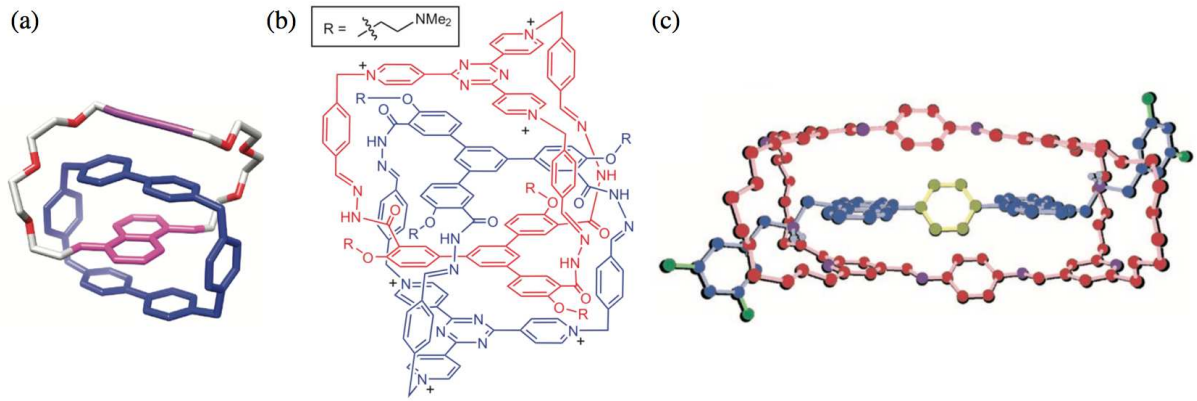

Figure 1.42: Organic cation templated MIMs: (a) crystal structure of a bis-viologen-based [2]catenane,[239] (b) hexa-pyridinium templated interlocked cages,[240] and (c) the first example of a 'suitane' templated by secondary ammoniums.[241] Figures reproduced from references.

Active Metal Templation

Transition metals have more potential in MIM synthesis than just simple templates, as they can also simultaneously catalyse covalent bond formation. Compared to the passive metal template approach, MIM syntheses harnessing this active metal template (AMT) property are in their early stages. The first [2]rotaxane synthesized this way was reported by Leigh and co-workers in 2006.[242] A Cu^{I} species bound endotopically within the macrocycle cavity catalysed the formation of an axle, from azide- and alkyne-functionalized half thread components, via a copper-catalysed azide-alkyne cycloaddition (CuAAC) *snapping* reaction to form a [2]rotaxane.

This first example set out the general form of AMT rotaxane synthesis, shown schematically below in Figure 1.43: first endotopic coordination of an 'active' metal species within a macrocycle, then subsequent introduction and coordination of appropriately functionalized half-axle components, metal-catalysed covalent bond formation and finally demetallation.[215] Unlike passive metal templation, precursor molecules do not need to incorporate permanent metal cation recognition sites, and catalytic, rather than stoichiometric, quantities of metal cations can be used. Active template CuAAC (AT-CuAAC) reactions will be discussed in detail in Chapter 2.

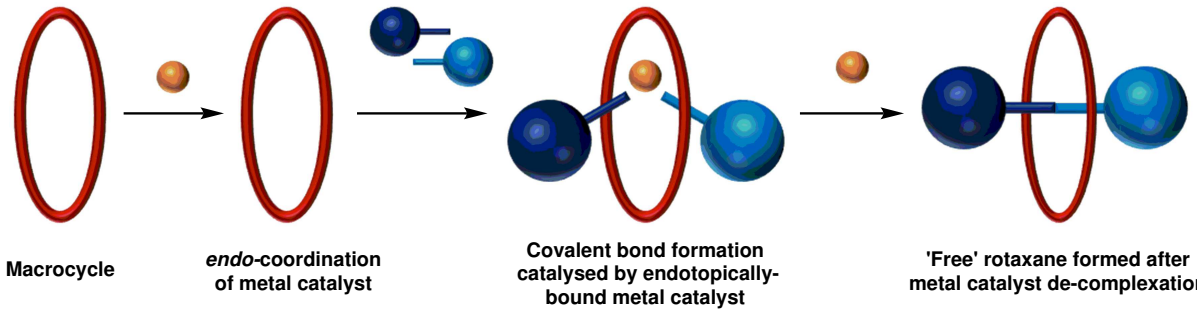

Figure 1.43: Schematic of the AMT strategy.

While these reactions are the most commonly employed, they are not the only ones available, with examples of Cu^{I}-mediated Glaser,[243] Ullmann[244] and Goldberg[245] reactions, Pd^{II}-mediated Michael addition,[246] Heck cross-coupling,[247] Pd^{II}-[248] and Ni^{II}-mediated[249] alkyne, Ni^{II} $C(sp^3)-C(sp^3)$ homocoupling[250] and Zn^{II}-mediated Diels-Alder reactions[251] being used to produce a diverse array of MIMs, in very high yields, notably including a quantitative example reported by Goldup and co-workers in 2011.[201] Higher-order MIM highlights include a dual active-passive copper(I)-templated trefoil knot reported by Leigh and co-workers in 2011 (Figure 1.44a),[252] a double-threaded polyyne [3]rotaxane reported by Anderson and co-workers in 2016 formed *via* a Cu^{I}-catalyzed Cadiot-Chodkiewicz cross-coupling (Figure 1.44b),[253]

and an oligo[n]rotaxane reported by Lewis *et al* in 2016, which used iterative Cu^{I}-templated CuAAC reactions that each proceeded with over 90% yield (Figure 1.44c).[254] The high potential yields of AMT routes to MIMs, catalytic dependence on the metals themselves, as well as decreased need for dedicated recognition sites make AMT a highly promising new route to functional interlocked structures.

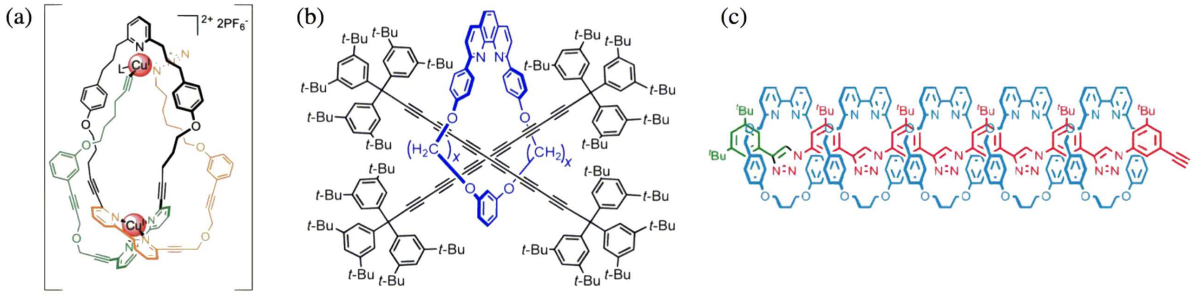

Figure 1.44: Higher-order AMT products: (a) The dual templated precursor to a trefoil knot,[252] (b) a polyyne [3]rotaxane,[253] and (c) an oligo[n]rotaxane from iterative AT-CuAAC reactions.[254] Figures reproduced from references.

1.6.2 Neutral Template Synthesis

Neutral templates were first reported in 1992 by Hunter and Vögtle *et al*.[255,256] They independently synthesized [2]catenanes which were templated through a combination of donor-acceptor interactions and HB between the isophthalamide groups of the macrocycle and macrocycle precursor. A later, self-templating example harnessing the same interactions was reported by Gatti *et al* in 2001, which relies on initial amide formation and resulting N–H···O HB interactions to template pseudorotaxane formation (Figure 1.45a).[257] A [2]catenane reported by Sanders and co-workers in 1997 exploits aromatic donor-acceptor interactions between naphthalendiimide and dihydroxynaphthalene moieties (Figure 1.45b),[258] with a later example also exploiting solvophobic interactions.[259] Solvophobic interactions can be the primary driving force behind self-assembly of MIMs, especially under aqueous conditions,[260,261] with examples of inclusion complexes between cyclodextrins and hydrophobic extended-π motifs such as anthracene derivatives (Figure 1.45c).[262]

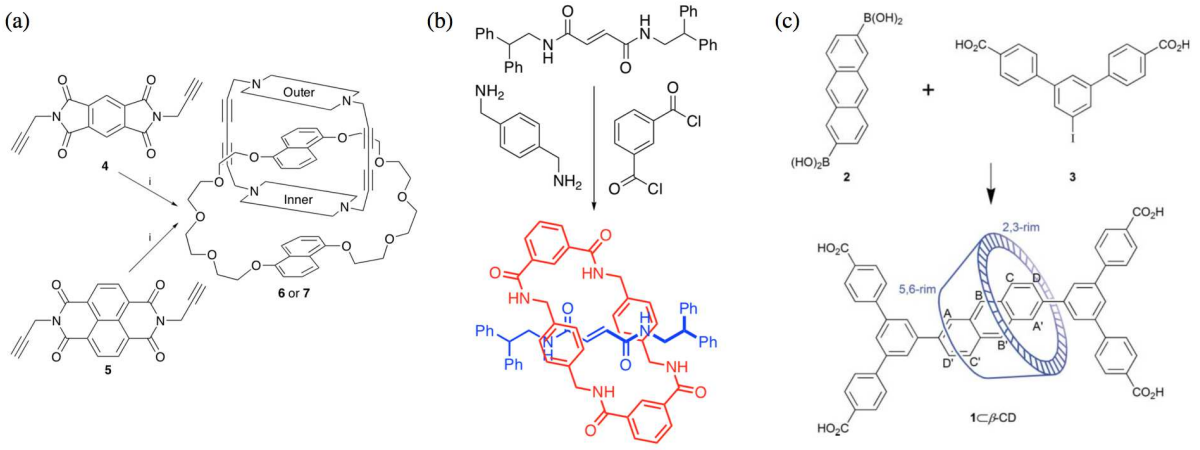

Figure 1.45: MIMs accessed by neutral template synthesis: (a) [2]rotaxane formation driven by HB self-templation,[257] (b) [2]catenane formed using donor–acceptor interactions,[258] and (c) solvophobically driven cyclodextrin [2]rotaxane.[262]

1.6.3 Anion Template Synthesis

The first example of an anion-based templation method for MIM construction was reported by Vögtle *et al* in 1999, using the *snapping* method, wherein a phenoxide half axle forms a 1:1 HB inclusion complex with a bis-amide macrocycle.[214] Subsequent reaction with a bromobenzyl stopper produced the neutral [2]rotaxane in very high yield (Figure 1.46a). Another mode of anion templation, reported in 2002 by Schalley and co-workers relied on the formation of a pseudorotaxane *via* interaction between the central phenolate functionality of a protected bis-amine axle precursor, and macrocycle isophthalamide HB donor groups. The [2]rotaxane product was completed through deprotection of the axle precursor amine functionality, and subsequent reaction with triphenylacetic acid chloride stoppers.[263] A more recent example of this method can be seen in the [3]rotaxane reported by Flood and co-workers in 2016, which makes use of the formation of 2:1 sandwich complexes of dialkyl phosphates with the 'cyanostar' macrocycle to form a pseudorotaxane (Figure 1.46b), which undergoes subsequent CuAAC-stoppering reactions, affording [3]rotaxanes in yields upto 80%.[264]

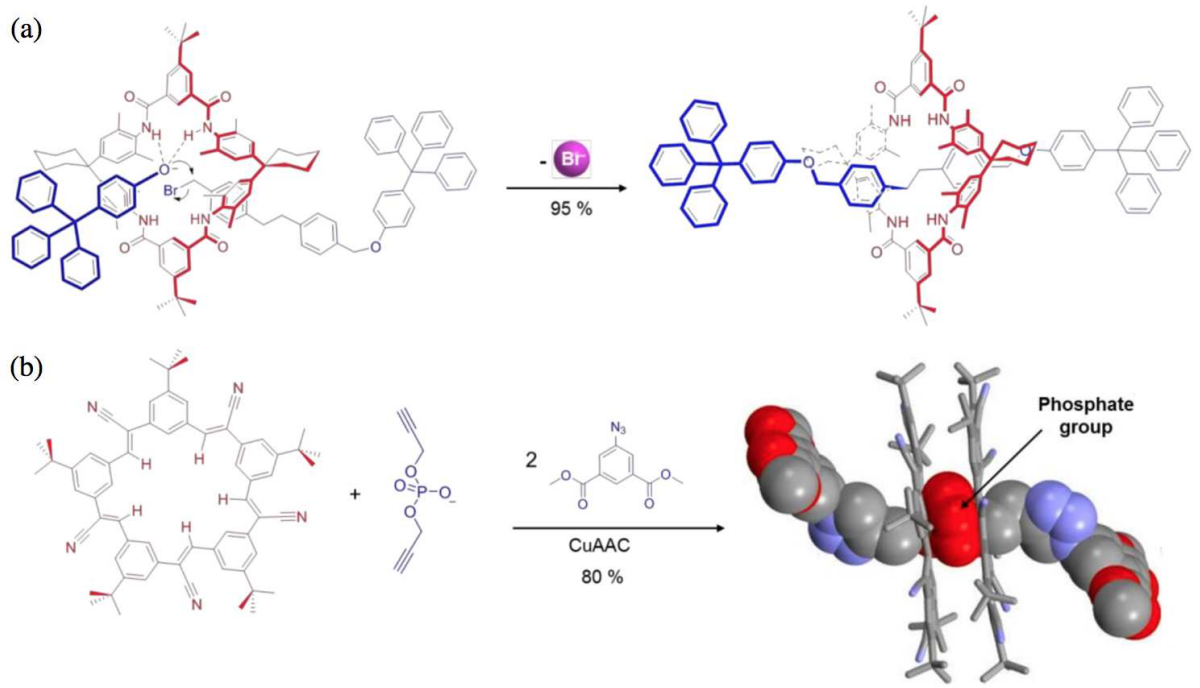

Figure 1.46: (a) First example of anion templated MIM formation,[214] (b) More recent work where an anion-templated pseudorotaxane is formed before stoppering.[264] Figures reproduced from references.

Discrete anion templates, where the anion coordinates to both components of the interpenetrated assembly are now more commonly used, and have facilitated access to a wide variety of more complex structures, including [3]rotaxanes,[265] handcuff catenanes[266] and a Janus [2]rotaxane.[267] Subsequent removal of the template affords an anion binding cavity far more potent than that of the acyclic analogue. This is clearly demonstrated in the first example of this manner of construction, reported by Beer and co-workers in 2002, wherein the rotaxane host structure that results after chloride anion template removal was demonstrated to bind chloride selectively over acetate and dihydrogen phosphate in a competitive organic-aqueous solvent mixture (Figure 1.47a).[117] Many template anions of different geometries, such as nitrite (bent),[268] nitrate (trigonal planar),[269] and anion binding motifs including pyridinium, imidazolium, and indolocarbazole have been reported as viable. Particularly of note is the value of the linear XB interaction in affording a further degree of preorganization, exemplified in bromide templated synthesis of a XB [2]catenane reported in 2012 (Figure 1.47b).[270]

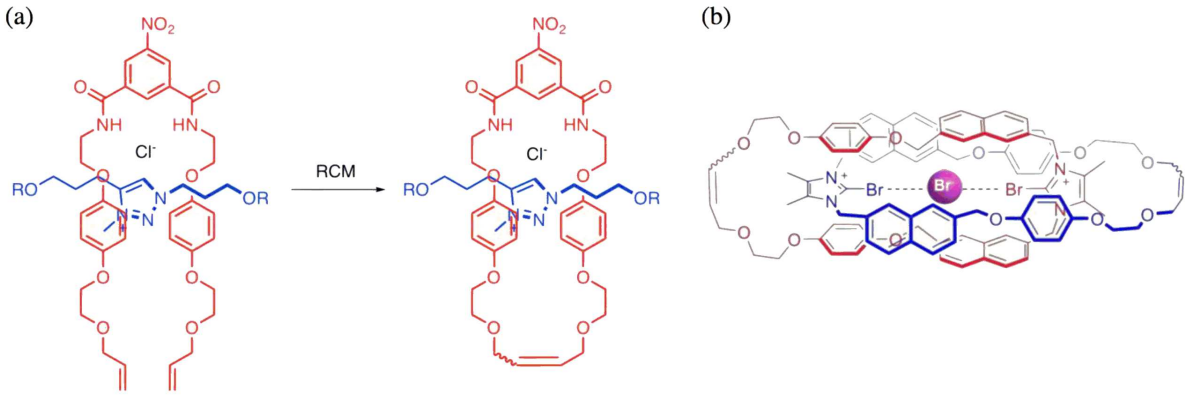

Figure 1.47: Examples of discrete anion MIM templation: (a) The first example of such, a chloride templated [2]rotaxane,[117] (b) a bromide templated [2]catenane.[270]

1.7 Applications of Mechanically Interlocked Molecules

The improvements in yield granted by advances in synthetic methods, especially through templating strategies, have enabled the exploration of a range of applications of MIMs in a variety of fields where the unique properties afforded by the mechanical bond can be capitalized upon. The unique ability of the molecular components to move independently of each other is a key strength in the application of MIMs,[271] enabling switchable responses for binding events in host-guest recognition and sensing,[272,273] multi-mode or condition dependent catalysis,[274,275] and stimulus-responsive properties for functional materials.[276–278] The following section is a brief overview of some of the most active and best developed areas.

1.7.1 Receptors and Sensors

The void space between interlocked components of MIMs can, especially when functionalized with appropriate moieties, ably serve as a highly preorganised cavity for three-dimensional encapsulation of charged guests.[279] Incorporation of Lewis basic groups enables rotaxanes and catenanes to act as alkali metal,[280,281] alkaline earth metal,[282,283] and transition metal cation hosts.[284] Conversely decoration with Lewis acidic groups results in an anion host instead. The discrete anion templation strategy is particularly potent when making a receptor of this nature, with many examples reported by Beer *et al* containing convergent electron-deficient HB and XB donor groups capable of selectivity for different halides[50,65,266,270,285–288] and oxoanions[265,269,289–291] in a range of media. Selectivity is altered by modifying the size of the cavity and the geometry of the binding moieties within. Recent work has extended these principles

to XB [2]rotaxanes capable of strong and selective iodide association in pure water (K_a >2000 M^{-1}), an order of magnitude higher than the axle alone.[292] A more complex [3]rotaxane example achieves nitrate selectivity in 1:1 $CHCl_3$:CD_3OD (K_a = 1782 M^{-1}) through a binding site composed of two nitroisophthalamide groups, one from each macrocycle, and two iodotriazoliums from the axle (Figure 1.48).[273]

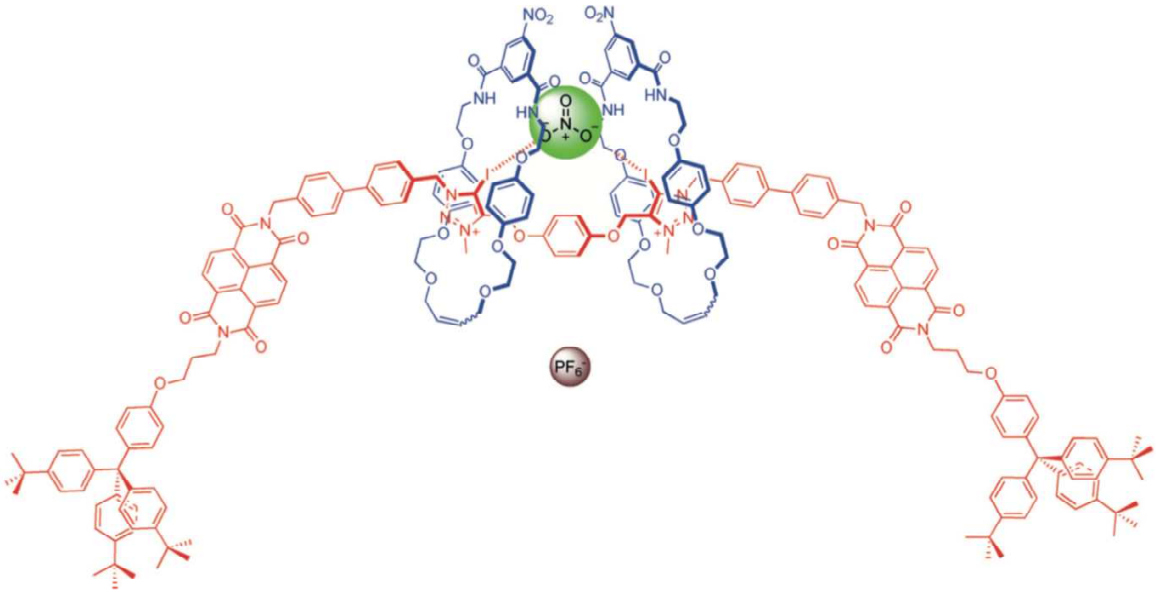

Figure 1.48: A NO_3^--selective [3]rotaxane.[273]

A crucial further step in applying systems of this type is the incorporation of a reporter group, to allow ready detection and quantification of binding events. An example of this is a neutral ferrocene-functionalized [2]rotaxane, reported by Beer and co-workers in 2014, which was capable of electrochemical sensing of halides through the ferrocene-ferrocenium redox couple in 1:1 CH_2Cl_2:CH_3CN (Figure 1.49a).[293] Electrochemical sensing can be augmented by attachment to an electrode surface, demonstrated by an osmium-containing [2]rotaxane assembled on a gold electrode reported in 2013 by Davis and co-workers (Figure 1.49b), which proved to be electrochemically and optically responsive for Cl^- over acetate and $H_2PO_4^-$ in CH_3CN.[294]

Optical responses are available in a variety of forms, being either switch-on or switch-off on a guest binding event, and responding by changes in wavelength or intensity of emission. A recent example of note is a Zn^{2+}-selective [2]rotaxane (Figure 1.49c) reported by Goldup and co-workers in 2018,[283] in which a heteroatom-substituted naphthalamide incorporated in the axle produces transition metal cation guest-dependent fluorescent responses from complete quenching upon binding of Zn^{2+} to weak amplification on exposure to Fe^{2+}. The list of optical groups used in interlocked sensors includes perylene/napththaline diimide,[295,296] squaraine,[297,298] anthracene[299,300] and acridine,[301] among others.

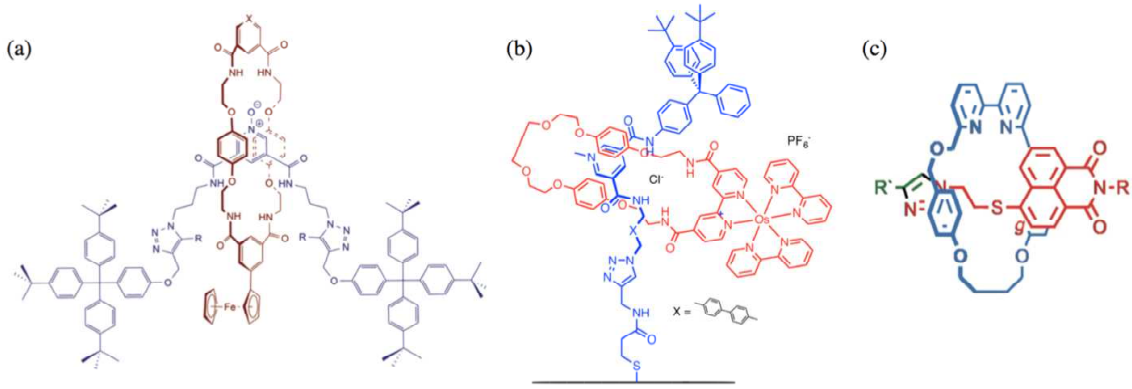

Figure 1.49: (a) A neutral, electrochemically active [2]rotaxane,[293] (b) surface assembled [2]rotaxane,[294] and (c) Zn^{2+}-selective [2]rotaxane.[283] Figures reproduced from references.

1.7.2 Switches and Machines

The potential for controlling the reversible relative motion of the axle and macrocycle components in MIMs via stimulus-driven conformational changes has propelled investigations into their potential for nanoscale switches and machines. These stimuli include pH changes, metal complexation, anion coordination, photoisomerism or redox activity.[271] Rotaxanes are capable of translational motion of the macrocyclic component along the axle, termed *shuttling*, or rotation of the macrocycle around it, termed *pirouetting*, while catenanes are capable of rotary motion in similar fashion, with each ring capable of rotating through the other. The Stoddart group reported the first example of a rotaxane molecular shuttle in 1991,[302] and since then many systems have been developed, including nanoscale elevators,[303] rotaxane-based molecular muscles, capable of mimicking muscle fiber contraction and relaxation by harnessing daisy-chained [2]rotaxane station shuttling *via* Zn^{II} metal cation coordination (Figure 1.50a),[230,278] surface-attached UV-light driven rotaxane systems which can move liquids against gravity,[276]

bi-stable switchable [2]catenanes[304,305] and unidirectional molecular rotors.[306,307] A subset of these works includes studies in varying the rate and sensitivity of these geometric transformations, with discoveries by the Leigh, Teixidor and Beer groups showing that simple changes to solvent,[308] counterion[309] or binding moiety[296] can result in large changes to system behaviour. Other particularly interesting applications include encryption, where the fluorescent emission of heterorotaxane complexes is highly dependent on complex equilibria between initial components, enabling unique chemical signatures,[310] and mechanochromic force transduction in polymers, where deformation of the bulk material causes displacement of the macrocycle and fluorescence switch-on (Figure 1.50b),[311].

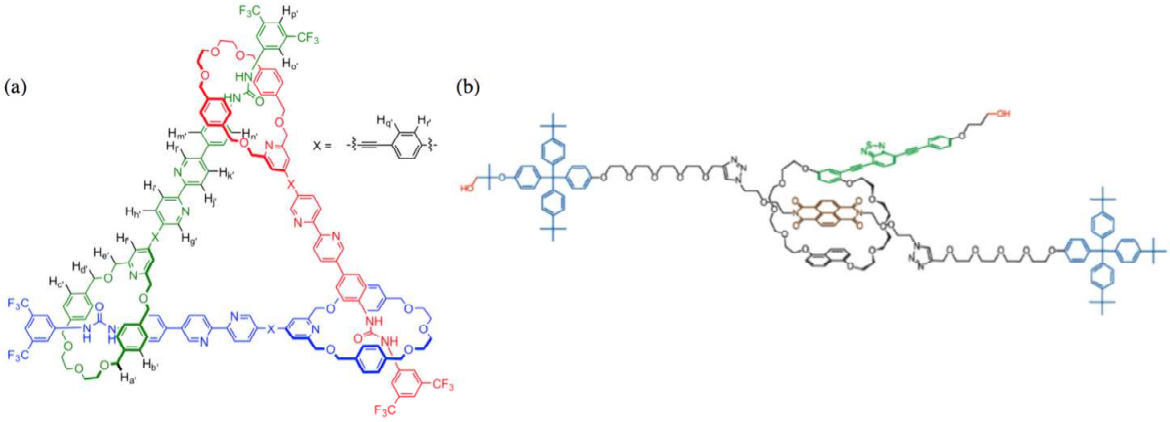

Figure 1.50: Examples of molecular machines: (a) A molecular muscle system capable of contracting in two dimensions,[230] (b) A [2]rotaxane incorporated as a mechanochromic force transducer by Sagara.[311] Figures reproduced from references.

1.7.3 Catalytic Applications

The degree of control afforded over the topology of MIMs, and the ease of incorporating a wide array of functionalities affords a lot of possibility in catalytic applications. Rotaxanes have been favoured due to their relatively greater ease of synthesis. The first examples of interlocked catalysts were [2]rotaxanes reported by Tachibana *et al* in 2004,[312] which demonstrated a modest 30% enatiomeric excess (ee) in asymmetric benzoin condensations, a result not replicated by the axle alone (Figure 1.51). This was achieved *via* close proximity of a chiral macrocycle to the catalytically active thiazolium group of the axle, demonstrating the possibility of through-space chiral information transfer in such systems.

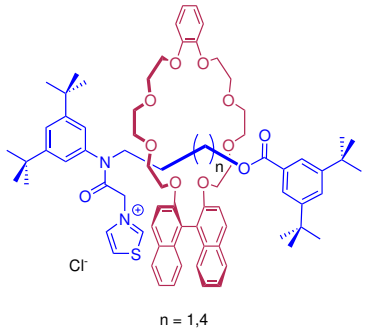

Figure 1.51: First example of an interlocked catalyst.[312]

This concept has since been extended to metal catalyzed reactions, with examples including conjugate addition,[245] and hydrogenation,[313] and to organocatalysts based on motifs such as chiral amines.[314] A recent example of particular note reported by Goldup and co-workers displays catalytic activity and stereoselectivity dictated by a Cu^{I} cofactor, which changes the active site conformation by binding within the rotaxane cavity.[315] Another notable form of catalytic MIM was first reported by Leigh and co-workers in 2012.[316] In this kind of catalyst, a stimulus responsive molecular shuttling event switches catalytic activity on or off. The initial example was a pH-switched crown ether macrocycle translocation between a triazolium station and a secondary amine on the axle component blocking iminium catalysis when the amine is protonated. This idea was extended in 2014, where the shuttling event instead alters chemoselectivity by exposing different catalytically active groups (Figure 1.52),[274] an idea that has since been demonstrated for a few other systems.[275,317]

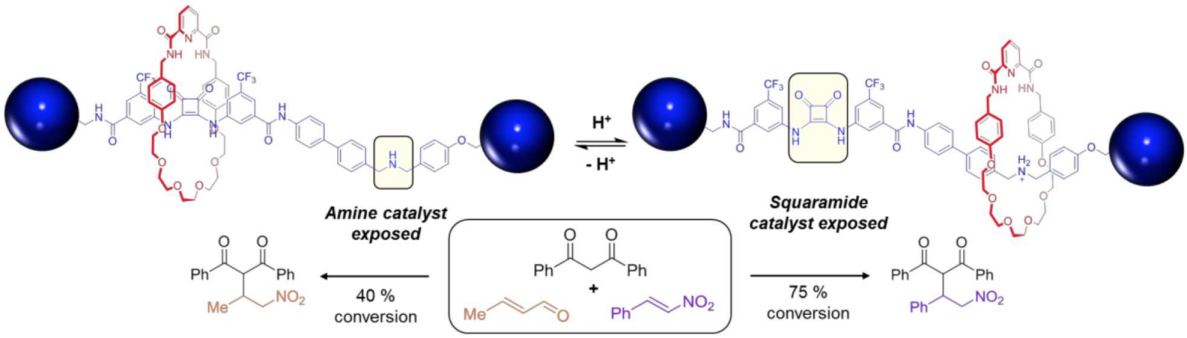

Figure 1.52: A pH-switchable [2]rotaxane catalyst from the Leigh group, figure reproduced from reference.[274]

1.8 Project Aims

Halogen bonding mechanically interlocked molecules designed for anion recognition are still rare, due to their challenging synthesis and the relative youth of the field. To date, anion templation has dominated synthetic routes, however recent successes have been reported exploiting the newly discovered AMT approach.[318,319] The theme of this thesis is to build upon these initial examples containing bis-iodotriazole macrocycle components systematically. Experimental and computational methods are used to investigate how parameters of halogen bonding macrocycle design, such as flexibility and size, impact the production of halogen bonding mechanically interlocked molecules.

Chapter 2 focuses on investigating the impact of macrocycle flexibility on AMT potency, through the synthesis of a series of novel macrocycles containing propyl and 1,2-hydroxymethyl benzene linked bis-iodotriazole motifs, detailing efforts to incorporate these novel macrocycles into [2]rotaxanes via AT-CuAAC reactions.

Chapter 3 seeks to build on these outcomes, using computational methods to investigate correlations between lowest energy conformations of various bis-iodotriazole macrocycles complexed with Cu^{I} cations, and AT-CuAAC rotaxane yield. The computational outcomes are discussed in light of their related experimental performance, and a few hypothetical systems are considered.

Chapter 4 investigates the effect of macrocycle size variation on AT-CuAAC rotaxane yield through the synthesis of a series of novel HB and XB macrocycles which are designed around a 1,3-bis(iodo)triazole benzene motif. Attempts to incorporate these macryccles into [2]rotaxanes are undertaken.

Chapter 2

Novel bis-triazole macrocylic motifs for AT-CuAAC synthesis of interlocked anion hosts

2.1 Introduction

With the aim of constructing novel XB based MIMs for anion recognition applications, this chapter focuses on the synthesis of a range of macrocycles with varying anion binding motifs, detailing efforts to exploit active metal template synthesis to incorporate them into rotaxane host structural frameworks. The triazole motif possesses a number of characteristics which highlight its Lewis-acidic HB and XB donor group potency for strong and directional anion binding: facile synthesis through the CuAAC reaction,[320–322] aromatic stability,[323] electron-deficient character,[324] possibility of 5-position functionalisation with a range of groups,[325] and further augmentation of its electron-deficient character by *N*-methylation or metal cation coordination at the 3-position nitrogen.[326]

2.1.1 AT-CuAAC Synthesis of Interlocked Structures

While many reactions available for AMT synthesis of MIMs were discussed earlier in Section 1.6.1, the CuAAC reaction is most prevalent.[327] The first protocol for rotaxane formation through an AT-CuAAC reaction was described in a seminal study published in 2006 by Leigh and coworkers,[242] in which they detail optimised reaction conditions to form the interlocked product using a macrocycle containing a 2,6-functionalised pyridine. Importantly, the authors determined that for the AT-CuAAC reaction to occur, a good ligating group such as a pyridyl nitrogen should be used, and incorporated into the macrocycle component such that it favours *endotopic* orientation, *i.e.* pointing into the macrocycle cavity, for Cu^{I} metal cation coordination. Their experimentation with denticity revealed that macrocycles should contain at most two coordination sites for the Cu^{I} species, with tridentate macrocycles failing to produce rotaxane products. They also observed that the macrocycle to Cu^{I} stoichiometry affected rotaxane yield, with sub-stoichiometric copper favouring rotaxane production over the free axle, albeit with longer completion times. These findings led to the proposal of the mechanism shown below (Figure 2.1) where a catalytic Cu^{I} species, coordinated endotopically, coordinates both azide and alkyne components through the macrocycle cavity, driving the formation of a Cu^{I}-triazolide species, which was subsequently characterised via X-ray crystallography.[328] Decomplexation afforded the free rotaxane, which was isolated in yields of up to 94%. Notably, the AT-CuAAC reaction was also found to be tolerant of Cu^{I} source, solvent choice (coordinating *e.g.* DME, NMP, THF, or non-coordinating *e.g.* toluene, DCM, $CHCl_3$) and elevated temperature.[329]

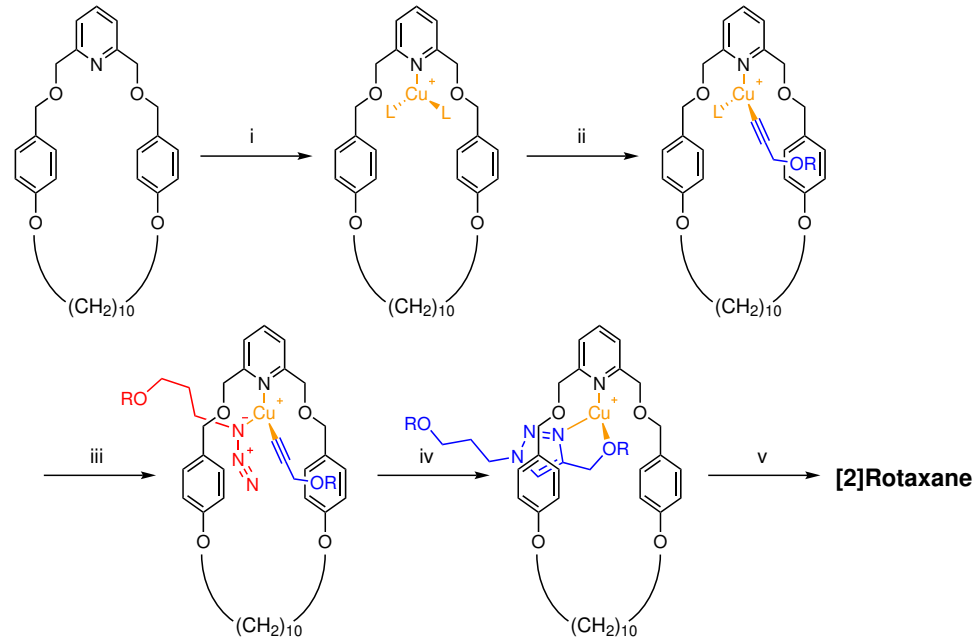

Figure 2.1: Initially proposed mechanism for AT-CuAAC rotaxanation: i) Ligation of CuI species by macrocycle, ii) coordination of alkyne half-thread, iii) coordination of azide half-thread, iv) CuAAC reaction, v) demetallation.

The AT-CuAAC reaction has also been used to afford higher-order MIMs, particularly poly-rotaxanes. This was first observed in a follow-up paper to the initial 2006 study by Leigh and coworkers, where they discovered that at high macrocycle:Cu^{I} stoichiometry ratios (10:1) a [3]rotaxane (Figure 2.2a) formed in yields of up to 33%.[215] Using bipyridine-based macrocycles, Goldup and coworkers observed [3]rotaxane products were favoured over [2]rotaxane analogues when using higher Cu^{I} loadings, larger macrocycle sizes and elevated temperatures, but suggested that the full set of determining factors is yet to be understood.[330] More recent work from the Goldup group has demonstrated size-driven kinetic self-sorting resulting in a heterocircuit [3]rotaxane composed of two different macrocycles,[329] as well as harnessing a related high-yielding (>90%) AT-CuAAC macrocyclic system iteratively to produce a [6]rotaxane (Figure 2.2b) in 67% overall yield,[254] and trigonal [4]rotaxane (Figure 2.2c).[331]

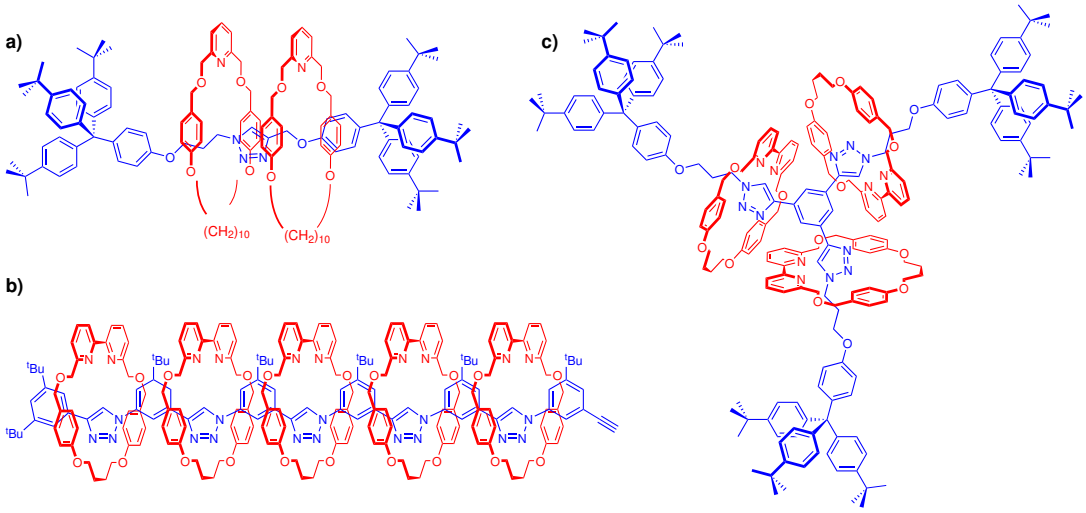

Figure 2.2: Examples of higher order MIMs formed through AT-CuAAC reactions: a) [3]rotaxane from the Leigh group, (b) an iteratively generated [6]rotaxane from the Goldup group, and (c) a trigonal [4]rotaxane from the same group.

The ability of triazoles to act as N-donor ligands for the coordination of metal cations such as Cu^{I} has been established in a number of solution-phase and solid-state studies.[332–334] Within the Beer group, initial investigations of the utility of AT-CuAAC rotaxanation for interlocked XB anion receptor synthesis have already proven it a promising avenue of research. The first system reported used a macrocycle containing a directly linked bis-iodotriazole motif, which afforded a 25% yield of the XB [2]rotaxane. Subsequent exotopic complexation with Re^{I} directed the XB donor iodine atoms into the macrocycle cavity. The resulting tridentate anion binding site of the rotaxane proved selective for chloride, binding it twice as strongly as the acyclic analogue, while acetate binding was significantly reduced (Scheme 2.1).[318]

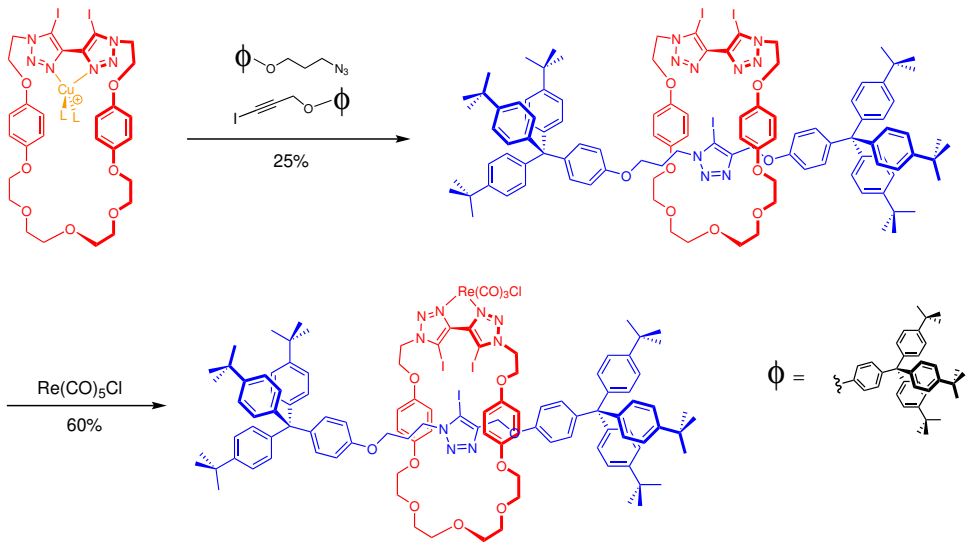

Scheme 2.1: The first example of an AT-CuAAC all-XB [2]rotaxane from the Beer group.

Macrocycles with integrated 1,3- and 1,2-bis(iodotriazole)benzene-based motifs were also demonstrated to be capable of AT-CuAAC rotaxanation, with yields of up to 41% demonstrated for the rotaxane examples shown below (Figure 2.3).[319] For these two systems, there was ^{1}H NMR evidence in the 1,3-bis(iodotriazole) case, and X-ray crystallographic evidence in the 1,2-bis(iodotriazole) case, for an inability of both 3-position triazole nitrogens to be involved in the Cu^{I} binding event. This was attributed to geometric and steric constraints respectively, as the two triazoles are far apart in the 1,3- system, and they are very close, with a narrow bite angle in the 1,2- system.

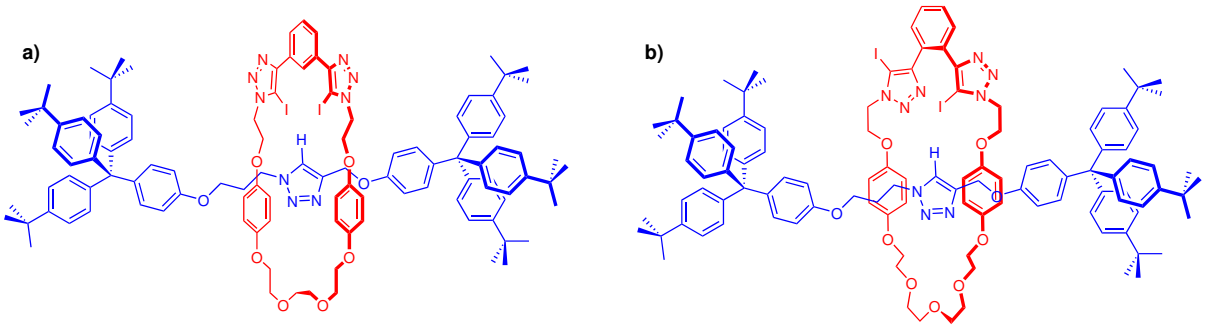

Figure 2.3: Further examples of early AT-CuAAC [2]rotaxanes from the Beer group: a) 1,3-bis(iodoethynyl)benzene-based, and b) 1,2-bis(iodoethynyl)benzene-based systems.

2.2 Chapter Aims

This chapter seeks to build on the prior work outlined above for the construction of interlocked XB anion hosts *via* the AT-CuAAC reaction. The macrocycle systems studied all incorporate a bis-triazole structural motif, where the spacer unit covalently linking the two triazole groups is varied to determine if macrocycle flexibility can be harnessed to enhance the outcome of the interlocking reaction, and if so, where the limit may lie. Towards this end, this chapter will introduce two novel macrocycle motifs, the first containing a propyl-linked bis-iodotriazole motif, and the second with the iodotriazole groups covalently linked *via* a 1,2-hydroxymethyl benzene group. Integration of these macrocycles into rotaxane structural frameworks through AT-CuAAC reactions is then investigated.

2.3 Propyl Bis-iodotriazole Macrocycle

2.3.1 Design and Synthesis of Hydrogen and Halogen Bonding Macrocycles

The initial macrocycle design chosen for synthesis and AT-CuAAC rotaxane formation was considered a direct analogue of the 1,3-bis(iodotriazole)benzene macrocycle component of the [2]rotaxane shown previously (Figure 2.3a), where the benzene ring is replaced with a propyl chain (Figure 2.4a). This system was chosen to investigate whether the flexible propyl spacer would facilitate endotopic Cu^{I} binding.

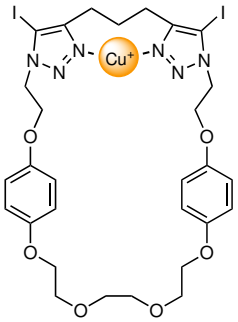

Figure 2.4: Propyl spaced bis-iodotriazole macrocycle structure in desired Cu^{I} binding conformation.

There are two readily accessed routes to making a bis-triazole macrocycle of this general form, hinging on whether the final ring closing step is a double CuAAC ring closing between a bis-azide and bis-alkyne (or iodoalkyne analogue) or a double Williamson ether synthesis involving the S_N2 nucleophilic substitution of a bis-tosylate polyether with a bis-phenoxide macrocycle precursor. For macrocycles **7** and **8** the ether synthesis route was attempted first, shown below (Scheme 2.2). This route was chosen as it had proved higher yielding than the CuAAC closing route for the previously reported systems (Figure 2.3).[319]

Initially an azide intermediate **2** was prepared from commercially available hydroquinone in two steps, first reacting with an excess of 1,2-dibromoethane under reflux conditions to obtain intermediate **1** using a modified literature procedure,[335] followed by a nucleophilic substitution reaction with sodium azide in DMSO. The bis-CuAAC reaction using an equimolar mixture of **2** and 1,6-heptadiyne, with catalytic quantities of $[Cu(CH_3CN)_4]PF_6$ and TBTA ligand,[336] afforded bis-triazole compound **4** in 80% yield.

The iodo-analogue **5** was produced by a 'two-pot iodo-click' route, requiring the synthesis of bis-iodoalkyne **3** from 1,6-heptadiyne, *via* Ag^{I}-catalysed iodination with *N*-iodosuccinimide,[337] then a subsequent bis-CuAAC reaction in the absence of light, which resulted in a 69% yield of compound **5**. S_N2 ring closing was then performed for both **4** and **5** using a 1:1 molar ratio of the bis-phenols **4** or **5** and triethylene glycol bis-tosylate **6** respectively in dry, degassed DMF with excess Cs_2CO_3 base, taking advantage of the 'caesium effect' to suppress oligomerisation in favour of macrocycle formation.[338] This cyclisation step resulted in both macrocycles being successfully formed, the proto-analogue **7** in 40% yield, and the iodo-analogue **8** in 32% yield.

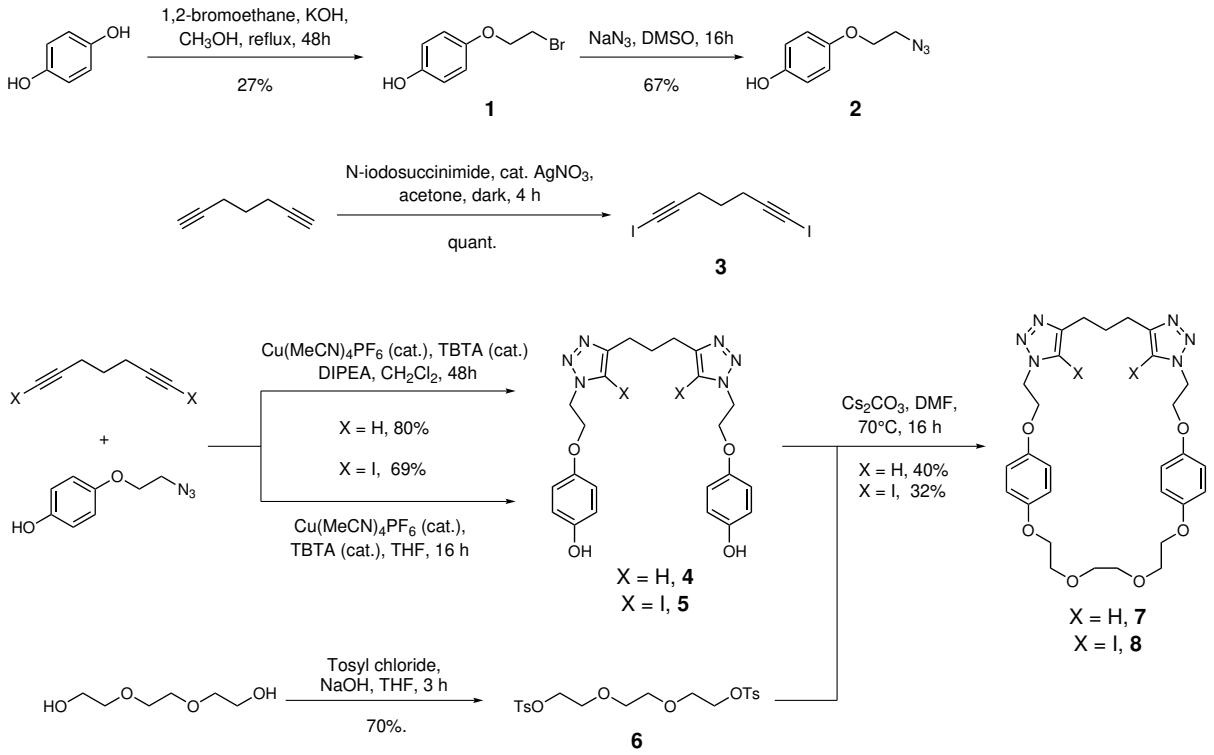

Scheme 2.2: Synthesis of macrocycles **7** and **8**

2.4 1,2-Hydroxymethyl Benzene Bis-iodotriazole Macrocycle

2.4.1 Design and Rationale

As the 1,3-bis(iodotriazole)benzene motif was understood to result in the triazoles being too far apart to bind Cu^{I} in a bidentate fashion,[319] a new binding motif based on 1,2-hydroxymethyl benzene bis(iodotriazole) substitution was targeted. This motif incorporated flexible methylene spacer units to overcome the steric Cu^{I} coordination restrictions of the previous 1,2-bis(iodotriazole)benzene macrocycle example (Figure 2.3b).

2.4.2 Synthesis of Hydrogen and Halogen Bonding Macrocycles

The reaction of catechol with 2.5 equivalents of propargyl bromide under basic conditions afforded bis-alkyne **9** in almost quantitative yield. Reaction with *N*-iodosuccinimide gave the corresponding bis-iodoalkyne **10** (Scheme 2.3).

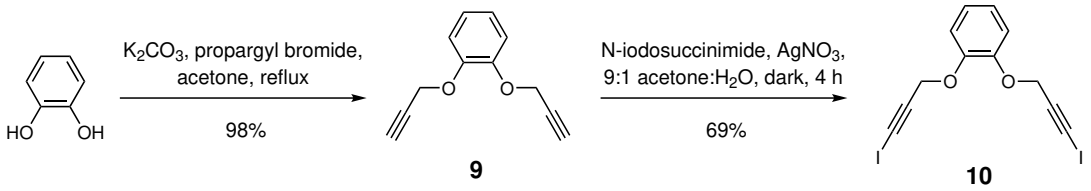

Scheme 2.3: Synthesis of bis-alkyne **9** and iodinated analogue **10**.

Initial synthesis of the target XB and HB macrocycles was carried out *via* CuAAC reaction between **9** or **10** and methoxymethyl acetal (MOM) protected phenol azide **11**,[319] followed after deprotection by ring closure *via* S_N2 reaction as previously described (Scheme 2.2). The proto-click CuAAC reaction to synthesize **12** proceeded in 63% yield. Increasing TBTA loading to 10 mol% significantly improved the yield of **12** to 79 %.[154] The one-pot iodo-click CuAAC synthesis of **13** resulted in a low yield of 31%, however the two-pot iodo-click methodology led to an increased yield of 76%. Quantitative removal of the MOM protecting group to afford precursors **14** and **15** was achieved using *in-situ* generated hydrochloric acid from the reaction of acetyl chloride and methanol solvent.

The S_N2 ring closing reactions between **14** or **15** and triethylene ditosylate, under basic conditions, produced their respective macrocyclic products in modest yields: 17% for **16** and 18% for **17** after isolation by column chromatography (Scheme 2.4).

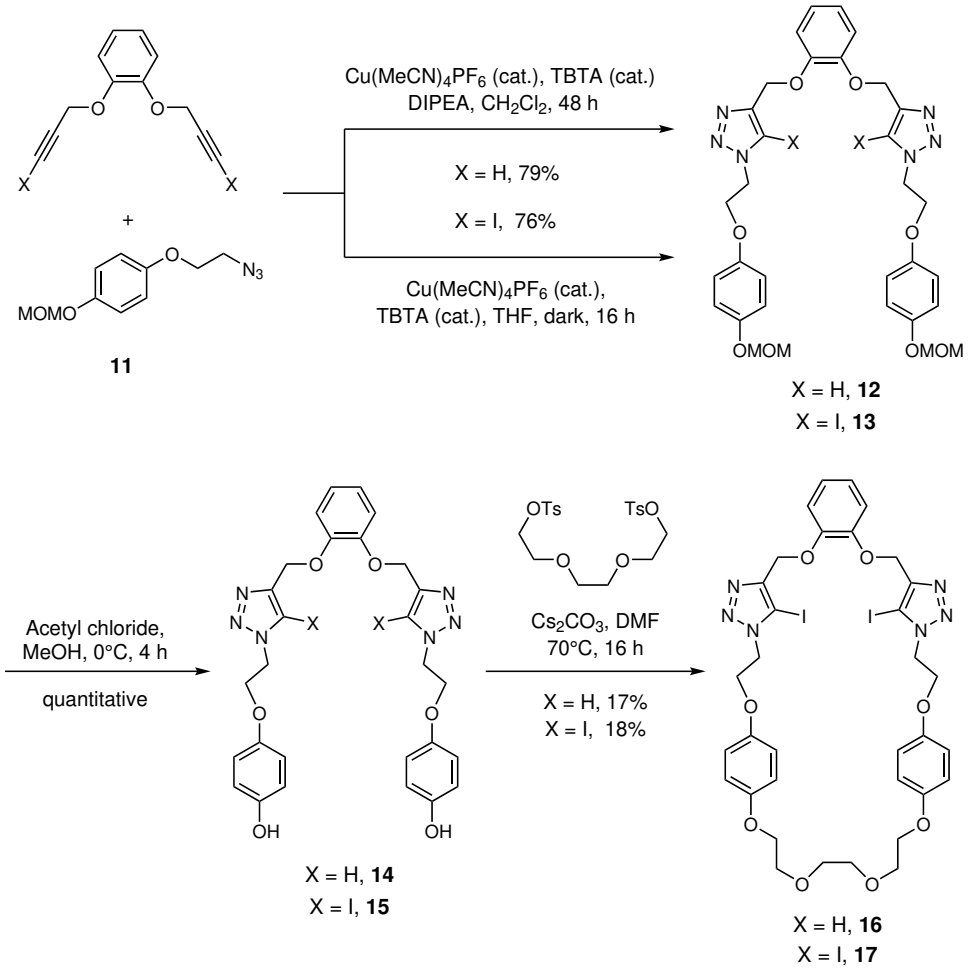

Scheme 2.4: First synthetic route towards novel macrocycles **16** and **17**, using a double Williamson ether reaction as the closing step.

In an effort to improve the cyclised product yields, an alternative synthetic route wherein ring closing was accomplished *via* a double CuAAC reaction between bis-azide and bis-(iodo)alkyne components was undertaken (Scheme 2.5). Bis-azide precursor **18** was isolated in 95% yield after a Williamson ether reaction between **2** and **6**. Subsequent CuAAC ring closing reactions between an equimolar mixture of **10** and **18** under high-dilution conditions (10 mM) with catalytic quantities of $[Cu(CH_3CN)_4]PF_6$ and 10 mol% of TBTA, afforded macrocycle **17** in an improved yield of 33%, proving superior to the bis-tosylate, phenolic ether forming route. Buoyed by this doubling of the yield, an identical reaction protocol was followed using protoalkyne **9**. Unfortunately, despite numerous attempts, isolation of macrocycle **16** was unsuccessful, as the TBTA contaminant could not be separated from the macrocycle *via* column chromatography.

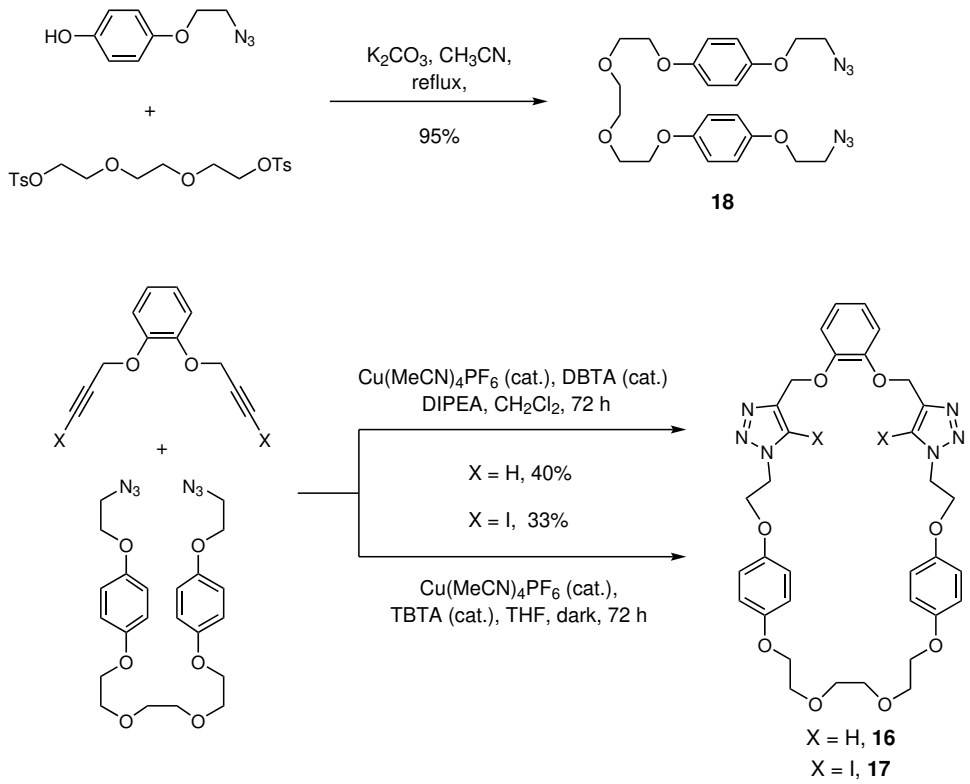

Scheme 2.5: Second synthetic route towards novel macrocycles **16** and **17**, employing a double CuAAC reaction in the closing step.

To overcome this purification issue, trial reactions where the rate accelerating TBTA ligand was replaced with DBTA and BTA (Figure 2.5) were carried out. Both resulted in straightforward purification by preparative TLC (prep-TLC). Isolated **16** was obtained in 40% yield for DBTA and 28 % yield for BTA. As a consequence DBTA was chosen as the ligand for use in scaled up production of macrocycle **16**.

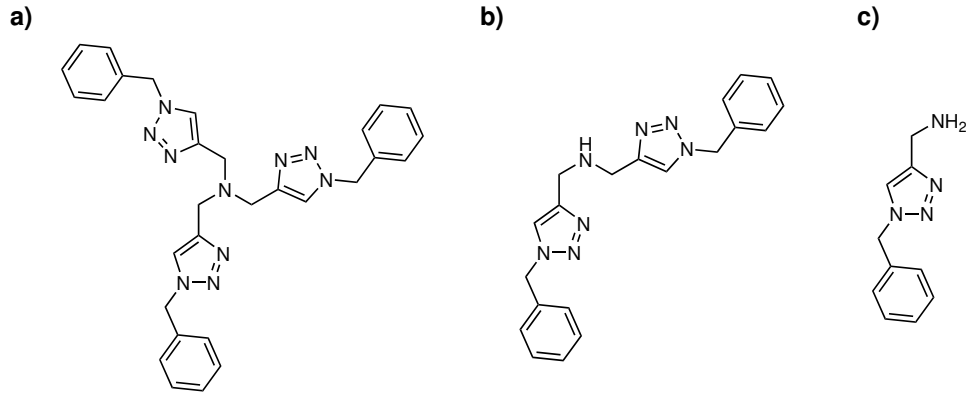

Figure 2.5: Structures of rate-accelerating ligands a) TBTA, b) DBTA, and c) BTA for comparison.

Subsequent to this successful isolation, characterisation of all macrocycles **7**, **8**, **16** and **17** was performed by ^{1}H NMR, ^{13}C NMR and high resolution ESI-MS. Assigned ^{1}H NMR spectra for all four macrocycles are shown below (Figure 2.6).

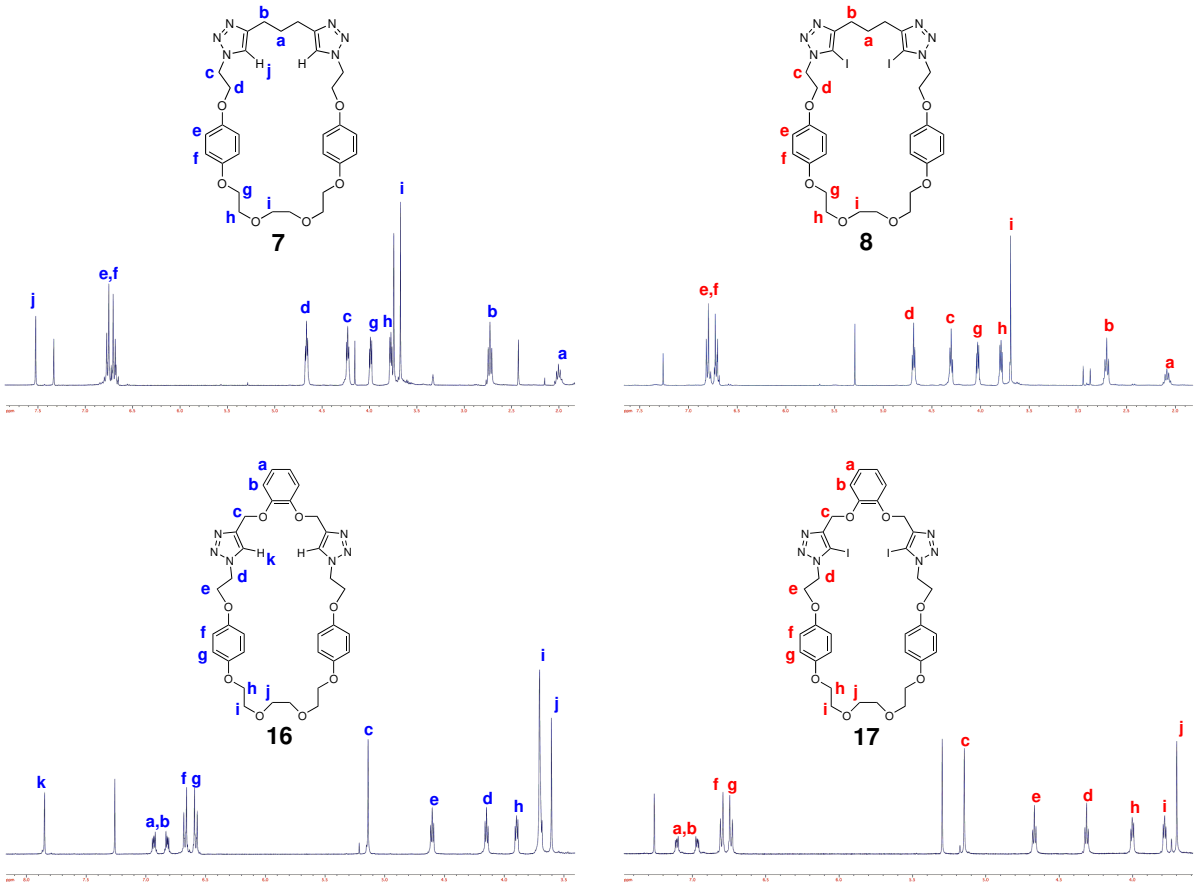

Figure 2.6: ^{1}H NMR spectra of HB and XB macrocycles incorporating novel bis-triazole motifs ($CDCl_3$, T = 298 K).

2.4.3 Attempted AT-CuAAC Rotaxane Formation with Propyl Spaced Bis-iodotriazole Macrocycle

The active metal template synthesis of a rotaxane was first explored with the XB macrocycle **8**, with the expectation that the iodine steric bulk would favour endotopic Cu^{I} binding. First, terphenyl-stoppered azide **19** and alkyne **20** were synthesized according to literature procedures.[242] Subsequently, an equimolar mixture of macrocycle **8** and $[Cu(CH_3CN)]_4PF_6$ was dissolved in thoroughly degassed CH_2Cl_2 before 5.0 equivalents of azide **19** and alkyne **20** were added (Scheme 2.6). After stirring under an atmosphere of N_2 for 72 hours, complete consumption of the axle precursors **19** and **20** was observed by thin layer chromatography (TLC) analysis, concomitant with the formation of a product. ESI-MS analysis of the crude reaction mixture revealed the product to be the free axle component with no evidence of target [2]rotaxane **21** formation.

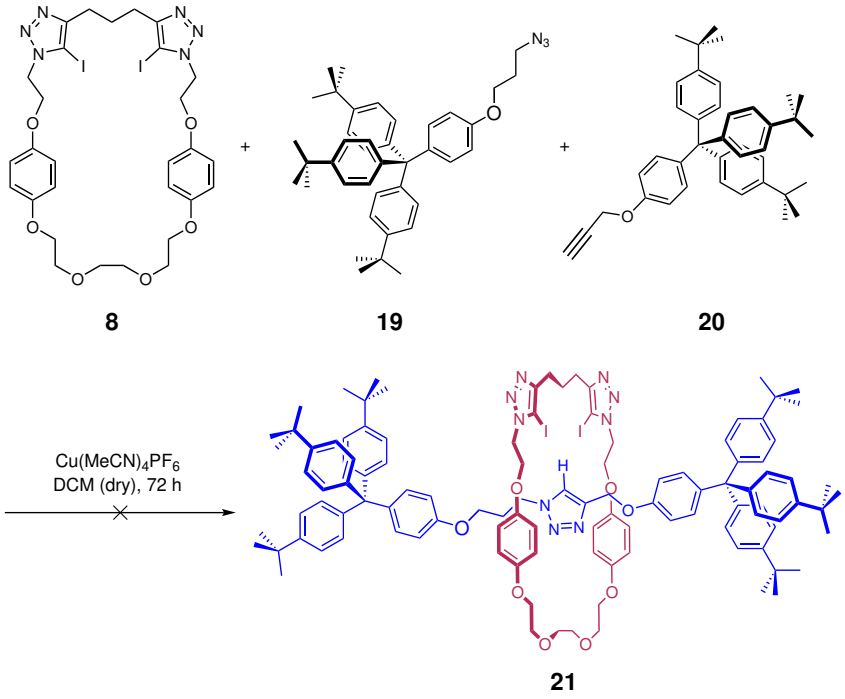

Scheme 2.6: Attempted AT-CuAAC synthesis of [2]rotaxane **21**.

Following the addition of a solution of ethylenediamine-tetraacetate (EDTA) in dilute aqueous ammonia to remove the copper catalyst, column chromatography confirmed the lack of an interlocked product and led to the isolation of the free axle, recovery of the macrocycle, and trace amounts of the axle precursors **19** and **20**. The reaction was subsequently repeated with substoichiometric Cu^{I} (0.9 equivalents), confirming the result. This disappointing outcome defied expectations of the macrocycle iodotriazole iodines being predominantly exotopic due

to their relative bulk, which would favour endotopic Cu^{I} coordination. The result may be rationalised by the flexibility of the propyl linker between the iodotriazole groups facilitating their free rotation, resulting in conformations where both bulky iodines and the complexed copper cation are facially oriented on opposite faces of the macrocycle, in an unproductive conformation for AT-CuAAC mechanical bond formation. This hypothesis is discussed further alongside the computational results shown in Chapter 3. In light of this outcome, AT-CuAAC testing of the HB analogue **7** was not undertaken: lacking even the steric bulk of the iodines to favour endotopic Cu^{I} coordination, an interlocked rotaxane is very unlikely to be produced.

2.4.4 Qualitative Cu^{I}-binding

After the disappointing result with macrocycle **8**, and prior to AT-CuAAC reactions with macrocycles **16** and **17**, a Cu^{I} complexation titration ^{1}H NMR experiment with macrocycle **16** was undertaken to determine the metal cation coordinated to the macrocycle's triazole motifs in a symmetric fashion as desired, and to probe whether an endotopic binding geometry was supported by the macrocycle ^{1}H shifts on complexation. The HB macrocycle was chosen in order to gain additional information about the binding from the triazole protons. Figure 2.7 compares the ^{1}H NMR spectrum of **16** with the spectrum obtained on addition of excess (three equivalents) $[Cu(CH_3CN)_4]PF_6$, in 1:1 $CDCl_3$:d_6-acetone. The HB macrocycle was chosen to gain additional information about the binding from the triazole protons. Significant downfield perturbations of the macrocycle protons suggested Cu^{I} complexation. Looking at the magnitude of the changes in chemical shifts, protons *c*, *d*, *e* and *f* display large downfield shift, with triazole proton *d* displaying the greatest perturbation. Comparing these changes with those for protons *a* and *b*, *g*-*k* suggests the Cu^{I} species is bound by the triazole nitrogens, as the magnitude of the downfield shifts diminishes as the protons are more distant from the triazole groups. No increase in complexity of the spectrum was observed, suggesting the presence of only one coordinated species in solution, most likely with the Cu^{I} cation complexed in a symmetric bidentate binding mode, but fast exchange between monodentate binding modes is also possible.

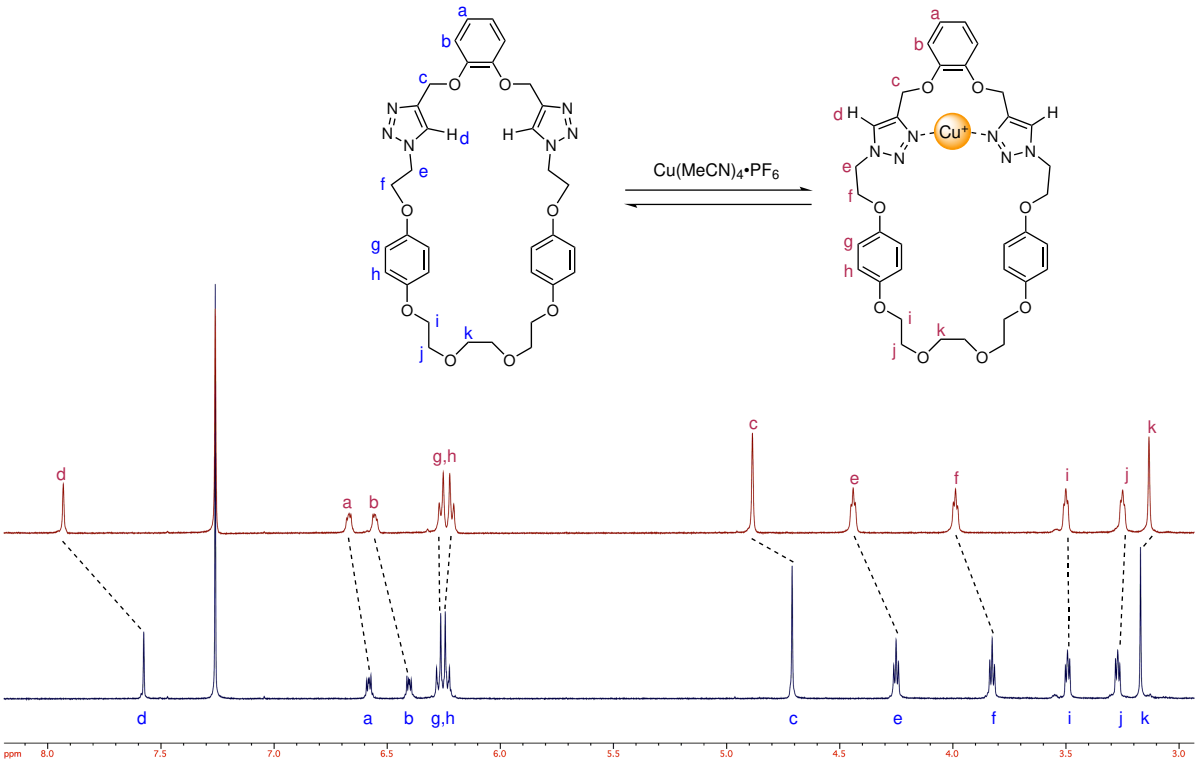

Figure 2.7: ^{1}H NMR binding study to probe Cu^I-binding behaviour: a) Assigned ^{1}H NMR spectrum of macrocycle **16** and b) in the presence of 3.0 equivalents of $[Cu(CH_3CN)_4]PF_6$ in 1:1 $CDCl_3$:d_6-acetone.

2.4.5 Attempted AT-CuAAC Rotaxane Formation with 1,2-hydroxymethyl Benzene Spaced Bis-iodotriazole Macrocycle

AT-CuAAC rotaxane synthesis was explored with macrocycles **16** and **17**, following the same procedure as outlined in section 2.4.3 (Scheme 2.7). After 72 hours, ESI-MS analysis of the respective crude reaction mixtures revealed a peak corresponding to the presence of target rotaxane **23** (*m/z* = 2041 $[M + H]^+$), but none corresponding to **22** (*m/z* = 1789 $[M + H]^+$).

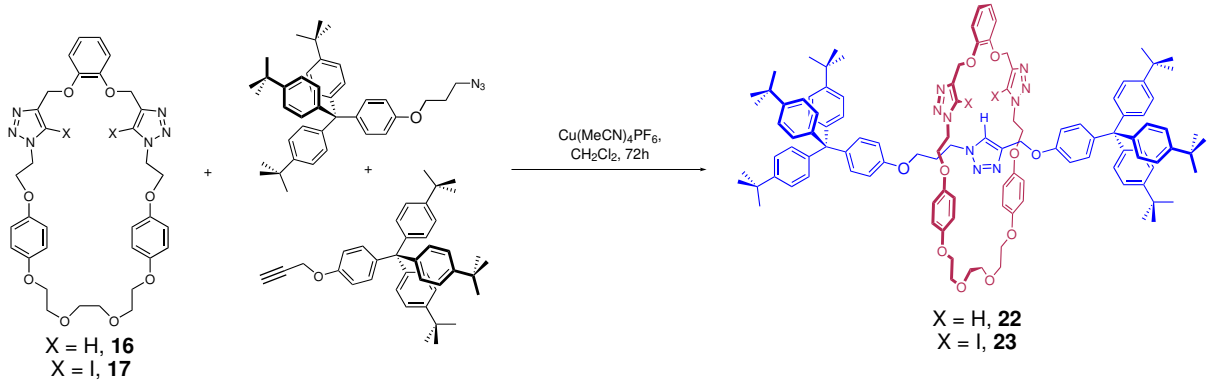

Scheme 2.7: Synthesis of [2]rotaxanes **22** and **23** via AT-CuAAC reaction.

Initial attempts to isolate products from the respective reaction mixtures were carried out using prep-TLC. As expected from the ESI-MS analysis, only free axle and macrocycle were isolated from the AT-CuAAC reaction using macrocycle **16**. For the AT-CuAAC reaction with macrocycle **17**, a single band containing the target rotaxane peak in ESI-MS was isolated by prep-TLC, representing 17% potential yield by mass. This band proved to have limited solubility in common organic reagents, but was eventually solubilised in a 2:1 $CDCl_3$:CD_3OD mixture for ^{1}H NMR analysis.

The ^{1}H NMR spectrum revealed that a mixture of the target [2]rotaxane **23** and free axle was present, shown below in proposed assignment on a stacked plot with the component macrocycle **17** and free axle (Figure 2.8). The primary evidence for [2]rotaxane **23** formation is found in the upfield shift of macrocycle hydroquinone protons *f* and *g*, suggesting interaction with the axle triazole, for which the proton *6* is correspondingly shifted downfield. The integration value of the macrocycle 1,2-hydroxymethyl benzene protons *c* compared to the axle triazole proton *6* suggested that the principle impurity was an equivalent of free axle, further supported by the additional complexity and approximately doubled integration values for many of the aromatic stopper proton signals.

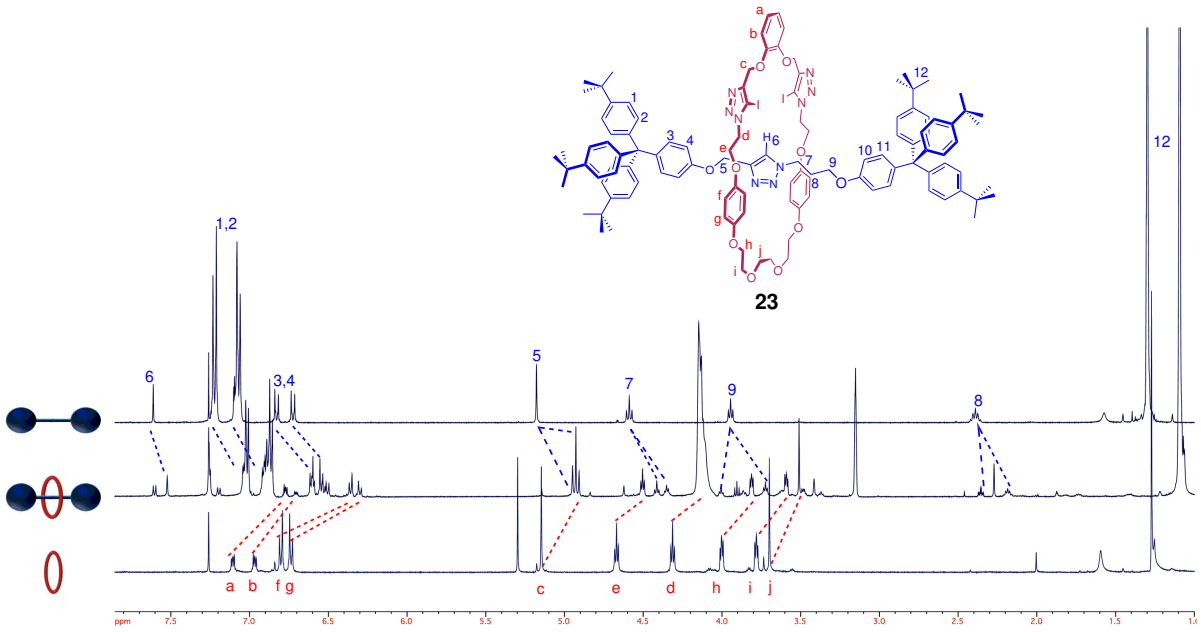

Figure 2.8: Stacked plot of ^{1}H NMR spectra of free axle (top), impure [2]rotaxane **23** (middle) and macrocycle **17** (bottom), indicating key protons (rotaxane mixture in 2:1 $CDCl_3$:CD_3OD, axle and macrocycle in $CDCl_3$, T = 298 K).

Further purification by prep-TLC was attempted, using a less polar eluent to increase band separation and prevent co-elution, resulting in a 3% yield from the band corresponding to target rotaxane **23**. The limited amount of rotaxane material isolated (4 mg) resulted in a very broad ^{1}H NMR spectrum, despite extended scanning time. Over subsequent ^{1}H NMR analyses, the growth of an additional peak was observed next to the axle triazole proton (Figure 2.9). ESI-MS analysis revealed new mass peaks corresponding to the free axle and macrocycle **17**, indicating the [2]rotaxane was dethreading into separate axle and macrocycle components.

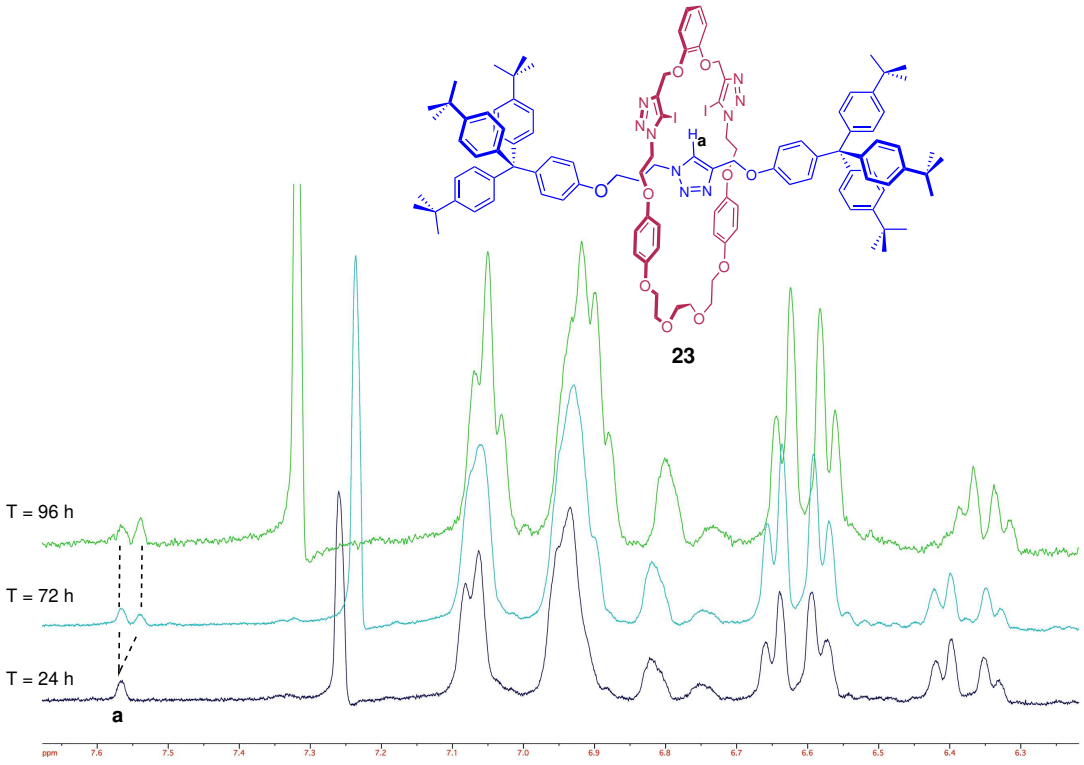

Figure 2.9: ^{1}H NMR spectra indicating dethreading of rotaxane **23** over time, monitoring axle triazole proton *a* (all in 2:1 $CDCl_3$:CD_3OD, T = 298 K).

Within the Beer group, the standard stopper group used to make rotaxanes is based on a 4-(tris-(4-^{t}butylphenyl)methyl)phenol motif (Figure 2.10a), which is functionalised as required at the phenolic oxygen. The largest ring-size bis-triazole macrocycle successfully incorporated into a [2] rotaxane using this stopper group is 33 atoms in circumference when counting round the shortest path (Figure 2.11a).[319] An unpublished isophthalamide-based macrocycle of 36 atom circumference previously studied in the Beer group (Figure 2.11b), required synthesis of an extended 'super stopper' to prevent dethreading when anion-templated rotaxanation was attempted (Figure 2.10b). This dethreading with the standard stopper was attributed to a combination of increased ring size and flexibility.

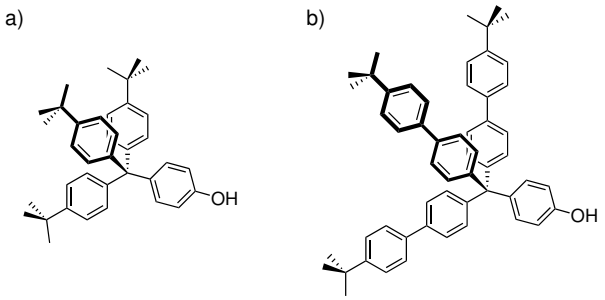

Figure 2.10: Stoppers for rotaxane formation: a) the standard design used within the Beer group, and b) an expanded 'super stopper' design.

Macrocycle **17** is a 36-membered ring (Figure 2.11c), albeit a more rigid one, and hence may be too large for a kinetically stable rotaxane structure containing the standard terphenyl stopper to be isolated.

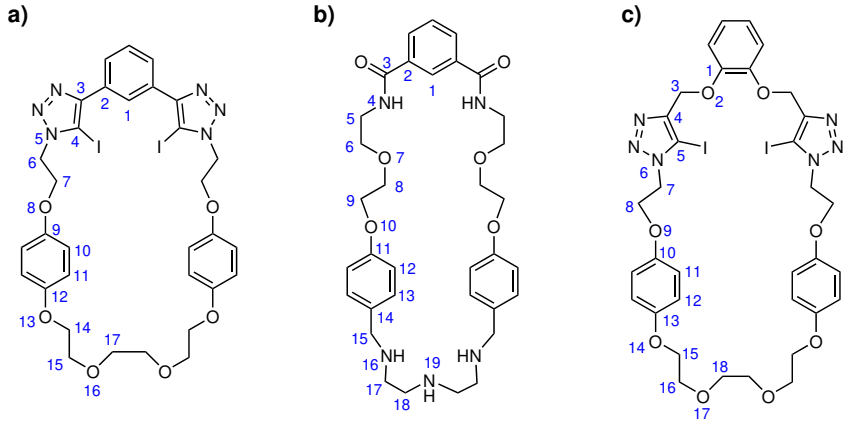

Figure 2.11: Macrocycle ring-size limits for successful [2]rotaxane synthesis using the standard stopper shown with partial ring counts: a) The largest known macrocycle within the Beer group that forms a [2]rotaxane N = 33, b) a macrocycle which is too large for the standard terphenyl stopper N = 36, and c) macrocycle **17** N = 36.

Taking into account the above, the incorporation of the 1,2-hydroxymethyl benzene bis-iodotriazole motif into a macrocycle component to form a kinetically stable rotaxane requires reducing the macrocycle ring-size, or employing a stopper of increased size. The decision was made to target smaller ring-size macrocyclic analogues, as this approach would also determine whether certain structural features such as the hydroquinone moiety were a necessity for mechanical bond formation via the AT-CuAAC reaction.

2.4.6 Synthesis of Smaller Ring-size 1,2-hydroxymethyl Benzene Bis-iodotriazole Containing Macrocycles

The decision to synthesise smaller macrocycles containing the 1,2-hydroxymethyl benzene bis-iodotriazole motif for potential AT-CuAAC synthesis of rotaxanes afforded the opportunity to begin to investigate the role of ring size, a theme developed in Chapter 4, as well as the impact of replacing the hydroquinone spacer groups with an aryl group directly conjugated to each triazole, or the removal of aromatic groups entirely. To this end, a series of smaller ring-size analogues were targeted (Figure 2.12) and prepared *via* double CuAAC reactions between appropriate bis-azide and bis-alkyne reactants, as successfully employed in the synthesis of macrocycles **16** and **17**.

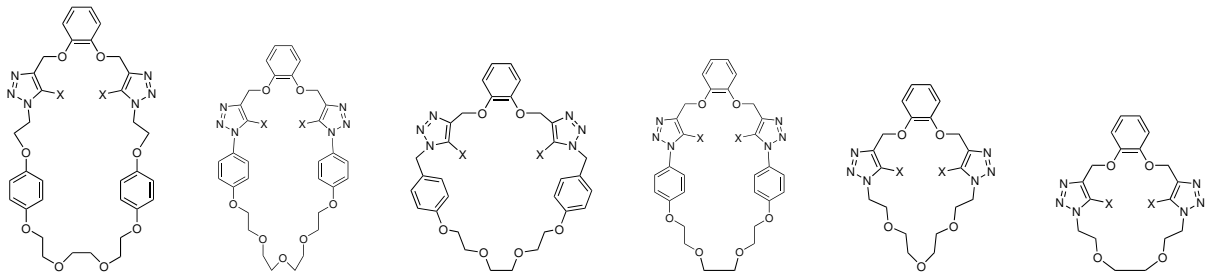

Figure 2.12: Smaller ring-size macrocycle targets (X = H, I) where **N defines the number of atoms in each macrocycle.**

Bis-azide precursors **24** and **25** were synthesised *via* reaction of di- and triethylene glycol with tosyl chloride under basic conditions in dry THF, followed by purification by column chromatography and subsequent reaction with sodium azide in DMSO. Bis-azide precursors **28** and **29** were synthesised *via* Williamson reaction between 4-iodophenol and the corresponding bis-tosylate polyether chain to afford **26** and **27**, followed by Ullman-type coupling with NaN_3, catalysed by a Cu^I/DMEDA complex. Bis-azide precursor **32** was synthesised *via* Williamson reaction between 4-hydroxybenzyl alcohol and the corresponding bis-tosylate polyether chain to yield **30**, following literature conditions.[339] Following this, conversion to the chloride **31** was achieved using $SOCl_2$ in dioxane, which was then reacted with NaN_3 in DMSO(Scheme 2.8).

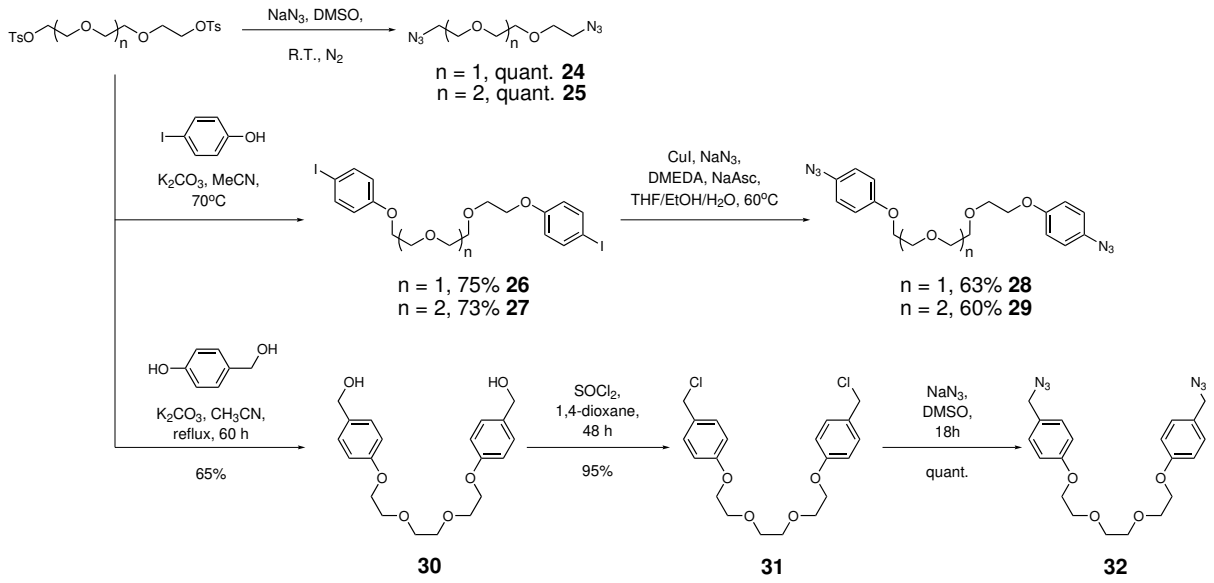

Scheme 2.8: Synthesis of bis-azides for diminished ring-size target macrocycles.

Double CuAAC ring-closing reactions were carried out at 10 mM, with 10 mol% TBTA for XB bis(iodotriazole) macrocycle formation, and DBTA for the HB macrocycle analogues (Scheme 2.9). Yields for these nine smaller macrocycles were generally good, excepting the smallest iodo-analogue **34**, where steric hindrance to macrocycle formation from the iodotriazoles is likely to be at its greatest. Macrocycles **37**, **38** with 30-atom ring sizes, **39** and **40** with 32-atom ring sizes, and macrocycle **41** with 35-atom ring sizes, all displayed isolated yields after prep-TLC exceeding 50%. Each macrocycle was characterised by ^{1}H NMR (Figure 2.13, ^{13}C NMR and high-resolution ESI-MS.

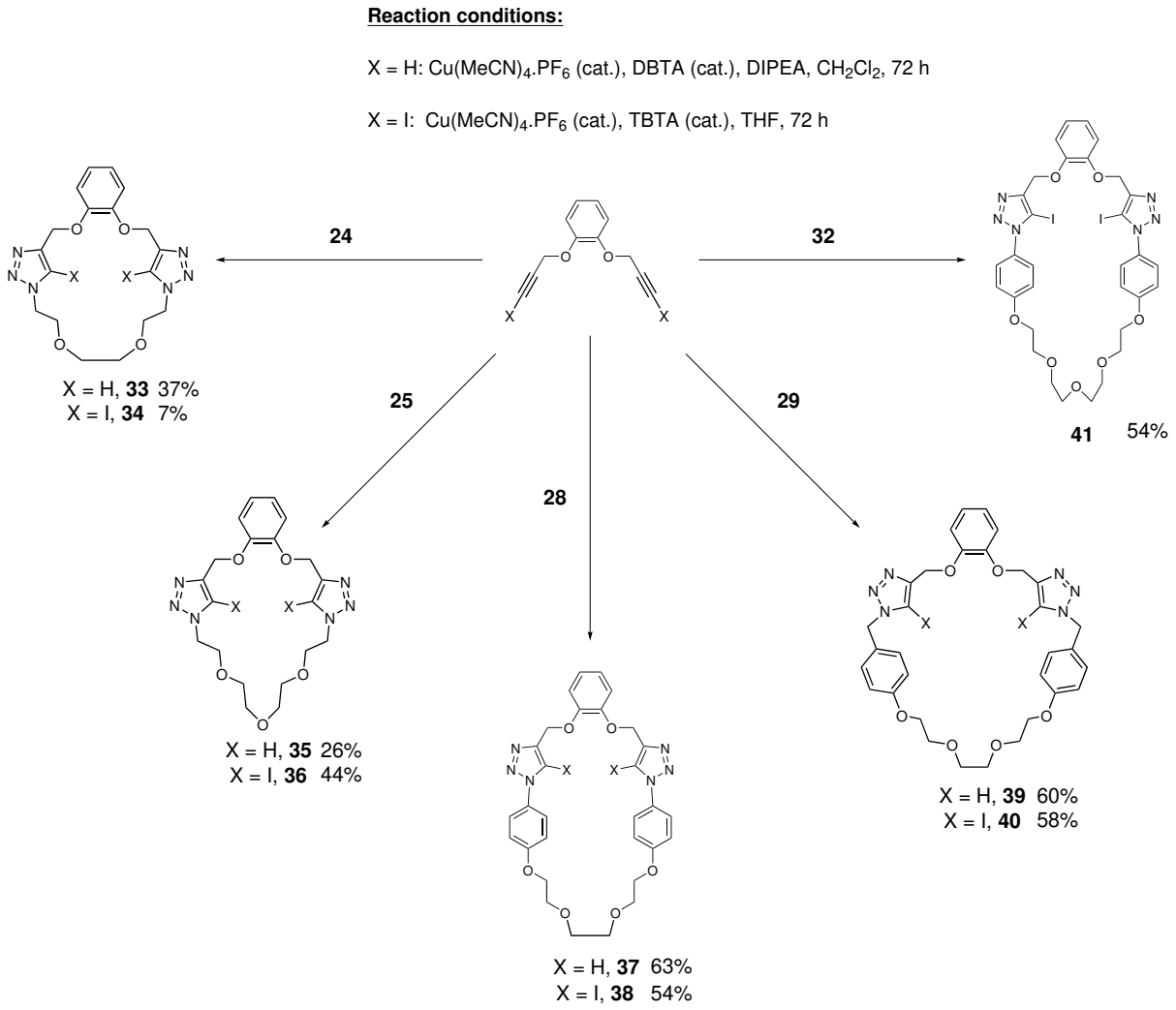

Scheme 2.9: Synthesis of diminished ring-size target macrocycles.

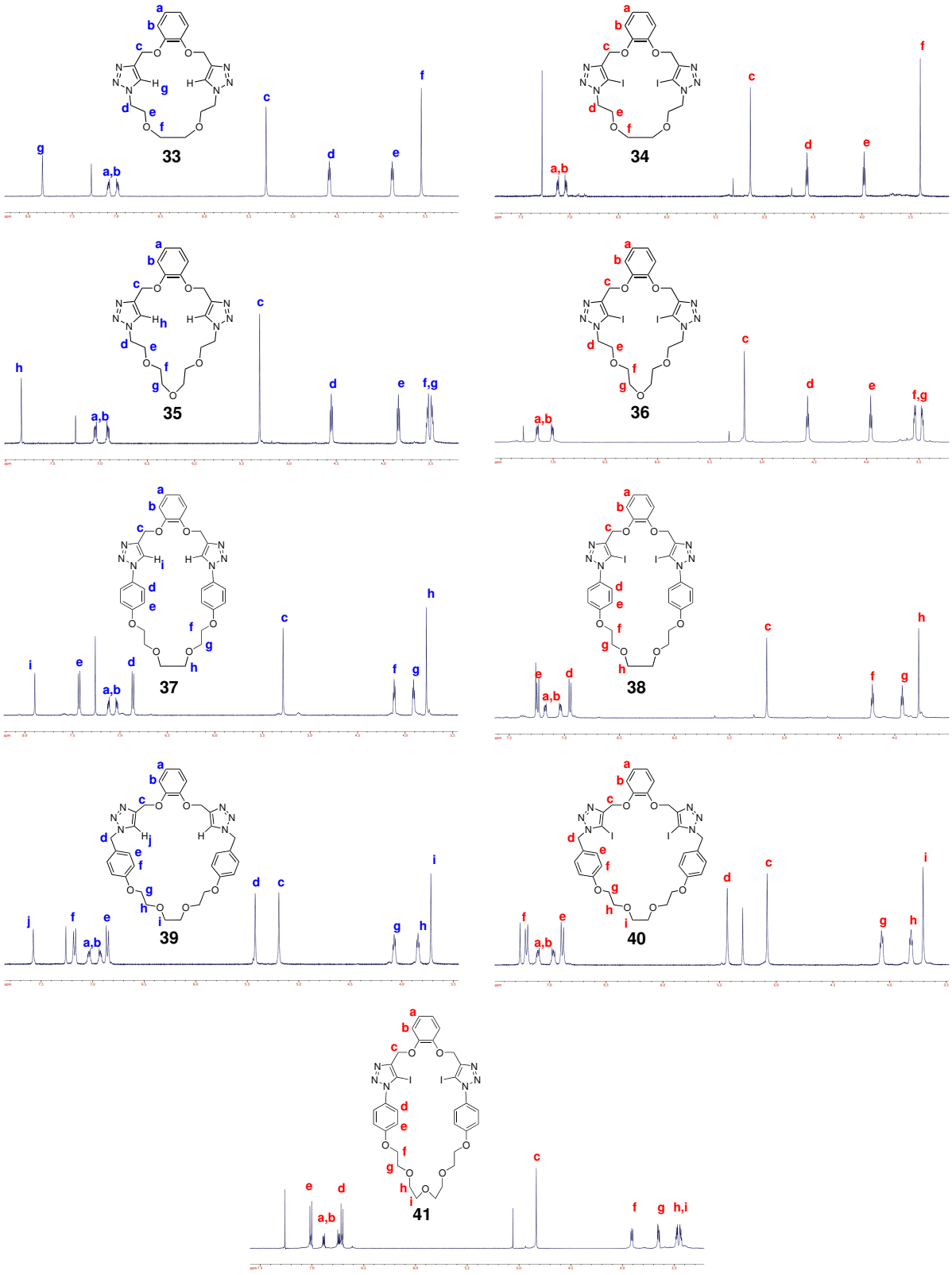

Figure 2.13: ^{1}H NMR spectra of smaller ring-size macrocycles ($CDCl_3$, T = 298 K).

2.4.7 Small Macrocycle AT-CuAAC Rotaxane Formation Investigation

Due to the limited supply of the macrocycles, AT-CuAAC rotaxane synthetic studies were initially undertaken on a small scale with the XB analogues, and the macrocycles with promising rotaxane formation reactions were then prepared on a larger scale along with their HB macrocycle analogues for further testing. AT-CuAAC reactions were carried out using the previously established conditions with macrocycles **33**-**41**. Of the initial test-scale reactions, ESI-MS analysis of the crude reaction mixtures for **34** (20-atom ring size) and **36** (23-atom ring size) displayed no ESI-MS evidence of [2]rotaxane formation indicating the macrocycles were too small for rotaxane formation. Rotaxanation reactions using **38** and **40** (30-atom ring size) and **41** (33-atom ring size), showed evidence of [2]rotaxane formation, for **38** and **41** in the form of $[M + Cu]^+$ peaks (Figure 2.14a & c), and for **40** in the form of a peak corresponding to the rotaxane having lost one iodine (Figure 2.14b).

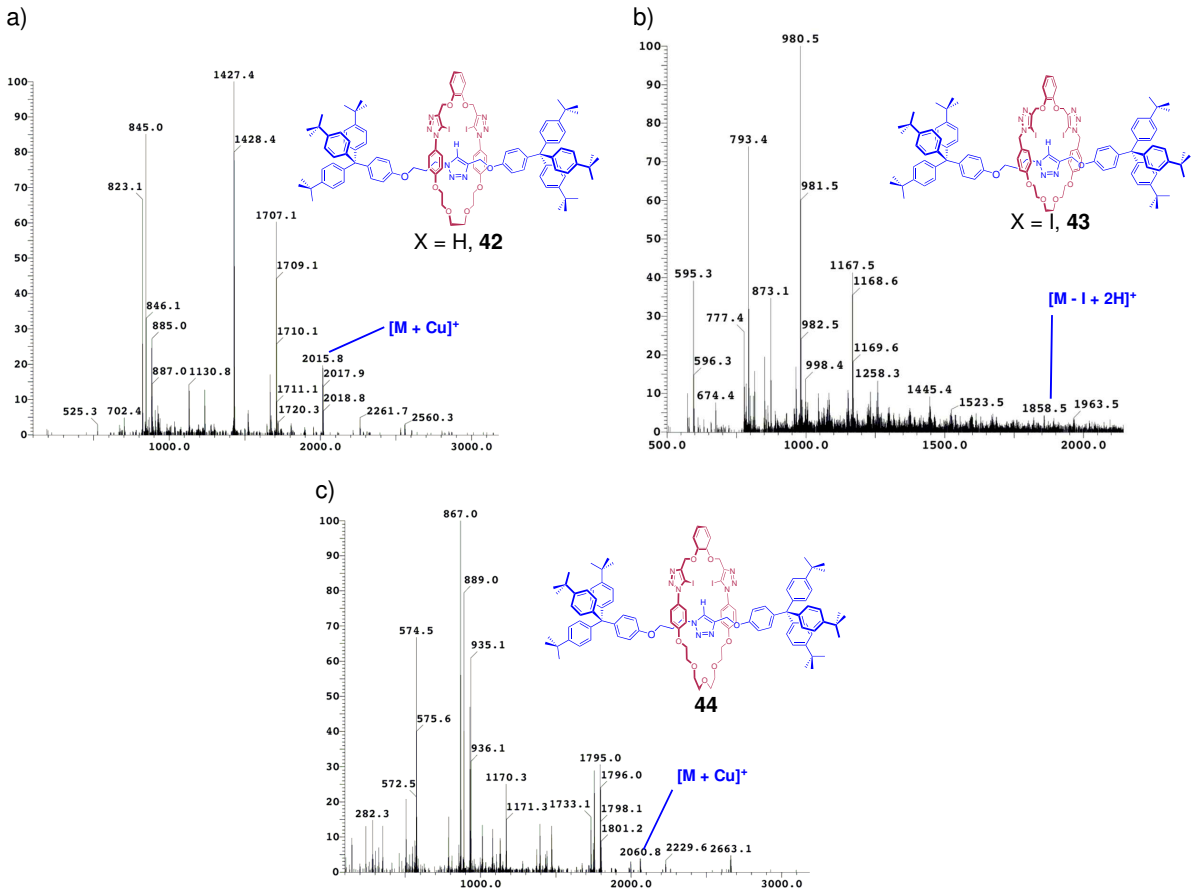

Figure 2.14: ESI-MS evidence for [2]rotaxane formation in crude reaction mixtures.

Scaled up AT-CuAAC reactions were then set for the 35-atom and 32-atom ring size macrocycles **36**-**41** (Scheme 2.10). During the setup of these AT-CuAAC reactions, incomplete dissolution was observed after addition of the alkyne half-axle **20** to the reaction mixture at its target 50 mM concentration (five-fold excess over the macrocycle component). In several cases, the dissolution in the CH_2Cl_2 solvent was simply slow, perhaps driven by interaction with the Cu^I-coordinated macrocycle, serving to solubilise the half-axle. After 72 hours, ESI-MS analysis of these reactions only revealed the presence of free axle and corresponding free macrocycle, with no interlocked product mass peaks observed.

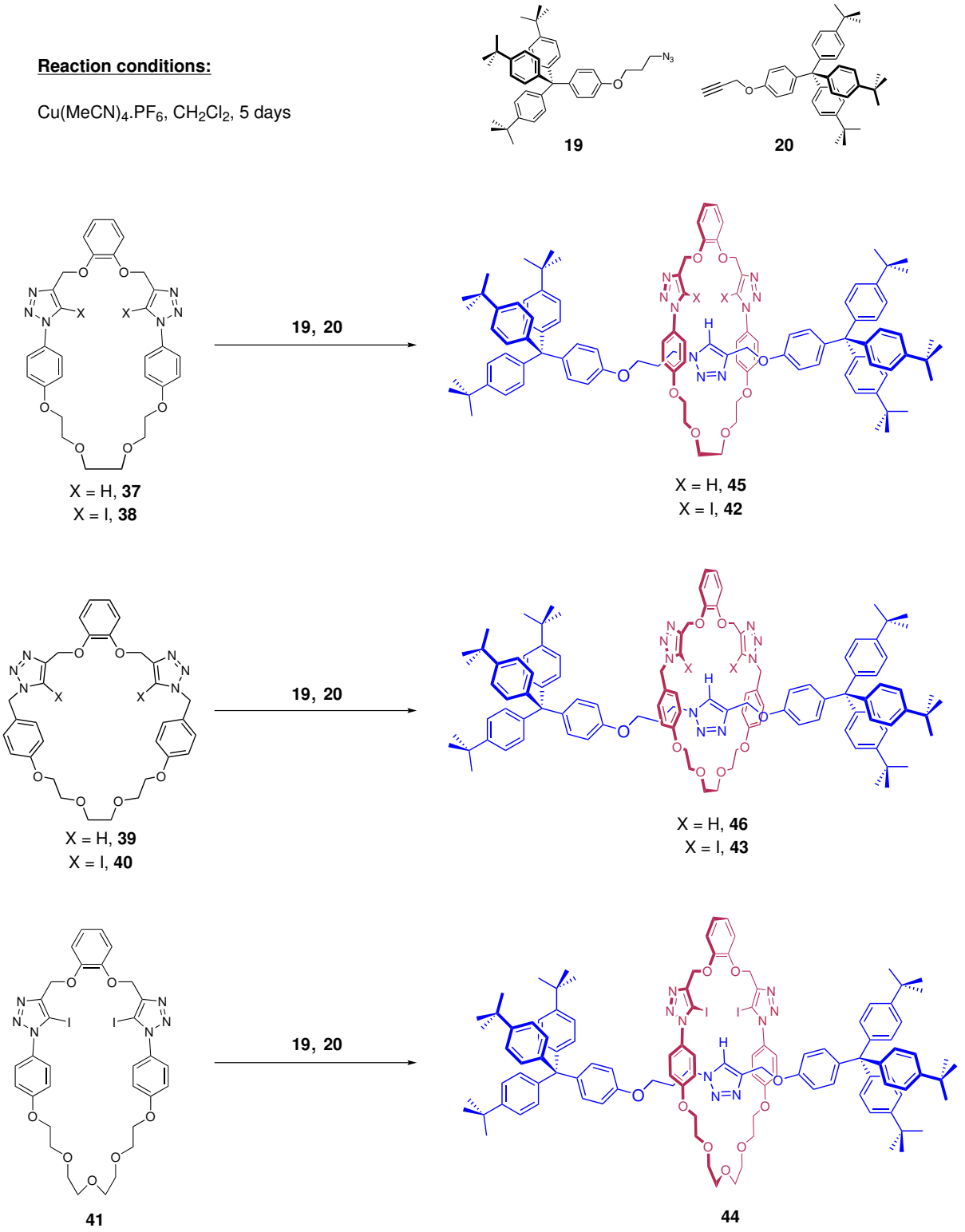

Scheme 2.10: AT-CuAAC synthesis of [2]rotaxanes **42**-**46**.

Undeterred, in order to aid solubility, the second scaled-up AT-CuAAC tests were undertaken at the lower concentration of 5 mM, resulting in homogeneous solutions. After 72 hours, ESI-MS analysis indicated rotaxane mass peaks were present corresponding to **46** (*m/z* = 1730 $[M + H]^+$) and **44** (*m/z* = 1998 $[M + H]^+$). Disappointingly, after prep-TLC purification attempts

for rotaxane **46**, there proved too little material to isolate from the free axle, suggesting the AT-CuAAC bond forming reaction was inefficient. Similarly for rotaxane **44**, it proved challenging to separate out the free axle side product, but there was sufficient isolated material to obtain a ^{1}H NMR spectrum Figure 2.15.

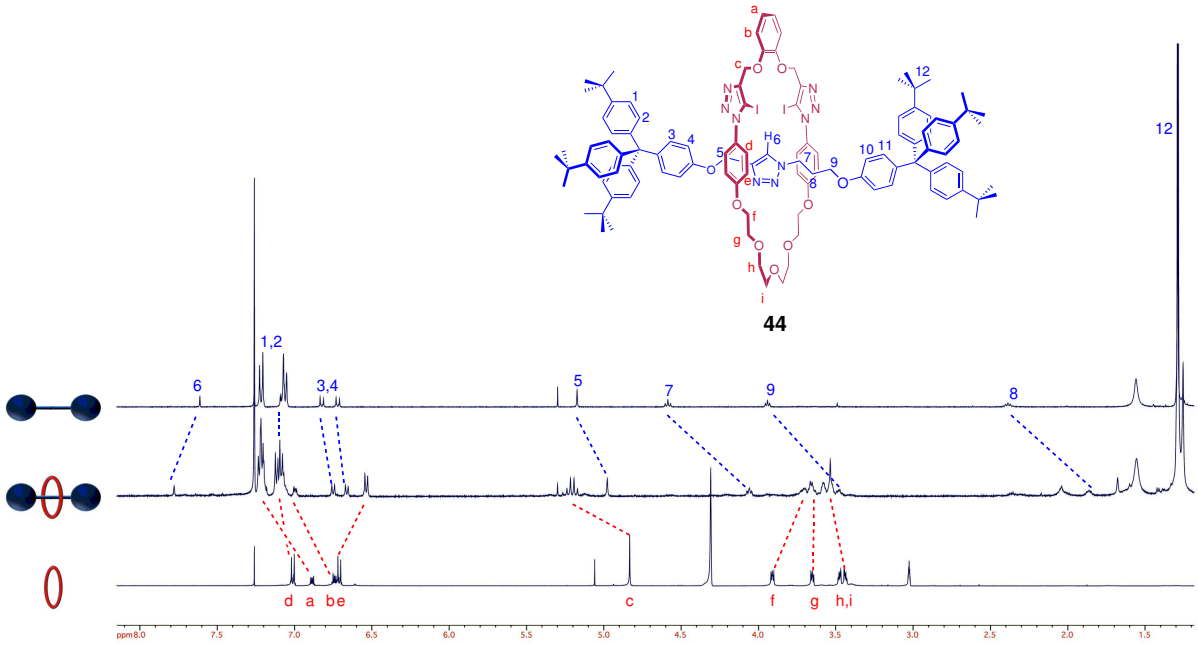

Figure 2.15: Stacked plot of partial ^{1}NMR spectra of free axle (top), [2]rotaxane **44** (middle), and macrocycle **41** (bottom), indicating key proton shift changes ($CDCl_3$, T = 298 K).

The strongest evidence of successful rotaxane formation comes from macrocycle component perturbations compared to the free macrocycle. The splitting and downfield shifting of proton *c*, is consistent with axle interpenetration causing the protons in each methylene pair to be in different environments. Hydroquinone protons *d* and *e* are further split, with the former moving downfield and the latter significantly upfield, indicative of macrocycle aromatic donor-axle triazole acceptor interactions.[285,340,341] Macrocycle protons *a* and *b* also move downfield, suggesting a folded conformation and interaction with stopper protons *3* or *4*. Further evidence can be found in the shift of proton *6* upfield, indicative of an interaction with the iodotriazoles of the macrocycle. While high-resolution ESI-MS also supported the formation of rotaxane **44**, there proved to be insufficient material for full characterisation by ^{13}C NMR and the ^{1}H–^{1}H ROESY NMR experiments required to prove the interlocked nature of the products.

2.5 Conclusions

The goal of this work was to explore how the flexibility of the linking moiety between two triazole groups incorporated into a macrocycle affected their ability to act in concert to bind Cu^{I} endotopically for AT-CuAAC rotaxanation reactions. It was considered a possibility that a flexible system incorporating iodotriazoles might favour an endotopic Cu^{I} binding mode, driven by the steric bulk of the iodines. To investigate this, two bis(iodo)triazole motifs were explored, one incorporating a highly flexible alkyl linker, analogous in size to a previous 1,3-functionalised benzene linker, and a second incorporating a more rigid 1,2-hydroxymethyl benzene linker, which represented an increase in flexibility over a previous 1,2-functionalised benzene linker. Macrocycles incorporating both novel motifs were successfully synthesized, with testing of the former proving that incorporation of so much flexibility was detrimental to AT-CuAAC efficacy, to an extent where no interlocked product was observed. In the case of the more structured 1,2-hydroxymethyl benzene linker, the motif was determined to be a likely candidate through a Cu^{I} binding study, but the initial macrocycle design proved too large for the stoppers, resulting in dethreading. Fueled by evidence of the motif being competent in AT-CuAAC reactions, a series of smaller macrocycles incorporating the motif were synthesized. While initial tests appeared promising for some of the larger analogues, issues with solubility were found on scaling the reactions up, which required reduced concentrations.

2.6 Future Work

The synthesis of sufficient quantity of [2]rotaxane for effective isolation and characterisation is a necessary step to further study systems incorporating this 1,2-hydroxymethyl benzene bis-triazole motif. This might be achieved by using macrocycles **16** and **17** with larger stopper-size axle precursors. Doing so would increase understanding of the impact of flexibility, in both the motif and the macrocycle in total, and whether it might be harnessed in subsequent receptor design. Synthesis of a 1,3-functionalised benzene with additional methylene units represents another ready avenue for exploration, with hopefully good comparison between such synthons and the 1,2-functionalised benzene motifs detailed above. Looking towards greater rigidification, exploration of directly attaching triazoles to polyaromatic motifs such as phenanthroline or anthracene may present the opportunity to strictly control geometry further.

Chapter 3

Computational investigation of Cu(I) binding by bis-triazole macrocycles

3.1 Introduction

The previous chapter demonstrates that it can be a non-trivial task to design a macrocycle which is competent for both anion binding and AT-CuAAC. A large degree of structural permutation around the anion binding motif may be required until a viable macrocycle is obtained. The challenge is, at heart, a consequence of the limits of the chemist's intuition into how a novel structure will behave in solution, concomitant with understanding where the balance of enthalpic and entropic contributions from metal ligation, and the desired endotopic Cu^{I} macrocycle complex conformation, lies. Determining the limits of these factors, and so how much potential the AT-CuAAC reaction has in the synthesis of anion receptors, is a subject of particular interest, and sometime frustration, within the Beer group. This chapter details an investigation into the application of relatively computationally inexpensive methods to the study of macrocyclic systems made within the Beer group, seeking to determine if the results can be used to indicate the likelihood of a given macrocyclic structure being competent in AT-CuAAC reactions. This competency is evaluated through the proxy of endotopic Cu^{I} binding favorability, which is understood to be the key conformational feature of successful AT-CuAAC rotaxanation reactions.

3.1.1 Density Functional Theory in Brief

This being a predominantly synthetic thesis in nature, the following explanation of density functional theory (DFT) is intended to be an introduction to the what and the why of key assumptions and approximations involved in the method.

The quantum mechanical (QM) wavefunction Ψ contains, in principle, all of the information about a given system. For the case of a hydrogen atom, a two-body problem involving the interaction of the positively charged nucleus and a negative electron, the Schrödinger equation can be solved exactly, *via* separation of variables, yielding the wavefunction of the system, Ψ. This Ψ then allows determination of the permitted energy states in the system. For a many-electron system it is not possible to solve the Schrödinger equation directly, as an additional term, arising from the interaction between electrons, prevents separation of variables. This necessitates approximations to render the system tractable.

The first, and most important of these assumptions is the Born-Oppenheimer approximation, which presumes that due to differing masses (an electron mass being approx. 1/1850 the mass of a proton) and resulting much slower speeds, nuclei can be considered fixed at a particular geometry relative to electrons. This enables the electronic Schrödinger equation to be considered independently of the nuclear Schrödinger equation, with an energetic term depending on nuclear position at that geometry. While computationally intensive methods exist to determine approximate Ψ under this assumption, such as the configuration interaction method, this is not currently feasible for large molecules. A compromise which works for large molecules is the use of density functional theory (DFT), which is built upon Hartree-Fock theory, itself a more simple, approximate approach.

3.1.2 Hartree-Fock Theory

Hartree-Fock theory provides a method of approximation of the Ψ and energy of a many-body system in a stationary state. It assumes that the Ψ of a polyatomic, many-electron system can be approximated by a Slater determinant, an expression capable of describing the Ψ of a multi-electron (or other fermion) system while satisfying anti-symmetry requirements, and hence the Pauli exclusion principle, which states:

$$\Psi(x_1, x_2) = -\Psi(x_2, x_1) \tag{3.1}$$

This Slater determinant is built using Hartree products, which assume that Ψ for a polyatomic many-electron system can be expressed as the product of wavefunctions, χ, of the corresponding single-atom systems. An example Hartree product for a two-particle case is shown below:

$$\Psi(x_1, x_2) = \chi_1(x_1)\chi_2(x_2) \tag{3.2}$$

These Hartree products must be used in a normalized, linear combination, as individually they are unable to satisfy the Pauli exclusion principle:

$$\Psi(x_1, x_2) = \frac{1}{\sqrt{2}}[\chi_1(x_1)\chi_2(x_2) - \chi_1(x_2)\chi_2(x_1)] \tag{3.3}$$

Once constructed, this trial Ψ can be used to find an approximation to the ground-state energy. This approximation, the Hartree-Fock energy can be written as:

$$E_{HF} = 2\sum_{i}^{N} h_{ii} + \sum_{i}^{N}\sum_{j}^{N}(2J_{ij} - K_{ij}) \tag{3.4}$$

The first term is a summation of the one-electron Hamiltonians, which contain operators for the kinetic energy of the electrons, and the potential they experience due to an external field. The second term contains the *Coulomb* and *exchange* integrals. The Coulomb integral, J, represents the classical repulsion between pairs of electrons, while the exchange integral, K, represents the repulsion between electrons of like spins.

The energy yielded by the Hartree-Fock method is a good upper bound, but makes several further approximations: relativistic effects are completely ignored, with momentum assumed to be completely non-relativistic; further, it is assumed that electron-electron repulsion is suitably approximated by an average value, rather than treating them as discrete point particles. While the exchange integral successfully accounts for the Fermi hole, this mean field approximation neglects the Coulomb hole, the region around an electron where the probability of finding another electron falls to zero, allowing the electrons to approach too closely. The energy associated with this permitted electron correlation serves to raise the Hartree-Fock energy above the exact ground state energy. This difference in energy only grows as the system grows in complexity, or when a large number of electrons are in similar regions of space with similar energies, such as for the non-diffuse 3d orbitals of 1st row transition metals.[342,343] The configuration interaction method mentioned previously attempts to solve this problem by fully correlating the electrons, but rapidly proves too computationally expensive as the system becomes more complex.

3.1.3 Kohn-Sham Density Functional Theory

Kohn-Sham DFT builds on Hartree-Fock theory to obtain a more accurate solution. The many electron wavefunction is again approximated as a single Slater determinant, but a further interaction, between the electrons and an external potential is assumed (in a molecule, the electronic attraction to the nucleus, diminished by the presence of the other electrons). Kohn and Sham considered a Schrödinger-like equation for a fictitious system of non-interacting particles possessing a ground state with the same density as a real system involving interacting particles.[344] This equation is defined by the local value of an external potential in which the non-interacting particles move, termed the Kohn-Sham potential. Within this framework, the total energy of the electrons in the system can be considered as a summation of the individual kinetic and potential energy terms (as the electrons no longer interact) and the exchange-correlation energy term. Refinement of the determination of this exchange-correlation energy is an active area of research in computational chemistry method development.[345]

Moving to considering a system in terms of electron density instead of N discrete electrons significantly reduces the computational complexity, requiring consideration of 3 spatial terms (the electron density at a given coordinate) instead of 3N (the coordinates of N electrons), but makes the calculation of electron kinetic energy more difficult (though still cheap and straightforward compared to exchange-correlation energy calculations), due to the loss of the explicit electronic Ψ. To rectify this, a set of (physically meaningless) one-electron Kohn-Sham orbitals are constructed from the Slater determinant for a single electron spin orbital. The total electron density is then constructed from, and minimized, using a set of these orbitals. These orbitals are varied by altering the Kohn-Sham potential iteratively until the change in calculated electron density with respect to the orbitals is zero. Per the variational principle, which determines that any energy found through approximation will always be greater than or equal to the ground state energy, the energy at this point must be the ground energy.

3.1.4 Functionals

The correct form of the exchange-correlation energy is not known for anything other than a free electron gas, and while formulae for exchange-correlation energy density have been constructed from quantum Monte Carlo simulations, it is only a viable approach for the smallest systems. This again necessitates approximations to accurately calculate physical properties within DFT, found in the form of functionals (functions of a function). The simplest of these is the local density approximation (LDA) which considers only the electron density of the system, tending to bind electrons too strongly as a result. Generalized gradient approximation functionals (GGA) are more refined, considering both the electron density and its first derivative with respect to position, which allows a better representation of the non-homogeneity of the true electron density, and so see wide use. These GGA functionals can be expanded to the second derivative for further accuracy, then termed meta-GGA functionals. Finally, hybrid functionals combine the exact Hartree-Fock exchange with DFT exchange-correlation energy, but are computationally more expensive. In general, as more parameters are used, and the complexity of the exchange-correlation energy description increases, so too does computational cost.

3.1.5 Basis Sets

Determining the exact nature of these constructed Kohn-Sham orbitals is very computationally intensive, so again, an approximation is used to calculate the electron density. Linear combination of atomic orbitals enables an orbital to be represented by a combination of basis functions, the complexity of which is determined by the system investigated, as there is an asymptotic relationship between the number of basis functions, and so the computational cost, and the accuracy of the representation of the atomic orbital afforded. Further complexity exists in the form of polarization functions, which serve to describe valence electron density inhomogeneity as a result of asymmetric orbitals (p-, d-type), as well as diffuse functions, which improve the accuracy of the model at describing orbitals far from the nucleus, particularly important for anions or dipole moments, as well as modeling of non-covalent interactions.

Initially basis functions were of two types, Gaussian- and Slater-type, with Slater-type functions providing much more accurate representation of electron density when very close or distant to a nucleus than the Gaussian-type functions, at the cost of computational complexity. This trade-off was resolved by Francis Boys, who realized that these Slater-type orbitals could themselves be approximated by a linear combination of Gaussian-type orbitals.[346] Subsequent work by John Pople *et al* to implement this computationally resulted in the first version of the GAUSSIAN program released in 1970, a later version of which was used to carry out the work laid out in this chapter.[347,348]

A final key approximation which has proved a powerful accelerant to computational methods is the separation of electrons into valence and core electrons. Within this approximation, core electrons are considered to be strongly bound, having no significant role in chemical bonding, serving only to screen the charge of the nucleus. All bonding properties are attributed to the valence electrons, and the atom is reduced to an ionic core which interacts with valence electrons *via* a pseudopotential, calculated *ab initio* through inversion of the free-electron Schrödinger equation for a given reference electronic configuration.

3.1.6 Chapter Aims

This chapter aims to serve as a pilot study into the utility of computational modeling of simplified versions of supramolecular systems for predicting synthetic outcomes when building higher architectures, in this case the [2]rotaxane. The desired outcome for the project is observable, quantifiable correlation between experimental and computational results, with sufficient confidence to prioritize, permute or discard macrocycles incorporating an anion binding motif for use in the AT-CuAAC reaction. Use of computational methods in this manner, while common in areas such as medicinal chemistry, is unprecedented in the field, with existing studies which seek to probe structure activity relationships for the AT-CuAAC reaction being purely synthetic in nature. A key goal for such a screening approach is for it to be fast, here dictated by computational complexity, hence termed 'cost', allowing many structures to be evaluated within a reasonably short period of time (here determined by the relative time required for synthesis of a system, approximately one to two weeks). A further complication compared to these studies is that while they have predominantly focused on macrocycles with little if any other functionality beyond the single purpose ligating motif, we are focusing on the construction of interlocked structures for anion binding, so all macrocycles must include an anion-binding motif.

3.2 Methodology

For each macrocycle studied, initial 3D coordinates were generated from a ChemDraw structure using Avogadro 1.2. These atomic coordinates were then subjected to energy minimization using molecular mechanics with the Universal Force Field (UFF), which is known to better represent transition metals.[349] In brief, molecular mechanics approaches model the atom, without consideration of electrons, as single particles with a radius, polarizability and constant net charge, taken as the average of experimental values across many molecules. Bonding interactions are modelled as springs, with an equilibrium distance again based on experimental data.

To this macrocycle model was added a $[Cu(CH_3CN)_2]^+$ unit, in a variety of different relative positions, the number being dependent on the degree of symmetry in the macrocycle and the number of likely ligating groups for the Cu^I species within the macrocycle. These interactions were modelled under molecular mechanics by the addition of a dummy bond between the copper and one or two ligating groups. This new set of ligating macrocycle models were again minimized using the UFF, and checked to ensure the outcome made chemical sense, *i.e.* exhibited staggered rather than eclipsed carbon chains, had planar sp^2 bonds etc. At least 6 conformations were evaluated for each macrocycle, and these minimized conformations were used as the starting points for DFT energy minimization in Gaussian16. This energy minimization was carried out over five steps:

1. Initial DFT geometry optimisation using the B3LYP method, employing the 6-31g basis sets for all atoms except iodine, for which the LANL2DZ basis set was used.

2. Vibrational frequency calculation at the same level of theory, to determine that each stationary point reached by DFT minimization step was indeed a minimum with respect to the vibrational modes of the molecule, not a saddle point. This serves as a check beyond visual inspection of the conformation that nothing has gone wildly awry in setting up the calculation.

3. Once satisfied, a second geometry optimization step was carried out, using the 6-31+G(d,p) basis sets for all atoms except iodine, where the LANL2DZ basis set, augmented by polarization functions of d symmetry and diffuse functions of p symmetry (here abbreviated LANL2DZdp), was used instead.

4. Vibrational frequency calculations were again carried out at the same level of theory to verify minima.

5. Finally, a basis set superposition error (BSSE) calculation was carried out, to generate the final energies used for comparison between conformations. This is necessary due to the nature of the Gaussian functions used to approximate the electron density of the component atoms: comparison of the energies of the isolated macrocycle and $[Cu(CH_3CN)_2]^+$ complex with that of the ligated complex reveals that the ligated complex is slightly lower. This is due to the basis functions being used to describe electron density in a region near an atom, irrespective of whether that electron density originates from that atom.

The second geometry optimization is more computationally costly than the first, as the basis sets used contain significantly more basis functions. Thus, a stepwise approach, wherein the first, lower detail minimization step is used to generate a better approximation to the lowest energy conformation than that granted by the molecular mechanics step. The general principle adopted is to do as much of the optimization at as low a level of theory as possible. Discussion of the choices of functional and basis sets follows below.

3.2.1 Functionals

When simulating supramolecular systems using DFT, balancing computational cost against molecule size is one of the predominant factors affecting the functionals and basis sets chosen. A survey of the computational literature on solution phase supramolecular chemistry indicates a strong preference for functionals that have lower computational cost[350,351] generally those developed by, or based on the work of, Becke *et al* such as the B97, B98 and B3LYP families.[352] B3LYP is well established, representing one of the first DFT methods to show significant improvement over Hartree-Fock.[353] It has also been shown to yield similar results to more parameterised and expensive functionals in supramolecular systems.

3.2.2 Basis Sets

Beyond simple computational cost, the balance of the number of basis functions used to describe the electron density around various atoms, compared to neighbouring atoms of different electronic configuration, must be mentioned. As the basis functions are used to describe the electron density around the molecule, each centred on their parent atom, it should be apparent that if there are many more functions available to describe electron density around one atom, e.g. an iodine, than its neighbouring (here carbon) atom, the most accurate depiction of the overall electron density will result in the many functions on the iodine being used to also describe the electron density around the neighbouring carbon. This can become a problem particularly with longer ranged diffuse functions, critical for modelling anionic behaviour and van der Waals interactions, and valuable in this case to describe the longer range interactions that iodine and copper may be involved in within the systems under study. This potential source of error must be weighed against the computational cost of increasing the number of basis functions on the less important atoms in the molecule, such as backbone carbon and hydrogen atoms, or the loss of confidence in the results resulting from decreasing the number of basis functions used to describe the atoms more likely to be involved in longer ranged interactions, such as iodine and copper.

The choice of basis sets indicated above was informed primarily by the works of Chudzinski *et al*[351] on comparison of DFT determined binding constants with experiment, and Félix *et al*[292,354] on solution-phase halogen bonding simulation, with the aug-cc-pVDZ-dp basis set used in the latter's work judged overly computationally expensive for the purposes of this pilot project, and the LANL2DZdp chosen by the former a suitable alternative. A large part of this decision was based on the demonstrated agreement between calculations run with the 6-31+G(d,p)/LANL2DZdp mixed basis sets and experimental data for systems of fairly similar complexity to those modeled in this work, which allows better confidence in the results.

3.2.3 Conformational Sampling

A challenge of modelling a large system with many σ-bonds is the size of the potential conformational space. This is especially true for most of the systems considered. While there is some conformational restriction of the upper half of the macrocycle by the Cu^{I}, the lower half of the macrocycle is a highly flexible polyethylene glycol (PEG) chain largely uninvolved in the binding. This results in many potential conformations which are very similar in energy.

To simplify this problem, starting conformations were chosen based on an understanding of the major potential binding modes, in part supported by ^{1}H NMR data on Cu^{I} binding for some of the systems studied. These conformations are shown in schematic form below using one of the systems studied as the example structure (Figure 3.1) and reflect three main classes of binding geometry; endotopic *i.e.* within the macrocycle cavity, facial *i.e.* above the face of the macrocycle, and exotopic *i.e.* outside the macrocycle. For all systems studied, binding modes investigated involve interaction with Cu^{I} in a mono- or bi-dentate fashion, so for each of the three main relative positions detailed above, these two binding modes are used, resulting in six or nine starting conformations, depending on macrocycle symmetry.

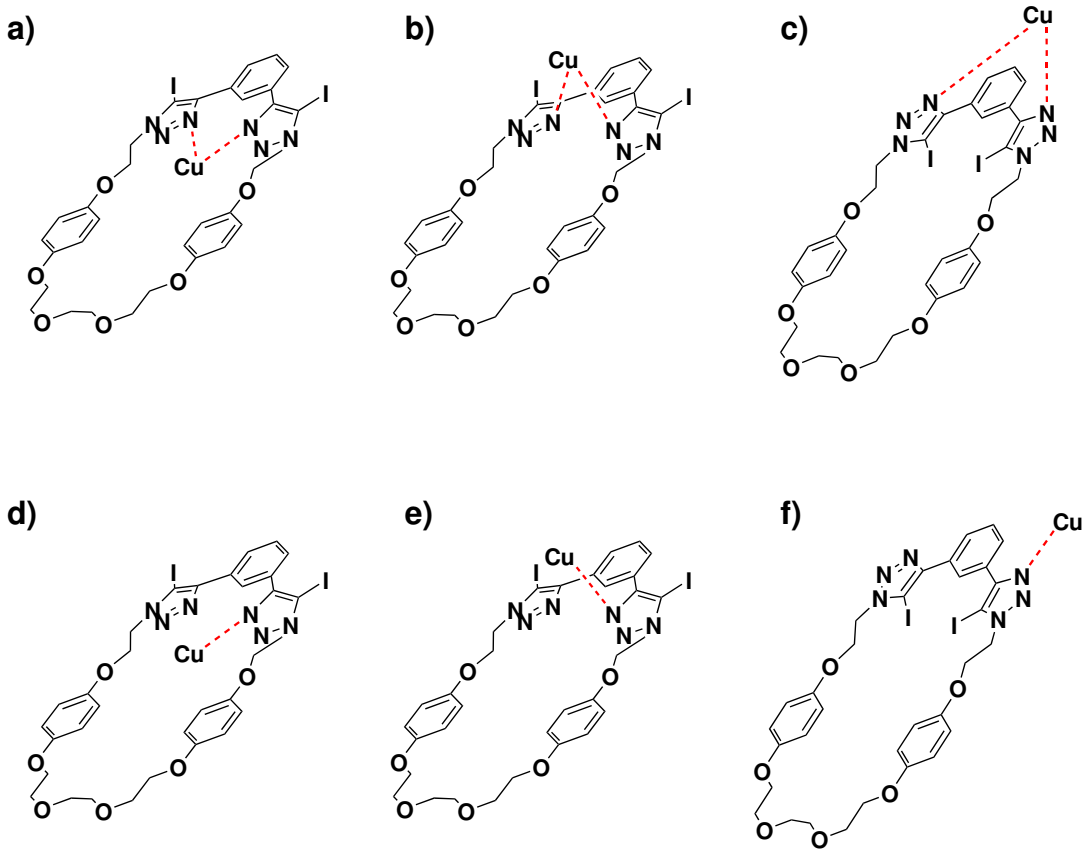

Figure 3.1: Schematic representations of types of starting conformations used in this study, reflecting the three main classes, endotopic, facial and exotopic, and two main binding modes, mono- and bidentate. (a) bidentate endotopic, (b) bidentate facial, (c) bidentate exotopic, (d) monodentate endotopic, (e) monodentate facial, and (f) monodentate exotopic.

As illustrated in the AT-CuAAC rotaxanation schematic shown in the introduction (Figure 1.43), it is expected that a macrocycle that demonstrates a consistent energetic preference for endotopically bound Cu^{I} should perform better in AMT rotaxanation reactions than one that shows preference for facial or exotopic Cu^{I} binding.

3.2.4 Limitations of Approach

It is important to note two assumptions that were made at the start of this study. First, that if the PEG chain loop at the 'bottom' of the macrocycle is in a chemically sensible, *i.e.* predominantly staggered, geometry, its conformation is unlikely to change significantly during energy minimization. This is rationalized by its distance from, and lack of involvement in, the key Cu^{I} binding events being considered. This means that the difference in energy between conformations is assumed to have no significant contribution from the PEG chain component of the macrocycle.

The second, and more important assumption relates to the lack of any solvent model in the DFT methods used, particularly as the study is attempting to model solution phase behaviour. The thermodynamic balance of desolvation often plays a key role in binding interactions, with ligand-metal interactions in solution often driven by the increase in entropy resulting from freed solvent molecules on complexation, especially so when the solvent is unable to form strong donor-acceptor interactions with the metal, such as in DCM, the medium the Beer group predominantly uses for its AT-CuAAC rotaxanations. It is assumed that macrocycle conformations which more effectively encapsulate the Cu^{I} on ligation should more strongly desolvate the metal species, so increasing this entropic contribution to the system energy. Thus, inclusion of an implicit or explicit solvent model should serve to favour endotopic binding modes more, so neglecting it should only result in borderline cases looking less promising, *i.e.* there may be an increase in false negatives. This is judged vastly preferable to increased false positives, as it minimizes the chance of weeks of following synthetic effort for naught.

3.2.5 Predictive Capacity

What level of insight could this pilot study hope to provide? Within the group of macrocycles studied for which experimental data exists, there are several close structural analogues, with interlocked yields in the AT-CuAAC reaction ranging from 0-40%, which provide the best opportunity to answer this question. The results will be presented in two ways. First, the minimal conformations and associated energies will be discussed for systems with known experimental performance in the AT-CuAAC rotaxanation reaction, ordered by yield. Following this, conformations and energies of previously synthesized and as yet unmade macrocycles will be discussed together, grouped by structural similarity. It is important to note that direct comparison of energies between different macrocyclic systems are meaningless unless they have the same molecular formula and are isoelectronic, as energy is dependent on the number of atoms and electrons present. For all minimum conformations shown, where multiple minima exist for a particular macrocycle, their energies are shown relative to the other minima of the same system.

3.3 Results

For convenience, all macrocycles presented are named according to their iodotriazole motif. In all systems modelled, unless otherwise specified, tetradentate copper species display approximately tetrahedral geometry, and tridentate copper species display approximately trigonal planar geometry, with variation of Cu–N(triazole) and Cu–N(CH_3CN) bond lengths of $<$0.1 Å.

3.3.1 Macrocycles with Known AT-CuAAC Performance

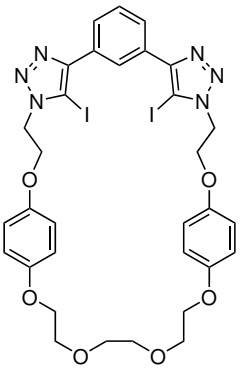

Figure 3.2: 1,3-bis(iodotriazole)benzene macrocycle.

This macrocyclic structure has shown consistent good performance in the AT-CuAAC rotaxanation reaction, repeatedly yielding 40%.[319] For all starting points, the minimized geometries were very similar, featuring endotopic monodentate binding of the $[Cu(CH_3CN)_2]^+$ unit to one triazole nitrogen, with approximately trigonal planar geometry, as illustrated below (Table 3.1). As variation of the optimized structures energies was $<$2 kJ mol^{-1}, it is probable that the optimized geometry is the lowest point on the potential surface. Experimentally, this macrocycle has been reported to bind Cu^I in a monodentate fashion, as evinced by ^{1}H NMR titration experiments.

Table 3.1: Schematic and 3D representations of calculated minimal geometry for 1,3-bis(iodotriazole)benzene macrocycle, showing endotopic monodentate triazole binding.

Schematic Representation	3D representation
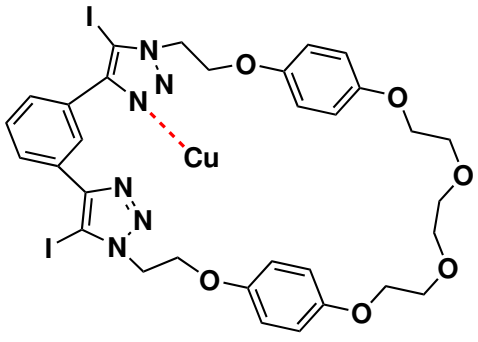	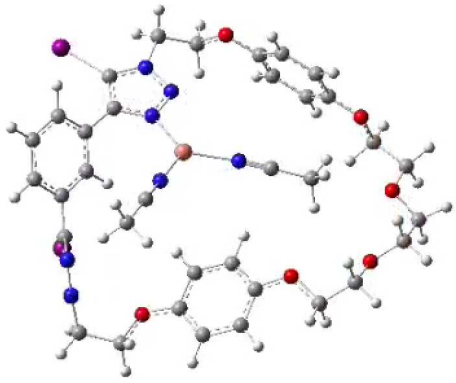

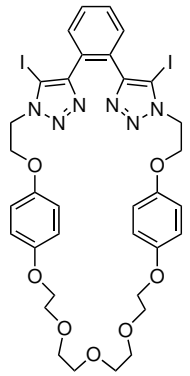

Figure 3.3: 1,2-bis(iodotriazole)benzene macrocycle.

For the macrocycle shown in Figure 3.3, 3 minimal conformations were found, with the lowest two being within 2 kJ mol^{-1} (Table 3.2). In these lowest energy conformations, the $[Cu(CH_3CN)_2]^+$ unit is facially bound, with the higher energy minimum exhibiting endotopic binding geometry. This apparent preference for facial conformations over endotopic can be expected from the narrow bite angle and spatial proximity of the triazole nitrogens, and is supported by ^{1}H NMR and crystallographic data collected on this system. Asymmetry is observed between the two triazoles, with the crystal structure showing them spun out of the plane of the macrocycle, as in the lower energy conformations displayed below. Experimentally this macrocycle has produced yields of 30% in AT-CuAAC rotaxanation reactions.

Table 3.2: Schematic and 3D representations of calculated minimal geometries for 1,2-bis(iodotriazole)benzene macrocycle, ordered by energy.

Schematic Representation	3D representation	Relative Energy (kJ mol^{-1})
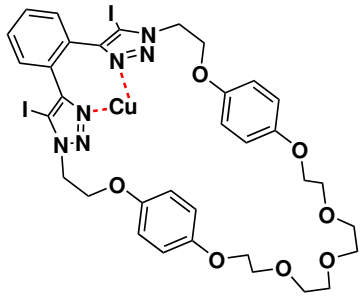	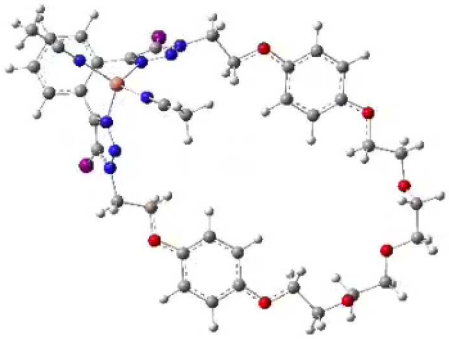	0
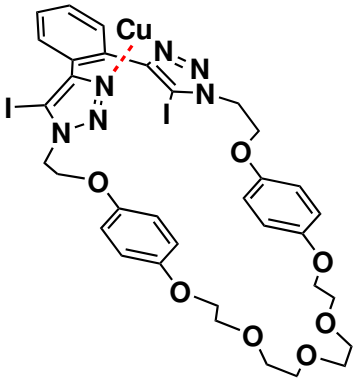	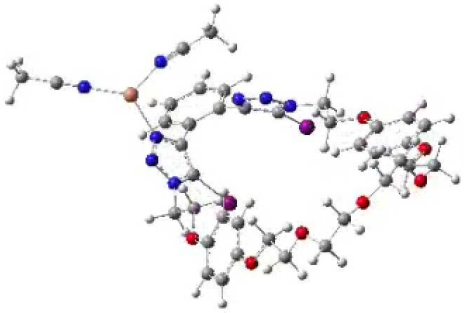	1.4
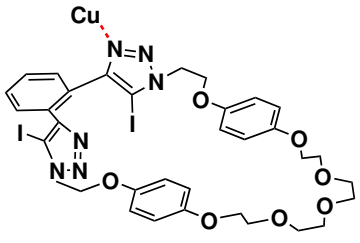	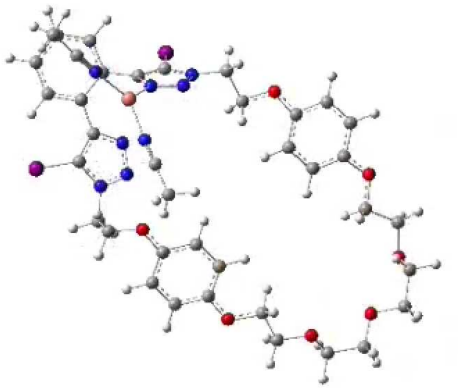	7.8

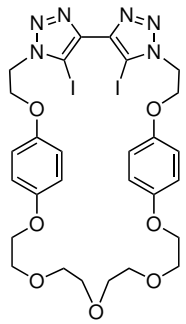

Figure 3.4: Bis(iodotriazole) macrocycle.

The minimal structures found for the macrocycle in Figure 3.4 are very similar (Table 3.3), both being bidentate facial, differing almost solely in the alignment of the hydroquinone groups and PEG loop at the bottom of the macrocycle. In the higher energy structure, the macrocycle is skewed to one side, and the PEG chain is disordered, whereas in the lower energy structure, the PEG chain is symmetrical, and bends out of the plane slightly. As the structures show good agreement otherwise, it supports these geometries being at, or close to, the lowest energy point of the potential surface in the region defined by the starting geometries. Experimentally, this was the first macrocycle made in the Beer group for use in the AT-CuAAC rotaxanation reaction, yielding 30% of interlocked product.[318]

Table 3.3: Schematic and 3D representations of calculated minimal geometries for bis(iodotriazole) macrocycle, ordered by energy.

Schematic Representation	3D representation	Relative Energy (kJ mol^{-1})
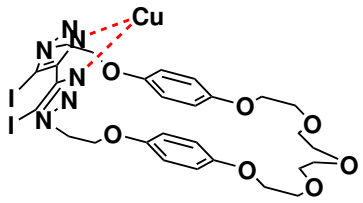	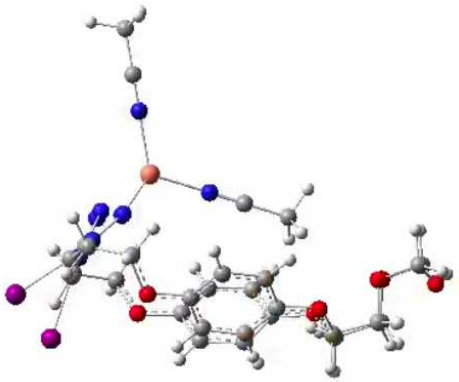	0
	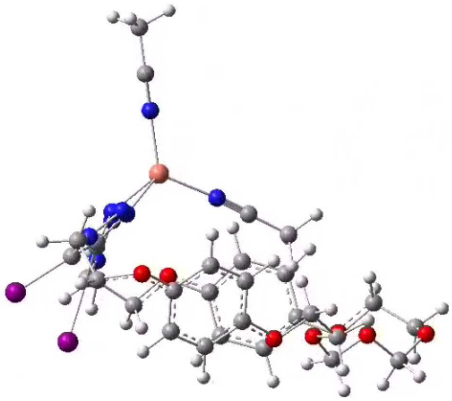	6.8

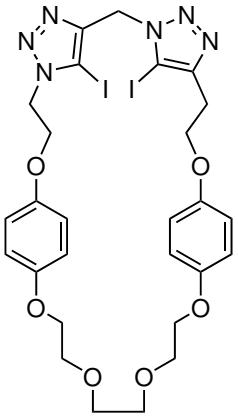

Figure 3.5: Head-to-tail bis(iodotriazole) macrocycle.

Of the five minimal geometries for the macrocyclic system in Figure 3.5 shown below (Table 3.4), most are very similar in energy differing by $<$4 kJ mol^{-1}, with the second structure differing from the first in its loss of the capability for a bidentate facial binding interaction due to the antisymmetric rotation of a triazole group. This bidentate binding is unexpectedly a result of the 2-position nitrogen on one of the two triazoles, likely a feature of restricted relative motion due to the methylene spacer unit. Most of the energy difference between the first four conformations could reasonably be attributed to the PEG chain variation, and indeed they are all within error. The unfavourability of exotopic binding modes is illustrated by the rise in energy for the final conformation, in part a consequence of the impossibility of a bidentate binding mode. From the lower energy conformations, it seems reasonable to postulate that the true minimum for the potential surface is a bidentate binding mode somewhere between facial and endotopic, with range of movement towards exotopic. This decreased observed preference for a facial or endotopic conformation matches the experimental data, where it has been shown to reach 20% yield in AT-CuAAC rotaxanations.

Table 3.4: Schematic and 3D representations of calculated minimal geometries for head-to-tail bis(iodotriazole) macrocycle, ordered by energy.

Schematic Representation	3D representation	Relative Energy (kJ mol^{-1})
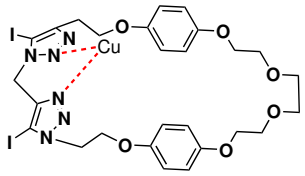	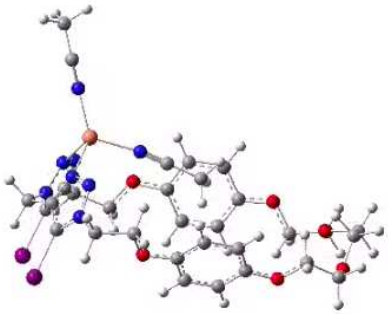	0
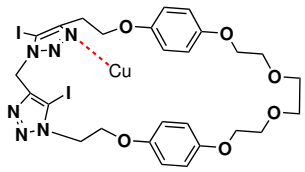	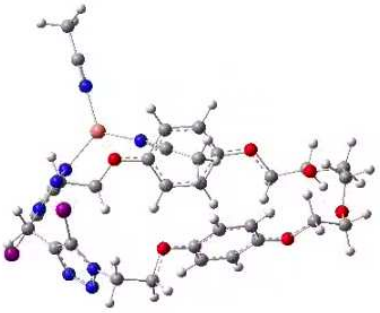	1.8
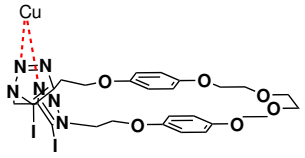	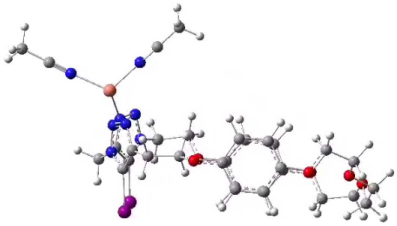	2.8
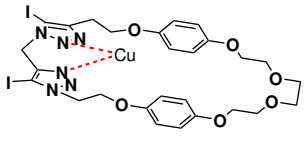	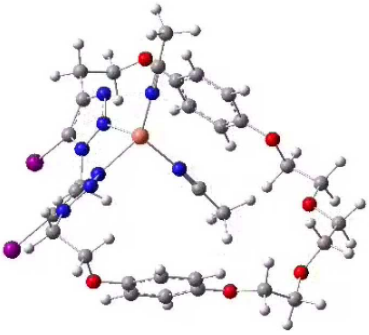	3.4
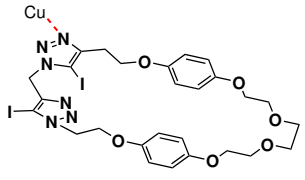	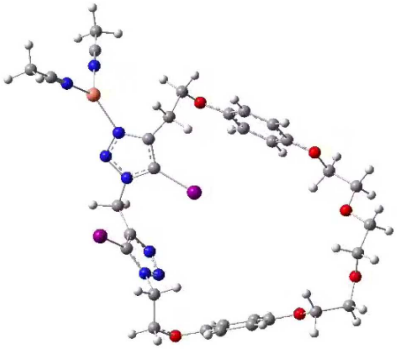	16.3

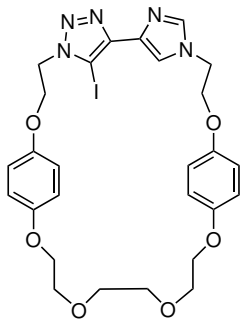

Figure 3.6: Imidazole-iodotriazole macrocycle.

From the three minimal geometries found for the macrocycle in Figure 3.6, there is a small energetic preference for bidentate Cu^{I} binding, but again, the energy difference between endotopic and exotopic conformations is very small (Table 3.5). From the structure it is easy to see that the imidazole-triazole unit is capable of acting as an almost entirely unhindered rotor at the top of the macrocycle. The consequent absence of an energetic preference for endotopic or facial binding modes is born out by the experimental data, with $<$3% yield in AT-CuAAC reactions observed from crude reaction mixture ^{1}H NMR data.

Table 3.5: Schematic and 3D representations of calculated minimal geometries for imidazole-iodotriazole macrocycle, ordered by energy.

Schematic Representation	3D representation	Relative Energy (kJ mol^{-1})
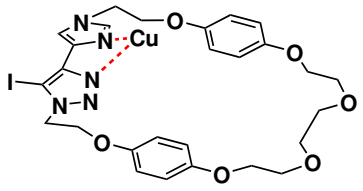	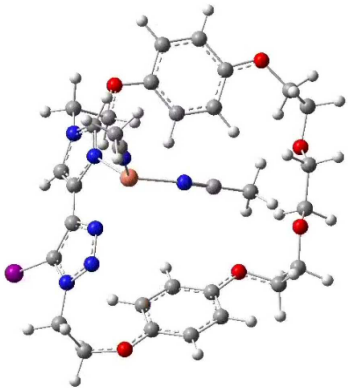	0
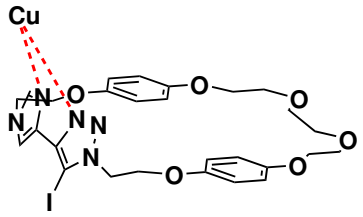	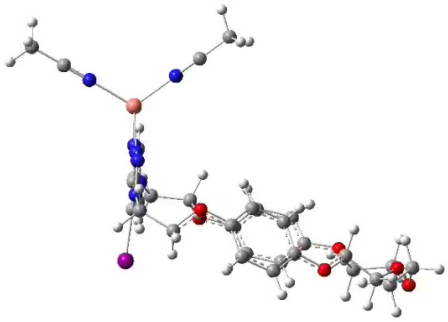	2.4
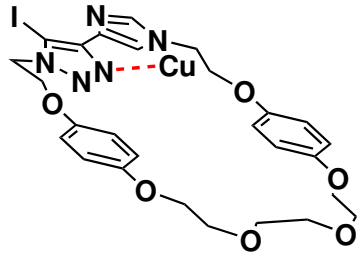	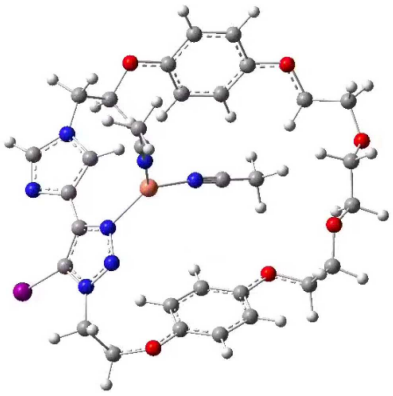	8.1

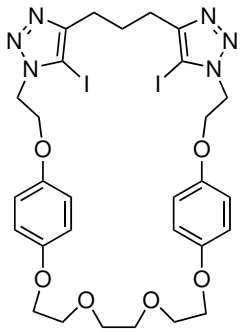

Figure 3.7: 1,3-bis(iodotriazole) propane macrocycle.

The two minimal conformations of the macrocycle in Figure 3.7 are identical in energy within error, with one appearing favourable for AT-CuAAC, being monodentate facial, while the the other is bidentate exotopic (Table 3.6). It is likely that the potential energy surface for this molecule is very flat, as for the previous structure, possessing little to no preference for the desired binding modes. Experimentally, this macrocycle has yielded no interlocked product on every AT-CuAAC reaction tested.

Table 3.6: Schematic and 3D representations of calculated minimal geometries for 1,3-bis(iodotriazole) propane macrocycle, ordered by energy.

Schematic Representation	3D representation	Relative Energy (kJ mol^{-1})
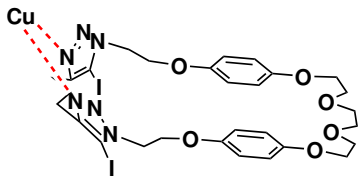	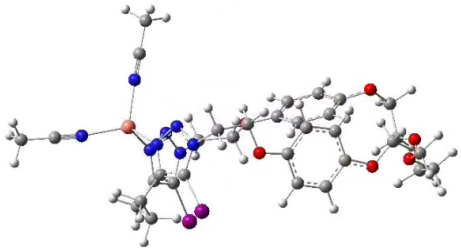	0
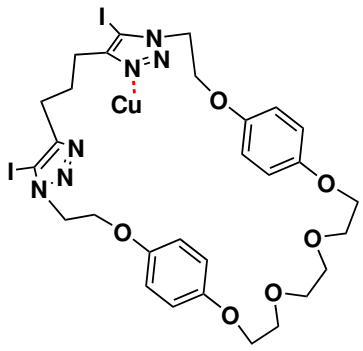	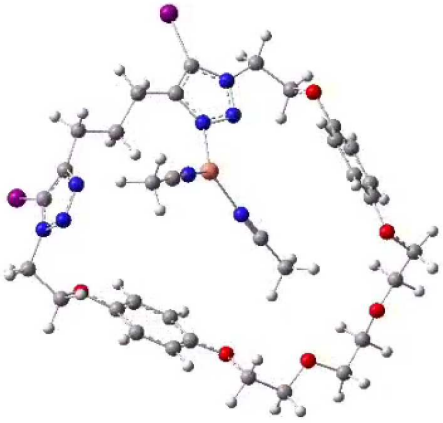	0.4

3.3.2 Comparison of Minimal Conformations and AT-CuAAC Yield

Table 3.7: Schematic and 3D representations of lowest energy conformations found for systems ordered by experimental AT-CuAAC performance.

Schematic Representation	3D representation	AT-CuAAC Yield
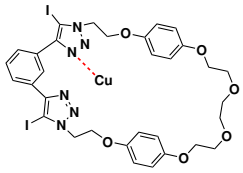	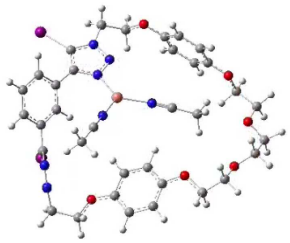	40%
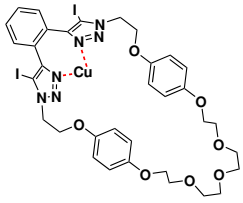	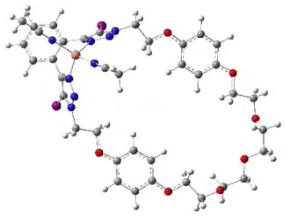	30%
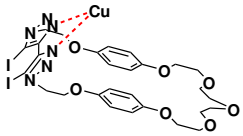	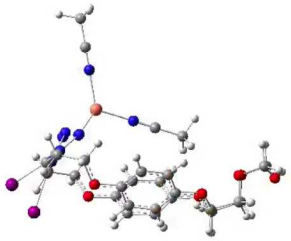	30%
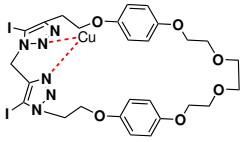	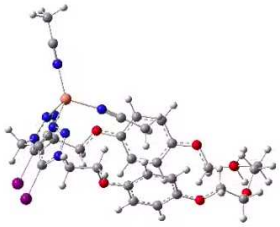	20%
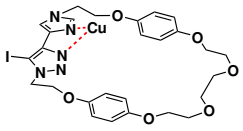	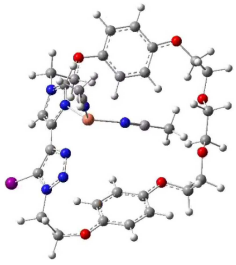	<3%
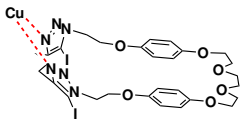	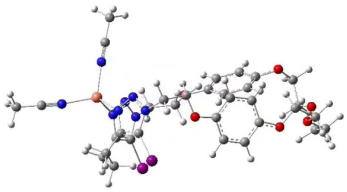	0%

Comparing the structures in Table 3.7 lends support to the hypothesis advanced earlier that energetic preference for an endotopic or facial binding mode is a key factor for AT-CuAAC success. One of the factors that seems to facilitate this preference is increased rigidity, with the macrocycles with more rigid precursor units showing greatest, and those with more unrestricted rotatable bonds showing least preference for these desired binding modes, a result mirrored by their performance synthetically. Computationally, another point to note about the more flexible systems beyond their flatter potential energy landscape, is that there is greater energetic variation in minimal structures observed due to PEG chain conformation, with the more rigid systems restricting PEG chain variation to as close to completely staggered as possible, as long as it results in no steric clash in the rest of the system. With these results as basis, hypothetical macrocycle structures which are equivalently synthetically accessible have been proposed and investigated, attempting to leverage the apparent structure-activity relationship information gleaned to improve the energetic preference for the desired endotopic binding mode. These prospective systems are designed with aromatic linkers between the triazoles at the 'top', for the additional rigidity granted, while varying the angle and distance of the triazole groups relative to each other.

3.3.3 Prospective Macrocycles

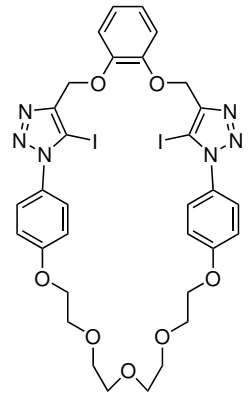

Figure 3.8: 1,2-hydroxymethyl benzene bis-iodotriazole macrocycle.

The two minimal conformations adopted by macrocycle Figure 3.8, which both bind Cu^{I} in a bidentate endotopic manner, differ by the absence of a CH_3CN ligand in the higher energy structure, which has adopted an approximately trigonal planar geometry about the Cu^{I} (Table 3.8). The energy difference between them being so small ($<$4 kJ mol^{-1}) suggests that the macrocycle is capable of accommodating the Cu^{I} endotopically over a range of positions and bite angles, with a tetrahedral bidentate mode being preferred, and that the minima found are at or close to the true minimum. This structure was discussed in Chapter 2, demonstrating some success in AT-CuAAC rotaxanation.

Table 3.8: Schematic and 3D representations of calculated minimal geometries for 1,2-hydroxymethyl benzene bis-iodotriazole macrocycle, ordered by energy.

Schematic Representation	3D representation	Relative Energy (kJ mol^{-1})
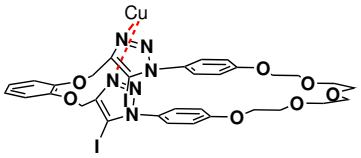	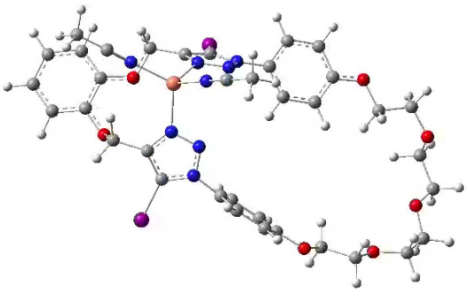	0
	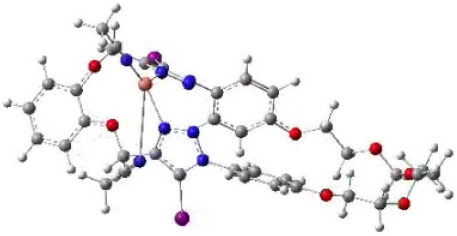	4.1

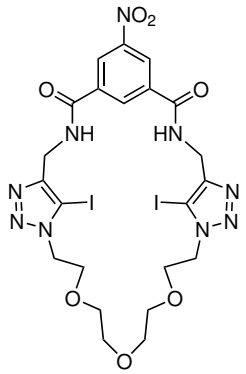

Figure 3.9: 5-nitroisophthalamide bis-iodotriazole macrocycle.

The minimal conformations of the macrocycle depicted in Figure 3.9, shown below (Table 3.9) occupy predominantly endotopic bidentate conformations which are approximately tetrahedral about Cu^{I}. The lowest energy conformation involves the coordination of three nitrogens in the macrocycle, two from the triazoles, both at the 3-position, and an amide nitrogen, with the final coordination site occupied by one of the two CH_3CN ligands. The chair-like and boat-like bidentate conformations above it in energy are comparable, possibly exhibiting a similar energetic hurdle to overcome for their interconversion. The highest energy conformation is also of note, as it appears to be stabilized by a σ-hole interaction between the endotopic iodine of one triazole and the adjacent 3-position nitrogen of the other, being 2.9 Å apart. The significantly different conformations at fairly similar energies indicate that there are multiple possible conformational barriers which must be overcome to reach the true minimum, but there is good agreement between the two lowest energy structures, so it is likely that they are close to it.

Table 3.9: Schematic and 3D representations of calculated minimal geometries for 5-nitroisophthalamide bis-iodotriazole macrocycle, ordered by energy.

Schematic Representation	3D representation	Relative Energy (kJ mol^{-1})
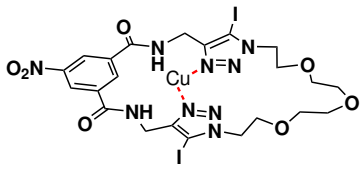	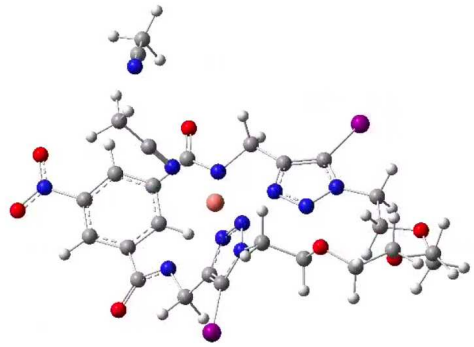	0
	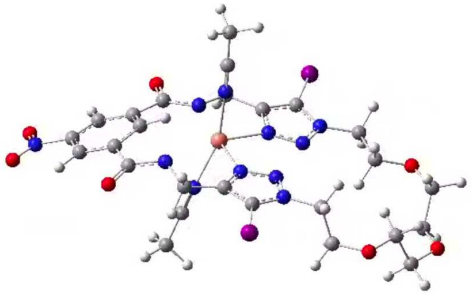	8.3
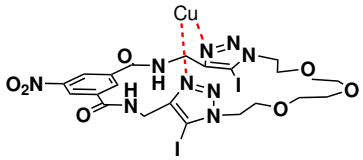	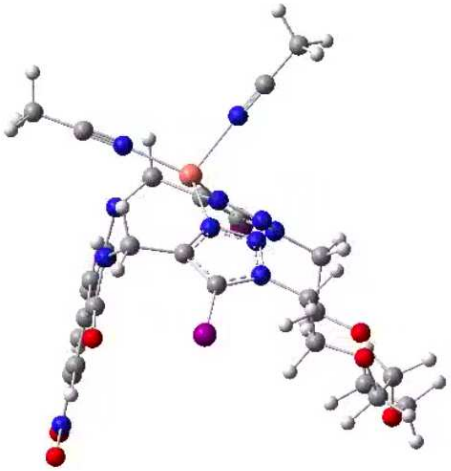	13.3
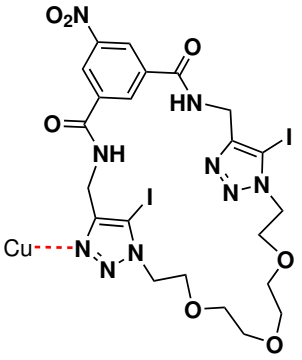	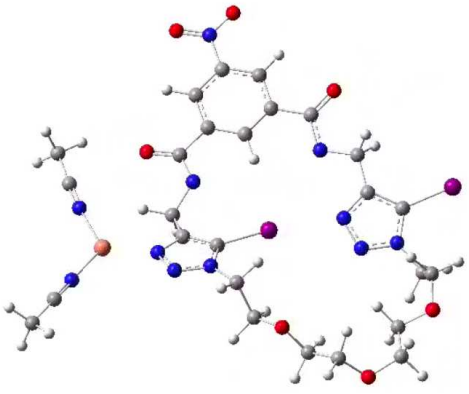	13.3

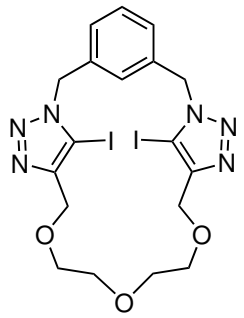

Figure 3.10: 1,3-bis(iodotriazolemethyl)benzene macrocycle.

The three minimal geometries of the macrocycle in Figure 3.10 shown below (Table 3.10) all exhibit facial or endotopic binding, with an indication of the facial binding conformation being preferred. The similarity of the two lowest energy conformations suggests that they are close to the true minimum, but the bidentate tetrahedral conformation being higher in energy implies an energetic cost associated with the contraction necessary to achieve it. Further evidence for this strain is the Cu–triazole bond being 0.2 Å shorter in the monodentate structure.

Table 3.10: Schematic and 3D representations of calculated minimal geometries for 1,3-bis(iodotriazoleomethyl)benzene macrocycle, ordered by energy.

Schematic Representation	3D representation	Relative Energy (kJ mol^{-1})
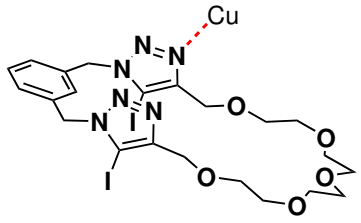	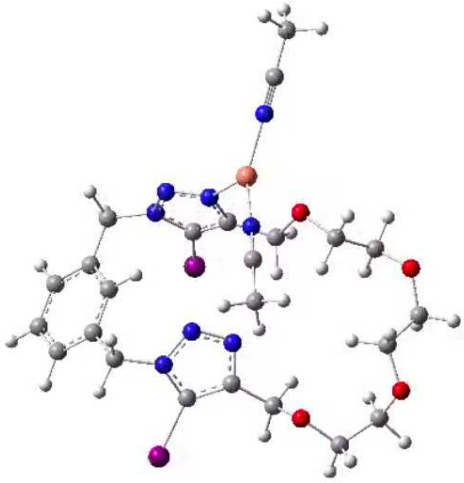	0
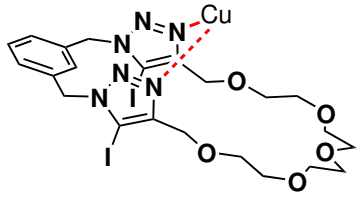	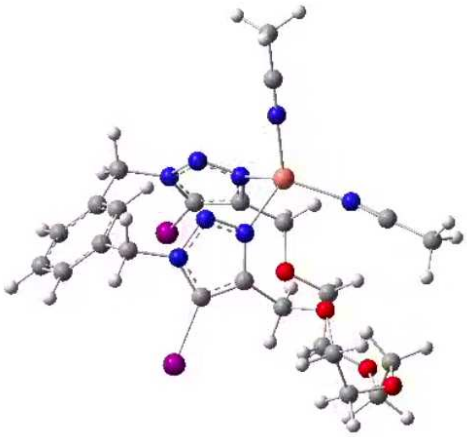	0.8
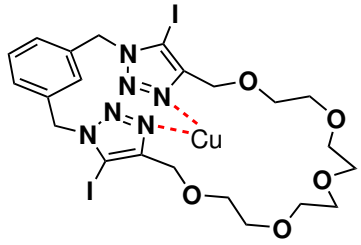	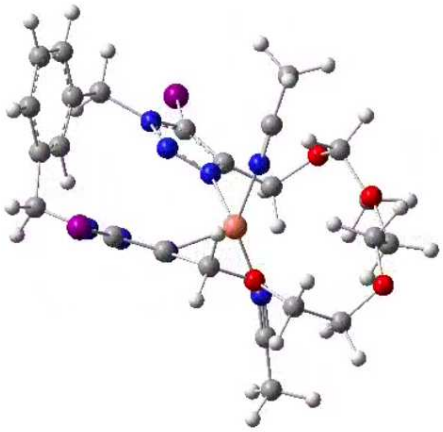	9.9

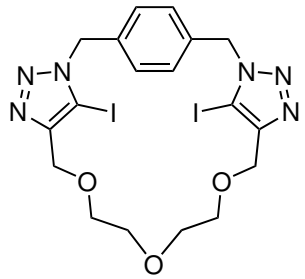

Figure 3.11: 1,4-bis(iodotriazolemethyl)benzene macrocycle.

The small energy differences found between the found minimal conformations for macrocycle Figure 3.11 below (Table 3.11) suggest the relative potential energy surface is quite flat, with possible preference for a facial bidentate binding conformation over an endotopic one. The exotopic conformation shown resulted from a starting conformation almost identical to it, implying a rotational energy barrier which prevents adoption of a bidentate binding mode. Unlike previously (Table 3.9), the iodine and nitrogen are too far apart for there to be much of an interaction ($>$3.9 Å) and offset, rather than coplanar.

Table 3.11: Schematic and 3D representations of calculated minimal geometries for 1,4-bis(iodotriazolemethyl)benzene macrocycle, ordered by energy.

Schematic Representation	3D representation	Relative Energy (kJ mol^{-1})
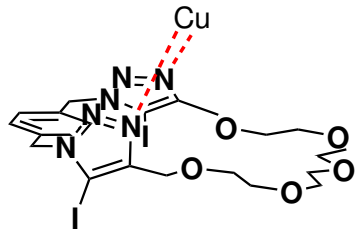	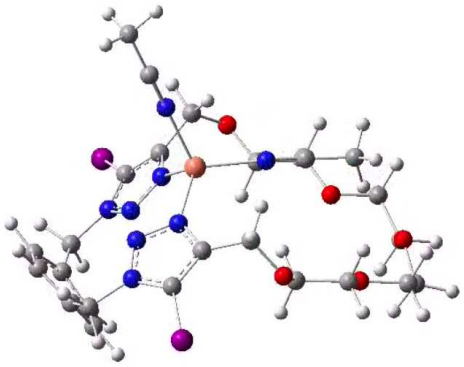	0
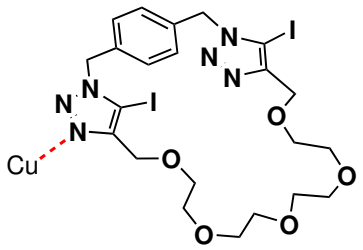	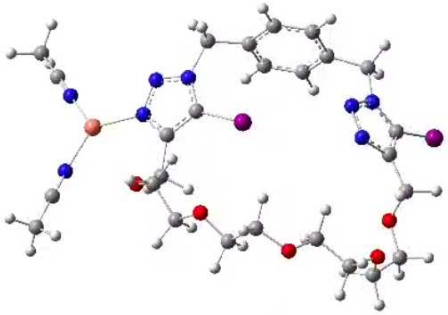	3.9
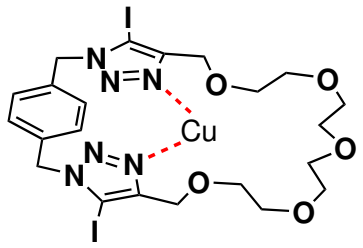	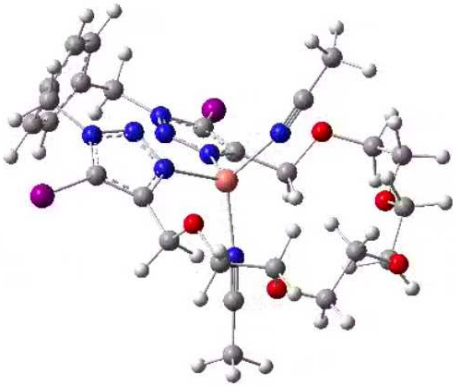	4.5

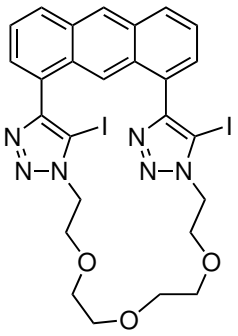

Figure 3.12: 1,8-bis(iodotriazole)anthracene macrocycle.

All of the minimal conformations found for the cyclic system in Figure 3.12 exhibit facial binding, predominantly bidentate, with the main structural differences lying in whether the macrocycle is in a boat-like or chair-like conformation, and whether the triazoles are syn or anti with respect to the iodines (Table 3.12). In a boat-like conformation, with the anthracene and PEG units pointing away from the face on which Cu^{I} is bound, it exhibits approximately tetrahedral geometry, whereas when the face is more crowded, an approximately trigonal planar geometry with the displacement of a CH_3CN results. The highest energy, monodentate, conformation is probably the result of restricted rotation of the iodotriazoles due to steric clash. The lower energy conformations showing good agreement and readily rationalized differences in their energies suggests the true minimum is close.

Table 3.12: Schematic and 3D representations of calculated minimal geometries for 1,8-bis(iodotriazole)anthracene macrocycle, ordered by energy.

Schematic Representation	3D representation	Relative Energy (kJ mol^{-1})
	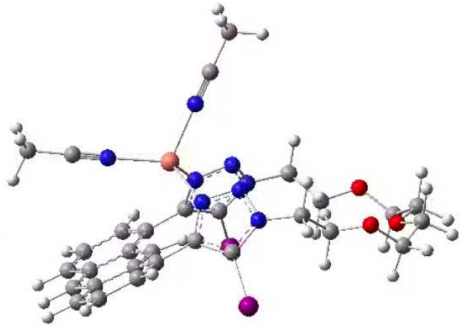	0
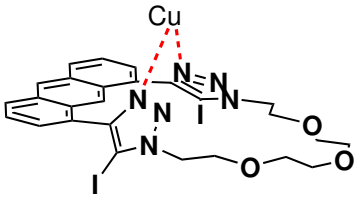	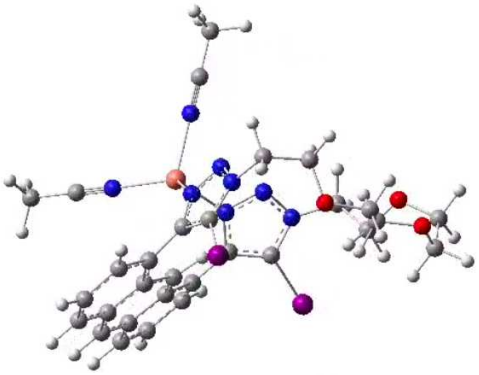	4.8
	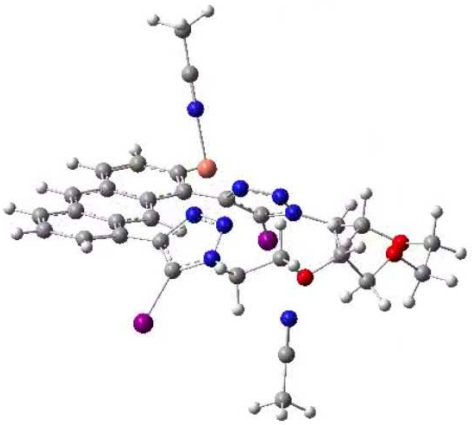	8.4
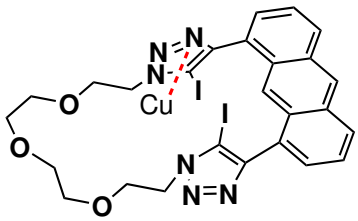	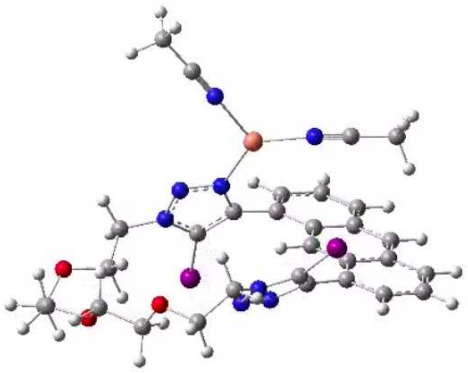	8.5

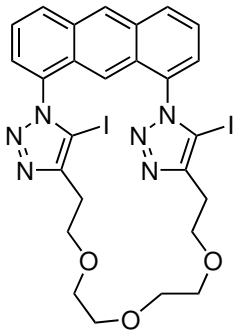

Figure 3.13: 1,8-N-linked-bis(iodotriazole)athracene macrocycle.

The similarity in energy ($<$4 kJ mol^{-1} difference in total) of the conformations found for macrocycle Figure 3.13 below (Table 3.13) suggests that the potential energy surface is quite flat, with facial binding modes again being the most common outcome, a likely result of the proximity of the two triazoles disfavouring an endotopic binding sterically. The restricted rotation suggested by the previous system is again visible, though in this case the anti conformation of iodotriazoles appears lower in energy. While it is difficult to say where the true minimum lies, all of the minimal conformations found seem well suited to AT-CuAAC rotaxanation by the criteria chosen.

Table 3.13: Schematic and 3D representations of calculated minimal geometries for 1,8-N-linked-bis(iodotriazole)anthracene macrocycle, ordered by energy.

Schematic Representation	3D representation	Relative Energy (kJ mol^{-1})
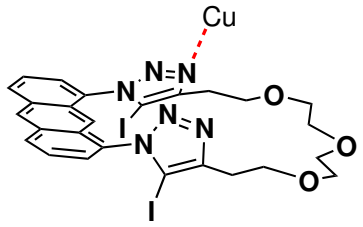	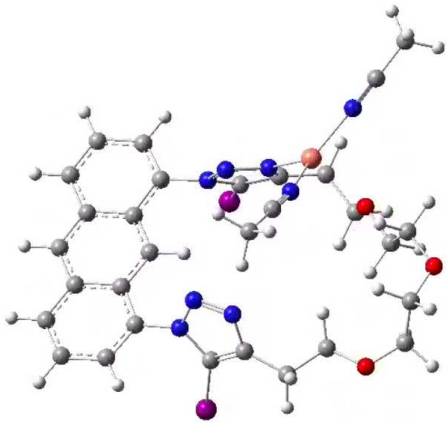	0
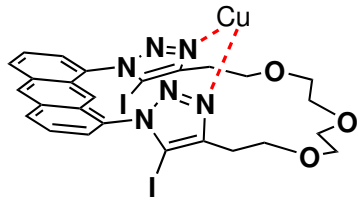	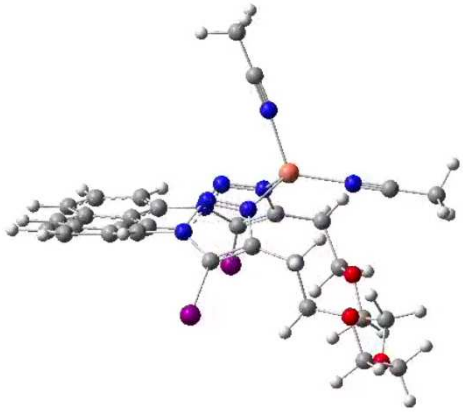	2.8
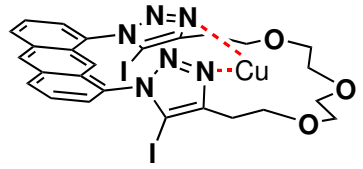	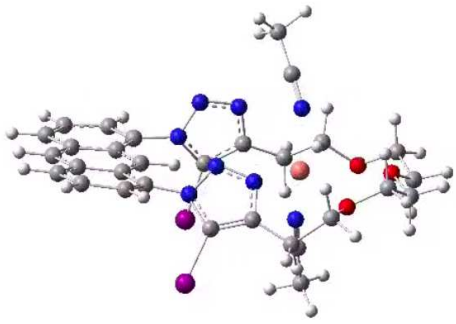	3.6

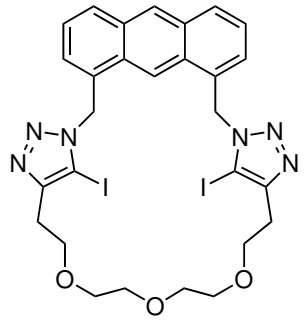

Figure 3.14: 1,8-N-linked-bis(iodotriazolemethyl)anthracene macrocycle.

Addition of a methylene spacer unit to the previous system as above (Figure 3.14) resulted in more diverse minimal conformations (Table 3.14), which again echoed the chair-like and boat-like conformations seen in the previous anthracene macrocycle (Figure 3.13). In this more flexible system, as previously, the boat-like conformation bent away from the face on which the Cu^{I} is bound is the lowest in energy, but the additional flexibility afforded by the additional methylene spacers allows a chair-like facial conformation of comparable energy. The true minimum is likely similar to these conformations, but may be difficult to determine due to conformational barriers as a consequence of the anthracene rigidity. The endotopic conformation is higher in energy, likely still due to steric clash as a consequence of the triazoles being too close to each other when required to remain coplanar. As in the 1,4-bis(iodotriazolemethyl)benzene system (Table 3.11) the persistence of a monodentate exotopic conformation indicates rotational restriction of the triazoles to some degree.

Table 3.14: Schematic and 3D representations of calculated minimal geometries for 1,8-N-linked-bis(iodotriazolemethyl)anthracene macrocycle, ordered by energy.

Schematic Representation	3D representation	Relative Energy (kJ mol^{-1})
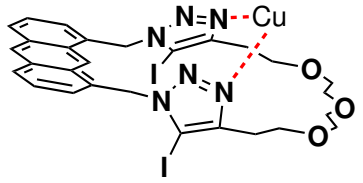	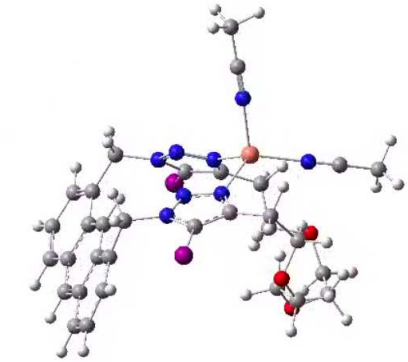	0
	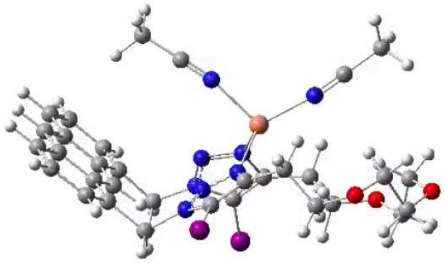	2.7
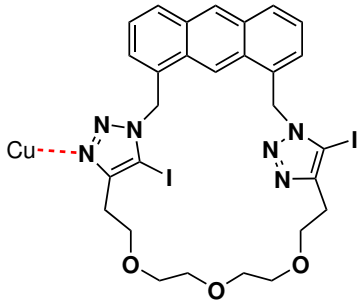	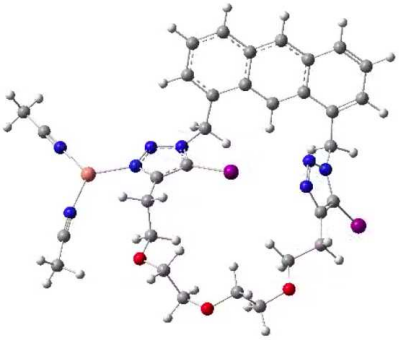	5.7
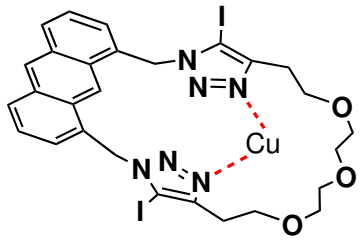	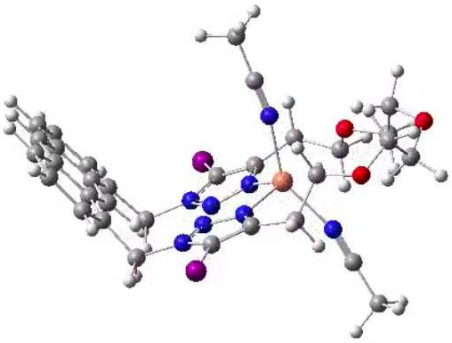	8.5

3.3.4 Comparison of Novel Macrocycle Conformations

Table 3.15: Schematic and 3D representations of minimal conformations found for novel systems inspired by known good AT-CuAAC candidates, ordered by apparent favorability.

Schematic Representation	3D representation
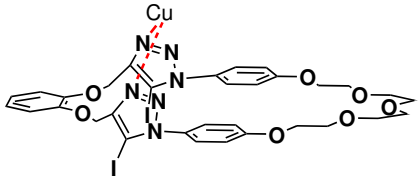	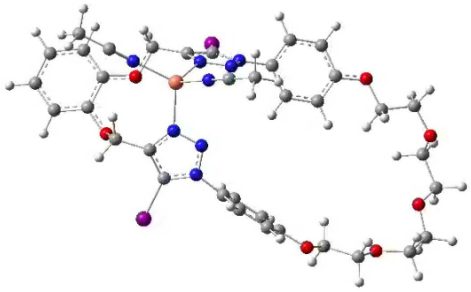
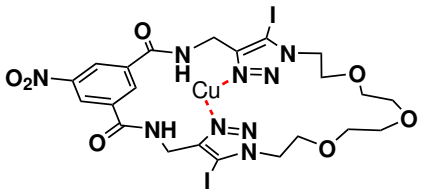	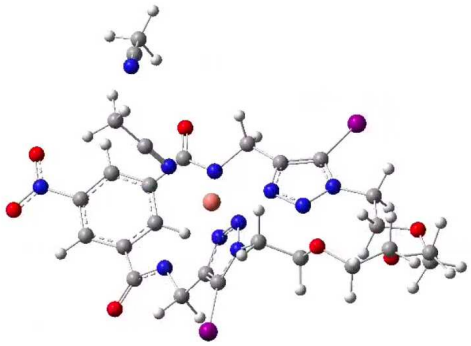
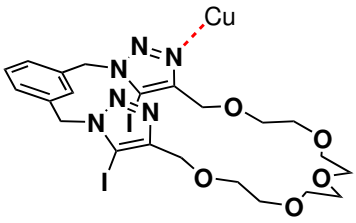	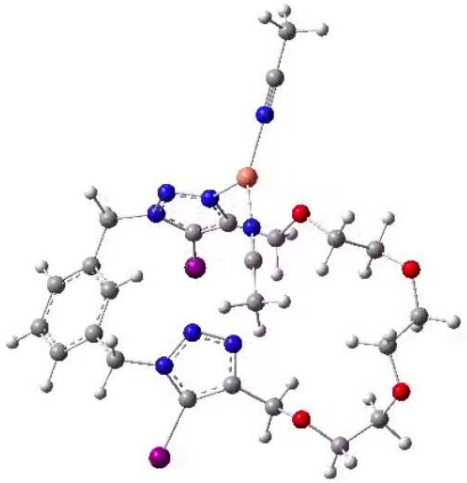
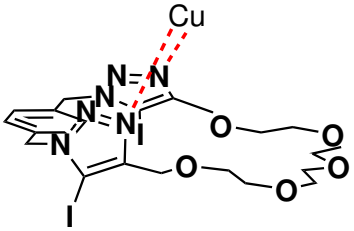	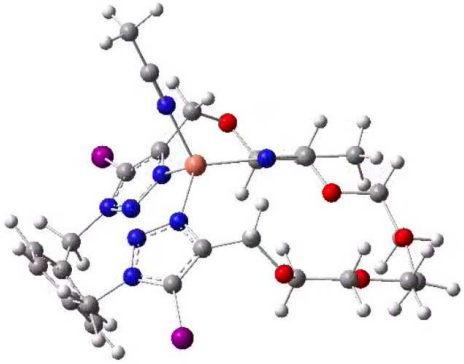

Most of these structures have an additional methylene linker compared to the 1,3-bis-iodotriazole benzene based system (Table 3.1), which seems to provide sufficient conformational flexibility to increase the likelihood of bidentate approximately tetrahedral binding of Cu^{I} being favoured, albeit at the cost of decreased certainty of the true minimal conformation. The central rigid aryl element seems an effective way of restricting free rotation of the triazoles, with exotopic conformations only observed when systems were capable of flexing to afford them 180° connections to the rest of the molecule, as for the 5-nitroisophthalamide bis-iodtriazole macrocycle (Table 3.9) and 1,4-bis(iodotriazolemethyl)benzene macrocycle (Table 3.11). The systems with reversed triazole connectivity (Table 3.10, Table 3.11, Figure 3.13 and Figure 3.14) allow the 3-position nitrogen donor to point down into the main volume of the macrocycle cavity, which potentially offers a route to low energy endotopic conformations, enabling the CH_3CN units, here serving as proxy for half-axle components, less steric constraint.

Table 3.16: Schematic and 3D representations of minimal conformations found for rigidified novel systems.

Schematic Representation	3D representation
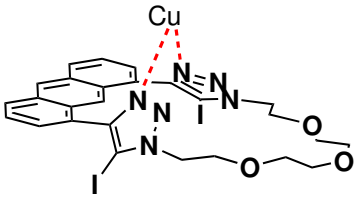	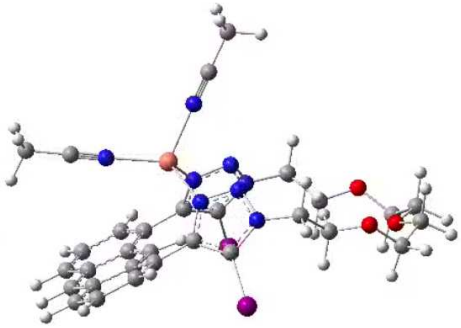
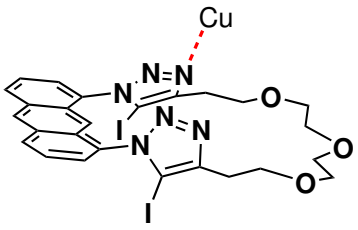	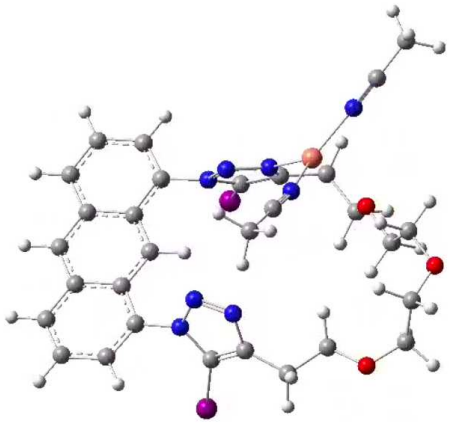
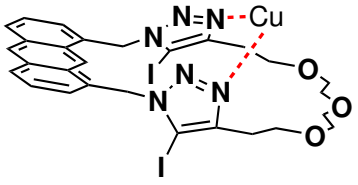	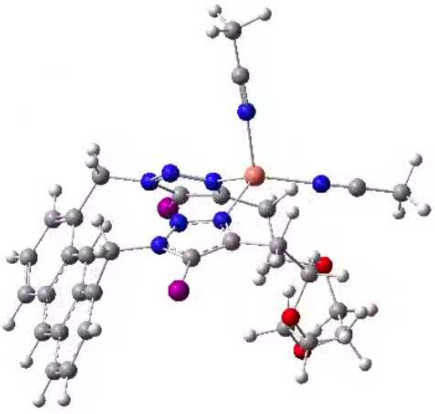

Taking the opposite approach and rigidifying the system further with an anthracene moiety produces conformational outcomes more closely resembling the 1,2-bis(iodotriazole)benzene system (Table 3.2). Here, because of steric constraints, facial conformations are predominant, again, almost all bidentate and approximately tetrahedral about Cu^{I}. The large planar anthracene also results in surprisingly consistent mimicry of the conformations of cyclohexane, a property that could probably be exploited with further tuning to favour potentially productive binding modes in AT-CuAAC. A potential issue with the boat-like conformations is that they risk blocking the approach of half-axle components on one side, but this is not determinable within the scope of this pilot computational investigation.

Another phenomenon only observed with these potential novel macrocycles is the displacement of a CH_3CN ligand due to the stricter geometric demands enforced. Interestingly, the addition of the two methylene spacers (Table 3.14) is sufficient for this to cease for the anthracene-based systems, but further sampling of the conformational space is required to have confidence in this behaviour being significant.

3.4 Conclusions

The work in this chapter sought to determine if there was correlation between AT-CuAAC rotaxanation experimental yields and minimal conformations found using gas-phase DFT calculations for systems consisting of a $[Cu(CH_3CN)_2]^+$ unit and the macrocycle in question. If correlation was found, an attempt to quantify it would be made. The expectation of correlation was predicated on the hypothesis that to a first approximation, the efficacy of a macrocycle in AT-CuAAC rotaxanation reactions can be determined by inspection of its preference for endotopic Cu^I binding. This correlation was sought to enable fast, accessible screening of potential macrocycles for use in generating interlocked anion hosts via AT-CuAAC rotaxanation.

First, the energy differences between most of the minimal conformations found are insufficient to draw any concrete or quantifiable conclusions on macrocycle preference for AMT. In most cases under the conditions considered, the potential energy surface in the region sampled by the starting conformations is flat, reflecting the lack of driving factors beyond structural restriction, such as solvation, in driving macrocycle conformational preference. With these factors missing, it is possible that some systems appear less favorable than the solvated reality, but crucially this outcome supports the goal of minimizing false positives.

Looking at the outcomes qualitatively, the structures of the known macrocycle minimal conformations correlate with the experimental results, where macrocycles that favoured endotopic Cu^I-complexed minimal conformations over facial and exotopic ones, and those with fewer, more favourable, conformations displayed better AT-CuAAC yields. As such, it seems reasonable to conclude that this method can be used to order a series of prospective cyclic structures in likelihood of success, and so prove of value for screening. The speed of the method is good, taking less than a week to complete all calculation steps for each macrocycle, and is highly scalable, with the number of parallel investigations limited only by available nodes on the cluster.

A number of the prospective macrocyclic systems investigated seem promising, with several of those investigated apparently favoring endotopic conformations, especially those that contain a degree of rigidity due to the use of an anthracene unit, which is potentially a desirable inclusion that offers fluorescent reporting capacity to the target interlocked rotaxane host anion sensor.

3.5 Further Work

An obvious path to building on the value of this computational method in its current form is to synthesize some of the prospective macrocycles and determine their efficacy in the AT-CuAAC reaction. Good candidates for synthesis and testing are macrocycles shown in figures Figure 3.9 and Figure 3.10, the former as it uses chemistry and synthons already established within the group, having been initially validated for anion binding, and the latter which allow inspections of the effect of swapping the connectivity of the triazoles in AT-CuAAC and anion binding. A synthetic route for the nitroisophthalamide-based macrocycle is proposed below (Figure 3.15) with yields stated where known.

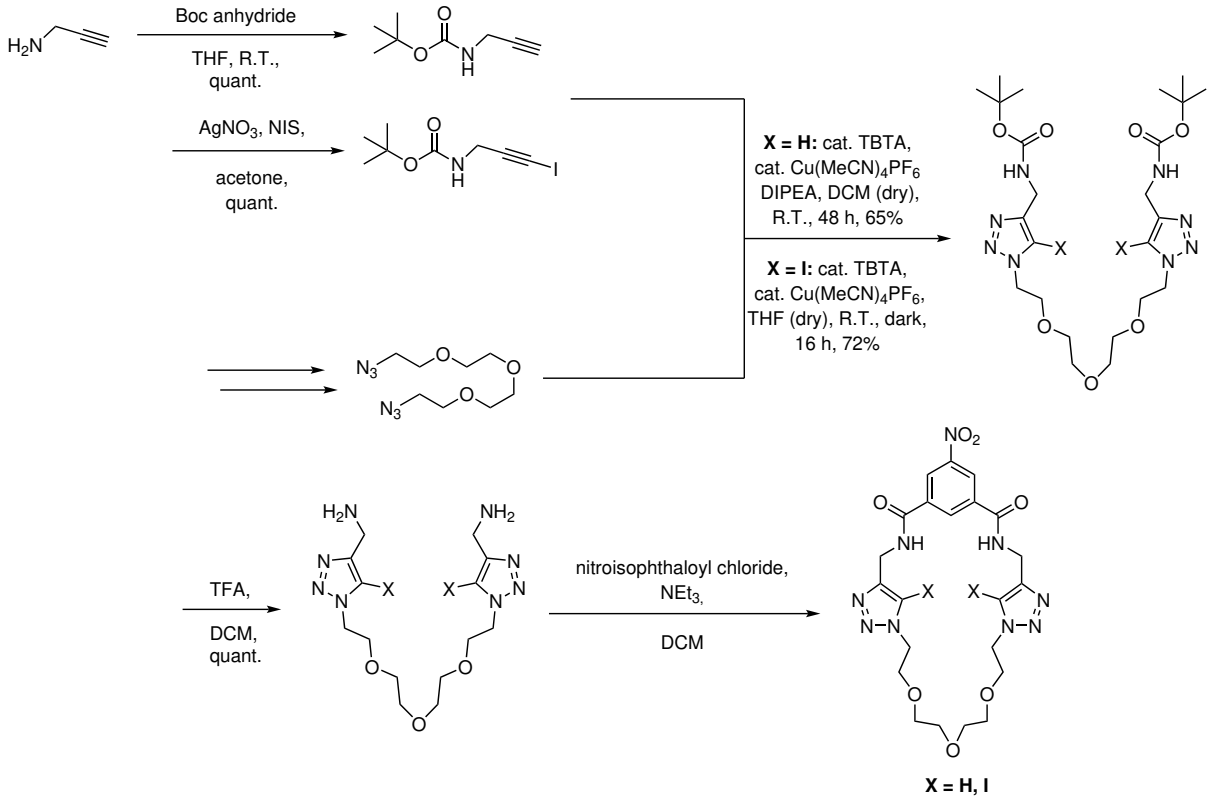

Figure 3.15: Proposed synthetic route to novel nitroisophthalamide-based macrocycle.

The second path to follow is to increase the fidelity of the simulated systems and see what effect this has on evaluating outcome. This has two major component steps: Gas-phase simulation of simplified half-axle components interacting with a Cu^{I} species bound in a variety of conformations by a macrocycle, and molecular dynamics (MD) simulations of simple macrocycle-ligated Cu^{I} systems, as a precursor to MD simulation of the transition state itself. This greater fidelity comes at the cost of significant computational time, but would enable inspection of the impact of solvent effects on macrocycle conformation while ligating Cu^{I}.

Chapter 4

Investigation of bis-triazole macrocycle ring-size in AT-CuAAC [2]rotaxane formation

4.1 Introduction

This chapter discusses efforts to establish a relationship between macrocycle ring-size and AT-CuAAC rotaxanation yield, ultimately aiming to investigate the subsequent impact on the anion binding properties of the [2]rotaxane host product containing the bis-triazole macrocycle component. Contrary to initial expectations, a recent paper by Goldup and coworkers observed improved AT-CuAAC yield on decreased macrocycle ring size with a simple bipyridine-containing macrocycle (Scheme 4.1).[201]

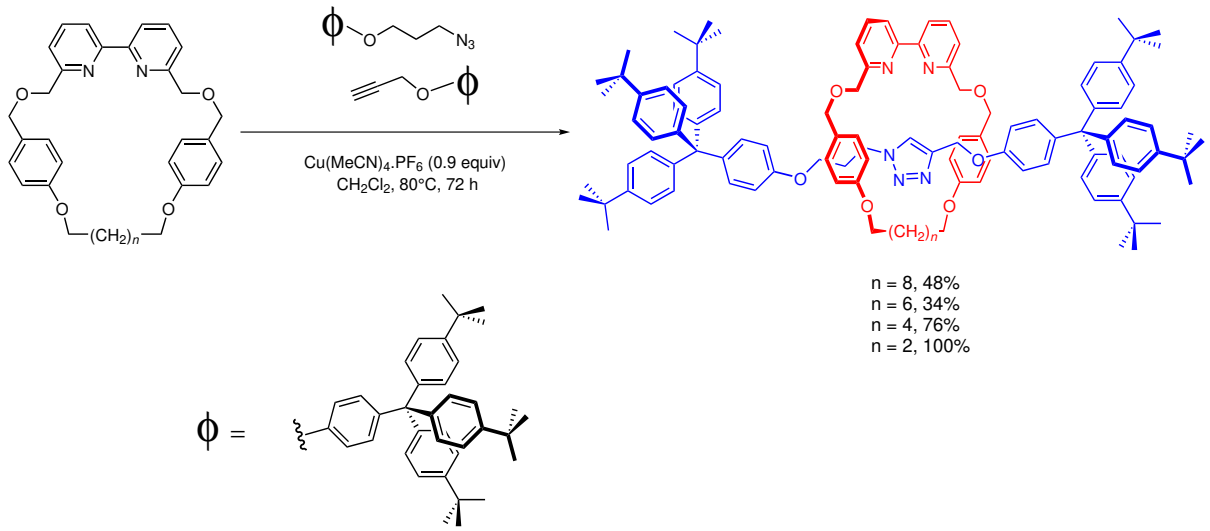

Scheme 4.1: The first macrocycle observed to display macrocycle ring-size dependent AT-CuAAC rotaxanation yields.

Subsequent work by the same group exploring the anomalous yield for n = 8 determined that macrocycle ring-size altered the mechanism of the AT-CuAAC reaction: smaller macrocycles were seen to favour a monometallic pathway, and larger macrocycles a bimetallic one, impacting relative rates of productive rotaxane and unproductive axle outcomes as a consequence. This phenomenon was behind the elevated yield of the n = 8 macrocycle: it was large enough to favour the bimetallic pathway, where the others favoured the monometallic one.[330]

A recent review describes the AT phenomenon as kinetically driven, with the yield of the interlocked product and free axle dependent on the pre-equilibrium between the starting materials and activated complexes, their relative rate of progress toward products, and any competing background reactions, much as in a catalytic process (Figure 4.1). This relationship is summarized in equation 4.1.

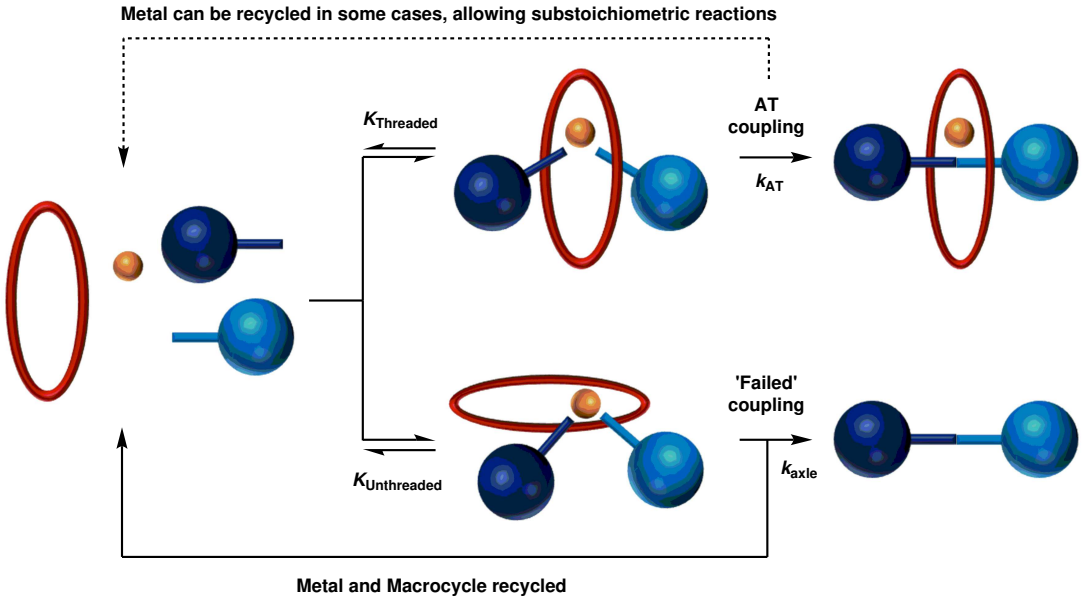

Figure 4.1: Schematic representation of the AMT approach to rotaxanes, showing key steps that determine selectivity.

$$\frac{Rotaxane}{Axle} = \frac{k_{AT}K(Threaded\ Complex)}{k_{axle}K(Unthreaded\ Complex)} \tag{4.1}$$

In this review, the authors also highlight the need for further study into this macrocycle size-dependent yield phenomenon, to establish whether observations to date were system specific or more generalizable.[355] Determining whether these reported trends in macrocycle ring size-dependent rotaxanation yield hold with different binding motifs and macrocycle structures, especially with additional functionality for purposes such as anion recognition, is of particular relevance to our group, and other groups seeking to use AT-CuAAC reactions as a route to interlocked structures for organocatalysis for example.

The work in this chapter builds on the observations and results of the preceding chapters in an effort to better understand how to exploit the fidelity and advantage of AT-CuAAC methodology for the construction of interlocked halogen bonding anion hosts. Chapter 2 focused on the exploration of hypotheses concerning the impact of macrocycle flexibility on AT-CuAAC yield through novel motifs, while Chapter 3 sought to shed light from a different angle, through a simplified computational approach exploring the effect of structural changes on Cu^{I} binding geometries, considered alongside experimental AT-CuAAC yield data. Both chapters indicated that a predominantly rigid Cu^{I} binding motif was preferable, as it allows direct control of binding geometry through chemical design, rather than indirect control through conformational equilibria. A fully rigid binding motif could be viewed as an extreme case, in which the problem of designing a motif for high-yielding AT-CuAAC reactions and subsequent anion binding is reduced to achieving a good balance between the respective steric and electronic demands of these two binding modes.

In order to minimize potential solubility issues as observed in Chapter 2, the decision was made to start from a 1,3-bis(iodo)triazole benzene motif that had already seen use in standard AT-CuAAC rotaxanation conditions with a broad range of axle precursors (see Scheme 4.2 for example), with the interlocked products shown to be capable of the strong binding of a variety of anions.[319]

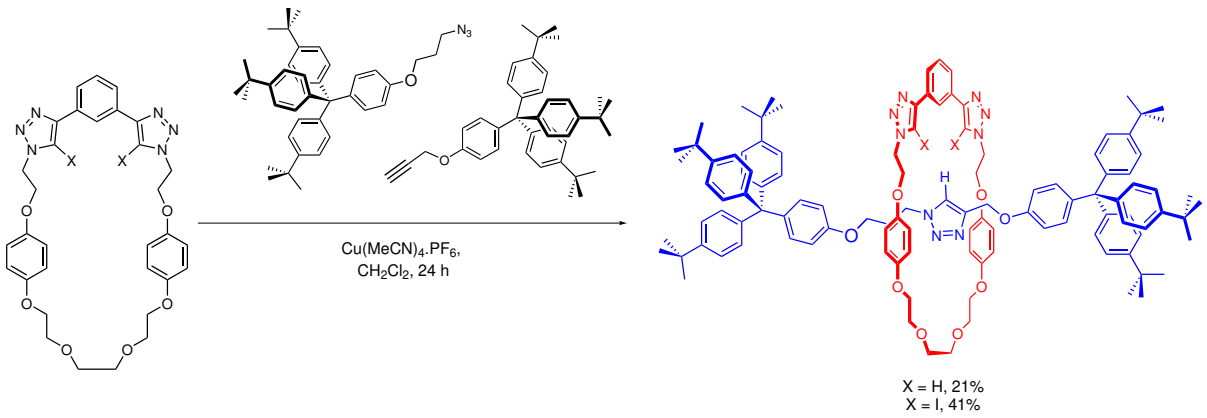

Scheme 4.2: Previous syntheses of [2]rotaxanes incorporating the 1,3-bis(iodo)triazole benzene motif.

4.2 Chapter Aims

A series of reduced ring-size 1,3-bis(iodo)triazole benzene macrocycles were targeted (Figure 4.2) for AT-CuAAC rotaxane synthesis. A comparison of isolated interlocked product yields would then provide evidence for macrocycle size dependence. The resulting rotaxane hosts could then also be evaluated for any size dependent trends in their anion binding properties.

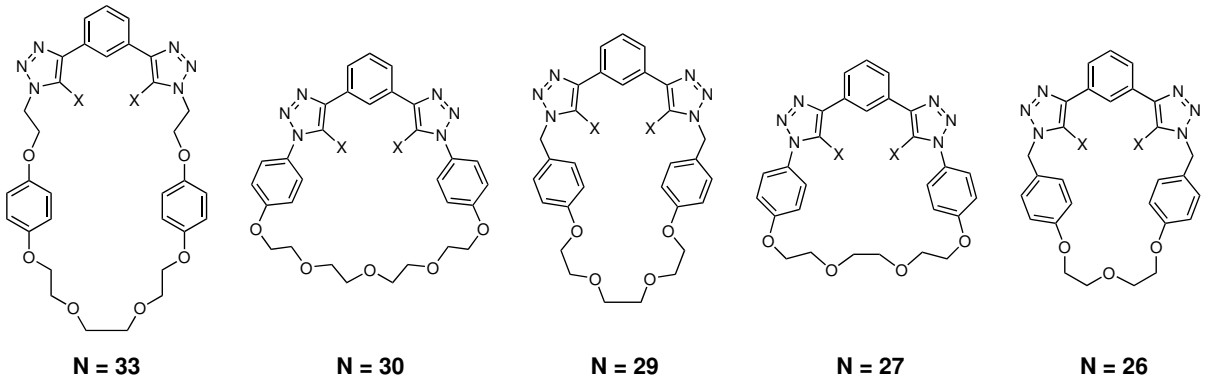

Figure 4.2: Diminished ring size targets incorporating the 1,3-bis(iodo)triazole benzene motif, with accompanying macrocycle ring size, original macrocycle shown for comparison on far left. X = H, I.

4.3 Synthesis of Smaller Ring-size 1,3-bis(iodo)triazole Benzene Containing Macrocycles

4.3.1 Design and Rationale

The geometry of the 1,3-bis(iodo)triazole benzene motif is better suited to anion binding than Cu^{I}-binding. Evidence for this comes from ^{1}H NMR, crystallographic and computational data which all indicate that the Cu^{I}-binding interaction can only be with the nitrogen donor of one triazole at a time, as they are too far apart to bind in a bidentate fashion. With solubility issues having caused problems in successful [2]rotaxane synthesis and isolation in Chapter 2, there was concern that decreasing the length of the solubilising PEG chain at the bottom of the macrocycle to afford a diminished circumference would result in the same outcome. To preempt this, and maximise the PEG chain length, the diminished ring-size 1,3-bis(iodo)triazole benzene macrocycles chosen saw the central benzene unit directly attached *via* triazoles to phenyl and benzyl motifs, with the macrocycle completed by 3-, 4- and 5-oxygen polyether chains Figure 4.3. The additional methylene spacers of the latter macrocycle contrast the relatively more rigid triazole-aryl conjugated covalent linkage of the first design, which should exhibit greater resistance to rotation as indicated in Figure 4.3.

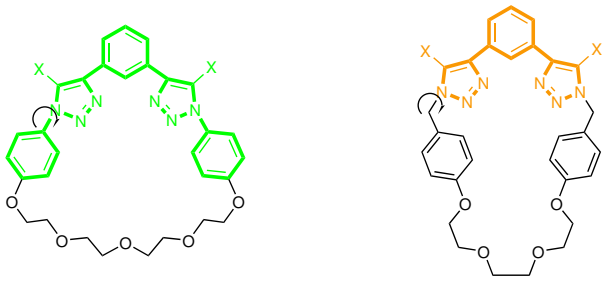

Figure 4.3: Target diminished ring-sized 1,3-bis(iodo)triazole benzene macrocycles.

4.3.2 Synthesis

The same synthetic protocol as established in Chapter 2, using a CuAAC reaction in the cyclisation step, was adopted for these macrocycle syntheses. The necessary precursors were synthesised using previously discussed methods (Scheme 4.3). The bis-azide precursors were prepared by reaction of di- and triethylene glycol with tosyl chloride under basic conditions in dry THF to afford the corresponding bis-tosylates, isolated by column chromatography. These bis-tosylates were subjected to a double Williamson etherification reaction with 4-iodophenol or 4-hydroxybenzyl alcohol, and the resulting compounds **26**, **27**, **48** and **30** were isolated by column chromatography. Subsequent Ullmann-type coupling of **26** and **27** with NaN_3, catalysed by a Cu^I/DMEDA complex gave the bis-azide precursors **28** and **29**. Compounds **48** and **30** were converted to bis-chlorides **49** and **31** using $SOCl_2$, followed by reaction with NaN_3 to give bis-azide precursors **50** and **32**. 1,3-Ethynyl benzene is commercially available, and the bis-iodoalkyne analogue **47** was prepared in 80% yield through Ag^I catalysed reaction with *N*-iodosuccinimide in an acetone:water mixture, which results in the target compound without further purification.

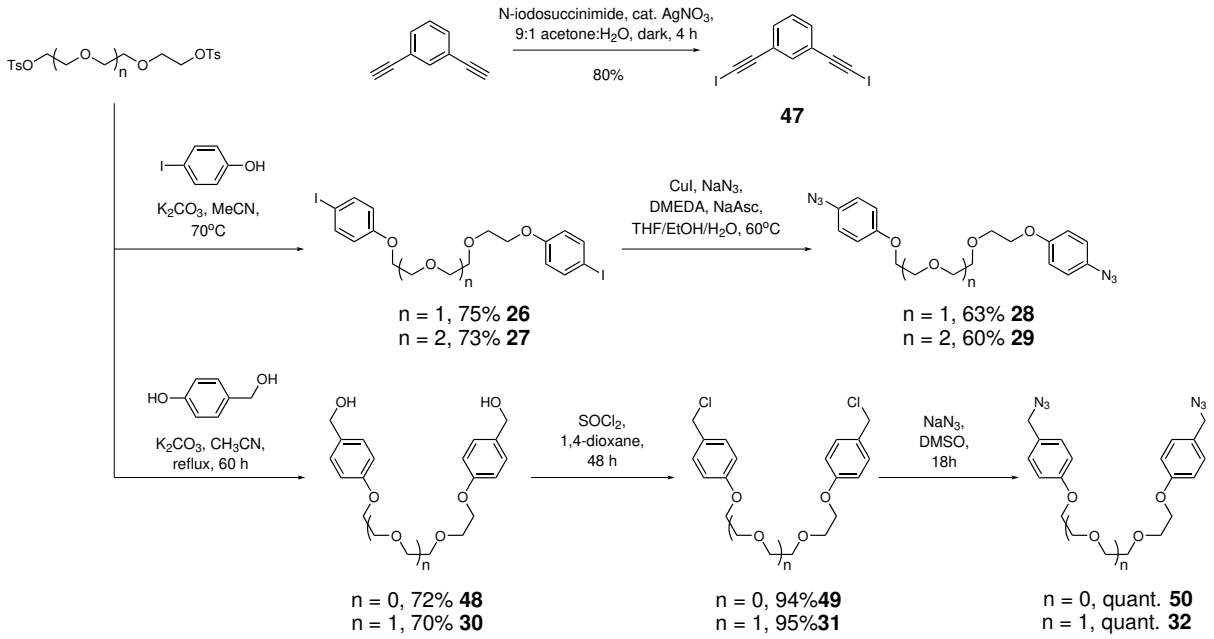

Scheme 4.3: Synthesis of bis-azide and bis-alkyne precursors.

Initial double CuAAC ring-closing reactions between aryl-azides **28** and **29** and the appropriate bis-alkyne were carried out in CH_2Cl_2 at 5 mM, in the presence of a catalytic amount of $[Cu(CH_3CN)_4]PF_6$ and TBTA (Scheme 4.4). ESI-MS analysis of the crude reaction mixtures after 24 and 48 hours showed no evidence of macrocycle formation.

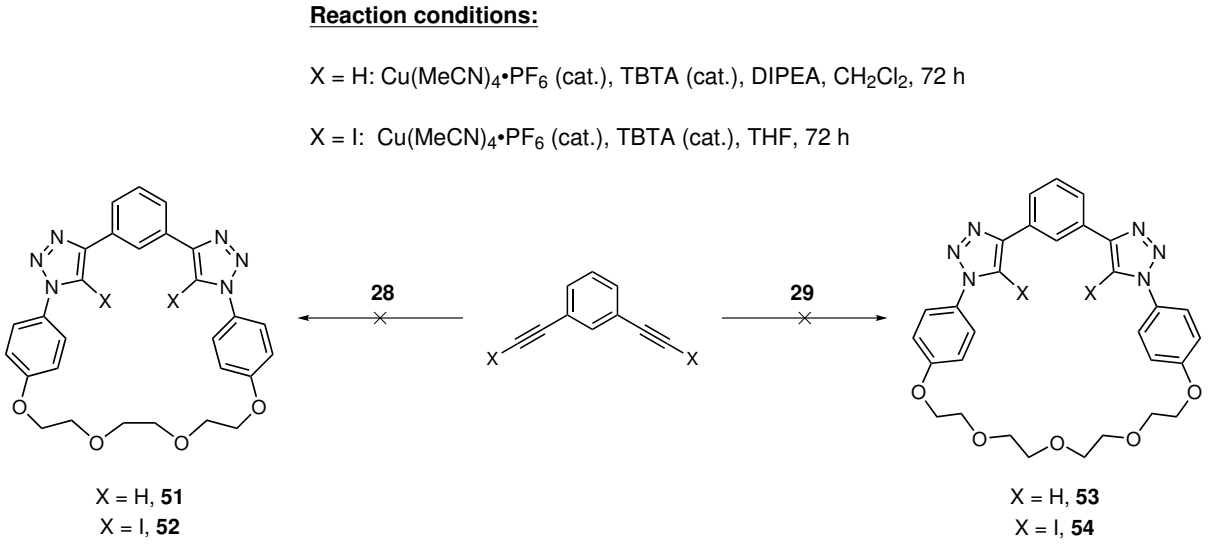

Scheme 4.4: Attempted synthesis of smaller ring macrocycles incorporating the 1,3-bis(iodo)triazole benzene motif.

After washing with NH_4OH/EDTA to remove the copper species, prep-TLC was carried out in order to identify side-products of the respective reactions. For the proto-reaction, the mixture proved inseparable, with mono-clicked product and unreacted azide identified from ESI-MS. Only starting materials were isolated from the corresponding iodotriazole reactions.

The presence of mono-clicked product, and no observable bis-clicked product in the protic systems suggests the electronics of the second click reaction are less favourable than the first, beyond the entropically disfavoured nature of the ring-closing step. While there are many mono-clicked, aryl-alkyne, aryl-azide examples in literature, there are only two prior bis-click examples, both simple acyclic bis-triazole molecules. One used a one-pot two-step process wherein phenylboronic acid was refluxed with NaN_3 and CuCl in methanol, subsequently adding 1,3-ethynyl benzene, $CuSO_4 \cdot 5\,H_2O$, Na_2CO_3, ascorbic acid and water and stirring for 24 hours at room temperature, resulting in a 45% isolated yield.[356] The second also followed a two-stage one-pot route, reacting bromobenzene in an Ullmann-type coupling with conditions as above, to which was added 1,3-ethynyl benzene, resulting in a 95% isolated yield after 24 hours stirring at room temperature.[357]

Examples of phenolic azide mono-clicked systems present in the literature are generally prepared by reflux in water:ethanol mixtures[358] or similarly forcing temperatures ($\geq$70°) in solvents such as DMSO[359] or glycerol.[360] Such high temperatures pose a concern during synthesis of the iodotriazole analogues, as iodo-alkynes do not tend to survive temperatures in excess of 60°C for extended time periods. An attempt was made to synthesise macrocycle **53** under the more forcing reaction conditions of higher temperature in THF, longer reaction time, and a stoichiometric amount of catalyst (Scheme 4.5). After workup, no macrocyclic product was isolated, only a mixture of mono-clicked product and unreacted azide.

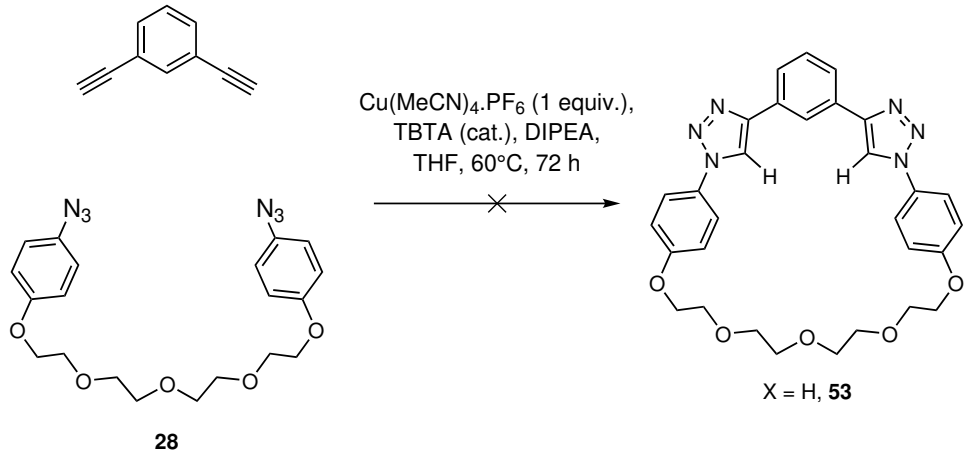

Scheme 4.5: Attempted synthesis of smaller ring macrocycle incorporating the 1,3-bistriazole benzene motif using aryl-azide and elevated temperature.

Alongside these efforts, double CuAAC ring-closing reactions were carried out using bis-azides **32** and **50**. With the former, after 24 hours ESI-MS analysis of the respective crude reaction mixtures showed evidence of both prototriazole **55** and **56** macrocycle formation. However, separating the macrocyclic product from the TBTA ligand again proved problematic. As a consequence, the reactions were repeated, using DBTA as the rate-accelerating ligand instead. Pleasingly, this time isolation proved straightforward by prep-TLC, resulting in good isolated yields of 37% for **55** and 25% for **56** (Scheme 4.6). Using these conditions with the smaller bis-azide precursor **50** also resulted in straightforward isolation of macrocycles **57** and **58** in similar yields of 41% and 28% respectively.

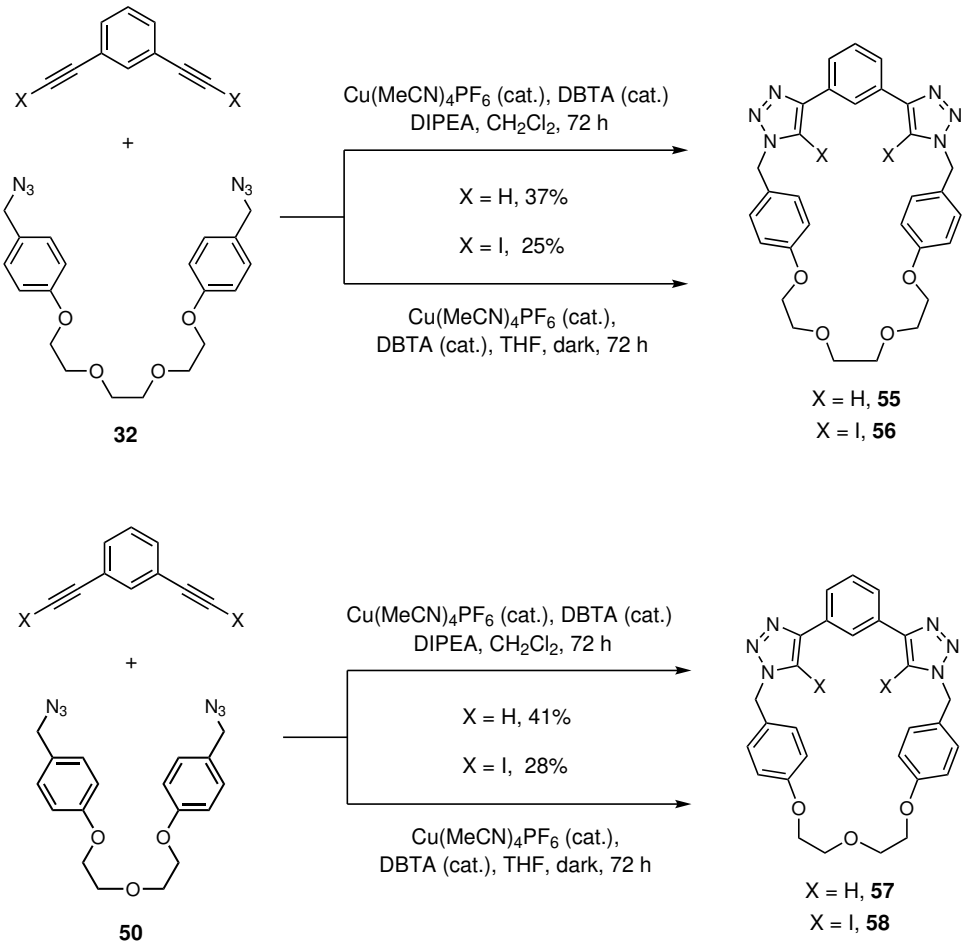

Scheme 4.6: Synthesis of smaller ring-size macrocycles incorporating the 1,3-bis(iodo)triazole benzene motif using alkyl-azide.

Macrocycles were characterised by ^{1}H NMR (Figure 4.4), ^{13}C NMR and high-resolution ESI-MS.

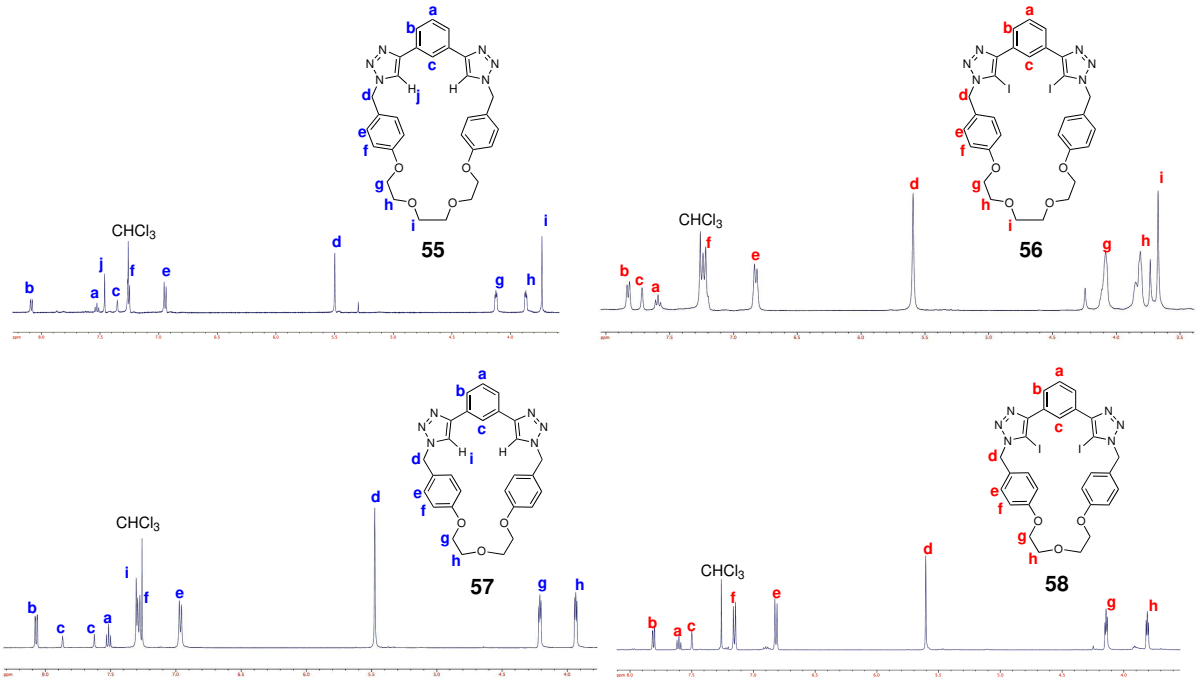

Figure 4.4: ^{1}H NMR characterisation data for reduced ring-size macrocycles incorporating 1,3-bis(iodo)triazole benzene motif ($CHCl_3$ T = 298 K).

4.4 AT-CuAAC [2]rotaxane Formation Investigation

4.4.1 Synthesis

Following repeat synthesis of the target macrocycles to accumulate enough material, AT-CuAAC rotaxanation reactions were undertaken using previously established conditions, adding a five-fold excess of azide **19** and alkyne **20** to a degassed CH_2Cl_2 solution of the respective macrocycle-Cu^I adduct (Scheme 4.7). Pleasingly, ESI-MS analysis of the crude reaction mixtures after 5 days indicated that all four test-scale AT-CuAAC rotaxanation reactions had been productive, with rotaxane $[M + H]^+$ peaks observed for all reactions: **59** $[M + H]^+$ = 1670, **60** $[M + H]^+$ = 1922, **61** $[M + H]^+$ = 1626 and **62** $[M + H]^+$ = 1877.

Purification by prep-TLC met with mixed results: for **59** isolation proved straightforward, yielding 16% of the pure [2]rotaxane. The halogen bonding analogue **60** had a very similar retention factor to the free macrocycle, but was eventually isolated in 9% yield. For both **61** and **62**, isolation was unsuccessful, with neither interlocked product found in the ^{1}H NMR spectra of the various fractions. This suggests rotaxanes **61** and **62** were formed in very poor yield, perhaps as a consequence of the decreased ring size. Unfortunately, insufficient free macrocycle was recovered from either reaction to undertake repeat rotaxanation attempts.

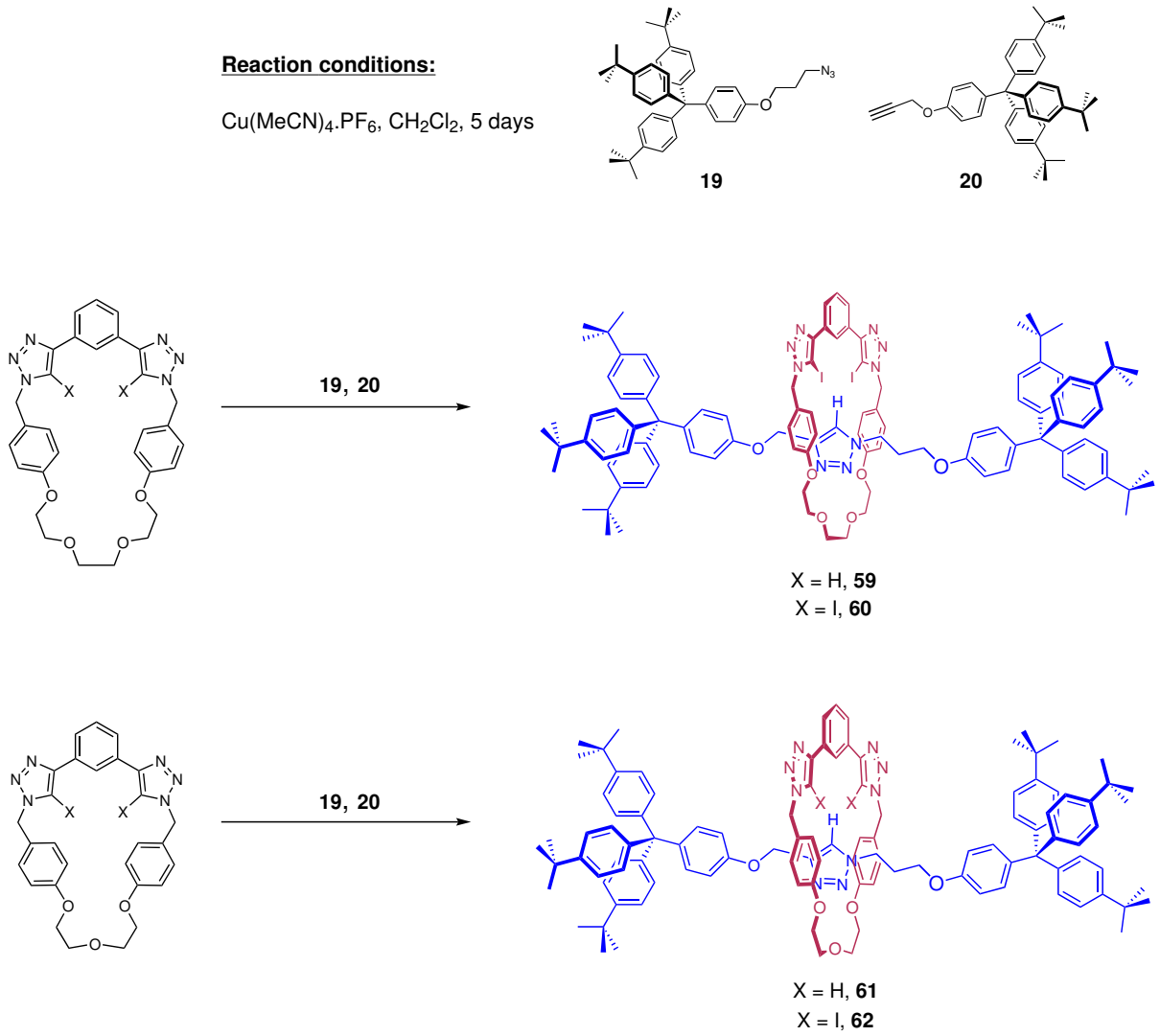

Scheme 4.7: Synthesis of [2]rotaxanes **59**-**62**.

^{1}H NMR, 2D ^{1}H–^{1}H ROESY spectroscopy and high-resolution ESI-MS data served to confirm the presence of interlocked product for both novel rotaxanes **59** and **60**. Partial ^{1}H NMR spectra together with free macrocycle and axle for comparison are shown below in Figure 4.5 and Figure 4.6 accompanied by the corresponding ^{1}H–^{1}H ROESY NMR and high-resolution ESI-MS data. Marked cross-peaks in the 2D ROESY spectra provide evidence of through-space interactions arising between the axle and macrocycle components in close proximity to each other, consistent with the interlocked nature of the [2]rotaxanes.

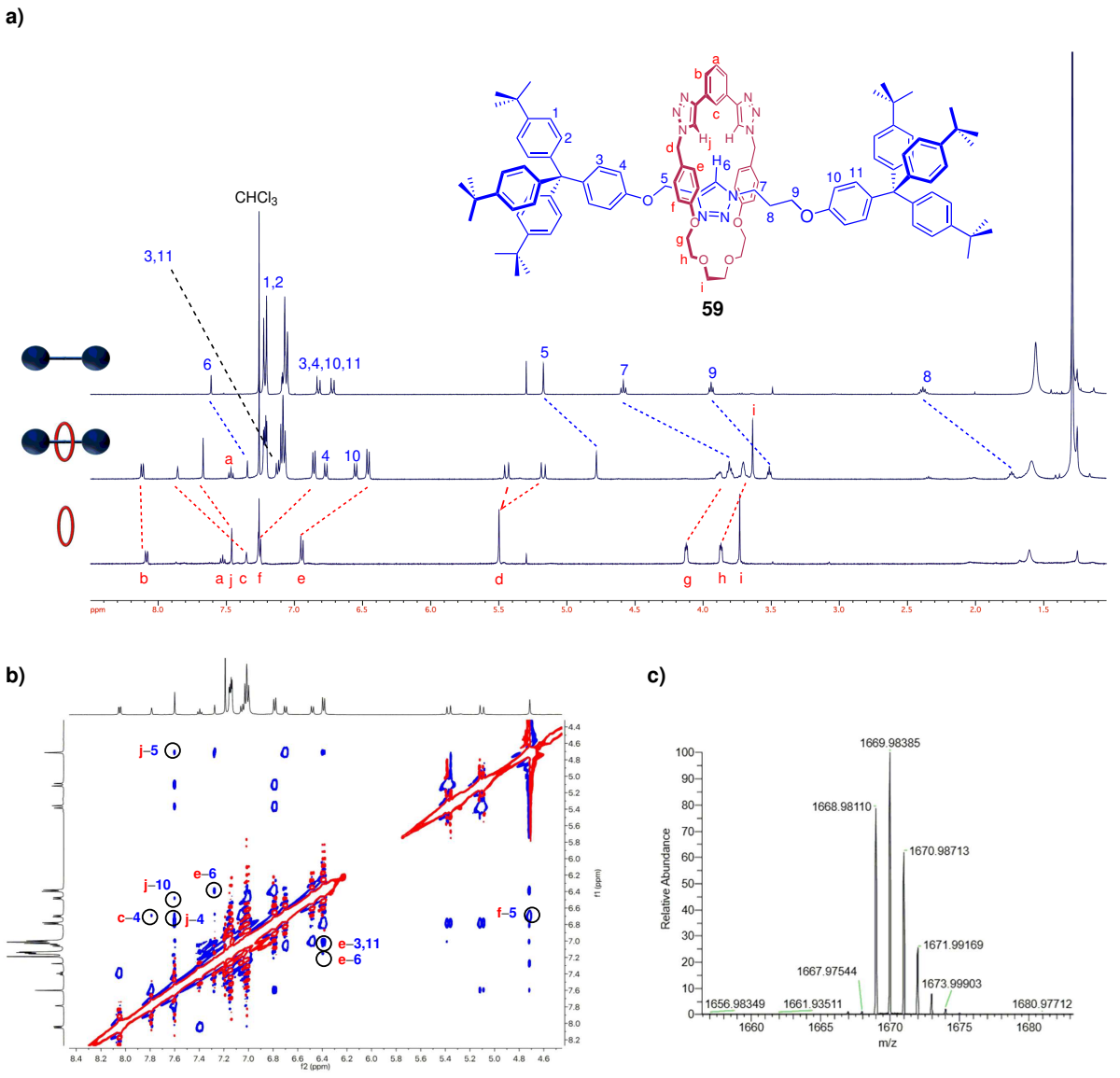

Figure 4.5: Characterisation data for [2]rotaxane **59**: a) Stacked plot of partial ^{1}H NMR spectrum of free axle (top), [2]rotaxane **59** (middle) and macrocycle **55** (bottom), b) partial 2D ROESY NMR spectrum of [2]rotaxane **59** (all in $CHCl_3$, T = 298 K) , and c) corresponding high-resolution ESI-MS spectrum.

There are several peak shifts compared to the free components worth noting in the ^{1}H NMR spectrum for **59** that indicate the successful formation of the interlocked product. The largest change is observed for methylene protons *d* of the macrocycle, which have moved upfield, and strongly split from a singlet in the free macrocycle into two environments (Figure 4.5a). The upfield shift is a reflection of the additional local electron density due to the axle, while the asymmetry of the axle in combination with the rigidity of the macrocycle (which leads to slow fluxion on the NMR timescale) explain the splitting. The effect of this asymmetry is magnified by the macrocycle apparently favouring a bent conformation, supported by interactions between macrocycle protons *c* and *j* and axle protons *4* and *10* (indicated in Figure 4.5b). The downfield shift of macrocycle proton *j* may be a consequence of interaction with the axle triazole nitrogen lone pair, with a commensurate upfield shift of axle proton *6*. Additional cross-peaks between macrocycle protons *e* and *f* and axle protons *5* and *6* also support interlocking with a bent conformation. The high-resolution ESI-MS spectrum shown matches theoretical prediction, further supporting formation of **59** (Figure 4.5c).

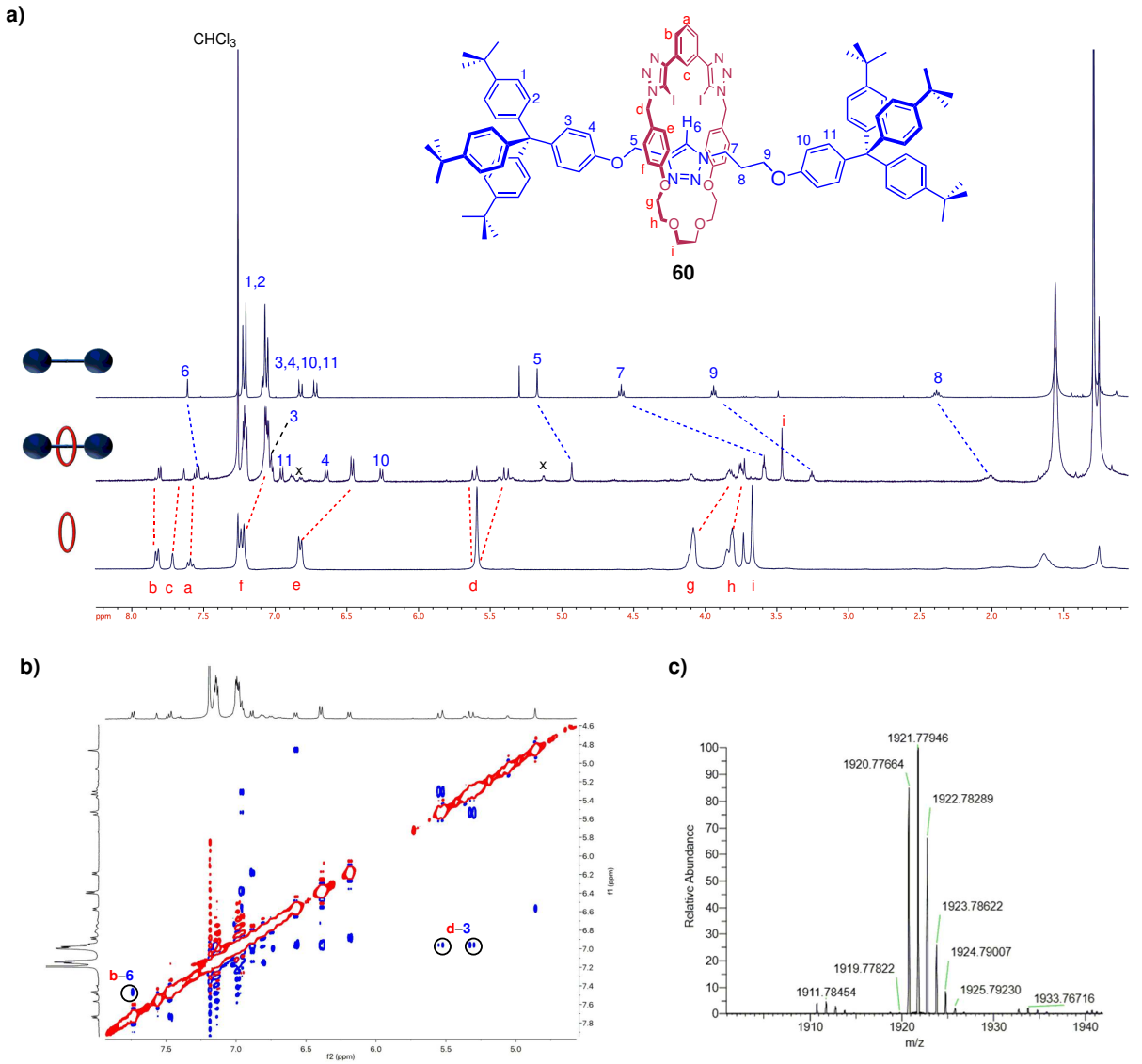

Figure 4.6: Characterisation data for [2]rotaxane **60**: a) Stacked plot of partial ^{1}H NMR spectrum of free axle (top), [2]rotaxane **60** (middle) and macrocycle **56** (bottom), b) partial 2D ROESY NMR spectrum of [2]rotaxane **60** (all in $CHCl_3$, T = 298 K), and c) corresponding high-resolution ESI-MS spectrum.

Many of the peaks identified previously prove diagnostic for **60** also. Evidence for successful formation of the interlocked product is provided by the methylene protons *d*, which are again upfield and strongly split into two environments (Figure 4.6a) by interaction with aromatic axle proton *3*. Axle proton *6* is moved upfield relative to free axle, which suggest a halogen bonding interaction between the iodotriazoles of the macrocycle and the axle triazole nitrogen lone pair. The other readily observed diagnostic cross-peak is seen between macrocycle aromatic proton *b* and axle triazole proton *6*, suggesting that this macrocycle also favours a bent conformation around the axle (Figure 4.6b). Dissection of further diagnostic cross-peaks is prevented by the overlap of aromatic stopper protons *1* and *2* with signals for protons *3* and *e*, as well as the presence of impurities. This can be addressed through use of a different solvent mixture to resolve the aromatic region better, and repeat synthesis to facilitate isolation. The high-resolution ESI-MS spectrum shown was a clear match to theoretical prediction, serving as further conformation of the formation of **60** (Figure 4.6c).

4.5 Conclusions

The objective of this chapter was to further probe the relationship between macrocycle ring-size and AT-CuAAC rotaxanation yield. To this end, a series of macrocycles of different sizes, incorporating the 1,3-bis(iodo)triazole benzene motif were targeted. Of these, the triazole-aryl conjugated macrocycles could not be prepared, however four macrocycles were successfully synthesised using bis-azide benzyl polyether, and 1,3-bis(ethynyl)benzene precursor synthons. Employing these macrocycles in the AT-CuAAC method for rotaxane formation led to the preparation of two novel halogen bonding and hydrogen bonding rotaxanes **59** and **60** containing the reduced ring-size macrocycle components **55** and **56**. With the further reduced ring-size macrocycles **57** and **58**, though ESI-MS analysis of the reaction mixtures indicated interlocked product formation, no rotaxane products could be isolated, suggesting macrocycle ring size was too small for efficient AT-CuAAC rotaxanation.

4.6 Future Work

The work presented in this chapter should first be extended by large scale AT-CuAAC synthesis of [2]rotaxane products **59** and **60** for an extensive anion binding investigation. As noted in Chapter 1, halogen bonding interlocked hosts are rare due to in part to their challenging multi-step synthesis. Further exploration of sub-stoichiometric Cu^{I} catalyst loadings, together with the effects of solvent variation on AT-CuAAC yield of these two new, and the previous rotaxanes incorporating the 1,3-bis(iodo)triazole benzene motif would confirm the importance of macrocycle ring-size in these systems.

To further investigate the impact of macrocycle design variation, a number of avenues worthy of study present themselves. First, the Cu^{I}-ligating motif for AT-CuAAC and the anion binding moiety can be separated, placed for example at opposite ends of the macrocycle, enabling each functionality to be devoted to a single purpose, and greatly increasing the variety of groups usable for each application. A second, related route of investigation is to incorporate binding sites suited for different metals, for example nickel or palladium, to harness alternative cross-coupling reactions such as Suzuki or Sonogashira in the rotaxane forming step between two half-axle components. A third option is to explore bis-triazole anion binding motifs that include between them non-nitrogen donor ligands such as sulfur or phosphorus donors, which offer potential post-rotaxanation conversion to a related group more suitable for anion binding, e.g. sulfide to sulfonium or sulfone, phosphine to phosphonium. Understanding the impact of the rest of the skeleton of the macrocycle, in an AMT or anion binding context, is another avenue of investigation that may prove important in understanding how to improve yields, or dial in selectivity of binding: the ethyl-hydroquinone spacer unit predominates in many rotaxane systems reported by the Beer group, with no deliberate comparison to other linkages having been previously attempted. Building up a library of similarly effective connecting units could also pay dividends in ameliorating difficulties of solubility or synthesis, as well as downstream applications.

Chapter 5

Conclusions

Conclusions

The work presented in this thesis sought to systematically investigate the impact of aspects of macrocycle structure, such as flexibility and ring-size, on the AT-CuAAC yield of XB and HB rotaxanes, whose anion binding properties would ultimately be investigated. The novelty of the target macrocycle design lies in the dual purpose bis-triazole motifs which can bind the Cu^{I} catalyst and act as anion binding groups *via* polarised C–I and C–H donors. As part of these efforts, computational studies of reported and novel macrocycles were undertaken. The outcomes of these simulations were compared with experimental data where available, to determine whether there was any predictive capacity in such an approach.

Chapter 2 explored the limits of additional flexibility in the bis-triazole binding motif, asking the question of whether a rigid, semi-rigid, or flexible connection between the two triazole groups provided the best outcome in AT-CuAAC reactions. To this end, 11 macrocycles based on two novel motifs (propyl bis(iodo)triazole and 1,2-hydroxymethyl benzene bis(iodo)triazole) were synthesised and efforts made to incorporate them into [2]rotaxanes. It was found that the highly flexible propyl bis(iodo)triazole macrocycles were incompetent for AT-CuAAC, while the 1,2-hydroxymethyl benzene bis(iodo)triazole macrocycles showed promise, though conclusive evidence was hindered by limited solubility of systems incorporating these macrocycles. Future work should seek to explore this, and other, semi-rigid linkages between the triazole groups, as well as considering even more rigid polyaromatic connections.

Chapter 3 built on the work in the previous chapter, attempting through computational investigations to gain further insight into how macrocycle structure affected AT-CuAAC performance. This work sought to answer the question of whether it was possible to predict the outcome of an AT-CuAAC reaction by inspecting the lowest energy conformations of a simplified system, that of a macrocycle binding a $[Cu(CH_3CN)_2]^+$ unit, simulated in the gas phase. There did appear to be a correlation between the degree of exotopicity in the lowest energy conformations and experimental yield, which makes the more complex molecular dynamic simulation studies required to validate this finding worthwhile in the future.

Chapter 4 returned to an established motif, 1,3-bis(iodo)triazole benzene, which has proven competent in AT-CuAAC rotaxanation and anion recognition. This motif was successfully incorporated into four novel macrocycles of reduced ring-size, which were then tested for AT-CuAAC performance, seeking to understand whether the outcomes were consistent with previously reported results, where reducing macrocycle ring-size improved AT-CuAAC rotaxanation yield. Two novel rotaxanes were isolated and fully characterised, while the smallest macrocycles yielded insufficient interlocked material for isolation, suggesting that at least in the case of this bifunctional macrocycle, the previously observed trend may not hold. Future work in exploring the size dependence of AMT reactions in systems intended for anion recognition purposes may benefit from separation of these concerns. Using anion binding and metal binding motifs on opposite sides of the macrocycle structural framework affords more freedom in the design of the motif for each purpose, and potentially opens up more diverse chemistry in the AMT reaction step.

Chapter 6

Experimental

6.1 General Considerations

6.1.1 Chemicals and Solvents

All solvents and reagents were purchased from commercial suppliers and used as received unless otherwise stated. Dry solvents were obtained by purging with nitrogen and then passing through an MBraun MPSP-800 column. H_2O was de-ionised and micro filtered using a Milli-Q® Millipore machine. TBA salts, $Pd_2(dba)_3$, $[Cu(MeCN)_4][PF_6]$, BTA, DBTA and TBTA were stored in a vacuum desiccator containing P_2O_5 prior to use. Where mixtures of solvents were used, ratios are reported by volume. Triethylamine was distilled from and stored over potassium hydroxide. Brine refers to a saturated aqueous solution of NaCl, $NH_4OH_{(aq.)}$ refers to a 28–30% solution of NH_3 in water. Petrol refers to the fraction of petroleum ether boiling between 40 and 60°C. Column chromatography was carried out on Merck® silica gel 60 under a positive pressure of nitrogen, preparative TLC was performed on 20 × 20 cm plates, with a silica layer of thickness 1 mm.

6.1.2 Instrumentation

NMR Spectra

Routine NMR spectra were recorded on either a Bruker AVIII 400 spectrometer, equipped with a 9.4T magnet or a Bruker AVIII 500 spectrometer, equipped with an 11.75T magnet. ^{1}H NMR titrations were recorded on the same Bruker AVIII 500 spectrometer. All chemical shifts are noted in parts per million (ppm) with signal splitting patterns denoted as singlet (s), doublet (d), triplet (t), quartet (quart.), quintet (quint.), septet (sep.) and multiplet (m). Coupling constants are reported as 3-bond (^{3}J) unless otherwise stated and are recorded to the nearest 0.1 ppm. Spectra are recorded relative to the residual solvent peak (for ^{1}H and ^{13}C), or the solvent with greatest number of deuterium atoms if mixed solvent systems are used, and are assigned with aid from 2D techniques such as COSY and ROESY.

Mass Spectra

Mass spectra were recorded on a Bruker μTOF spectrometer. Low resolution ESI mass spectra were recorded on a Waters LCT premier spectrometer.

6.1.3 Titration Protocols

All deuterated solvents used were purchased from chemical suppliers. Where available, all tetrabutylammonium (TBA) or sodium salts were used as purchased, with the former stored in vacuum desiccators at room temperature with P_2O_5 desiccant. ^{1}H NMR titrations were performed on the Bruker Avance 500 spectrometer at 298 K unless otherwise stated. In a typical titration experiment, a solution of the salt of interest was added to a 0.5 mL solution of the host (1.0 mM or 1.5 mM), and the chemical shift of the appropriate proton environments were monitored for at least 17 data points, or till saturation of the binding curve was seen. The spectra were referenced to the residual solvent peak. The observed chemical shift values at each guest concentration were entered into the WinEQNMR2 software[361] for every titration point, together with initial estimates of association constants and limiting chemical shifts. Nonlinear least squares analyses were then performed to refine the parameters using either a host-guest 1:1 or 1:2 stoichiometric binding model to obtain the best-fit between the empirical and calculated chemical shifts during convergence of the best-fit binding constant values and their errors.

6.1.4 Computational Methods

Theoretical calculations were performed using density functional theory (DFT). All calculations were performed with the Gaussian16 program package (Version A.03).[348] The B3LYP functional (Becke's three-parameter hybrid method using the correlation functional of Lee, Yang and Parr)[352,353] was selected, in combination with the double-ζ 6-31+G(d,p) Pople basis sets for all atoms except iodine,[362] for which the double-ζ LANL2DZ basis set and effective core potential (ECP) were used,[363] augmented by polarization functions of d symmetry and diffuse functions of p symmetry, here abbreviated LANL2DZdp.[364] The LANL2DZdp basis set was downloaded from the EMSL Basis Set Exchange.[365] Calculations were performed in the gas phase with default optimisation criteria and the true minimum of the optimised geometries confirmed by the absence of imaginary frequencies on vibrational analysis. Graphical visualisations were generated using GaussView 5.0.9.[366]

6.2 Synthesis

6.2.1 General Synthetic Methods

A: Bis-click Macrocycle Closure - Prototriazole

$[Cu(CH_3CN)_4]PF_6$ (0.02 mmol), DBTA (0.02 mmol), bis-azide (0.1 mmol) and bis-alkyne (0.1 mmol) were dissolved in dry, degassed CH_2Cl_2 (200 ml). To this was added DIPEA (0.22 mmol), and the mixture stirred under N_2 for 72 h at room temperature. The reaction was washed with NH_4OH/EDTA (2 x 20 ml), H_2O (2 x 40 ml) and brine (40 ml), then dried over $MgSO_4$. The solvent was removed *in vacuo*. Purification was undertaken *via* preparative thin layer chromatography (1-10% MeOH in CH_2Cl_2) to afford the macrocyclic product.

B: Bis-click Macrocycle Closure - Iodotriazole

$[Cu(CH_3CN)_4]PF_6$ (0.02 mmol) and TBTA (0.02 mmol) were dissolved in dry, degassed THF (200 ml). The mixture was allowed to stir for 5 m, after which it was covered in foil to keep the reaction in the dark, and bis-azide (0.1 mmol) added. After a further 5 min stirring, bis-alkyne (0.1 mmol) was added, and the mixture stirred in the dark under N_2 for 72 h at room temperature. The solvent was removed *in vacuo*, and the residue was taken up in CH_2Cl_2 (200 ml). The solution was washed with NH_4OH/EDTA (2 x 20 ml), H_2O (2 x 40 ml) and brine (40 ml), then dried over $MgSO_4$. The solvent was removed *in vacuo*. Purification was undertaken *via* preparative thin layer chromatography (1-5% MeOH in CH_2Cl_2) to afford the macrocyclic product.

C: AT-CuAAC [2]rotaxane Formation

$[Cu(CH_3CN)_4]PF_6$ (0.02 mmol) and macrocycle (0.02 mmol) were stirred in dry, degassed CH_2Cl_2 (2 ml) for 10 m. Stopper azide **19** (0.10 mmol) and stopper alkyne **20** (0.10 mmol) were then added and the reaction stirred under N_2 for 72-120 h, monitoring by TLC for complete consumption of axle precursors. On completion, the mixture was diluted with $CHCl_3$ (30 ml), washed with NH_4OH/EDTA (2 x 10 ml), H_2O (3 x 10 ml), dried over $MgSO_4$ and the solvent was removed *in vacuo*. Purification was undertaken *via* preparative thin layer chromatography (1-3% MeOH in CH_2Cl_2) to afford the interlocked product.

6.2.2 Compounds from Chapter 2

Propyl bis-triazole macrocycle precursor, 4

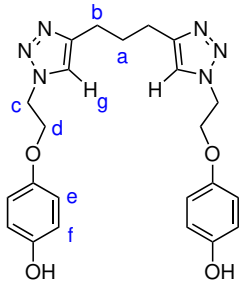

To $[Cu(CH_3CN)_4]PF_6$ (22.4 mg, 0.06 mmol), TBTA (6.0 mg, 0.01 mmol), 2-azidoethoxy phenol **2** (100 mg, 0.56 mmol), and 1,6-heptadiyne (25.7 mg, 0.28 mmol) dissolved in dry, degassed CH_2Cl_2 (10 ml) was added DIPEA (80.1 mg, 0.62 mmol), and the mixture stirred under N_2 for 48 h at room temperature. The reaction was diluted with CH_2Cl_2 (50 ml) and washed with NH_4OH (2 x 20 ml) and brine (1 x 20 ml), then dried over $MgSO_4$. The solvent was removed *in vacuo*. Purification by silica gel column chromatography (10% MeOH in CH_2Cl_2) to afford **4** (101 mg, 80%). ^{1}**H NMR** (400 MHz; MeOD) δ (ppm): 7.53 (2H, s, H_g), 6.67 (8H, m, $H_{e,f}$), 4.63 (4H, t, $J_{d|c} = 4.9$ Hz, H_d), 4.23 (4H, t, $J_{c|d} = 4.9$ Hz, H_c), 2.69 (4H, t, $J_{b|a} = 7.6$ Hz, H_b), 1.97 (2H, quintet, $J_{a|b} = 7.6$ Hz, H_a). ^{13}**C NMR** (101 MHz; MeOD) δ (ppm): 151.43, 151.21, 147.31, 122.55, 115.96, 115.83, 67.22, 49.91, 28.77, 24.61. **HRESI-MS** (pos.): 451.20871, calc. for $[C_{23}H_{26}O_4N_6 \cdot H]^+ = 451.20883$.

Propyl bis-iodotriazole macrocycle precursor, 5

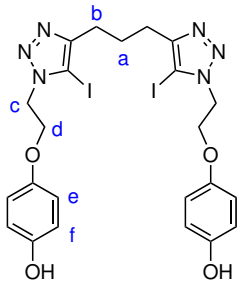

$[Cu(CH_3CN)_4]PF_6$ (24.2 mg, 0.065 mmol) and TBTA (6.4 mg, 0.01 mmol) were dissolved in dry, degassed THF (5 ml). The mixture was allowed to stir for 5 min, after which it was covered in foil and 2-azidoethoxyphenol **2** (100 mg, 0.559 mmol) was added. After a further 5 m stirring, **3** (96.0 mg, 0.279 mmol) was added and the mixture stirred under N_2 for 18 h at room temperature. The solvent was removed *in vacuo*, and the residue taken up in CH_2Cl_2 (50 ml). The solution was washed with NH_4OH/EDTA (20 ml), H_2O (20ml) and brine (20 ml), dried over $MgSO_4$ and the solvent was removed *in vacuo*. Purification by silica gel column chromatography (7% MeOH in CH_2Cl_2) to afford **5** (135 mg, 69%). ^{1}**H NMR** (400 MHz; MeOD) δ (ppm): 6.66 (8H, s, $H_{e,f}$), 4.65 (4H, t, $J_{d|c} = 5.5$ Hz, H_d), 4.29 (4H, t, $J_{c|d} = 5.5$ Hz, H_c), 2.67 (4H, t, $J_{b|a} = 7.4$ Hz, H_b), 2.00 (2H, quintet, $J_{a|b} = 7.4$ Hz, H_a). ^{13}**C NMR** (101 MHz; MeOD) δ (ppm): 151.23, 119.98, 115.89, 115.77, 66.85, 49.96, 27.79, 25.20. **HRESI-MS** (pos.): 703.00154, calc. for $[C_{23}H_{24}O_4N_6I_2 \cdot H]^+ = 703.00212$.

Propyl bis-triazole macrocycle, 7

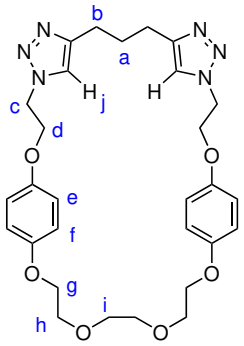

Triethylene glycol di-tosylate **6** (25.2 mg, 0.055 mmol) and bis-phenol macrocycle precursor **4** (24.8 mg, 0.055 mmol) were dissolved in degassed, anhydrous DMF (10 ml). Cs_2CO_3 (71.4 mg, 0.219 mmol) was added, and the suspension vigorously stirred for 16 h at 70°C under N_2. The solvent was removed *in vacuo*, and the resulting solid stirred in a mixture of $CHCl_3$ (50 ml) and H_2O (50 ml). The aqueous and organic layers were separated, and the aqueous layer extracted thoroughly with $CHCl_3$ (4 x 30 ml). The combined organics were washed with brine (20 ml), dried over $MgSO_4$ and the solvent was removed *in vacuo*. Purification was undertaken *via* preparative thin layer chromatography (2.5% MeOH in CH_2Cl_2) to afford **7** (20 mg, 40%). ^{1}**H NMR** (400 MHz; MeOD) δ (ppm): 7.52 (2H, s, H_j), 6.68-6.77 (8H, m, $H_{e,f}$), 4.66 (4H, t, $J_{d|c} = 4.8$ Hz, H_d), 4.23 (4H, t, $J_{c|d} = 4.8$ Hz, H_c), 3.99 (4H, t, $J_{g|h} = 4.6$ Hz, H_g), 3.77 (4H, t, $J_{h|g} = 4.6$ Hz, H_h), 3.67 (4H, s, H_i), 2.73 (4H, t, $J_{b|a} = 7.6$ Hz, H_b), 2.01 (2H, quintet, $J_{a|b} = 7.6$ Hz, H_a). ^{13}**C NMR** (101 MHz; MeOD) δ (ppm): 153.62, 152.07, 147.32, 116.32, 115.85, 115.50, 70.74, 69.66, 68.14, 67.13, 49.82, 28.65, 24.61. **HRESI-MS** (pos.): 565.27671, calc. for $[C_{29}H_{36}O_6N_6 \cdot H]^+ = 565.27691$.

Propyl bis-iodotriazole macrocycle, 8

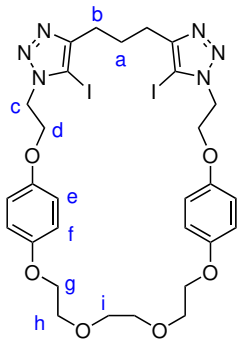

Triethylene glycol di-tosylate **6** (25.2 mg, 0.055 mmol) and bis-phenol macrocycle precursor **5** (38.6 mg, 0.055 mmol) were dissolved in anhydrous degassed DMF (10 ml). Cs_2CO_3 (71.4 mg, 0.219 mmol) was added, and the suspension vigorously stirred for 16 h at 70°C under N_2. The solvent was removed *in vacuo*, and the resulting solid stirred in a mixture of $CHCl_3$ (50 ml) and H_2O (50 ml). The aqueous and organic layers were separated, and the aqueous layer extracted thoroughly with $CHCl_3$ (4 x 30 ml). The combined organics were washed with brine (20 ml), dried over $MgSO_4$ and the solvent was removed *in vacuo*. Purification was undertaken *via* preparative thin layer chromatography (2.5% MeOH in CH_2Cl_2) to afford **8** (20.4 mg, 32%). ^{1}**H NMR** (400 MHz; $CDCl_3$) δ (ppm): 6.76 (8H, m, $H_{e,f}$), 4.69 (4H, t, $J_{d|c} = 5.2$ Hz, H_d), 4.30 (4H, t, $J_{c|d} = 5.2$ Hz, H_c), 4.03 (4H, t, $J_{g|h} = 4.7$ Hz, H_g), 3.79 (4H, t, $J_{h|g} = 4.7$ Hz, H_h), 3.69 (4H, s, H_i), 2.70 (4H, t, $J_{b|a} = 7.4$ Hz, H_b), 2.09 (2H, quintet, $J_{a|b} = 7.4$ Hz, H_a). ^{13}**C NMR** (101 MHz; $CDCl_3$) δ (ppm): 153.60, 152.18, 151.12, 116.43, 116.05, 115.54, 115.51, 70.93, 69.79, 68.40, 67.07, 49.68, 28.04, 25.18. **HRESI-MS** (pos.): 817.06947, calc. for $[C_{29}H_{34}O_6N_6I_2 \cdot H]^+ = 817.07020$.

1,2-(Iodopropargyloxy)benzene, 10

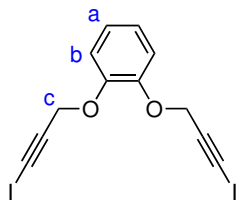

N-iodosuccinimide (266 mg, 1.18 mmol) was added to a stirred solution of **9** (100 mg, 0.537 mmol) in acetone (10 ml) covered in foil. A solution of $AgNO_3$ (18.2 mg, 0.107 mmol) in H_2O (1 ml) was then added and the mixture stirred under N_2 for 4 h. H_2O (20 ml) was added and the mixture extracted with CH_2Cl_2 (5 x 20 ml). The combined organic layers were washed with 10% $Na_2S_2O_3$ solution (10 ml), brine (20 ml), dried over $MgSO_4$ and the solvent was removed *in vacuo*, affording **10** (163 mg, 69%). ^{1}**H NMR** (400 MHz; $CDCl_3$) δ (ppm): 7.04 (2H, m, H_b), 6.99 (2H, m, H_a), 4.89 (4H, s, H_c). ^{13}**C NMR** (101 MHz; $CDCl_3$) δ (ppm): 147.55, 122.26, 114.97, 89.17, 58.45, 4.97. **HRESI-MS** (pos.): 460.85018, calc. for $[C_{12}H_8O_2I_2 \cdot Na]^+ = 460.85059$.

MOM-protected 1,2-hydroxymethyl benzene bis-triazole macrocycle precursor, 12

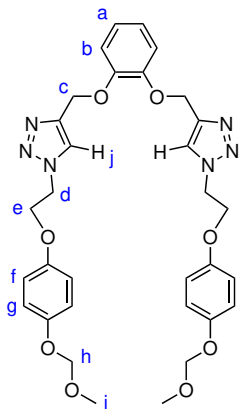

To $[Cu(CH_3CN)_4]PF_6$ (40.0 mg, 0.107 mmol), TBTA (57.0 mg, 0.107 mmol), **11** (264 mg, 1.18 mmol),[319] and **9** (100 mg, 0.537 mmol) dissolved in dry, degassed CH_2Cl_2 (20 ml) was added DIPEA (153 mg, 1.18 mmol), and the mixture stirred under N_2 for 48 h at room temperature. The reaction was diluted with CH_2Cl_2 (50 ml) and washed with NH_4OH (2 x 20 ml) and brine (1 x 20 ml), then dried over $MgSO_4$. The solvent was removed *in vacuo*. Purification by silica gel column chromatography (5% MeOH in CH_2Cl_2) afforded **12** (268 mg, 79%). ^{1}**H NMR** (400 MHz; $CDCl_3$) δ (ppm): 7.84 (2H, s, H_j), 7.04 (2H, m, H_b), 6.94 (4H, d, $J_{f|g} = 9.2$ Hz, H_f), 6.90 (2H, m, H_a), 6.74 (4H, d, $J_{g|f} = 9.2$ Hz, H_g), 5.27 (4H, s, H_c), 5.09 (4H, s, H_h), 4.69 (4H, t, $J_{e|d} = 5.1$ Hz, H_e), 4.28 (4H, t, $J_{d|e} = 5.1$ Hz, H_d), 3.46 (6H, s, H_i). ^{13}**C NMR** (101 MHz; $CDCl_3$) δ (ppm): 152.85, 152.02, 148.45, 144.40, 124.11, 122.15, 117.64, 115.64, 115.53, 95.14, 66.97, 63.50, 55.89, 49.80. **HRESI-MS** (pos.): 655.24754, calc. for $[C_{32}H_{36}O_8N_6 \cdot Na]^+ = 655.24868$.

MOM-protected 1,2-hydroxymethyl benzene bis-iodotriazole macrocycle precursor, 13

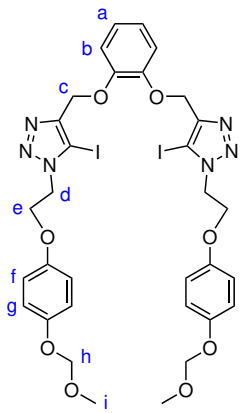

$[Cu(CH_3CN)_4]PF_6$ (20.4 mg, 0.055 mmol) and TBTA (29,1 mg, 0.055 mmol) were dissolved in dry, degassed THF (4 ml). The mixture was allowed to stir for 5 m, after which it was covered in foil and **11** (135 mg, 0.603 mmol) was added.[319] After a further 5 m stirring, **10** (120 mg, 0.274 mmol) was added and the mixture stirred under N_2 for 18 h at room temperature. The solvent was removed *in vacuo*, and the residue taken up in CH_2Cl_2 (50 ml). The solution was washed with NH_4OH/EDTA (20 ml), H_2O (20ml) and brine (20 ml), dried over $MgSO_4$ and the solvent was removed *in vacuo*. Purification by silica gel column chromatography (3% MeOH in CH_2Cl_2) afforded **13** (184 mg, 76%). ^{1}**H NMR** (400 MHz; $CDCl_3$) δ (ppm): 7.07 (2H, m, H_a), 6.90-6.95 (6H, m, $H_{b,f}$), 6.76 (4H, d, $J_{g|f} = 9.1$ Hz, H_g), 5.17 (4H, s, H_c), 5.08 (4H, s, H_h), 4.69 (4H, t, $J_{e|d} = 5.7$ Hz, H_e), 4.34 (4H, t, $J_{d|e} = 5.7$ Hz, H_d), 3.45 (6H, s, H_i). ^{13}**C NMR** (101 MHz; $CDCl_3$) δ (ppm): 153.03, 152.00, 148.91, 147.66, 122.59, 117.68, 116.77, 115.70, 95.26, 82.39, 66.76, 63.39, 55.98, 49.83. **HRESI-MS** (pos.): 655.24754, calc. for $[C_{32}H_{36}O_8N_6 \cdot Na]^+ = 655.24868$.

1,2-Hydroxymethyl benzene bis-triazole macrocycle precursor, 14

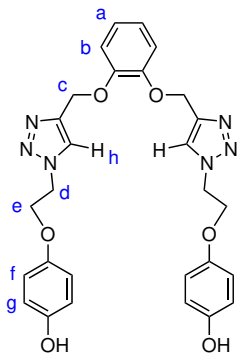

Acetyl chloride (0.5 ml, 7.0 mmol) was added to MeOH (2 ml) at 0 °C and stirred for 5 m, before being warmed to room temperature and stirred for a further 15 m. **12** (135 mg, 0.213 mmol) was dissolved in CH_2Cl_2 (5 ml) and added portionwise to the acidic MeOH solution, and stirred for 4 h. After the reaction was complete (monitored by TLC using 5% MeOH in CH_2Cl_2 as eluent) the solvent was removed *in vacuo*, and the product dried under high vacuum, affording **14** (116 mg, quant.). ^{1}**H NMR** (400 MHz; MeOD) δ (ppm): 8.11 (2H, s, H_h), 6.91 (2H, m, H_a), 6.83 (2H, m, H_b), 6.54 (8H, m, $H_{f,g}$), 5.11 (4H, s, H_c), 4.65 (4H, t, $J_{e|d} = 4.4$ Hz, H_e), 4.15 (4H, t, $J_{d|e} = 4.4$ Hz, H_d). ^{13}**C NMR** (101 MHz; MeOD) δ (ppm): 151.62, 150.90, 147.96, 125.82, 122.94, 116.05, 115.96, 115.94, 115.85, 66.63, 62.09, 51.19. **HRESI-MS** (pos.): 545.28845, calc. for $[C_{28}H_{28}O_6N_6 \cdot H]^+ = 545.21431$.

1,2-Hydroxymethyl benzene bis-iodotriazole macrocycle precursor, 15

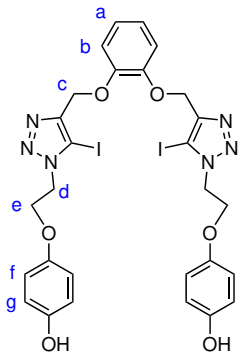

Acetyl chloride (0.5 ml, 7.0 mmol) was added to MeOH (2 ml) at 0 °C and stirred for 5 m, before being warmed to room temperature and stirred for a further 15 m. **12** (185 mg, 0.209 mmol) was dissolved in CH_2Cl_2 (5 ml) and added portionwise to the acidic MeOH solution, and stirred for 4 h. After the reaction was complete (monitored by TLC using 5% MeOH in CH_2Cl_2 as eluent) the solvent was removed *in vacuo*, and the product dried under high vacuum, affording **14** (166 mg, quant.). ^{1}**H NMR** (400 MHz; MeOD) δ (ppm): 6.88 (2H, m, H_a), 6.78 (2H, m, H_b), 6.53 (8H, m, $H_{f,g}$), 4.98 (4H, s, H_c), 4.55 (4H, t, $J_{e|d} = 5.4$ Hz, H_e), 4.17 (4H, t, $J_{d|e} = 5.4$ Hz, H_d). ^{13}**C NMR** (101 MHz; MeOD) δ (ppm): 151.36, 151.16, 148.51, 147.08, 122.74, 116.69, 115.84, 115.81, 83.89, 66.72, 62.96, 50.27. **HRESI-MS** (pos.): 797.00724, calc. for $[C_{28}H_{26}I_2N_6O_6 \cdot H]^+ =$ 797.00760.

1,2-Hydroxymethyl benzene bis-triazole macrocycle, 16

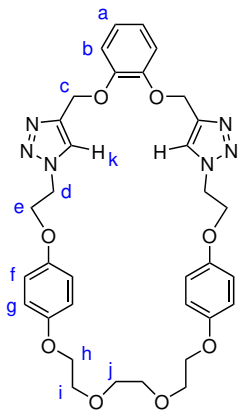

Williamson Ether Synthesis

Triethylene glycol di-tosylate **6** (97.6 mg, 0.213 mmol) and bis-phenol macrocycle precursor **14** (116 mg, 0.213 mmol) were dissolved in anhydrous, degassed DMF (20 ml). Cs_2CO_3 (277mg, 0.851 mmol) was added and the suspension stirred under N_2 at 70 °C for 16 h. Subsequently the reaction was allowed to cool to room temperature, and stirred in a mixture of $CHCl_3$ (20 ml) and H_2O (20 ml). The aqueous and organic layers were separated, and the aqueous layer extracted with $CHCl_3$ (4 x 20 ml). The combined organics were washed with brine (20 ml), dried over $MgSO_4$ and the solvent was removed *in vacuo*. Purification was undertaken *via* preparative thin layer chromatography (4% MeOH in CH_2Cl_2) to afford **16** (23 mg, 17%).

CuAAC Synthesis

Synthesis follows general synthetic procedure A. Quantities used: $[Cu(CH_3CN)_4]PF_6$ (7.5 mg, 0.02 mmol), DBTA (7.17 mg, 0.02 mmol), bis-azide **18** (47.2 mg, 0.1 mmol), bis-alkyne **9** (18.6 mg, 0.1 mmol), CH_2Cl_2 (100 ml) and DIPEA (28.4 mg, 0.22 mmol). Purification was undertaken *via* preparative thin layer chromatography (3% MeOH in CH_2Cl_2) to afford the macrocyclic product **16** (26 mg, 40%).

Characterisation

^{1}**H NMR** (400 MHz; MeOD) δ (ppm): 7.85 (2H, s, H_k), 6.93 (2H, m, H_a), 6.82 (2H, m, H_b), 6.67 (4H, d, $J_{f|g} = 9.1$ Hz, H_f), 6.58 (4H, d, $J_{g|f} = 9.1$ Hz, H_g), 5.14 (4H, s, H_c), 4.60 (4H, t, $J_{e|d} = 5.0$ Hz, H_e), 4.15 (4H, t, $J_{d|e} = 5.0$ Hz, H_d), 3.90 (4H, t, $J_{h|i} = 4.6$ Hz, H_h), 3.70 (4H, t, $J_{i|h} = 4.6$ Hz, H_i), 3.60 (4H, s, H_j). ^{13}**C NMR** (101 MHz; MeOD) δ (ppm): 153.66, 152.03, 148.39, 144.28, 124.35, 122.40, 115.91, 115.73, 115.61, 70.79, 69.73, 68.17, 66.95, 63.44, 49.93. **HRESI-MS** (pos.): 659.28222, calc. for $[C_{34}H_{38}O_8N_6 \cdot H]^+ = 659.28239$.

1,2-Hydroxymethyl benzene bis-iodotriazole macrocycle, 17

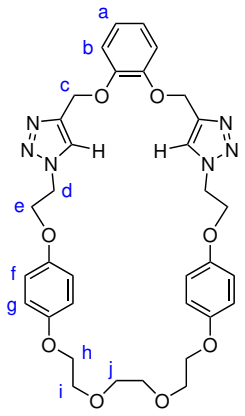

Williamson Ether Synthesis

Triethylene glycol di-tosylate **6** (28.8 mg, 0.063 mmol) and bis-phenol macrocycle precursor **15** (50.0 mg, 0.063 mmol) were dissolved in anhydrous, degassed DMF (12 ml). Cs_2CO_3 (81.8mg, 0.0.251 mmol) was added and the suspension stirred under N_2 at 70 °C for 16 h. Subsequently the reaction was allowed to cool to room temperature, and stirred in a mixture of $CHCl_3$ (20 ml) and H_2O (20 ml). The aqueous and organic layers were separated, and the aqueous layer extracted with $CHCl_3$ (4 x 15 ml). The combined organics were washed with brine (20 ml), dried over $MgSO_4$ and the solvent was removed *in vacuo*. Purification was undertaken *via* preparative thin layer chromatography (3% MeOH in CH_2Cl_2) to afford **16** (10.3 mg, 18%).

CuAAC Synthesis

Synthesis follows general synthetic procedure B. Quantities used: $[Cu(CH_3CN)_4]PF_6$ (20 mg, 0.05 mmol), TBTA (26.5 mg, 0.05 mmol), bis-azide **18** (94.4 mg, 0.2 mmol), bis-alkyne **9** (87.6 mg, 0.2 mmol) and CH_2Cl_2 (200 ml). Purification was undertaken *via* preparative thin layer chromatography (2.5% MeOH in CH_2Cl_2) to afford the macrocyclic product **16** (60 mg, 33%).

Characterisation

^{1}**H NMR** (400 MHz; $CDCl_3$) δ (ppm): 7.11 (2H, m, H_a), 6.97 (2H, m, H_b), 6.80 (4H, d, $J_{f|g} = 9.0$ Hz, H_f), 6.74 (4H, d, $J_{g|f} = 9.0$ Hz, H_g), 5.15 (4H, s, H_c), 4.67 (4H, t, $J_{e|d} = 5.6$ Hz, H_e), 4.31 (4H, t, $J_{d|e} = 5.6$ Hz, H_d), 4.00 (4H, t, $J_{h|i} = 4.7$ Hz, H_h), 3.78 (4H, t, $J_{i|h} = 4.7$ Hz, H_i), 3.70 (4H, s, H_j). ^{13}**C NMR** (101 MHz; $CDCl_3$) δ (ppm): 153.84, 152.21, 149.04, 147.73, 122.68, 116.61, 116.16, 115.81, 82.37, 71.14, 70.03, 68.41, 66.89, 63.44, 49.86. **HRESI-MS** (pos.): 911.07552, calc. for $[C_{34}H_{36}O_8N_6I_2 \cdot H]^+ = 911.07567$.

1,2-Hydroxymethyl benzene bis-triazole macrocycle, 33

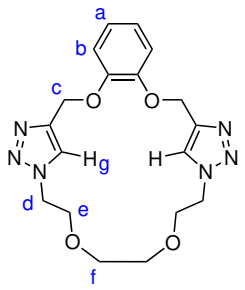

Synthesis follows general synthetic procedure A with TBTA instead of DBTA. Quantities used: $[Cu(CH_3CN)_4]PF_6$ (10.0 mg, 0.025 mmol), TBTA (10.1 mg, 0.02 mmol), bis-azide **24** (20.2 mg, 0.10 mmol), bis-alkyne **9** (18.6 mg, 0.10 mmol), CH_2Cl_2 (200ml) and DIPEA (28.4 mg, 0.22 mmol). Purification was undertaken *via* preparative thin layer chromatography (4% MeOH in CH_2Cl_2) to afford the macrocyclic product **33** (14 mg, 37%). ^{1}**H NMR** (400 MHz; $CDCl_3$) δ (ppm): 7.84 (2H, s, H_g), 7.09 (2H, m, H_b), 6.99 (2H, m, H_a), 5.30 (4H, s, H_c), 4.59 (4H, t, $J_{d|e} = 4.6$ Hz, H_d), 3.87 (4H, t, $J_{e|d} = 4.6$ Hz, H_e), 3.55 (4H, s, H_f). ^{13}**C NMR** (101 MHz; $CDCl_3$) δ (ppm): 148.40, 144.72, 123.46, 122.26, 115.17, 70.75, 69.86, 63.80. **HRESI-MS** (pos.): 387.17750, calc. for $[C_{18}H_{22}O_4N_6 \cdot H]^+ = 387.17753$.

1,2-Hydroxymethyl benzene bis-iodotriazole macrocycle, 34

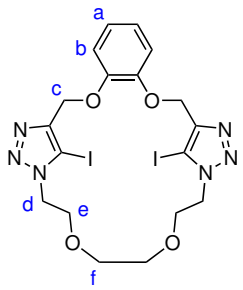

Synthesis follows general synthetic procedure B. Quantities used: $[Cu(CH_3CN)_4]PF_6$ (10.0 mg, 0.025 mmol), TBTA (12.0 mg, 0.02 mmol), bis-azide **24** (20.0 mg, 0.10 mmol), bis-alkyne **10** (43.8 mg, 0.10 mmol) and THF (200 ml). Purification was undertaken *via* preparative thin layer chromatography (3% MeOH in CH_2Cl_2) to afford the macrocyclic product **34** (4.5 mg, 7%). ^{1}**H NMR** (400 MHz; $CDCl_3$) δ (ppm): 7.12 (2H, m, H_b), 7.04 (2H, m, H_a), 5.15 (4H, s, H_c), 4.56 (4H, t, $J_{d|e} = 5.1$ Hz, H_d), 3.98 (4H, t, $J_{e|d} = 5.1$ Hz, H_e), 3.40 (4H, s, H_f). ^{13}**C NMR** (101 MHz; $CDCl_3$) δ (ppm): 148.90, 138.55, 122.14, 114.77, 84.35, 71.67, 70.37, 63.00, 50.98. **HRESI-MS** (pos.): 638.97044, calc. for $[C_{18}H_{20}O_4N_6I_2 \cdot H]^+ = 638.97082$.

1,2-Hydroxymethyl benzene bis-triazole macrocycle, 35

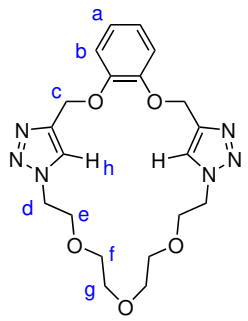

Synthesis follows general synthetic procedure A. Quantities used: $[Cu(CH_3CN)_4]PF_6$ (10.0 mg, 0.025 mmol), DBTA (7.20 mg, 0.02 mmol), bis-azide **25** (24.2 mg, 0.10 mmol), bis-alkyne **9** (18.6 mg, 0.10 mmol), CH_2Cl_2 (200ml) and DIPEA (28.4 mg, 0.22 mmol). Purification was undertaken *via* preparative thin layer chromatography (3.5% MeOH in CH_2Cl_2) to afford the macrocyclic product **35** (11 mg, 26%). ^{1}**H NMR** (400 MHz; $CDCl_3$) δ (ppm): 7.83 (2H, s, H_h), 7.05 (2H, m, H_b), 6.92 (2H, m, H_a), 5.31 (4H, s, H_c), 4.55 (4H, t, $J_{d|e} = 4.7$ Hz, H_d), 3.84 (4H, t, $J_{e|d} = 4.7$ Hz, H_e), 3.54 (4H, t, $J_{f|g} = 4.4$ Hz, H_f), 3.48 (4H, t, $J_{g|f} = 4.4$ Hz, H_g). ^{13}**C NMR** (101 MHz; $CDCl_3$) δ (ppm): 148.23, 144.49, 124.02, 121.93, 114.75, 70.79, 70.63, 69.66, 63.52, 50.50. **HRESI-MS** (pos.): 431.20360, calc. for $[C_{20}H_{26}O_5N_6 \cdot H]^+ = 431.20374$.

1,2-Hydroxymethyl benzene bis-iodotriazole macrocycle, 36

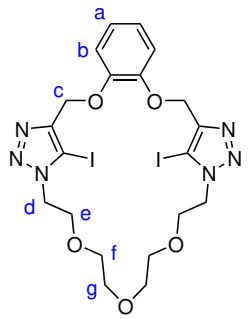

Synthesis follows general synthetic procedure B. Quantities used: $[Cu(CH_3CN)_4]PF_6$ (10.0 mg, 0.025 mmol), TBTA (12.0 mg, 0.02 mmol), bis-azide **25** (24.4 mg, 0.10 mmol), bis-alkyne **10** (43.8 mg, 0.10 mmol) and THF (200 ml). Purification was undertaken *via* preparative thin layer chromatography (2.5% MeOH in CH_2Cl_2) to afford the macrocyclic product **36** (30 mg, 44%). ^{1}**H NMR** (400 MHz; $CDCl_3$) δ (ppm): 7.15 (2H, m, H_b), 7.01 (2H, m, H_a), 5.17 (4H, s, H_c), 4.57 (4H, t, $J_{d|e} = 5.1$ Hz, H_d), 3.96 (4H, t, $J_{e|d} = 5.1$ Hz, H_e), 3.54 (4H, t, $J_{f|g} = 4.3$ Hz, H_f), 3.47 (4H, t, $J_{g|f} = 4.3$ Hz, H_g). ^{13}**C NMR** (101 MHz; $CDCl_3$) δ (ppm): 148.98, 129.97, 122.57, 116.33, 82.78, 70.86, 70.72, 69.49, 63.28, 50.52. **HRESI-MS** (pos.): 682.99633, calc. for $[C_{20}H_{24}O_5N_6I_2 \cdot H]^+ = 682.99703$.

1,2-Hydroxymethyl benzene bis-triazole macrocycle, 37

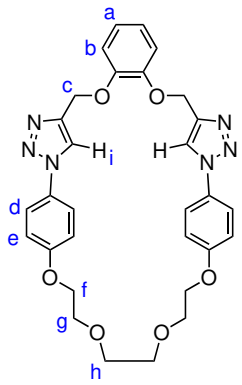

Synthesis follows general synthetic procedure A. Quantities used: $[Cu(CH_3CN)_4]PF_6$ (10.0 mg, 0.025 mmol), DBTA (7.20 mg, 0.02 mmol), bis-azide **28** (38.4 mg, 0.10 mmol), bis-alkyne **9** (18.6 mg, 0.10 mmol), CH_2Cl_2 (200ml) and DIPEA (28.4 mg, 0.22 mmol). Purification was undertaken *via* preparative thin layer chromatography (3% MeOH in CH_2Cl_2) to afford the macrocyclic product **35** (36 mg, 63%). ^{1}**H NMR** (400 MHz; $CDCl_3$) δ (ppm): 7.90 (2H, s, H_i), 7.43 (4H, d, $J_{e|d} = 8.9$ Hz, H_e), 7.12 (2H, m, H_b), 7.03 (2H, m, H_a), 6.86 (4H, d, $J_{d|e} = 8.9$ Hz, H_d), 5.28 (4H, s, H_c), 4.11 (4H, d, $J_{f|g} = 4.7$ Hz, H_f), 3.91 (4H, t, $J_{g|f} = 4.7$ Hz, H_g), 3.78 (4H, s, H_h). ^{13}**C NMR** (101 MHz; $CDCl_3$) δ (ppm): 159.11, 148.90, 145.27, 130.37, 122.54, 121.77, 120.86, 115.51, 115.48, 71.11, 69.62, 67.99, 64.05. **HRESI-MS** (pos.): 571.22972, calc. for $[C_{30}H_{30}O_6N_6 \cdot H]^+ = 571.22996$.

1,2-Hydroxymethyl benzene bis-iodotriazole macrocycle, 38

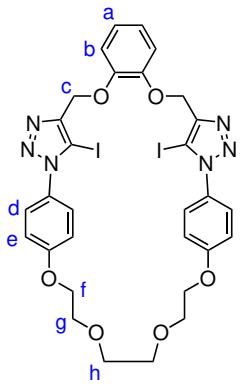

Synthesis follows general synthetic procedure B. Quantities used: $[Cu(CH_3CN)_4]PF_6$ (10.0 mg, 0.025 mmol), TBTA (12.0 mg, 0.02 mmol), bis-azide **28** (38.4 mg, 0.10 mmol), bis-alkyne **10** (43.8 mg, 0.10 mmol) and THF (200 ml). Purification was undertaken *via* preparative thin layer chromatography (2% MeOH in CH_2Cl_2) to afford the macrocyclic product **38** (45 mg, 54%). ^{1}**H NMR** (400 MHz; $CDCl_3$) δ (ppm): 7.24 (4H, d, $J_{e|d} = 8.8$ Hz, H_e), 7.17 (2H, m, H_b), 7.04 (2H, m, H_a), 6.95 (4H, d, $J_{d|e} = 8.8$ Hz, H_d), 5.16 (4H, s, H_c), 4.20 (4H, t, $J_{f|g} = 4.8$ Hz, H_f), 3.93 (4H, t, $J_{g|f} = 4.8$ Hz, H_g), 3.78 (4H, s, H_h). ^{13}**C NMR** (101 MHz; $CDCl_3$) δ (ppm): 159.96, 148.96, 148.07, 129.80, 127.42, 122.20, 115.22, 115.06, 82.86, 71.13, 69.52, 67.94, 63.36. **HRESI-MS** (pos.): 823.02263, calc. for $[C_{30}H_{28}O_6N_6I_2 \cdot H]^+ = 823.02325$.

1,2-Hydroxymethyl benzene bis-triazole macrocycle, 39

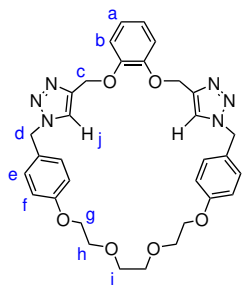

Synthesis follows general synthetic procedure A. Quantities used: $[Cu(CH_3CN)_4]PF_6$ (10.0 mg, 0.025 mmol), DBTA (7.20 mg, 0.02 mmol), bis-azide **32** (49.2 mg, 0.10 mmol), bis-alkyne **9** (18.6 mg, 0.10 mmol), CH_2Cl_2 (200ml) and DIPEA (28.4 mg, 0.22 mmol). Purification was undertaken *via* preparative thin layer chromatography (2.5% MeOH in CH_2Cl_2) to afford the macrocyclic product **39** (36 mg, 60%). ^{1}**H NMR** (400 MHz; $CDCl_3$) δ (ppm): 7.57 (2H, s, H_j), 7.18 (4H, d, $J_{f|e} = 8.6$ Hz, H_f), 7.04 (2H, m, H_b), 6.93 (2H, m, H_a), 6.86 (4H, d, $J_{e|f} = 8.6$ Hz, H_e), 5.42 (4H, s, H_d), 5.19 (4H, s, H_c), 4.07 (4H, t, $J_{g|h} = 4.5$ Hz, H_g), 3.84 (4H, t, $J_{h|g} = 4.5$ Hz, H_h), 3.72 (4H, s, H_i). ^{13}**C NMR** (101 MHz; $CDCl_3$) δ (ppm): 159.18, 148.53, 144.78, 129.69, 126.73, 122.59, 122.23, 115.47, 115.27, 71.00, 69.67, 67.74, 63.82, 53.74. **HRESI-MS** (pos.): 599.26102, calc. for $[C_{32}H_{34}O_6N_6 \cdot H]^+ = 599.26126$.

1,2-Hydroxymethyl benzene bis-iodotriazole macrocycle, 40

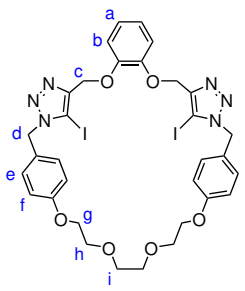

Synthesis follows general synthetic procedure B. Quantities used: $[Cu(CH_3CN)_4]PF_6$ (10.0 mg, 0.025 mmol), TBTA (10.6 mg, 0.02 mmol), bis-azide **32** (49.2 mg, 0.10 mmol), bis-alkyne **10** (43.8 mg, 0.10 mmol) and THF (200 ml). Purification was undertaken *via* preparative thin layer chromatography (1.5% MeOH in CH_2Cl_2) to afford the macrocyclic product **40** (49 mg, 58%). ^{1}**H NMR** (400 MHz; $CDCl_3$) δ (ppm): 7.20 (4H, d, $J_{f|e} = 8.7$ Hz, H_f), 7.10 (2H, m, H_b), 6.97 (2H, m, H_a), 6.89 (4H, d, $J_{e|f} = 8.7$ Hz, H_e), 5.43 (4H, s, H_d), 5.08 (4H, s, H_c), 4.07 (4H, t, $J_{g|h} = 4.7$ Hz, H_g), 3.81 (4H, t, $J_{h|g} = 4.7$ Hz, H_h), 3.70 (4H, s, H_i). ^{13}**C NMR** (101 MHz; $CDCl_3$) δ (ppm): 159.09, 148.87, 129.52, 126.44, 122.49, 116.33, 115.29, 80.78, 71.00, 69.79, 67.76, 63.28, 53.78, 53.43. **HRESI-MS** (pos.): 851.05431, calc. for $[C_{32}H_{32}O_6N_6I_2 \cdot H]^+ = 851.05455$.

1,2-Hydroxymethyl benzene bis-iodotriazole macrocycle, 41

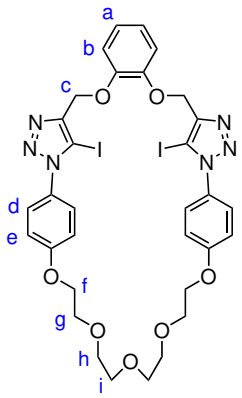

Synthesis follows general synthetic procedure B. Quantities used: $[Cu(CH_3CN)_4]PF_6$ (10.0 mg, 0.025 mmol), TBTA (10.6 mg, 0.02 mmol), bis-azide **29** (42.8 mg, 0.10 mmol), bis-alkyne **10** (43.8 mg, 0.10 mmol) and THF (200 ml). Purification was undertaken *via* preparative thin layer chromatography (1% MeOH in CH_2Cl_2) to afford the macrocyclic product **41** (47 mg, 54%). ^{1}**H NMR** (400 MHz; MeOD) δ (ppm): 7.01 (4H, d, $J_{e|d} = 9.0$ Hz, H_e), 6.89 (2H, m, H_b), 6.74 (2H, m, H_a), 6.71 (4H, d, $J_{d|e} = 9.0$ Hz, H_d), 4.83 (4H, s, H_c), 3.91 (4H, t, $J_{f|g} = 4.6$ Hz, H_f), 3.65 (4H, t, $J_{g|f} = 4.6$ Hz, H_g), 3.48 (4H, t, $J_{h|i} = 4.4$ Hz, H_h), 3.44 (4H, t, $J_{i|h} = 4.4$ Hz, H_i). ^{13}**C NMR** (101 MHz; MeOD) δ (ppm): 159.84, 148.58, 147.66, 129.40, 127.16, 122.03, 114.88, 114.61, 84.12, 70.35, 70.26, 69.08, 67.66, 62.88. **HRESI-MS** (pos.): 867.04891, calc. for $[C_{32}H_{32}O_7N_6I_2 \cdot H]^+ = 867.04946$.

6.2.3 Compounds from Chapter 4

1,3-Bistriazole benzene macrocycle, 55

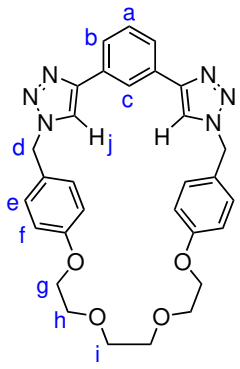

Synthesis follows general synthetic procedure A. Quantities used: $[Cu(CH_3CN)_4]PF_6$ (10.0 mg, 0.025 mmol), DBTA (7.20 mg, 0.02 mmol), bis-azide **32** (41.2 mg, 0.10 mmol), 1,3-bis(ethynyl)benzene (12.6 mg, 0.10 mmol), CH_2Cl_2 (200ml) and DIPEA (28.4 mg, 0.22 mmol). Purification was undertaken *via* preparative thin layer chromatography (2.5% MeOH in CH_2Cl_2) to afford the macrocyclic product **55** (20 mg, 37%). ^{1}**H NMR** (400 MHz; $CDCl_3$) δ (ppm): 8.09 (2H, dd, $J_{b|a} = 7.8$ Hz, $^4J_{b|c} = 1.5$ Hz, H_b), 7.53 (1H, t, $J_{a|b} = 7.8$ Hz, H_a), 7.46 (2H, s, H_j), 7.35 (1H, t, $^4J_{c|b} = 1.5$ Hz, H_c), 7.26 (4H, d, $J_{f|e} = 8.5$ Hz, H_f), 6.95 (4H, d, $J_{e|f} = 8.5$ Hz, H_e), 5.50 (4H, s, H_d), 4.12 (4H, t, $J_{g|h} = 4.1$ Hz, H_g), 3.87 (4H, t, $J_{h|g} = 4.1$ Hz, H_h), 3.73 (4H, s, H_i). ^{13}**C NMR** (101 MHz; $CDCl_3$) δ (ppm): 159.49, 147.96, 131.07, 130.34, 129.87, 126.34, 125.81, 123.10, 119.16, 115.29, 71.11, 69.83, 67.72, 54.06. **HRESI-MS** (pos.): 539.23995, calc. for $[C_{30}H_{30}O_4N_6 \cdot H]^+ = 539.24013$.

1,3-Bis(iodotriazole) benzene macrocycle, 56

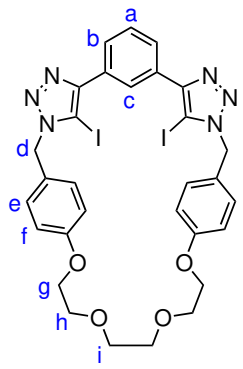

Synthesis follows general synthetic procedure B. Quantities used: $[Cu(CH_3CN)_4]PF_6$ (10.0 mg, 0.025 mmol), TBTA (10.6 mg, 0.02 mmol), bis-azide **32** (41.2 mg, 0.10 mmol), bis-alkyne **47** (37.8 mg, 0.10 mmol) and THF (200 ml). Purification was undertaken *via* preparative thin layer chromatography (1% MeOH in CH_2Cl_2) to afford the macrocyclic product **56** (20 mg, 25%). ^{1}**H NMR** (400 MHz; $CDCl_3$) δ (ppm): 7.83 (2H, d, $J_{b|a} = 7.4$ Hz, H_b), 7.72 (1H, s, H_c), 7.59 (1H, t, $J_{a|b} = 7.4$ Hz, H_a), 7.22 (4H, d, $J_{f|e} = 7.9$ Hz, H_f), 6.81 (4H, d, $J_{e|f} = 7.9$ Hz, H_e), 5.59 (4H, m, H_d), 4.08 (4H, t, $J_{g|h} = 3.7$ Hz, H_g), 3.81 (4H, t, $J_{h|g} = 3.7$ Hz, H_h), 3.67 (4H, s, H_i). ^{13}**C NMR** (101 MHz; $CDCl_3$) δ (ppm): 158.89, 129.98, 129.81, 129.80, 129.44, 128.61, 114.94, 114.78, 70.77, 69.69, 69.68, 67.46, 54.34, 54.34. **HRESI-MS** (pos.): 791.03310, calc. for $[C_{30}H_{28}O_4N_6I_2 \cdot H]^+ = 791.03342$.

1,3-Bistriazole benzene macrocycle, 57

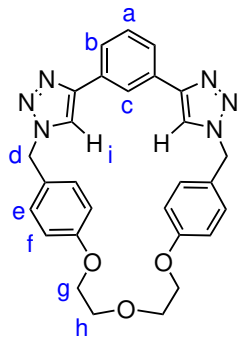

Synthesis follows general synthetic procedure A. Quantities used: $[Cu(CH_3CN)_4]PF_6$ (10.0 mg, 0.025 mmol), DBTA (7.20 mg, 0.02 mmol), bis-azide **50** (36.8 mg, 0.10 mmol), 1,3-bis(ethynyl)benzene (12.6 mg, 0.10 mmol), CH_2Cl_2 (200ml) and DIPEA (28.4 mg, 0.22 mmol). Purification was undertaken *via* preparative thin layer chromatography (3% MeOH in CH_2Cl_2) afforded the macrocyclic product **57** (18 mg, 37%). ^{1}**H NMR** (400 MHz; $CDCl_3$) δ (ppm): 8.07 (2H, dd, $J_{b|a} = 7.8$ Hz, $^4J_{b|c} = 1.5$ Hz, H_b), 7.87 (1H, t, $^4J_{c|b} = 1.5$ Hz, H_c), 7.52 (1H, t, $J_{a|b} = 7.8$ Hz, H_a), 7.30 (2H, s, H_i), 7.28 (4H, d, $J_{f|e} = 8.4$ Hz, H_f), 6.97 (4H, d, $J_{e|f} = 8.4$ Hz, H_e), 5.48 (4H, s, H_d), 4.21 (4H, t, $J_{g|h} = 4.4$ Hz, H_g), 3.94 (4H, t, $J_{h|g} = 4.4$ Hz, H_h). ^{13}**C NMR** (101 MHz; $CDCl_3$) δ (ppm): 159.56, 147.34, 130.91, 129.79, 129.68, 125.56, 125.51, 123.05, 119.07, 115.46, 115.43, 69.95, 68.03, 54.00. **HRESI-MS** (pos.): 495.21382, calc. for $[C_{28}H_{26}O_3N_6 \cdot H]^+ = 495.21392$.

1,3-Bis(iodotriazole) benzene macrocycle, 58

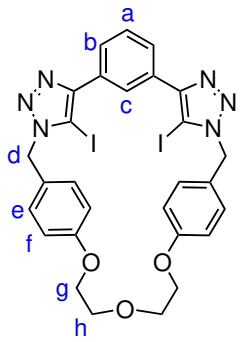

Synthesis follows general synthetic procedure B, with DBTA used instead of TBTA. Quantities used: $[Cu(CH_3CN)_4]PF_6$ (10.0 mg, 0.025 mmol), DBTA (7.2 mg, 0.02 mmol), bis-azide **50** (36.8 mg, 0.10 mmol), bis-alkyne **47** (37.8 mg, 0.10 mmol) and THF (200 ml). Purification was undertaken *via* preparative thin layer chromatography (1.5% MeOH in CH_2Cl_2) to afford the macrocyclic product **58** (20 mg, 25%). ^{1}**H NMR** (400 MHz; $CDCl_3$) δ (ppm): 7.81 (2H, dd, $J_{b|a} = 7.7$ Hz, $^4J_{b|c} = 1.5$ Hz, H_b), 7.60 (1H, t, $J_{a|b} = 7.7$ Hz, H_a), 7.50 (1H, t, $^4J_{c|b} = 1.5$ Hz, H_c), 7.15 (4H, d, $J_{f|e} = 8.6$ Hz, H_f), 6.82 (4H, d, $J_{e|f} = 8.6$ Hz, H_e), 5.60 (4H, s, H_d), 4.14 (4H, t, $J_{g|h} = 4.7$ Hz, H_g), 3.81 (4H, t, $J_{h|g} = 4.7$ Hz, H_h). ^{13}**C NMR** (101 MHz; $CDCl_3$) δ (ppm): 158.86, 152.17, 130.56, 129.82, 129.72, 129.63, 129.52, 128.48, 126.75, 115.06, 69.79, 67.70, 54.54. **HRESI-MS** (pos.): 747.00675, calc. for $[C_{28}H_{24}O_3N_6I_2 \cdot H]^+ = 747.00720$.

[2]rotaxane, 59

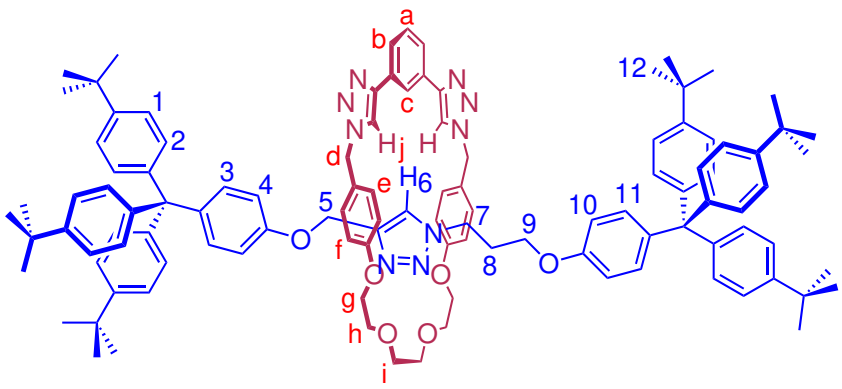

Synthesis follows general synthetic procedure C. Quantities used: $[Cu(CH_3CN)_4]PF_6$ (6.2 mg, 0.0167 mmol), macrocycle **55** (10 mg, 0.0186 mmol), CH_2Cl_2 (1.9 ml) stopper azide **19** (54.6 mg, 0.0928 mmol) and stopper alkyne **20** (50.3 mg, 0.0928 mmol). Purification was undertaken *via* preparative thin layer chromatography (1.5% MeOH in CH_2Cl_2) afforded the interlocked product **59** (5 mg, 16%). ^{1}**H NMR** (500 MHz; $CDCl_3$) δ (ppm): 8.12 (2H, dd, $J_{b|a} = 7.8$ Hz, $J_{b|c} = 1.4$ Hz, H_b), 7.86 (1H, t, $J_{c|b} = 1.4$ Hz, H_c), 7.67 (2H, s, H_j), 7.47 (1H, t, $J_{a|b} = 7.8$ Hz, H_a), 7.35 (2H, s, H_6), 7.06-7.23 (28H, m, $H_{1,2,3,11}$), 6.86 (4H, d, $J_{e|f} = 8.5$ Hz, H_e), 6.77 (2H, d, $J_{4|3} = 8.9$ Hz, H_4), 6.55 (2H, d, $J_{10|11} = 8.8$ Hz, H_{10}), 6.46 (4H, d, $J_{f|e} = 8.5$ Hz, H_f), 5.31 (4H, dd, $J_{d|d} =$, Hz $J_{d|5} = 14.6$ Hz, H_d), 4.78 (2H, s, H_5), 3.78-3.90 (4H, m, H_g), 3.81 (2H, t, $J_{7|8} = 6.0$ Hz, H_7), 3.71 (4H, t, $J_{h|g} = 5.36$ Hz, H_h), 3.64 (4H, s, H_i), 3.51 (2H, t, $J_{9|8} = 6.0$ Hz, H_9), 1.74 (2H, quintet, $J_{8|7,9} = 6.0$ Hz, H_8), 1.29 (54H, s, H_{12}). ^{13}**C NMR** (126 MHz; $CDCl_3$) δ (ppm): 158.51, 156.19, 156.14, 148.51, 148.45, 148.04, 144.22, 144.20, 142.96, 140.39, 140.31, 132.48, 132.39, 131.20, 130.78, 130.75, 129.84, 129.68, 126.51, 125.26, 124.26, 123.06, 119.94, 114.57, 113.14, 112.92, 71.07, 69.76, 67.64, 64.01, 63.19, 61.31, 46.86, 34.44, 31.53. **HRESI-MS** (pos.): 1669.98385, calc. for $[C_{110}H_{125}O_6N_9 \cdot H]^+ =$ 1669.98591.

[2]rotaxane, 60

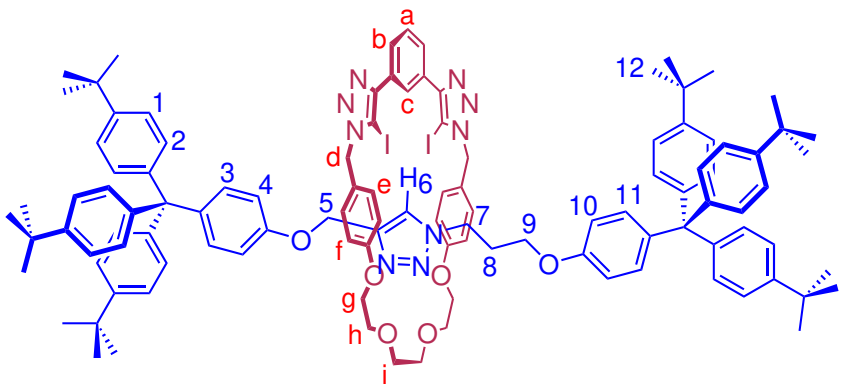

Synthesis follows general synthetic procedure C. Quantities used: $[Cu(CH_3CN)_4]PF_6$ (4.2 mg, 0.0114 mmol), macrocycle **56** (10 mg, 0.0127 mmol), CH_2Cl_2 (1.3 ml) stopper azide **19** (37.2 mg, 0.0633 mmol) and stopper alkyne **20** (34.3 mg, 0.0633 mmol). Purification was undertaken *via* preparative thin layer chromatography (1% MeOH in CH_2Cl_2) afforded the interlocked product **60** (2.3 mg, 9.5%). ^{1}**H NMR** (500 MHz; $CDCl_3$) δ (ppm): 7.81 (2H, dd, $J_{b|a} = 7.9$ Hz, $J_{b|c} = 1.5$ Hz, H_b), 7.64 (1H, t, $J_{c|b} = 1.5$ Hz, H_c), 7.55 (1H, t, $J_{a|b} = 7.9$ Hz, H_a), 7.53 (1H, s, H_6), 7.05-7.22 (24H, m, $H_{1,2}$), 7.04 (4H, d, $J_{e|f} = 8.5$ Hz, H_e), 7.02 (2H, d, $J_{3|4} = 8.8$ Hz, H_3), 6.96 (2H, d, $J_{11|10} = 8.8$ Hz, H_{11}), 6.64 (2H, d, $J_{4|3} = 8.8$ Hz, H_4), 6.46 (4H, d, $J_{f|e} = 8.5$ Hz, H_f), 6.26 (2H, d, $J_{10|11} = 8.8$ Hz, H_{10}), 5.50 (4H, dd, $J_{d|d} =$, Hz $J_{d|3} = 14.8$ Hz, H_d), 4.93 (2H, s, H_5), 3.82 (4H, t, $J_{g|h} = 6.3$ Hz, H_g), 3.75 (4H, t, $J_{h|g} = 6.3$ Hz, H_h), 3.59 (4H, t, $J_{7|8} = 6.4$ Hz, H_7), 3.47 (4H, s, H_i), 3.26 (2H, t, $J_{9|8} = 6.4$ Hz, H_9), 2.02 (2H, quintet, $J_{8|7,9} = 6.4$ Hz, H_8), 1.29 (54H, s, H_{12}). ^{13}**C NMR** (126 MHz; $CDCl_3$) δ (ppm): 148.16, 144.19, 144.08, 138.59, 136.71, 133.33, 130.71, 130.68, 130.61, 130.56, 129.83, 125.35, 124.36, 124.13, 124.07, 124.05, 114.51, 112.94, 107.29, 104.10, 99.99, 98.57, 96.02, 85.72, 69.47, 63.03, 47.34, 34.30, 31.40. **HRESI-MS** (pos.): 1921.77946, calc. for $[C_{110}H_{123}O_6N_9I_2 \cdot H]^+ =$ 1921.77920.

Chapter 7

References

Bibliography

[1] J. M. Lehn, *Angewandte Chemie International Edition*, 1988, **27**, 89–112.
[2] C. J. Pedersen, *Journal of the American Chemical Society*, 1967, **89**, 7017–7036.
[3] J. M. Lehn, *Chemical Society Reviews*, 2007, **36**, 151–160.
[4] D. J. Cram, *Angewandte Chemie International Edition*, 1988, **27**, 1009–1020.
[5] M. J. Webber, E. A. Appel, E. W. Meijer and R. Langer, *Nature Materials*, 2016, **15**, 13–26.
[6] E. V. Anslyn, *The Journal of Organic Chemistry*, 2007, **72**, 687–699.
[7] L. You, D. Zha and E. V. Anslyn, *Chemical Reviews*, 2015, **115**, 7840–7892.
[8] D. K. Smith, *Journal of Chemical Education*, 2005, **82**, 393.
[9] M. J. Webber and R. Langer, *Chemical Society Reviews*, 2017, **46**, 6600–6620.
[10] Z. Liu, M. Frasconi, J. Lei, Z. J. Brown, Z. Zhu, D. Cao, J. Iehl, G. Liu, A. C. Fahrenbach, Y. Y. Botros, O. K. Farha, J. T. Hupp, C. A. Mirkin and J. F. Stoddart, *Nature Communications*, 2013, **4**, 1855.
[11] C. Cheng, P. R. McGonigal, J. F. Stoddart and R. D. Astumian, *ACS Nano*, 2015, **9**, 8672–8688.
[12] R. D. Astumian, *Chemical Science*, 2017, **8**, 840–845.
[13] P. Atkins and J. de Paula, *Atkins' Physical Chemistry*, Oxford University Press, USA, 2010.
[14] H. J. Schneider, *Angewandte Chemie International Edition*, 2009, **48**, 3924–3977.
[15] J. W. Steed and J. L. Atwood, *Supramolecular Chemistry*, John Wiley & Sons, 2013.
[16] T. Steiner, *Angewandte Chemie International Edition*, 2002, **41**, 48–76.
[17] E. Arunan, G. R. Desiraju, R. A. Klein, J. Sadlej, S. Scheiner, I. Alkorta, D. C. Clary, R. H. Crabtree, J. J. Dannenberg, P. Hobza, H. G. Kjaergaard, A. C. Legon, B. Mennucci and D. J. Nesbitt, *Pure Applied Chemistry*, 2011, **83**, 1619–1636.
[18] J. Emsley, *Chemical Society Reviews*, 1980, **9**, 91–124.
[19] J. C. Ma and D. A. Dougherty, *Chemical Reviews*, 1997, 1303–1324.
[20] L. M. Salonen, M. Ellermann and F. Diederich, *Angewandte Chemie International Edition*, 2011, **50**, 4808–4842.
[21] J. P. Gallivan and D. A. Dougherty, *Journal of the American Chemical Society*, 2000, **122**, 870–874.
[22] B. L. Schottel, H. T. Chifotides and K. R. Dunbar, *Chemical Society Reviews*, 2007, **37**, 68–83.
[23] D. Quiñonero, C. Garau, A. Frontera, P. Ballester, A. Costa and P. M. Deyà, *Chemical Physics Letters*, 2002, **359**, 486–492.
[24] C. Garau, A. Frontera, D. Quiñonero, P. Ballester, A. Costa and P. M. Deyà, *ChemPhysChem*, 2003, **4**, 1344–1348.
[25] A. Frontera, P. Gamez, M. Mascal, T. J. Mooibroek and J. Reedijk, *Angewandte Chemie International Edition*, 2011, **50**, 9564–9583.
[26] C. Estarellas, A. Bauzá, A. Frontera, D. Quiñonero and P. M. Deyà, *Physical chemistry chemical physics : PCCP*, 2011, **13**, 5696–5702.
[27] F. Inokuchi, Y. Miyahara, T. Inazu and S. Shinkai, *Angewandte Chemie (International ed. in English)*, 1995, **34**, 1364–1366.
[28] D. X. Wang, Q. Y. Zheng, Q.-Q. Wang and M. X. Wang, *Angewandte Chemie (International ed. in English)*, 2008, **47**, 7485–7488.
[29] S. K. Burley and G. A. Petsko, *Science (New York, N.Y.)*, 1985, **229**, 23–28.
[30] C. A. Hunter and J. K. M. Sanders, *Journal of the American Chemical Society*, 1990, **112**, 5525–5534.
[31] S. Grimme, *Angewandte Chemie International Edition*, 2008, **47**, 3430–3434.
[32] C. R. Martinez and B. L. Iverson, *Chemical Science*, 2012, **3**, 2191–2201.
[33] S. E. Wheeler, *Journal of the American Chemical Society*, 2011, **133**, 10262–10274.
[34] A. Sygula, F. R. Fronczek, R. Sygula, P. W. Rabideau and M. M. Olmstead, *Journal of the American Chemical Society*, 2007, **129**, 3842–3843.
[35] P. W. Snyder, J. Mecinović, D. T. Moustakas, S. W. Thomas, M. Harder, E. T. Mack, M. R. Lockett, A. Héroux, W. Sherman and G. M. Whitesides, *Proceedings of the National Academy of Sciences of the United States of America*, 2011, **108**, 17889–17894.
[36] M. B. Hillyer and B. C. Gibb, *Annual Review of Physical Chemistry*, 2016, **67**, 307–329.
[37] M. S. Cubberley and B. L. Iverson, *Journal of the American Chemical Society*, 2001, **123**, 7560–7563.
[38] J. Seelig and P. Ganz, *Biochemistry*, 2002, **30**, 9354–9359.
[39] M. Fernández-Vidal, S. H. White and A. S. Ladokhin, *The Journal of Membrane Biology*, 2010, **239**, 5–14.
[40] M. Yaacobi and A. Ben-Naim, *J Phys Chem . . .*, 1974, **78**, 175–178.
[41] Q. F. Sun, J. Iwasa, D. Ogawa, Y. Ishido, S. Sato, T. Ozeki, Y. Sei, K. Yamaguchi and M. Fujita, *Science (New York, N.Y.)*, 2010, **328**, 1144–1147.
[42] P. D. Beer, P. A. Gale and D. K. Smith, *Supramolecular Chemistry*, Oxford University Press on Demand, 1999.
[43] E. Galbraith and T. D. James, *Chemical Society Reviews*, 2010, **39**, 3831–3842.
[44] D. Fujita, Y. Ueda, S. Sato, N. Mizuno, T. Kumasaka and M. Fujita, *Nature*, 2016, **540**, 563–566.
[45] A. Bundhun, P. Ramasami, J. S. Murray and P. Politzer, *Journal of Molecular Modeling*, 2012, **19**, 2739–2746.
[46] P. Politzer and J. S. Murray, *ChemPhysChem*, 2013, **14**, 278–294.

[47] J.-W. Zou, Y.-J. Jiang, M. Guo, G.-X. Hu, B. Zhang, H.-C. Liu and Q.-S. Yu, *Chemistry-A European Journal*, 2005, **11**, 740–751.
[48] Y.-X. Lu, J.-W. Zou, Y.-H. Wang, Y.-J. Jiang and Q.-S. Yu, *The journal of physical chemistry. A*, 2007, **111**, 10781–10788.
[49] M. H. Kolář and P. Hobza, *Chemical Reviews*, 2016, **116**, 5155–5187.
[50] A. Brown and P. D. Beer, *Chemical Communications (Cambridge, England)*, 2016, **52**, 8645–8658.
[51] J. S. Murray, P. Lane and P. Politzer, *Journal of Molecular Modeling*, 2008, **15**, 723–729.
[52] A. C. Legon, *Physical chemistry chemical physics : PCCP*, 2017, **19**, 14884–14896.
[53] A. Mohajeri, A. H. Pakiari and N. Bagheri, *Chemical Physics Letters*, 2009, **467**, 393–397.
[54] J. Y. C. Lim, I. Marques, V. Félix and P. D. Beer, *Angewandte Chemie International Edition*, 2017, **57**, 584–588.
[55] A. Bauzá and A. Frontera, *Angewandte Chemie (International ed. in English)*, 2015, **54**, 7340–7343.
[56] G. R. Desiraju, P. S. Ho, L. Kloo, A. C. Legon, R. Marquardt, P. Metrangolo, P. Politzer, G. Resnati and K. Rissanen, *Pure Applied Chemistry*, 2013, **85**, 1711–1713.
[57] F. Guthrie, *Journal of the Chemical Society (Resumed)*, 1863, **16**, 239–244.
[58] G. Cavallo, P. Metrangolo, R. Milani, T. Pilati, A. Priimagi, G. Resnati and G. Terraneo, *Chemical Reviews*, 2016, **116**, 2478–2601.
[59] R. S. Mulliken, *Journal of the American Chemical Society*, 1952, 811–824.
[60] O. Hassel and K. O. STRØMME, *Nature*, 1958, **182**, 1155–1156.
[61] E. K. Plyler and R. S. Mulliken, *Journal of the American Chemical Society*, 1959, 823–826.
[62] T. Brinck, J. S. Murray and P. Politzer, *International Journal of Quantum Chemistry*, 1992, **44**, 57–64.
[63] T. Brinck, J. S. Murray and P. Politzer, *International Journal of Quantum Chemistry*, 1993, **48**, 73–88.
[64] J. S. Murray, K. Paulsen and P. Politzer, *Proceedings of the Indian Academy of Sciences - Chemical Sciences*, 1994, **106**, 267–275.
[65] S. W. Robinson, C. L. Mustoe, N. G. White, A. Brown, A. L. Thompson, P. Kennepohl and P. D. Beer, *Journal of the American Chemical Society*, 2014, **137**, 499–507.
[66] C. C. Robertson, R. N. Perutz, L. Brammer and C. A. Hunter, *Chemical Science*, 2014, **5**, 4179–4183.
[67] T. Clark, M. Hennemann, J. S. Murray and P. Politzer, *Journal of Molecular Modeling*, 2007, **13**, 291–296.
[68] D. J. Pascoe, K. B. Ling and S. L. Cockroft, *Journal of the American Chemical Society*, 2017, **139**, 15160–15167.
[69] W. Wang, B. Ji and Y. Zhang, *The journal of physical chemistry. A*, 2009, **113**, 8132–8135.
[70] Y. Nagao, T. Hirata, S. Goto, S. Shigeki, A. Kakehi, K. Iizuka and M. Shiro, *Journal of the American Chemical Society*, 1998, **120**, 3104–3110.
[71] S. P. Thomas, K. Satheeshkumar, G. Mugesh and T. N. G. Row, *Chemistry-A European Journal*, 2015, **21**, 6793–6800.
[72] H. Park, L. J. Edgar, M. A. Lumba, L. M. Willis and M. Nitz, *Organic & biomolecular chemistry*, 2015, **13**, 7027–7033.
[73] T. Chivers and R. S. Laitinen, *Chemical Society Reviews*, 2015, **44**, 1725–1739.
[74] R. Thirumoorthi, T. Chivers and I. Vargas-Baca, *Dalton transactions (Cambridge, England : 2003)*, 2011, **40**, 8086–8088.
[75] A. Bauzá, I. Alkorta, A. Frontera and J. Elguero, *Journal of chemical theory and computation*, 2013, **9**, 5201–5210.
[76] M. D. Esrafili and F. Mohammadian-Sabet, *Journal of Molecular Modeling*, 2015, **21**, 60.
[77] N. C. Norman, *Phosphorus, Sulfur, and Silicon and the Related Elements*, 1994, **87**, 167–176.
[78] I. A. Mustafa and A. A. Taqa, *Synthesis and Reactivity in Inorganic and Metal-Organic Chemistry*, 2006, **31**, 517–526.
[79] E. Fischer, *Berichte der deutschen chemischen Gesellschaft*, 1894, **27**, 2985–2993.
[80] D. E. Koshland, *Proceedings of the National Academy of Sciences of the United States of America*, 1958, **44**, 98–104.
[81] D. E. Koshland, *Angewandte Chemie International Edition*, 1995, **33**, 2375–2378.
[82] D. J. Cram and G. M. Lein, *Journal of the American Chemical Society*, 1985, **107**, 3657–3668.
[83] E. P. Kyba, R. C. Helgeson, K. Madan, G. W. Gokel, T. L. Tarnowski, S. S. Moore and D. J. Cram, *Journal of the American Chemical Society*, 1977, **99**, 2564–2571.
[84] A. E. Martell, R. D. Hancock and R. J. Motekaitis, *Coordination Chemistry Reviews*, 1994, **133**, 39–65.
[85] Y. Li and A. H. Flood, *Angewandte Chemie International Edition in English*, 2008, **47**, 2649–2652.
[86] N. Busschaert, C. Caltagirone, W. Van Rossom and P. A. Gale, *Chemical Reviews*, 2015, **115**, 8038–8155.
[87] R. Dutzler, E. B. Campbell and R. MacKinnon, *Science (New York, N.Y.)*, 2003, **300**, 108–112.
[88] B. S. Meldrum, *The Journal of Nutrition*, 2000, **130**, 1007S–15S.
[89] A. Cavallero, A. Marte and E. Fedele, *Journal of Neurochemistry*, 2009, **110**, 924–934.
[90] L. B. Gladden, *The Journal of Physiology*, 2004, **558**, 5–30.
[91] L. R. Gray, S. C. Tompkins and E. B. Taylor, *Cellular and Molecular Life Sciences*, 2014, **71**, 2577–2604.
[92] M. P. Anderson, R. J. Gregory, S. Thompson, D. W. Souza, S. Paul, R. C. Mulligan, A. E. Smith and M. J. Welsh, *Science (New York, N.Y.)*, 1991, **253**, 202–205.

[93] V. H. Smith, G. D. Tilman and J. C. Nekola, *Environmental Pollution (Barking, Essex : 1987)*, 1999, **100**, 179–196.
[94] S. R. La Brooy, H. G. Linge and G. S. Walker, *Minerals Engineering*, 1994, **7**, 1213–1241.
[95] E. H. Schulte and P. Scoppa, *The Science of The Total Environment*, 1987, **64**, 163–179.
[96] H. Oliveira, *Journal of Botany*, 2012, 1–9.
[97] R. D. Shannon, *Acta Crystallographica Section A*, 1976, **32**, 751–767.
[98] C. Caltagirone, G. W. Bates, P. A. Gale and M. E. Light, *Chemical Communications (Cambridge, England)*, 2007, **0**, 61–63.
[99] A. E. Hargrove, S. Nieto, T. Zhang, J. L. Sessler and E. V. Anslyn, *Chemical Reviews*, 2011, **111**, 6603–6782.
[100] U. Mayer, *Coordination Chemistry Reviews*, 1976, **21**, 159–179.
[101] F. Hofmeister, *Archiv für experimentelle Pathologie und Pharmakologie*, 1888, **24**, 247–260.
[102] K. D. Collins, *Biophysical Chemistry*, 2006, **119**, 271–281.
[103] M. A. Yawer, V. Havel and V. Sindelar, *Angewandte Chemie International Edition*, 2015, **54**, 276–279.
[104] P. Sokkalingam, J. Shraberg, S. W. Rick and B. C. Gibb, *Journal of the American Chemical Society*, 2016, **138**, 48–51.
[105] J. D. Watson and E. J. Milner-White, *Journal of Molecular Biology*, 2002, **315**, 171–182.
[106] K. A. Denessiouk, M. S. Johnson and A. I. Denesyuk, *Journal of Molecular Biology*, 2005, **345**, 611–629.
[107] M. Saraste, P. R. Sibbald and A. Wittinghofer, *Trends in Biochemical Sciences*, 1990, **15**, 430–434.
[108] T. Sheet and R. Banerjee, *RSC Advances*, 2016, **6**, 54129–54141.
[109] J. J. He and F. A. Quiocho, *Science (New York, N.Y.)*, 1991, **251**, 1479–1481.
[110] J. M. Fox, K. Kang, W. Sherman, A. Héroux, G. M. Sastry, M. Baghbanzadeh, M. R. Lockett and G. M. Whitesides, *Journal of the American Chemical Society*, 2015, **137**, 3859–3866.
[111] M. Elias, A. Wellner, K. Goldin-Azulay, E. Chabriere, J. A. Vorholt, T. J. Erb and D. S. Tawfik, *Nature*, 2012, **491**, 134–137.
[112] C. H. Park and H. E. Simmons, *Journal of the American Chemical Society*, 1968, **90**, 2431–2432.
[113] E. Graf and J. M. Lehn, *Journal of the American Chemical Society*, 1976, **98**, 6403–6405.
[114] F. P. Schmidtchen, *Angewandte Chemie International Edition*, 1981, **20**, 466–468.
[115] R. A. Pascal Jr, J. Spergel and D. Van Engen, *Tetrahedron letters*, 1986, **27**, 4099–4102.
[116] K. Kavallieratos, S. R. de Gala, D. J. Austin and R. H. Crabtree, *Journal of the American Chemical Society*, 1997, **119**, 2325–2326.
[117] J. A. Wisner, P. D. Beer, M. G. B. Drew and M. R. Sambrook, *Journal of the American Chemical Society*, 2002, **124**, 12469–12476.
[118] F. Sommer and S. Kubik, *Organic & biomolecular chemistry*, 2014, **12**, 8851–8860.
[119] M. A. Hossain, S. O. Kang, J. M. Llinares, D. Powell and K. Bowman-James, *Inorganic Chemistry*, 2003, **42**, 5043–5045.
[120] T. Zieliński and J. Jurczak, *Tetrahedron*, 2005, **61**, 4081–4089.
[121] V. Blažek Bregović, N. Basarić and K. Mlinarić-Majerski, *Coordination Chemistry Reviews*, 2015, **295**, 80–124.
[122] S. Byrne and K. M. Mullen, *Supramolecular Chemistry*, 2017, **30**, 196–205.
[123] D. E. Gómez, L. Fabbrizzi, M. Licchelli and E. Monzani, *Organic & biomolecular chemistry*, 2005, **3**, 1495–1500.
[124] P. J. Smith, M. V. Reddington and C. S. Wilcox, *Tetrahedron letters*, 1992, **33**, 6085–6088.
[125] C. Jia, Q.-Q. Wang, R. A. Begum, V. W. Day and K. Bowman-James, *Organic & biomolecular chemistry*, 2015, **13**, 6953–6957.
[126] N. Busschaert, M. Wenzel, M. E. Light, P. Iglesias-Hernández, R. Pérez-Tomás and P. A. Gale, *Journal of the American Chemical Society*, 2011, **133**, 14136–14148.
[127] K. H. Lee and J.-I. Hong, *Tetrahedron letters*, 2000, **41**, 6083–6087.
[128] R. Prohens, S. Tomàs, J. Morey, P. M. Deyà, P. Ballester and A. Costa, *Tetrahedron letters*, 1998, **39**, 1063–1066.
[129] D. Quiñonero, R. Prohens, C. Garau, A. Frontera, P. Ballester, A. Costa and P. M. Deyà, *Chemical Physics Letters*, 2002, **351**, 115–120.
[130] V. Amendola, L. Fabbrizzi, L. Mosca and F.-P. Schmidtchen, *Chemistry-A European Journal*, 2011, **17**, 5972–5981.
[131] N. Busschaert, R. B. P. Elmes, D. D. Czech, X. Wu, I. L. Kirby, E. M. Peck, K. D. Hendzel, S. K. Shaw, B. Chan, B. D. Smith, K. A. Jolliffe and P. A. Gale, *Chemical Science*, 2014, **5**, 3617–3626.
[132] T. Lu and S. E. Wheeler, *Chemistry-A European Journal*, 2013, **19**, 15141–15147.
[133] L. Qin, A. Hartley, P. Turner, R. B. P. Elmes and K. A. Jolliffe, *Chemical Science*, 2016, **7**, 4563–4572.
[134] P. A. Gale, J. L. Sessler, V. Král and V. Lynch, *Journal of the American Chemical Society*, 1996, **118**, 5140–5141.
[135] P. Sokkalingam, D. S. Kim, H. Hwang, J. L. Sessler and C.-H. Lee, *Chemical Science*, 2012, **3**, 1819–1824.
[136] B. Turner, M. Botoshansky and Y. Eichen, *Angewandte Chemie International Edition*, 1998, **37**, 2475–2478.
[137] P. A. Gale, *Chemical Communications (Cambridge, England)*, 2008, **37**, 4525.
[138] J.-m. Suk and K.-S. Jeong, *Journal of the American Chemical Society*, 2008, **130**, 11868–11869.

[139] Z. Rappoport, S. E. Biali and M. Kaftory, *Journal of the American Chemical Society*, 1990, **112**, 7707–7718.
[140] S. Lee, C.-H. Chen and A. H. Flood, *Nature Chemistry*, 2013, **5**, 704–710.
[141] P. Blondeau, M. Segura, R. Pérez-Fernández and J. de Mendoza, *Chemical Society Reviews*, 2007, **36**, 198–210.
[142] K. S. Jeong and Y. L. Cho, *Tetrahedron letters*, 1997, **38**, 3279–3282.
[143] Brian R Linton, M Scott Goodman, Erkang Fan, S. A. van Arman and Andrew D Hamilton, *The Journal of Organic Chemistry*, 2001, 7313–7319.
[144] K. J. Wallace, W. J. Belcher, D. R. Turner, K. F. Syed and J. W. Steed, *Journal of the American Chemical Society*, 2003, **125**, 9699–9715.
[145] H.-Y. Gong, B. M. Rambo, E. Karnas, V. M. Lynch and J. L. Sessler, *Nature Chemistry*, 2010, **2**, 406–409.
[146] A. Kumar and P. S. Pandey, *Organic Letters*, 2008, **10**, 165–168.
[147] B. Schulze, C. Friebe, M. D. Hager, W. Günther, U. Köhn, B. O. Jahn, H. Görls and U. S. Schubert, *Organic Letters*, 2010, **12**, 2710–2713.
[148] N. G. White, S. Carvalho, V. Félix and P. D. Beer, *Organic & biomolecular chemistry*, 2012, **10**, 6951–6959.
[149] L. C. Gilday, S. W. Robinson, T. A. Barendt, M. J. Langton, B. R. Mullaney and P. D. Beer, *Chemical Reviews*, 2015, **115**, 7118–7195.
[150] A. Mele, P. Metrangolo, H. Neukirch, T. Pilati and G. Resnati, *Journal of the American Chemical Society*, 2005, **127**, 14972–14973.
[151] M. G. Sarwar, B. Dragisic, S. Sagoo and M. S. Taylor, *Angewandte Chemie International Edition in English*, 2010, **49**, 1674–1677.
[152] M. G. Chudzinski, C. A. McClary and M. S. Taylor, *Journal of the American Chemical Society*, 2011, **133**, 10559–10567.
[153] L. C. Gilday, N. G. White and P. D. Beer, *Dalton transactions (Cambridge, England : 2003)*, 2013, **42**, 15766.
[154] W. S. Brotherton, R. J. Clark and L. Zhu, *The Journal of Organic Chemistry*, 2012, **77**, 6443–6455.
[155] J. E. Hein, J. C. Tripp, L. B. Krasnova, K. B. Sharpless and V. V. Fokin, *Angewandte Chemie International Edition in English*, 2009, **48**, 8018–8021.
[156] R. Tepper, B. Schulze, H. Görls, P. Bellstedt, M. Jäger and U. S. Schubert, *Organic Letters*, 2015, **17**, 5740–5743.
[157] N. Kuhn, T. Kratz and G. Henkel, *J. Chem. Soc., Chem. Commun.*, 1993, **0**, 1778–1779.
[158] C. J. Serpell, N. L. Kilah, P. J. Costa, V. Félix and P. D. Beer, *Angewandte Chemie (International ed. in English)*, 2010, **49**, 5322–5326.
[159] S. M. Walter, F. Kniep, E. Herdtweck and S. M. Huber, *Angewandte Chemie (International ed. in English)*, 2011, **50**, 7187–7191.
[160] S. M. Walter, F. Kniep, L. Rout, F. P. Schmidtchen, E. Herdtweck and S. M. Huber, *Journal of the American Chemical Society*, 2012, **134**, 8507–8512.
[161] M. Cametti, K. Raatikainen, P. Metrangolo, T. Pilati, G. Terraneo and G. Resnati, *Organic & biomolecular chemistry*, 2012, **10**, 1329–1333.
[162] F. Zapata, A. Caballero, N. G. White, T. D. W. Claridge, P. J. Costa, V. Félix and P. D. Beer, *Journal of the American Chemical Society*, 2012, **134**, 11533–11541.
[163] R. Lalrempuia, N. D. McDaniel, H. M. Bunz, S. Bernhard and M. Albrecht, *Angewandte Chemie (International ed. in English)*, 2010, **49**, 9765–9768.
[164] R. Tepper, B. Schulze, M. Jäger, C. Friebe, D. H. Scharf, H. Görls and U. S. Schubert, *The Journal of Organic Chemistry*, 2015, **80**, 3139–3150.
[165] F. Zapata, A. Caballero, P. Molina, I. Alkorta and J. Elguero, *The Journal of Organic Chemistry*, 2014, **79**, 6959–6969.
[166] P. D. Beer, P. A. Gale and G. Z. Chen, *J. Chem. Soc., Dalton Trans.*, 1999, 1897–1909.
[167] P. D. Beer, M. G. B. Drew, J. Hodacova and S. E. Stokes, *J. Chem. Soc., Dalton Trans.*, 1995, **0**, 3447–3453.
[168] Y. Willener, K. M. Joly, C. J. Moody and J. H. R. Tucker, *The Journal of Organic Chemistry*, 2008, **73**, 1225–1233.
[169] K. A. Nielsen, J. O. Jeppesen, E. Levillain and J. Becher, *Angewandte Chemie International Edition*, 2003, **42**, 187–191.
[170] C. Bejger, J. S. Park, E. S. Silver and J. L. Sessler, *Chemical Communications (Cambridge, England)*, 2010, **46**, 7745–7747.
[171] E. Alonso, A. Labande, L. Raehm, J.-M. Kern and D. Astruc, *Comptes rendus de l'Académie des Sciences*, 1999, 209–213.
[172] D. P. Cormode, A. J. Evans, J. J. Davis and P. D. Beer, *Dalton transactions (Cambridge, England : 2003)*, 2010, **39**, 6532–6541.
[173] S. Zhang and L. Echegoyen, *Journal of the American Chemical Society*, 2005, **127**, 2006–2011.
[174] T. Minami, T. Minamiki and S. Tokito, *Chemical Communications (Cambridge, England)*, 2015, **51**, 9491–9494.
[175] H. Miyaji, W. Sato and J. L. Sessler, *Angewandte Chemie*, 2000, **112**, 1847–1850.
[176] N. Ahmed, B. Shirinfar, I. Geronimo and K. S. Kim, *Organic Letters*, 2011, **13**, 5476–5479.
[177] R. Tirfoin, J. A. B. Abdalla and S. Aldridge, *Chemistry-A European Journal*, 2015, **21**, 11813–11824.

[178] S. E. Plush and T. Gunnlaugsson, *Organic Letters*, 2007, **9**, 1919–1922.
[179] D. G. Smith, R. Pal and D. Parker, *Chemistry-A European Journal*, 2012, **18**, 11604–11613.
[180] R. J. Warr, A. N. Westra, K. J. Bell, J. Chartres, R. Ellis, C. Tong, T. G. Simmance, A. Gadzhieva, A. J. Blake, P. A. Tasker and M. Schröder, *Chemistry-A European Journal*, 2009, **15**, 4836–4850.
[181] A. Rajbanshi, B. A. Moyer and R. Custelcean, *Crystal Growth & Design*, 2011, **11**, 2702–2706.
[182] G. Wu, *Advances in nutrition (Bethesda, Md.)*, 2010, **1**, 31–37.
[183] S. Kubik, *Chemical Society Reviews*, 2009, **38**, 585–605.
[184] J. M. Granda and J. Jurczak, *Chemistry-A European Journal*, 2015, **21**, 16585–16592.
[185] L. Pu, *Accounts of chemical research*, 2011, **45**, 150–163.
[186] F. Ulatowski and J. Jurczak, *The Journal of Organic Chemistry*, 2015, **80**, 4235–4243.
[187] K. Ohmatsu, M. Kiyokawa and T. Ooi, *Journal of the American Chemical Society*, 2011, **133**, 1307–1309.
[188] J.-P. Gliese, S. H. Jungbauer and S. M. Huber, *Chemical Communications (Cambridge, England)*, 2017, **53**, 12052–12055.
[189] J. A. Foster, M.-O. M. Piepenbrock, G. O. Lloyd, N. Clarke, J. A. K. Howard and J. W. Steed, *Nature Chemistry*, 2010, **2**, 1037–1043.
[190] Q. Lin, T.-T. Lu, X. Zhu, T.-B. Wei, H. Li and Y.-M. Zhang, *Chemical Science*, 2016, **7**, 5341–5346.
[191] Z.-X. Liu, Y. Sun, Y. Feng, H. Chen, Y.-M. He and Q.-H. Fan, *Chemical Communications (Cambridge, England)*, 2016, **52**, 2269–2272.
[192] J. T. Davis, O. Okunola and R. Quesada, *Chemical Society Reviews*, 2010, **39**, 3843–3862.
[193] J. Shang, W. Si, W. Zhao, Y. Che, J.-L. Hou and H. Jiang, *Organic Letters*, 2014, **16**, 4008–4011.
[194] E. Hernando, V. Capurro, C. Cossu, M. Fiore, M. García-Valverde, V. Soto-Cerrato, R. Pérez-Tomás, O. Moran, O. Zegarra-Moran and R. Quesada, *Scientific Reports*, 2018, **8**, 2608.
[195] X. Wei, G. Zhang, Y. Shen, Y. Zhong, R. Liu, N. Yang, F. Y. Al-mkhaizim, M. A. Kline, L. He, M. Li, Z.-L. Lu, Z. Shao and B. Gong, *Journal of the American Chemical Society*, 2016, **138**, 2749–2754.
[196] A. Vargas Jentzsch and S. Matile, *Journal of the American Chemical Society*, 2013, **135**, 5302–5303.
[197] A. H. Parham, B. Windisch and F. Vögtle, *European Journal of Organic Chemistry*, 1999, **1999**, 1233–1238.
[198] R. Barat, T. Legigan, I. Tranoy-Opalinski, B. Renoux, E. Péraudeau, J. Clarhaut, P. Poinot, A. E. Fernandes, V. Aucagne, D. A. Leigh and S. Papot, *Chemical Science*, 2015, **6**, 2608–2613.
[199] R. Mitra, H. Zhu, S. Grimme and J. Niemeyer, *Angewandte Chemie (International ed. in English)*, 2017, **56**, 11456–11459.
[200] H. Frisch, I. Martin and H. Mark, *Monatshefte für Chemie und verwandte Teile anderer Wissenschaften*, 1953, **84**, 250–256.
[201] H. Lahlali, K. Jobe, M. Watkinson and S. M. Goldup, *Angewandte Chemie International Edition*, 2011, **50**, 4151–4155.
[202] A. M. Albrecht-Gary, Z. Saad, C. O. Dietrich-Buchecker and J.-P. Sauvage, *Journal of the American Chemical Society*, 1985, **107**, 3205–3209.
[203] E. Wasserman, *Journal of the American Chemical Society*, 1960, **82**, 4433–4434.
[204] I. T. Harrison and S. Harrison, *Journal of the American Chemical Society*, 1967, **89**, 5723–5724.
[205] M. A. Trakselis, S. C. Alley, E. Abel-Santos and S. J. Benkovic, *Proceedings of the National Academy of Sciences of the United States of America*, 2001, **98**, 8368–8375.
[206] B. Hudson and J. Vinograd, *Nature*, 1967, **216**, 647–652.
[207] M. A. Krasnow, A. Stasiak, S. J. Spengler, F. Dean, T. Koller and N. R. Cozzarelli, *Nature*, 1983, **304**, 559–560.
[208] D. H. Busch, *Journal of Inclusion Phenomena and Macrocyclic Chemistry*, 1992, **12**, 389–395.
[209] T. J. Hubin and D. H. Busch, *Coordination Chemistry Reviews*, 2000, **200-202**, 5–52.
[210] M. C. Thompson and D. H. Busch, *Journal of the American Chemical Society*, 1962, **84**, 1762–1763.
[211] P. R. Aston, P. T. Glink, J. F. Stoddart, P. A. Tasker, A. J. P. White and D. J. Williams, *Chemistry-A European Journal*, 1996, **2**, 729–736.
[212] S. J. Cantrill, D. A. Fulton, M. C. T. Fyfe, J. F. Stoddart, A. J. P. White and D. J. Williams, *Tetrahedron letters*, 1999, **40**, 3669–3672.
[213] J. Wu, K. C.-F. Leung and J. F. Stoddart, *Proceedings of the National Academy of Sciences of the United States of America*, 2007, **104**, 17266–17271.
[214] G. M. Hübner, J. Gläser, C. Seel and F. Vögtle, *Angewandte Chemie International Edition*, 1999, **38**, 383–386.
[215] V. Aucagne, J. Berná, J. D. Crowley, S. M. Goldup, K. D. Hänni, D. A. Leigh, P. J. Lusby, V. E. Ronaldson, A. M. Z. Slawin, A. Viterisi and D. B. Walker, *Journal of the American Chemical Society*, 2007, **129**, 11950–11963.
[216] P. R. Ashton, M. Bělohradský, D. Philp and J. F. Stoddart, *J. Chem. Soc., Chem. Commun.*, 1993, **0**, 1269–1274.
[217] I. Yoon, M. Narita, T. Shimizu and M. Asakawa, *Journal of the American Chemical Society*, 2004, **126**, 16740–16741.
[218] C.-W. Chiu, C.-C. Lai and S.-H. Chiu, *Journal of the American Chemical Society*, 2007, **129**, 3500–3501.
[219] K. Zhu, G. Baggi and S. J. Loeb, *Nature Chemistry*, 2018, **56**, 1.
[220] C. O. Dietrich-Buchecker, J. P. Sauvage and J. P. Kintzinger, *Tetrahedron letters*, 1983, **24**, 5095–5098.
[221] M. Weck, B. Mohr, J.-P. Sauvage and R. H. Grubbs, *The Journal of Organic Chemistry*, 1999, **64**, 5463–5471.

[222] C. O. Dietrich-Buchecker and J.-P. Sauvage, *Chemical Reviews*, 1987, **87**, 795–810.
[223] J. S. Hannam, T. J. Kidd, D. A. Leigh and A. J. Wilson, *Organic Letters*, 2003, **5**, 1907–1910.
[224] S. M. Goldup, D. A. Leigh, P. J. Lusby, R. T. McBurney and A. M. Z. Slawin, *Angewandte Chemie International Edition*, 2008, **47**, 6999–7003.
[225] A. M. Fuller, D. A. Leigh, P. J. Lusby, I. D. H. Oswald, S. Parsons and D. B. Walker, *Angewandte Chemie (International ed. in English)*, 2004, **43**, 3914–3918.
[226] C. Hamann, J.-M. Kern and J.-P. Sauvage, *Inorganic Chemistry*, 2003, **42**, 1877–1883.
[227] A. I. Prikhod'ko, F. Durola and J.-P. Sauvage, *Journal of the American Chemical Society*, 2008, **130**, 448–449.
[228] D. A. Leigh, R. G. Pritchard and A. J. Stephens, *Nature Chemistry*, 2014, **6**, 978–982.
[229] C. S. Wood, T. K. Ronson, A. M. Belenguer, J. J. Holstein and J. R. Nitschke, *Nature Chemistry*, 2015, **7**, 354–358.
[230] J.-C. Chang, S.-H. Tseng, C.-C. Lai, Y.-H. Liu, S.-M. Peng and S.-H. Chiu, *Nature Chemistry*, 2017, **9**, 128–134.
[231] G. Kaiser, T. Jarrosson, S. Otto, Y. F. Ng, A. D. Bond and J. K. M. Sanders, *Angewandte Chemie (International ed. in English)*, 2004, **43**, 1959–1962.
[232] R. Mitra, M. Thiele, F. Octa-Smolin, M. C. Letzel and J. Niemeyer, *Chemical Communications (Cambridge, England)*, 2016, **52**, 5977–5980.
[233] F. Zapata, O. A. Blackburn, M. J. Langton, S. Faulkner and P. D. Beer, *Chemical Communications (Cambridge, England)*, 2013, **49**, 8157–8159.
[234] J.-F. Ayme, G. Gil-Ramírez, D. A. Leigh, J.-F. Lemonnier, A. Markevicius, C. A. Muryn and G. Zhang, *Journal of the American Chemical Society*, 2014, **136**, 13142–13145.
[235] S.-Y. Hsueh, K.-W. Cheng, C.-C. Lai and S.-H. Chiu, *Angewandte Chemie (International ed. in English)*, 2008, **47**, 4436–4439.
[236] S. J. Loeb and J. A. Wisner, *Chemical Communications (Cambridge, England)*, 2000, **0**, 845–846.
[237] S. Z. Hu and C.-F. Chen, *Chemistry-A European Journal*, 2011, **17**, 5424–5431.
[238] M. Xue, Y. Yang, X. Chi, Z. Zhang and F. Huang, *Accounts of chemical research*, 2012, **45**, 1294–1308.
[239] L. Fang, S. Basu, C.-H. Sue, A. C. Fahrenbach and J. F. Stoddart, *Journal of the American Chemical Society*, 2011, **133**, 396–399.
[240] H. Li, H. Zhang, A. D. Lammer, M. Wang, X. Li, V. M. Lynch and J. L. Sessler, *Nature Chemistry*, 2015, **7**, 1003–1008.
[241] A. R. Williams, B. H. Northrop, T. Chang, J. F. Stoddart, A. J. P. White and D. J. Williams, *Angewandte Chemie International Edition*, 2006, **45**, 6665–6669.
[242] V. Aucagne, K. D. Hänni, D. A. Leigh, P. J. Lusby and D. B. Walker, *Journal of the American Chemical Society*, 2006, **128**, 2186–2187.
[243] Y. Sato, R. Yamasaki and S. Saito, *Angewandte Chemie (International ed. in English)*, 2009, **48**, 504–507.
[244] S. Saito, E. Takahashi and K. Nakazono, *Organic Letters*, 2006, **8**, 5133–5136.
[245] S. Hoekman, M. O. Kitching, D. A. Leigh, M. Papmeyer and D. Roke, *Journal of the American Chemical Society*, 2015, **137**, 7656–7659.
[246] S. M. Goldup, D. A. Leigh, P. J. Lusby, R. T. McBurney and A. M. Z. Slawin, *Angewandte Chemie (International ed. in English)*, 2008, **47**, 3381–3384.
[247] J. D. Crowley, K. D. Hänni, A.-L. Lee and D. A. Leigh, *Journal of the American Chemical Society*, 2007, **129**, 12092–12093.
[248] J. Berná, J. D. Crowley, S. M. Goldup, K. D. Hänni, A.-L. Lee and D. A. Leigh, *Angewandte Chemie (International ed. in English)*, 2007, **46**, 5709–5713.
[249] J. D. Crowley, S. M. Goldup, N. D. Gowans, D. A. Leigh, V. E. Ronaldson and A. M. Z. Slawin, *Journal of the American Chemical Society*, 2010, **132**, 6243–6248.
[250] S. M. Goldup, D. A. Leigh, R. T. McBurney, P. R. McGonigal and A. Plant, *Chemical Science*, 2010, **1**, 383–386.
[251] J. D. Crowley, K. D. Hänni, D. A. Leigh and A. M. Z. Slawin, *Journal of the American Chemical Society*, 2010, **132**, 5309–5314.
[252] P. E. Barran, H. L. Cole, S. M. Goldup, D. A. Leigh, P. R. McGonigal, M. D. Symes, J. Wu and M. Zengerle, *Angewandte Chemie International Edition*, 2011, **50**, 12280–12284.
[253] L. D. Movsisyan, M. Franz, F. Hampel, A. L. Thompson, R. R. Tykwinski and H. L. Anderson, *Journal of the American Chemical Society*, 2016, **138**, 1366–1376.
[254] J. E. M. Lewis, J. Winn, L. Cera and S. M. Goldup, *Journal of the American Chemical Society*, 2016, jacs.6b08958.
[255] C. A. Hunter, *Journal of the American Chemical Society*, 1992, **114**, 5303–5311.
[256] F. Vögtle, S. Meier and R. Hoss, *Angewandte Chemie (International ed. in English)*, 1992, **31**, 1619–1622.
[257] F. G. Gatti, D. A. Leigh, S. A. Nepogodiev, A. M. Z. Slawin, S. J. Teat and J. K. Y. Wong, *Journal of the American Chemical Society*, 2001, **123**, 5983–5989.
[258] D. G. Hamilton, J. K. M. Sanders, J. E. Davies, W. Clegg and S. J. Teat, *Chemical Communications (Cambridge, England)*, 1997, **0**, 897–898.

[259] H. Y. Au-Yeung, G. D. Pantoş and J. K. M. Sanders, *Proceedings of the National Academy of Sciences of the United States of America*, 2009, **106**, 10466–10470.
[260] D. Armspach, P. R. Ashton, C. P. Moore, N. Spencer, J. F. Stoddart, T. J. Wear and D. J. Williams, *Angewandte Chemie (International ed. in English)*, 1993, **32**, 854–858.
[261] G. Wenz, B.-H. Han and A. Müller, *Chemical Reviews*, 2006, **106**, 782–817.
[262] M. T. Stone and H. L. Anderson, *Chemical Communications (Cambridge, England)*, 2007, **0**, 2387–2389.
[263] P. Ghosh, O. Mermagen and C. A. Schalley, *Chemical Communications (Cambridge, England)*, 2002, **0**, 2628–2629.
[264] B. Qiao, Y. Liu, S. Lee, M. Pink and A. H. Flood, *Chemical Communications (Cambridge, England)*, 2016, **52**, 13675–13678.
[265] M. J. Langton and P. D. Beer, *Chemistry-A European Journal*, 2012, **18**, 14406–14412.
[266] N. H. Evans, C. J. Serpell and P. D. Beer, *Angewandte Chemie (International ed. in English)*, 2011, **50**, 2507–2510.
[267] N. H. Evans and P. D. Beer, *Chemistry-A European Journal*, 2011, **17**, 10542–10546.
[268] M. J. Langton, O. A. Blackburn, T. Lang, S. Faulkner and P. D. Beer, *Angewandte Chemie (International ed. in English)*, 2014, **53**, 11463–11466.
[269] M. J. Langton, L. C. Duckworth and P. D. Beer, *Chemical Communications (Cambridge, England)*, 2013, **49**, 8608.
[270] A. Caballero, F. Zapata, N. G. White, P. J. Costa, V. Félix and P. D. Beer, *Angewandte Chemie (International ed. in English)*, 2012, **51**, 1876–1880.
[271] S. Erbas-Cakmak, D. A. Leigh, C. T. McTernan and A. L. Nussbaumer, *Chemical Reviews*, 2015, **115**, 10081–10206.
[272] J. J. Gassensmith, L. Barr, J. M. Baumes, A. Paek, A. Nguyen and B. D. Smith, *Organic Letters*, 2008, **10**, 3343–3346.
[273] T. A. Barendt, A. Docker, I. Marques, V. Félix and P. D. Beer, *Angewandte Chemie International Edition*, 2016, **55**, 11069–11076.
[274] J. Beswick, V. Blanco, G. De Bo, D. A. Leigh, U. Lewandowska, B. Lewandowski and K. Mishiro, *Chemical Science*, 2014, **6**, 140–143.
[275] V. Blanco, D. A. Leigh and V. Marcos, *Chemical Society Reviews*, 2015, **44**, 5341–5370.
[276] J. Berná, D. A. Leigh, M. Lubomska, S. M. Mendoza, E. M. Pérez, P. Rudolf, G. Teobaldi and F. Zerbetto, *Nature Materials*, 2005, **4**, 704–710.
[277] W. Lu, M. Zhang, K. Liu, B. Fan, Z. Xia and L. Jiang, *Sensors and Actuators B: Chemical*, 2011, **160**, 1005–1010.
[278] C. J. Bruns and J. F. Stoddart, *Accounts of chemical research*, 2014, **47**, 2186–2199.
[279] M. J. Langton and P. D. Beer, *Accounts of chemical research*, 2014, **47**, 1935–1949.
[280] K. Hiratani, M. Kaneyama, Y. Nagawa, E. Koyama and M. Kanesato, *Journal of the American Chemical Society*, 2004, **126**, 13568–13569.
[281] M. Kimura, T. Mizuno, M. Ueda, S. Miyagawa, T. Kawasaki and Y. Tokunaga, *Chemistry – An Asian Journal*, 2017, **12**, 1381–1390.
[282] X. Wang, J. Zhu and D. B. Smithrud, *The Journal of Organic Chemistry*, 2010, **75**, 3358–3370.
[283] M. Denis, J. Pancholi, K. Jobe, M. Watkinson and S. M. Goldup, *Angewandte Chemie (International ed. in English)*, 2018, **57**, 5310–5314.
[284] S. S. Zhu and T. M. Swager, *Journal of the American Chemical Society*, 1997, **119**, 12568–12577.
[285] J. M. Mercurio, F. Tyrrell, J. Cookson and P. D. Beer, *Chemical Communications (Cambridge, England)*, 2013, **49**, 10793–10795.
[286] L. C. Gilday and P. D. Beer, *Chemistry-A European Journal*, 2014, **20**, 8379–8385.
[287] J. M. Mercurio, R. C. Knighton, J. Cookson and P. D. Beer, *Chemistry-A European Journal*, 2014, **20**, 11740–11749.
[288] B. R. Mullaney, A. L. Thompson and P. D. Beer, *Angewandte Chemie International Edition in English*, 2014, **53**, 11458–11462.
[289] M. J. Langton and P. D. Beer, *Chemical Communications (Cambridge, England)*, 2014, **50**, 8124–8127.
[290] S. P. Cornes, C. H. Davies, D. Blyghton, M. R. Sambrook and P. D. Beer, *Organic & biomolecular chemistry*, 2015, **13**, 2582–2587.
[291] S. W. Robinson and P. D. Beer, *Organic & biomolecular chemistry*, 2017, **15**, 153–159.
[292] M. J. Langton, S. W. Robinson, I. Marques, V. Félix and P. D. Beer, *Nature Chemistry*, 2014, **6**, 1039–1043.
[293] J. Y. C. Lim, M. J. Cunningham, J. J. Davis and P. D. Beer, *Dalton transactions (Cambridge, England : 2003)*, 2014, **43**, 17274–17282.
[294] J. Lehr, T. Lang, O. A. Blackburn, T. A. Barendt, S. Faulkner, J. J. Davis and P. D. Beer, *Chemistry-A European Journal*, 2013, **19**, 15898–15906.
[295] J. Baggerman, D. C. Jagesar, R. A. L. Vallée, J. Hofkens, F. C. De Schryver, F. Schelhase, F. Vögtle and A. M. Brouwer, *Chemistry-A European Journal*, 2007, **13**, 1291–1299.
[296] T. A. Barendt, S. W. Robinson and P. D. Beer, *Chemical Science*, 2016, **7**, 5171–5180.

[297] E. Arunkumar, C. C. Forbes, B. C. Noll and B. D. Smith, *Journal of the American Chemical Society*, 2005, **127**, 3288–3289.
[298] S. Xiao, N. Fu, K. Peckham and B. D. Smith, *Organic Letters*, 2010, **12**, 140–143.
[299] W. Zhou, J. Li, X. He, C. Li, J. Lv, Y. Li, S. Wang, H. Liu and D. Zhu, *Chemistry-A European Journal*, 2008, **14**, 754–763.
[300] W.-Y. Wong, K. C.-F. Leung and J. F. Stoddart, *Organic & biomolecular chemistry*, 2010, **8**, 2332–2343.
[301] V. M. Centelles and P. D. Beer, *Chemistry-A European Journal*, 2015, **21**, 9397–9404.
[302] P. L. Anelli, N. Spencer and J. F. Stoddart, *Journal of the American Chemical Society*, 1991, **113**, 5131–5133.
[303] J. D. Badjić, V. Balzani, A. Credi, S. Silvi and J. F. Stoddart, *Science (New York, N.Y.)*, 2004, **303**, 1845–1849.
[304] A. Coskun, S. Saha, I. Aprahamian and J. F. Stoddart, *Organic Letters*, 2008, **10**, 3187–3190.
[305] T. A. Barendt, L. Ferreira, I. Marques, V. Félix and P. D. Beer, *Journal of the American Chemical Society*, 2017, **139**, 9026–9037.
[306] D. A. Leigh, J. K. Y. Wong, F. Dehez and F. Zerbetto, *Nature*, 2003, **424**, 174.
[307] M. R. Wilson, J. Solà, A. Carlone, S. M. Goldup, N. Lebrasseur and D. A. Leigh, *Nature*, 2016, **534**, 235.
[308] M. R. Panman, B. H. Bakker, D. den Uyl, E. R. Kay, D. A. Leigh, W. J. Buma, A. M. Brouwer, J. A. J. Geenevasen and S. Woutersen, *Nature Chemistry*, 2013, **5**, 929–934.
[309] P. Farràs, E. C. Escudero-Adán, C. Viñas and F. Teixidor, *Inorganic Chemistry*, 2014, **53**, 8654–8661.
[310] X. Hou, C. Ke, C. J. Bruns, P. R. McGonigal, R. B. Pettman and J. F. Stoddart, *Nature Communications*, 2015, **6**, 6884.
[311] Y. Sagara, M. Karman, E. Verde-Sesto, K. Matsuo, Y. Kim, N. Tamaoki and C. Weder, *Journal of the American Chemical Society*, 2018, jacs.7b12405.
[312] Y. Tachibana, N. Kihara and T. Takata, *Journal of the American Chemical Society*, 2004, **126**, 3438–3439.
[313] Y. Li, Y. Feng, Y.-M. He, F. Chen, J. Pan and Q.-H. Fan, *Tetrahedron letters*, 2008, **49**, 2878–2881.
[314] Y. Cakmak, S. Erbas-Cakmak and D. A. Leigh, *Journal of the American Chemical Society*, 2016, **138**, 1749–1751.
[315] M. Galli, J. E. M. Lewis and S. M. Goldup, *Angewandte Chemie International Edition*, 2015, **54**, 13545–13549.
[316] V. Blanco, A. Carlone, K. D. Hänni, D. A. Leigh and B. Lewandowski, *Angewandte Chemie International Edition*, 2012, **51**, 5166–5169.
[317] C.-S. Kwan, A. S. C. Chan and K. C.-F. Leung, *Organic Letters*, 2016, **18**, 976–979.
[318] M. J. Langton, Y. Xiong and P. D. Beer, *Chemistry-A European Journal*, 2015, **21**, 18910–18914.
[319] J. Y. C. Lim, T. Bunchuay and P. D. Beer, *Chemistry-A European Journal*, 2017, **23**, 4700–4707.
[320] V. V. Rostovtsev, L. G. Green, V. V. Fokin and K. B. Sharpless, *Angewandte Chemie International Edition*, 2002, **41**, 2596–2599.
[321] C. W. Tornøe, C. Christensen and M. Meldal, *The Journal of Organic Chemistry*, 2002, **67**, 3057–3064.
[322] E. Haldón, M. C. Nicasio and P. J. Pérez, *Organic & biomolecular chemistry*, 2015, **13**, 9528–9550.
[323] C. A. Ramsden, *Tetrahedron*, 2010, **66**, 2695–2699.
[324] K. Jug, S. Chiodo, P. Calaminici, A. Avramopoulos and M. G. Papadopoulos, *The journal of physical chemistry. A*, 2003, **107**, 4172–4183.
[325] B. T. Worrell, J. E. Hein and V. V. Fokin, *Angewandte Chemie (International ed. in English)*, 2012, **51**, 11791–11794.
[326] B. Schulze and U. S. Schubert, *Chemical Society Reviews*, 2014, **43**, 2522–2571.
[327] J. D. Crowley, S. M. Goldup, A.-L. Lee, D. A. Leigh and R. T. McBurney, *Chemical Society Reviews*, 2009, **38**, 1530–1541.
[328] J. Winn, A. Pinczewska and S. M. Goldup, *Journal of the American Chemical Society*, 2013, **135**, 13318–13321.
[329] E. A. Neal and S. M. Goldup, *Angewandte Chemie (International ed. in English)*, 2016, **55**, 12488–12493.
[330] E. A. Neal and S. M. Goldup, *Chemical Science*, 2015, **6**, 2398–2404.
[331] J. Lewis, J. Winn and S. Goldup, *Molecules*, 2017, **22**, 89.
[332] O. Fleischel, N. Wu and A. Petitjean, *Chemical Communications (Cambridge, England)*, 2010, **46**, 8454–8456.
[333] L. Jiang, Z. Wang, S.-Q. Bai and T. S. A. Hor, *Dalton transactions (Cambridge, England : 2003)*, 2013, **42**, 9437–9443.
[334] R. Qiu and H. Luo, *RSC Advances*, 2015, **5**, 96213–96221.
[335] T. R. Bell-Horwath, A. K. Vadukoot, F. S. Thowfeik, G. Li, M. Wunderlich, J. C. Mulloy and E. J. Merino, *Bioorganic & Medicinal Chemistry Letters*, 2013, **23**, 2951–2954.
[336] N. G. White, H. G. Lovett and P. D. Beer, *RSC Advances*, 2014, **4**, 12133–12147.
[337] J. Leroy, *Synthetic Communications*, 1992, 567–572.
[338] G. Dijkstra, W. H. Kruizinga and R. M. Kellogg, *The Journal of Organic Chemistry*, 1987, **52**, 4230–4234.
[339] M. J. Gunter, T. P. Jeynes, M. R. Johnston, P. Turner and Z. Chen, *Journal of the Chemical Society, Perkin Transactions 1*, 1998, **0**, 1945–1958.
[340] N. L. Kilah, M. D. Wise, C. J. Serpell, A. L. Thompson, N. G. White, K. E. Christensen and P. D. Beer, *Journal of the American Chemical Society*, 2010, **132**, 11893–11895.

[341] N. H. Evans, C. J. Serpell, N. G. White and P. D. Beer, *Chemistry-A European Journal*, 2011, **17**, 12347–12354.
[342] J. A. Pople, *Reviews of Modern Physics*, 1999, **71**, 1267.
[343] C. J. Cramer, *Essentials of Computational Chemistry*, John Wiley & Sons, 2013.
[344] W. Kohn and L. J. Sham, *Physical Review*, 1965, **140**, A1133.
[345] M. A. L. Marques, M. J. T. Oliveira and T. Burnus, *Computer Physics Communications*, 2012, **183**, 2272–2281.
[346] S. F. Boys, *Proc. R. Soc. Lond. A*, 1950, **200**, 542–554.
[347] W. J. Hehre, R. F. Stewart and J. A. Pople, *The Journal of Chemical Physics*, 2003, **51**, 2657.
[348] M. J. Frisch, G. W. Trucks, H. B. Schlegel, G. E. Scuseria, M. A. Robb, J. R. Cheeseman, G. Scalmani, V. Barone, G. A. Petersson, H. Nakatsuji, X. Li, M. Caricato, A. V. Marenich, J. Bloino, B. G. Janesko, R. Gomperts, B. Mennucci, H. P. Hratchian, J. V. Ortiz, A. F. Izmaylov, J. L. Sonnenberg, Williams, F. Ding, F. Lipparini, F. Egidi, J. Goings, B. Peng, A. Petrone, T. Henderson, D. Ranasinghe, V. G. Zakrzewski, J. Gao, N. Rega, G. Zheng, W. Liang, M. Hada, M. Ehara, K. Toyota, R. Fukuda, J. Hasegawa, M. Ishida, T. Nakajima, Y. Honda, O. Kitao, H. Nakai, T. Vreven, K. Throssell, J. A. Montgomery Jr, J. E. Peralta, F. Ogliaro, M. J. Bearpark, J. J. Heyd, E. N. Brothers, K. N. Kudin, V. N. Staroverov, T. A. Keith, R. Kobayashi, J. Normand, K. Raghavachari, A. P. Rendell, J. C. Burant, S. S. Iyengar, J. Tomasi, M. Cossi, J. M. Millam, M. Klene, C. Adamo, R. Cammi, J. W. Ochterski, R. L. Martin, K. Morokuma, O. Farkas, J. B. Foresman and D. J. Fox, 2016.
[349] A. K. Rappe, C. J. Casewit, K. S. Colwell, W. A. Goddard and W. M. Skiff, *Journal of the American Chemical Society*, 1992, **114**, 10024–10035.
[350] K.-Y. Ng, V. Félix, S. M. Santos, N. H. Rees and P. D. Beer, *Chemical Communications (Cambridge, England)*, 2008, 1281–1283.
[351] M. G. Chudzinski and M. S. Taylor, *The Journal of Organic Chemistry*, 2012, **77**, 3483–3491.
[352] A. D. Becke, *The Journal of Chemical Physics*, 1993, **98**, 5648–5652.
[353] C. Lee, W. Yang and R. G. Parr, *Physical Review B*, 1988, **37**, 785–789.
[354] N. G. White, P. J. Costa, S. Carvalho, V. Félix and P. D. Beer, *Chemistry-A European Journal*, 2013, **19**, 17751–17765.
[355] M. Denis and S. M. Goldup, *Nature Reviews Chemistry*, 2017, **1**, s41570–017–0061.
[356] S. Ø. Scott, E. L. Gavey, S. J. Lind, K. C. Gordon and J. D. Crowley, *J. Chem. Soc., Dalton Trans.*, 2011, **40**, 12117–12124.
[357] W.-W. Yang, L. Wang, Y.-W. Zhong and J. Yao, *Organometallics*, 2011, **30**, 2236–2240.
[358] B. Beyer, C. Ulbricht, A. Winter, M. D. Hager, R. Hoogenboom, N. Herzer, S. O. Baumann, G. Kickelbick, H. Görls and U. S. Schubert, *New Journal of Chemistry*, 2010, **34**, 2622–2633.
[359] J. Andersen, S. Bolvig and X. Liang, *Synlett*, 2005, **2005**, 2941–2947.
[360] A. Kafle and S. T. Handy, *Tetrahedron*, 2017, **73**, 7024–7029.
[361] M. J. Hynes, *Journal of the Chemical Society, Dalton Transactions*, 1993, 311–312.
[362] W. J. Hehre, L. Radom, P. v. R. Schleyer and J. A. Pople, *Journal of Computational Chemistry*, 1986.
[363] P. J. Hay and W. R. Wadt, *The Journal of Chemical Physics*, 1985, **82**, 270–283.
[364] C. E. Check, T. O. Faust, J. M. Bailey and B. J. Wright, *The Journal of Physical Chemistry A*, 2001, 8111–8116.
[365] K. L. Schuchardt, B. T. Didier, T. Elsethagen, L. Sun, V. Gurumoorthi, J. Chase, J. Li and T. L. Windus, *Journal of Chemical Information and Modeling*, 2007, **47**, 1045–1052.
[366] R. Dennington, T. A. Keith and J. M. Millam, 2016.